TECHNISCHE UNIVERSITÄT MÜNCHEN
Ingenieurfakultät Bau Geo Umwelt
Professur für Hangbewegungen

Debris Flows in the Northern Alps – Activity, Erosivity and Anticipated Volumes

Andreas Dietrich

Vollständiger Abdruck der von der Ingenieurfakultät Bau Geo Umwelt der Technischen Universität München zur Erlangung des akademischen Grades eines

Doktors der Naturwissenschaften (Dr. rer. nat.)

genehmigten Dissertation.

Vorsitzender:	Prof. Dr. Kurosch Thuro
Prüfer der Dissertation:	1. Prof. Dr. Michael Krautblatter
	2. Prof. Dr. Andreas Lang
	3. Prof. Dr. Martin Elsner

Die Dissertation wurde am 09.07.2019 bei der Technischen Universität München eingereicht und durch die Ingenieurfakultät Bau Geo Umwelt am 28.01.2020 angenommen.

Meiner Frau Maria, meinen Eltern und Geschwistern in großer Dankbarkeit gewidmet.

Declaration of authorship

I, Andreas Dietrich, declare that the thesis entitled *"Debris Flows in the Northern Alps – Activity, Erosivity and Anticipated Volumes"* and the work presented in this thesis are both my own, and have been generated by me as a result of my own original research. I conform that:

- where I have quoted from the work of others, the source is always given
- where any parts of this thesis have been previously submitted for a degree at the Technical University of Munich or any other institution, this has been clearly stated
- I have acknowledged all main sources of help
- all published own work (authorship) or co-authored published work, regarding paper and conference proceedings originating of this thesis, are given in the following:

Accepted publications (ISI-listed, full research paper, peer-reviewed):

Dietrich, A., Krautblatter, M. (2017): Evidence for enhanced debris-flow activity in the Northern Calcareous Alps since the 1980s (Plansee, Austria). Geomorphology 287: 144-158. DOI: http://dx.doi.org/10.1016/j.geomorph.2016.01.013

Dietrich, A., Krautblatter, M. (2019): Deciphering controls for debris-flow erosion derived from a LiDAR-recorded extreme event and a calibrated numerical model (Roßbichelbach, Germany). Earth Surface Processes and Landforms 44: 1346-1361.
DOI: https://doi.org/10.1002/esp.4578

Journal article to be submitted:

Dietrich, A., Keilig, K., Stammberger, V., Krautblatter, M.: A 4-D reconstruction of post debris-flow sediment redistribution inferred from multi-temporal terrestrial laser scanning and photogrammetry (Roßbichelgraben, Germany).

Conference proceedings (national):

Dietrich, A., Krautblatter, M. (2017): Erosionskapazität, Entwicklung des Geschiebehaushalts und Simulation potentieller Murgänge am Beispiel des Roßbichelbachs und Roßbichelgrabens (Oberstdorf). Fachtagung Obernach: Naturgefahren - von der Sturzflut zur Schwemmholzverklausung, Obernach, Deutschland, 06.07.2017.

Dietrich, A., Krautblatter, M. (2017): Was kontrolliert die Erosion bei Murgängen? - Ein Beispiel aus den Allgäuer Alpen (Oberstdorf, Deutschland). DGGT, Fachsektionstage Geotechnik Würzburg, Tagungsband: 320-323.

Conference proceedings (international):

Dietrich, A., Krautblatter, M. (2016): Evidence for enhanced debris-flow activity in the Northern Calcareous Alps since the 1980s (Plansee, Austria). EGU 2016, Vienna.

Dietrich, A., Krautblatter, M. (2017): What controls debris-flow channel-bed erosion? A LiDAR-based change detection compared to velocity, momentum and pressure derived from a calibrated model. EGU 2017, Vienna.

Keilig, K., **Dietrich, A.**, Krautblatter, M. (2018): Comparison of multi-temporal elevation models relating to movement rates and volume estimation of debris flows. IAEG 2018, San Francisco *(peer reviewed).*

Dietrich, A., Krautblatter, M. (2018): Exhaustion law for post debris-flow sediment redistribution inferred from terrestrial laser scanning and photogrammetry (Roßbichelgraben, Germany. EGU 2018, Vienna.

Dietrich, A., Krautblatter, M. (2018): Revealing controls for debris-flow erosion derived from a calibrated numerical one-phase model (Roßbichelbach, Germany). Central European Conference on Geomorphology and Quaternary Sciences 2018, Giessen.

Keilig, K., **Dietrich, A.**, Krautblatter, M. (2018): How to effectively monitor geomorphic changes in debris-flow channels. 5th International Conference "Debris Flows: disasters, risk, forecast, protection" 2018, Tiflis.

Dietrich, A., Krautblatter, M. (2019): Revealing controls for debris-flow erosion using a LiDAR-based geomorphic change detection and a calibrated numerical model. EGU 2019, Vienna.

Dietrich, A., Krautblatter, M. (2019): Quantitative controls of debris-flow erosion derived by a LiDAR-based geomorphic change detection and a calibrated numerical model. Annual Meeting of the German Geomorphology Group „AK Geomorphologie" 2019, Kiel.

The following (unpublished) master thesis has been incorporated in this thesis:

Dietrich A. (2014): Vergleich von potentiell mobilisierbaren Murvolumina mit rezenten Ereignissen und holozänen Murkegeln am Plansee (Tirol, Österreich), Ingenieurfakultät Bau Geo Umwelt, Technische Universität München, unpublished master thesis, 177 p.

This thesis is written in accordance to

- the “Regulations for the Award of Doctoral Degrees at the Technische Universität München (Promotionsordnung)” of 12 March 2012 as amended by the 2nd Amendment Regulations of 1 September 2013, with implementation on January 1, 2014,
- the “Leitfaden BGU Promotionen” (issued on 6 April 2016) and
- the “Leitfaden kumulative Promotionen” (issued July 2015).

The thesis is written in British English, except for Chapter 4 (American English).

Abstract

Debris flows occur globally in steep channelised torrents filled with loose debris, mostly due to heavy rainstorm events. Their destructive power caused tens of thousands of deaths in the last 70 years and destroyed a huge amount of economic goods in endangered areas. Especially the European Alps are affected by a large number of recorded damaging debris flows per year, e.g. more than 1,400 events occurred between 1972 and 2004 in Austria. Although their occurrence is bound to specific locations, limited evidence exists regarding (i) their decadal and annual activity, (ii) their erosivity and transported sediment volumes as well as (iii) the channel refill rates after an event. However, the size of hazard zones and the size and site of countermeasures strongly depend on the above specified aspects (i) to (iii), as the evaluation is – among others – based on *how frequently* debris flows occur in an area (*activity?*), *how much* material is eroded and transported during an event and *how fast* the channel bed is refilled with sediments after an event. As a consequence, in this thesis a trinity of manuscripts aims to gain further understanding of (i) factors conditioning long-term debris-flow activity (pre-depositional), (ii) factors controlling sediment erosion and volume increase during an event (syn-depositional) and (iii) factors governing sediment dynamic and channel refill after an event (post-depositional). Different methodological approaches were required for each objective. Data were gathered at three study sites, as each site had its own advantages and limitations concerning survey and measurement setup.

(i) To decipher the long-term debris-flow activity (pre-depositional), a combination of an analysis of aerial photographs since the 1940s and field mapping in eight catchments at the Plansee Lake in Austria was carried out. The lithology in these catchments consists of Upper-Triassic dolomites. The investigated catchments and fans supply large amounts of sediments available for transport, representing an ideal spot to study the debris-flow activity in a transport-limited system in times of frequently hypothesised, but rarely proven impacts of climate change. The individual spatial and temporal development of each catchment and fan could be tracked on seven photos from 1947 to 2010. The volumes of debris flows, which occurred between two consecutive photos, were quantified by an area-to-volume relationship of deposited material. Results of these normalised rates (m^3/yr) suggest a significant increase in the transported sediment rate from 1947-1952 ($0.23 \pm 0.07\ 10^3 m^3/yr$) to 1987-2000 ($2.41 \pm 0.66\ 10^3 m^3/yr$) with a following decrease to $1.4 \pm 0.4\ 10^3 m^3/yr$ (2000-2010). Thus, rates after 1980 raised on a more than three-fold elevated level compared to pre-1980 rates. These recently increased rates also exceed the Holocene/Lateglacial rate by a factor of two to three, which was revealed by an electrical resistivity tomography. The analysis of the aerial photographs also shows a strong correlation between vegetation-free catchment area and transported annual sediment rate (activity). Additionally, nearby located meteorological stations provide insights into changed rainfall patterns in the study area in the last decades. The data indicate an enhanced rainstorm frequency (doubled since the 1920s) with a coincidently increased debris-flow activity.

(ii) To reveal meaningful controlling factors for debris-flow erosion and the related volumetric growth of debris flows along the flow path (syn-depositional), the second study analyses geomorphic change

by means of a pre-and post-event digital elevation model for a debris flow occurred in June 2015 (Roßbichelbach, Oberstdorf, Germany). The debris flow deeply incised into the underlying substrate, which consists of Flysch bedrock and Quaternary deposits, resulting in a substantial volumetric growth along the 1,200-metre long channel. The spatial variable erosion and deposition of material in the torrent was recorded by a terrestrial laser scanning survey (> 50 scan positions) shortly after the event. The derived digital elevation model of 2015 was in turn compared to a digital elevation model recorded by an airborne laser scanning survey in 2007. The difference of both data set reveals massive erosion rates up to 5 m^3/m^2 resulting in a total erosion volume of 9,550 ± 1,550 m^3 and a deposition volume of 650 ± 150 m^3 in the channel. Flow properties of a calibrated numerical debris-flow model were compared to the results of the change detection. For the first time, flow momentum and shear stress at the base of the flow were found to be meaningful parameters of a real-scale debris flow to explain erosion rates (R^2 up to 0.7) and can be considered as substantial controlling factors. Disproportionally large erosion rates were observed at transitions of the substrate from bedrock to loose debris.

(iii) In contrast to most recently published studies, which often focus on syn-event debris-flow processes, the third study analyses the sediment dynamic and the channel refill after a debris-flow event (post-depositional). Especially in sediment-limited systems, the refill rate governs debris-flow magnitude and activity, which both largely depend on the supply of mobilisable loose debris, originating from adjacent slopes or from the above lying catchment. For this purpose, the channel refill of the Roßbichelgraben (Oberstdorf, Germany) was investigated after a debris-flow event in June 2015. Ten TLS surveys (> 360 laser scans) and nine temporally synchronised UAV surveys (> 7,000 photos) were carried out from June 2015 to October 2018 to decipher the temporal, spatial and seasonal sediment dynamic in the 400-metre long channel. With both techniques, TLS and SfM-based photogrammetry, very similar erosion and disposition volumes were obtained (difference < 5%). The results suggest that approx. 1,150 m^3 of material has been stored in the channel bed in the last 3.5 years (≈ 1 m^3/d), whereby material redistribution is more active in summer than in winter. The erosion, deposition and net volumes were compared to different rainfall intensities (mm/10 min to mm/72 h) to examine potential links between rainfall pattern and sediment redistribution. The novel approach shows that the post-event sediment dynamic can best be explained (R^2 up to 0.9) by short intense rainstorm events. Additionally, the elapsed time since the last debris flow influences the channel refill significantly, as many over-steepened river banks failed shortly after the event and subsequently stabilised over time.

This thesis (i) presents one of the first evidences for a presumably climate change based three-fold increase in debris-flow activity since the 1980s coincident to an increased frequency of heavy rainstorm events, (ii) reveals momentum and shear stress as meaningful controlling factors for debris-flow erosion to better predict and model potential future debris flows, (iii) deciphers short, intense rainstorms as substantial controls on the post-event sediment dynamic in channels and demonstrates that photogrammetry and terrestrial laser scanning provide equivalent results. This thesis contributes to a more reliable and reproducible assessment of debris-flow related hazards in alpine regions.

Zusammenfassung

Murgänge sind gravitationsbedingte Massenbewegungen, die in steilen, schuttgefüllten Wildbächen bei Starkniederschlägen auftreten können. Aufgrund der hohen Geschwindigkeit und Masse kamen in den letzten 70 Jahren zehntausende Menschen zu Tode. Auch die Europäischen Alpen sind jedes Jahr von einer großen Anzahl an Murgängen betroffen. Allein in Österreich wurden zwischen 1972 und 2004 mehr als 1400 Ereignisse registriert. Obwohl das Auftreten von Murgängen an bestimmte Gebiete und Voraussetzungen gebunden ist, gibt es nur sehr wenige Daten bezüglich (i) deren langjähriger Aktivität, (ii) deren Erosivität und der transportierten Volumina und (iii) der Wiederauffüllungsrate eines Wildbaches mit Sediment nach einem Ereignis. Allerdings sind genau diese Daten für die zuverlässige Konstruktion von Schutzmaßnahmen und die nachvollziehbare Ausweisung von Schutzgebieten unabdingbar, da die Bewertung vor allem darauf basiert, *wie häufig* Murgänge in einem Gebiet auftreten (*Aktivität?*), *wie viel* Material transportiert wird und *wie schnell* sich der Bach nach einem Ereignis wieder mit Material füllt. Deshalb zielt diese Arbeit mithilfe dreier Manuskripte darauf ab, (i) ein besseres Verständnis für die methodische Herangehensweise zur Bestimmung der langjährigen Murgangaktivität und deren beeinflussende Faktoren zu erhalten (Pre-Event), (ii) kontrollierende Faktoren für die Erosionsraten eines Murgangs zu erforschen (Syn-Event) und (iii) beeinflussende Faktoren für die Sedimentdynamik und die Wiederauffüllungsrate eines Wildbachs mit Material nach einem Ereignis reproduzierbar zu bestimmen (Post-Event). Für die Ziele wurden unterschiedliche methodische Ansätze und Untersuchungsgebiete gewählt, da jedes Gebiet Vorzüge und Einschränkungen bzgl. der Durchführbarkeit der entsprechenden Messungen und Begehungen hatte.

(i) Um die Murgangaktivität (Pre-Event) über einen längeren Zeitraum zu untersuchen, wurden Luftbilder seit 1947 ausgewertet und Kartierungen am Plansee in Österreich durchgeführt (Nördliche Kalkalpen). Die acht untersuchten Einzugsgebiete sind lithologisch aus obertriassischem Hauptdolomit aufgebaut. Diese stellen sehr große Mengen an Sediment bereit, wodurch die Murgangaktivität in Zeiten des Klimawandels in einem transportlimitierten System sehr gut untersucht werden kann. Mithilfe von sieben Luftbildern zwischen 1947 und 2010 konnte die räumliche und zeitliche Entwicklung jedes Murkegels und Einzugsgebiets genau nachvollzogen werden. Die Ablagerungen von Murgängen, die zwischen zwei zeitlich aufeinanderfolgenden Luftbildern auftraten, wurden über eine Fläche-Volumen-Beziehung quantifiziert und in eine durchschnittliche Rate (m^3/Jahr) umgerechnet (Aktivität). Die daraus resultierenden Ergebnisse deuten auf einen deutlichen Anstieg der transportierten Sedimentraten von 1947-1952 ($0,23 \pm 0,07\ 10^3 m^3$/Jahr) bis 1987-2000 ($2,41 \pm 0,66\ 10^3 m^3$/Jahr) hin. Darauf folgte von 2000-2010 ein Rückgang auf $1,4 \pm 0,4\ 10^3 m^3$/Jahr. Die Raten nach 1980 sind mehr als dreimal so hoch wie die Raten vor 1980. Ebenso übersteigen die durchschnittlichen Murvolumia seit 1980 auch die holozäne bzw. spätglaziale Rate um den Faktor 2-3, die durch eine elektrische Widerstandstomographie angenähert wurde. Die Daten zeigen zudem einen starken Zusammenhang zwischen der vegetationslosen Fläche eines Einzugsgebiets und der transportierten Sedimentrate. Zwei nahe gelegene Wetterstationen deuten außerdem auf ein verändertes Niederschlagsmuster in den letzten Jahrzehnten hin. Eine höhere

Frequenz von Starkniederschlägen in der Region (Verdoppelung seit den 1920igern) könnte für die erhöhte Murgangaktivität mit verantwortlich sein.

(ii) Um aussagekräftige kontrollierende Faktoren für die Murgangerosion und die damit verbundene Volumenvergrößerung des Murgangs während des Ereignisses zu untersuchen (Syn-Event), wurden in der zweiten Studie die Höhenänderungen in einem Gerinne durch einen Murgang hochauflösend bestimmt (Roßbichelbach, Oberstdorf). Durch das tiefe Einschneiden des Murgangs in das Substrat, das lithologisch überwiegend aus Flysch und quartären Sedimenten besteht, vergrößerte sich das transportierte Volumen deutlich auf dem 1200 Meter langen Fließweg ins Tal. Die Erosions- und Ablagerungsbereiche im Gerinne wurden mit einem terrestrischen Laserscanner kurz nach dem Ereignis erfasst (> 50 Scanpositionen). Das daraus entwickelte Geländemodell wurde mit einem luftgestützten Laserscan von 2007 verglichen. Die berechneten Erosionsraten zeigen z. T. extreme Werte bis 5 m^3/m^2. Insgesamt wurden bei dem Ereignis 9550 ± 1550 m^3 erodiert und 650 ± 150 m^3 im Gerinne abgelagert. Basierend auf Geländedaten wurde ein numerisches Murgangmodell kalibriert. Die daraus resultierenden Fließeigenschaften des Murgangs wurden mit den Höhenänderungen im Gerinne verglichen. Es zeigte sich, dass der Impuls und die basale Scherspannung des Murgangs die Erosionraten im Gerinne am besten erklären (R^2 bis 0,7) und somit die Volumenvergrößerung des Murgangs stark beeinflussen. Überproportional hohe Erosionsraten wurden an Übergängen von steilen Festgesteinspassagen zu Lockergesteinsbereichen festgestellt.

(iii) Im Gegensatz zu den meisten Studien, die oft die Prozesse während eines Murgangereignisses untersuchen, wurde im dritten Manuskript die Sedimentdynamik und die Wiederauffüllung eines Wildbachs mit Sediment aus den Böschungen und aus dem darüber liegenden Einzugsgebiet *nach* einem Ereignis analysiert (Post-Event). Insbesondere in sedimentlimitierten Systemen steuert die Wiederauffüllungsrate sowohl die Murgangaktivität als auch die Menge des transportierten Materials. Dafür wurden zwischen Juni 2015 und Oktober 2018 zehn TLS-Messkampagnen (> 360 Laserscans) und neun zeitlich synchron stattfindende Drohnenbefliegungen (> 7000 Fotos) im Roßbichelgraben (Oberstdorf, Deutschland) auf einer Länge von 400 Metern durchgeführt. Beide Messverfahren, TLS und Fotogrammetrie, ergeben sehr ähnliche Erosions- und Ablagerungsvolumina (Unterschied < 5%). Im Betrachtungszeitraum wurden ca. 1150 m^3 Material im Gerinne abgelagert (≈ 1 m^3/d), wobei eine höhere Aktivität im Sommer als im Winter festgestellt wurde. Die Ergebnisse wurden mit verschiedenen Niederschlagsintensitäten (mm/10 min bis mm/72 h) verglichen, um Zusammenhänge zwischen Niederschlag und Sedimentdynamik zu erforschen. Der neue Ansatz zeigt, dass sich die Sedimentdynamik nach einem Ereignis am besten durch kurze, intensive Niederschläge erklären lässt (R^2 bis 0,9). Ein weiterer Einflussfaktor ist die vergangene Zeit seit dem letzten Murgangereignis, da viele übersteilte Böschungen kurz nach dem Ereignis versagten und sich mit der Zeit stabilisierten.

Diese Arbeit (i) stellt einen der ersten Hinweise für eine (vermutlich) klimabedingte Verdreifachung der Murgangaktivität seit den 1980er Jahren dar. Diese Erhöhung geht mit einer ebenfalls belegbaren erhöhten Frequenz von Starkregenereignissen einher. Die Arbeit zeigt, dass (ii) die basale Scherspannung und der Impuls eines Murgangs aussagekräftige kontrollierende Fließparameter für die Murgangerosion sind. Dadurch wird eine reproduzierbare Vorhersage potenzieller zukünftiger Murgänge ermöglicht. Die Arbeit legt außerdem dar, dass (iii) die Umlagerung von Sediment nach einem Murgang und die Wiederauffüllungsrate stark von kurzen, intensiven Niederschlägen abhängen und dass Fotogrammetrie und terrestrisches Laserscanning äquivalente Resultate liefern. Die Ergebnisse dieser Arbeit tragen zu einer zuverlässigeren Analyse und Beurteilung von Risiken in Murgang-gefährdeten Gebieten in alpinen Regionen bei.

Acknowledgements

The following acknowledgements are by no means a comprehensive attempt to say thanks to everybody who made this thesis a reality. I probably forgot someone important and, thus, I apologise to all the individuals who are not mentioned in the acknowledgements but contributed in variable ways to this thesis. Paper-specific acknowledgements, e.g. concerning editors and reviewers, are given in the respective manuscript sections.

First of all, I would like to thank Prof. Dr. Michael Krautblatter for giving me the opportunity to work in the attractive field of debris-flow research. I strongly appreciate your great supervision in field, office and pub, your constant support and your valuable discussions whenever I came up with questions. Thank you for providing me a PhD position at the Landslide Research Group and thanks for your confidence and patience throughout the last years. These 4 years did not just provide me deeper insights into the research field, but also shaped me as a person. I am very pleased having you as doctoral father.

Another thank goes to Prof. Dr. Kurosch Thuro for encouraging me to get a PhD position at university. Without your support and helpful advices, since the bachelor's program, I would definitely not be at that point where I am now. I thank Prof. Dr. Martin Elsner and Prof. Dr. Andreas Lang for their participation as examiner. I also thank Dr. Andreas Rimböck and Karl Mayer from the Bavarian Environment Agency for setting up interesting projects with us and for your financial support during the last years. I thank my mentor Dr. Bettina Sellmeier for your numerous constructive discussions and ideas. Special thanks are offered to Benjamin Jacobs. Thank you for supporting me whenever I had questions in regard to the processing of point clouds.

Thanks go also to my colleagues Philipp Mamot, Theresa Raab, Sibylle Knapp, Riccardo Scandroglio, Benjamin Jacobs, Johannes Leinauer, Saskia Eppinger and Doris Hermle. I thank you for all the fun we had, for your constructive advices and intense discussions (both thematic and non-thematic) during countless coffee breaks and lunch times in the canteen. I am very pleased to say that the team spirit in this group is outstanding. Furthermore, I would like to thank all my colleagues from the Chair of Engineering Geology for their support. A special thank goes to Georg Stockinger for forcing me to the circuit training twice a week. I also thank Astrid Merling and Stephanie Schaidhammer for all your encouragement during the last years and for providing large quantities of jelly bears, which I often gladly accepted. That really brightened up everyday life.

I also want to thank all my master students for their contributions to this work. Thank you Klaus Keilig for your support in field and for your baking recipes for tasty leavened bread, thank you Verena Stammberger for your time-consuming work on numerical debris-flow modelling and for your delicious cheese noodles. Thank you Lukas Schrettenbrunner and Simon Mitterreiter for your commitment concerning ERT measurements in really nasty terrain.

My greatest thank goes to my wife Maria and my entire family. I want to thank my mum and my dad for your unlimited support during the whole course of study and for your ever-lasting patience. Thanks for everything. I thank my sister Agnes and my brothers, Georg and Johannes, for their help and commitment, e.g. supporting my laser scanning campaigns or being load carrier for diverse things in field. Maria, I thank you for your amazing support during the last years, especially when things did not work as expected. Thank you for making sacrifices to allow me to take and pursue this challenge. Thank you for encouraging me all the time. You are the best!

Thank you all, I am very grateful.

Table of Contents

List of acronyms

ALS: Airborne Laser Scanning

DEM: Digital Elevation Model

DoD: DEM of Difference

DTM: Digital Terrain Model

ERT: Electrical Resistivity Tomography

FIS: Fuzzy Interference System

ICP: Iterative Closest Point

ICSS: In-Channel Stored Sediment

LoD: Limit of Detection

MP: Mega Pixels

MSA: Multi-Station Adjustment

RTK: Real-Time Kinematic

SfM: Structure from Motion

TLS: Terrestrial Laser Scanning

UAV: Unmanned Arial Vehicle

List of figures

List of tables

1 Introduction

The following chapter contains, inter alia, contents of Dietrich and Krautblatter (2017) and Dietrich and Krautblatter (2019), but was significantly revised and extended.

Debris flows are continuously deforming, fast moving mass movements in alpine regions subject to intense rainstorms and mobilisable loose debris (Hungr *et al.*, 2014, Varnes, 1978). Destructive debris flows are documented in the European Alps (Bollschweiler *et al.*, 2007, Hürlimann *et al.*, 2003, Pavlova *et al.*, 2014, Rickenmann and Koschni, 2010, Stoffel, 2010), different sites in North America (Baum and Godt, 2010, Cannon and DeGraff, 2009), in the Andes in South America (Mothes *et al.*, 1998, Sepulveda *et al.*, 2015, Vilimek *et al.*, 2006) or in other earthquake-prone mountainous regions, e.g. China (Ma *et al.*, 2013, Yin *et al.*, 2009), just to name very few examples. From 1950 to 2011 debris flows have caused more than 75,000 fatalities worldwide (Dowling and Santi, 2014). As a consequence, the same questions arise repeatedly for every region: *How frequently* do debris flows occur in an area (*activity?*), *how much* material is transported during an event and *when* is it possible and probable that the next event happens? Although these questions usually cannot be answered in general, authors have investigated variable sources and causes for these problems and have sought novel solution approaches.

Concerning the frequency and activity of debris flows ("*how active?*"), debris-flow fans represent a unique record of past events revealing the long term dynamic of debris-flow activity (Bollschweiler and Stoffel, 2010a, Procter *et al.*, 2011, Schraml *et al.*, 2015a, Stoffel *et al.*, 2008). However, few studies provide deeper insights into reproducible and straightforward methodological approaches to decipher debris-flow activity over longer time scales (Procter *et al.*, 2012), although debris-flow history is a key requirement for sustainable hazard management in endangered areas (Fuchs *et al.*, 2007). Authors have hypothesised that the climate change is a result of the rising global air temperature (Saha *et al.*, 2010), which causes an increasing amount and intensity of precipitation in some parts of the world (Easterling, 2000, Frei and Schar, 1998, Hurrell, 1995). This, again, can be regionally linked to an increase (Evans and Clague, 1994, Frank *et al.*, 2019, Haeberli and Beniston, 1998, Haeberli *et al.*, 1993, Pelfini and Santilli, 2008, Zimmermann *et al.*, 1997) or decrease (Jomelli *et al.*, 2004) in debris-flow frequency and activity. However, reasonable activity trends can only be gained from areas with no sediment limitation in the channels (transport-limited systems). Thus, the above mentioned question concerning the frequency and activity of debris flows is still difficult to answer, especially for a longer period of time.

Besides limited data on fan evolution and activity (*"how active?"*), reasonable and plausible controls on debris-flow erosion and resulting debris-flow volumes (*"how much?"*) are still poorly understood. This questions gets even more challenging, as debris flows can be either initiated by landslide failures (e.g., Gabet and Mudd, 2006, Iverson, 1997) or by a critical runoff in a stream with progressive erosion of the channel bed (Berti *et al.*, 2000, Berti and Simoni, 2005). To estimate resulting potential debris-flow volumes thereof, simplified formula-based approaches use – among other things – the size of the

catchment area (Franzi and Bianco, 2001, Marchi *et al.*, 2019), the angle of the torrent thalweg (Guthrie *et al.*, 2010, Rickenmann, 1995) and lithological factors (Rickenmann and Koschni, 2010). As the explanatory power of these inductively derived formulas is often regionally limited, magnitude-frequency relationships (e.g., Riley *et al.*, 2013, Stoffel, 2010, van Steijn, 1996) and geomorphological field assessment guidelines (Gertsch, 2009, Hungr *et al.*, 1984) have been widely used in literature and practice. However, these methods lack controlling factors, e.g. flow properties, which could be used to predict debris-flow erosion rates on a physical-based approach. Besides, authors have tried to measure these erosion rates directly with different techniques, e.g. photogrammetry (Tsutsui *et al.*, 2007) or airborne and terrestrial laser scanning (Blasone *et al.*, 2015, Bremer and Sass, 2012, Cook, 2017, Perroy *et al.*, 2010, Theule *et al.*, 2015), but they often lack a transition between the methodological application and deeper insights into quantifiable controls on debris-flow erosion. Other studies investigated these controlling factors, but they are often carried out in small laboratory settings and, thus, suffer limited applicability in real-scale prediction models. Studies that combine detection of erosion processes in field with physical flow properties are rare and often investigate only small parts of the flow path (Berger *et al.*, 2011a, Kean *et al.*, 2015, McCoy *et al.*, 2013) or describe this relation for other landslide processes (Schneider *et al.*, 2010). Thus, total volume, runout and impact energies of debris flows are often unknown, guessed or significantly over- or underestimated.

Aside from physical factors controlling erosion, the total debris-flow volume ("*how much?*") and activity (*"how active?"*) strongly depend on the sediment supply in the channel. As the amount of in-channel stored sediment (ICSS) changes temporally and spatially, the susceptibility of the system changes temporally as well (*"when is it possible and probable that the next event happens?"*). To investigate the sediment dynamic over time, different methods have been applied. Scour or fill rates have been derived by field mapping (Glade, 2005) including simplified literature retreat rates, geometric approximations of newly deposited sediments in completely scoured bedrock channels (Jakob *et al.*, 2005) or terrestrial (Goodwin *et al.*, 2017, Staley *et al.*, 2014) and airborne laser scanning (Cavalli *et al.*, 2017). Recently, Structure-from-Motion (SfM) photogrammetry of UAV surveys has gained more and more attention in geomorphology, as this technique is able to produce high-resolution field records in less time and at lower costs compared to other well-established methods (Fonstad *et al.*, 2013, Javemick *et al.*, 2014, Kenner *et al.*, 2014, Westoby *et al.*, 2012). However, driving forces in regard to the recorded changes of ICSS are still poorly understood. The link between climatic factors, e.g. precipitation, and sediment dynamic is not straightforward (Fuller and Marden, 2011). Controls on the seasonal variability of material availability are difficult to decipher (Berger *et al.*, 2011b, Fuller and Marden, 2011) and studies are, if carried out, often limited to small spatial extents (Bezak *et al.*, 2017, Theule *et al.*, 2015). Though, data and knowledge in relation to controlling factors for sediment dynamics in channels and their refill with material are substantial, as the ICSS is a key control on debris-flow activity and volume (Hungr *et al.*, 2005, Hungr *et al.*, 1984) and, thus, influences runout and impact energies.

The aims and objectives of this thesis (Figure 1) are (i) to contribute to a scientific, controversial discussion concerning debris-flow activity in alpine regions in times of climate change (① pre-depositional), (ii) to reveal meaningful factors controlling debris-flow erosion (② syn-depositional), and (iii) to decipher post-event sediment dynamic and its controls (③ post-depositional). The key findings of this thesis have broader implications for the temporally variable activity of debris flows, for debris-flow modelling and hazard assessment in alpine regions. Objectives (i)-(iii) are individually presented in the following Chapter 2.

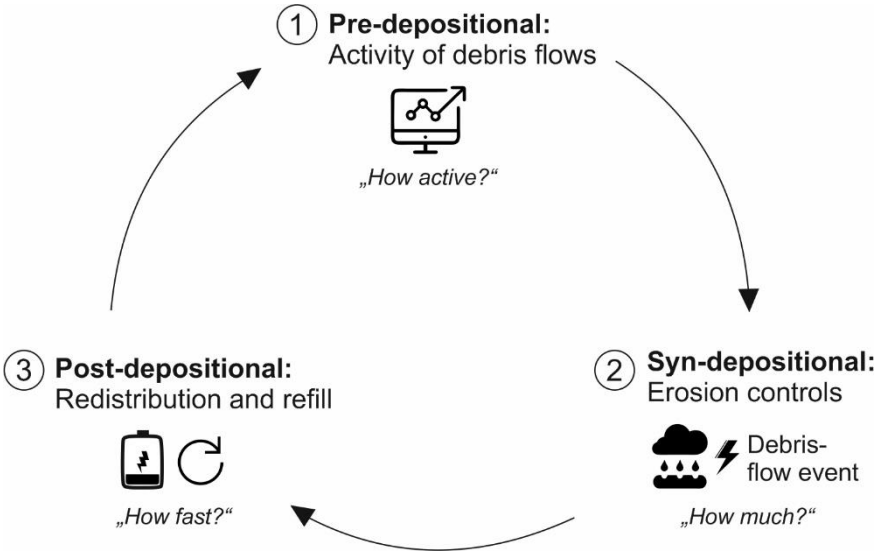

Figure 1: The three objectives and their relations covered in this thesis: ①: Pre-depositional – before a debris-flow event: Is an area prone to debris flows? How frequently do debris flows occur in a given area and which sediment volumes do they transport? ②: Syn-depositional – during an event: Which parameters control debris-flow erosion? ③: Post-depositional – after an event: How does a scoured channel and adjacent slopes react subsequent to a debris-flow event? How fast is a channel refilled with material?

2 Motivation and research gap

Why did I work exactly on the three topics shown in Figure 1 and the aims presented in the following Chapters 2.1, 2.2 and 2.3? On the one hand, the trinity is provoked by a scientific need and a research gap regarding these three specific topics. We have limited data to decipher the activity of debris flows in times of climate change. We have limited data on controlling physical properties of a flow to explain erosion and entrainment of material during an event. And we have limited data to make general statements regarding sediment recharge in channels. On the other hand, the trinity is provoked – to be honest – by chance. Just one month after I had joined the TUM Landslide Research Group, a debris flow occurred not far from the city where I was born. In addition, one of my master students had relatives, who had to be evacuated due to the event. Fortunately, these three topics have strong thematic relations to each other, because they are mutually dependent. The three topics are presented individually in the following subchapters.

2.1 Pre-depositional: Debris-flow activity in the last decades in the Northern Alps

2.1.1 Problem and background

In the past decades records of the fire department of Breitenwang, Austria, show repeatedly operations at the Plansee Lake due to debris-flow events. These debris flows often blocked a road (L255), which goes along the north side of the lake (Figure 2). First records reach back to the year 1851, in which King Maximilian II of Bavaria instructed to build a road at the north side of the Plansee Lake. The road was destroyed in the same year by a natural event, presumably a debris flow (Innsbrucker Zeitung, 1852). Other examples for documented events happened in 1929 (Außerferner Bote, 1929) or more recently in 2010 (Feuerwehr Breitenwang, 2010) and 2012 (Scheucher and Rudigier, 2012). Unfortunately, debris-flow events were just recorded, if economical goods were damaged or human lives were threatened. Thus, newspapers and magazines do not give detailed information about the debris-flow activity and frequency of events in that area, although more events were recorded in recent decades. In literature authors hypothesise an increase in activity and frequency of gravitational mass movements as a result of climate change (Beniston and Douglas, 1996, Evans and Clague, 1994, Haeberli and Beniston, 1998, Pelfini and Santilli, 2008). In contrast, other authors show that the rising temperature affects, regarding debris-flow activity, only higher located areas above the permafrost boarder line (Jomelli *et al.*, 2004).

2.1.2 Aims and key questions

Considering the background and problems mentioned in Chapter 2.1.1, the following questions arise:

1. How can we reveal debris-flow activity for a longer period of time?
2. How did mean annual debris-flow transport change in the last decades and can we compare these rates to mean Holocene/Lateglacial debris-flow transport rates?
3. Can we link debris-flow activity with rainstorm frequency?

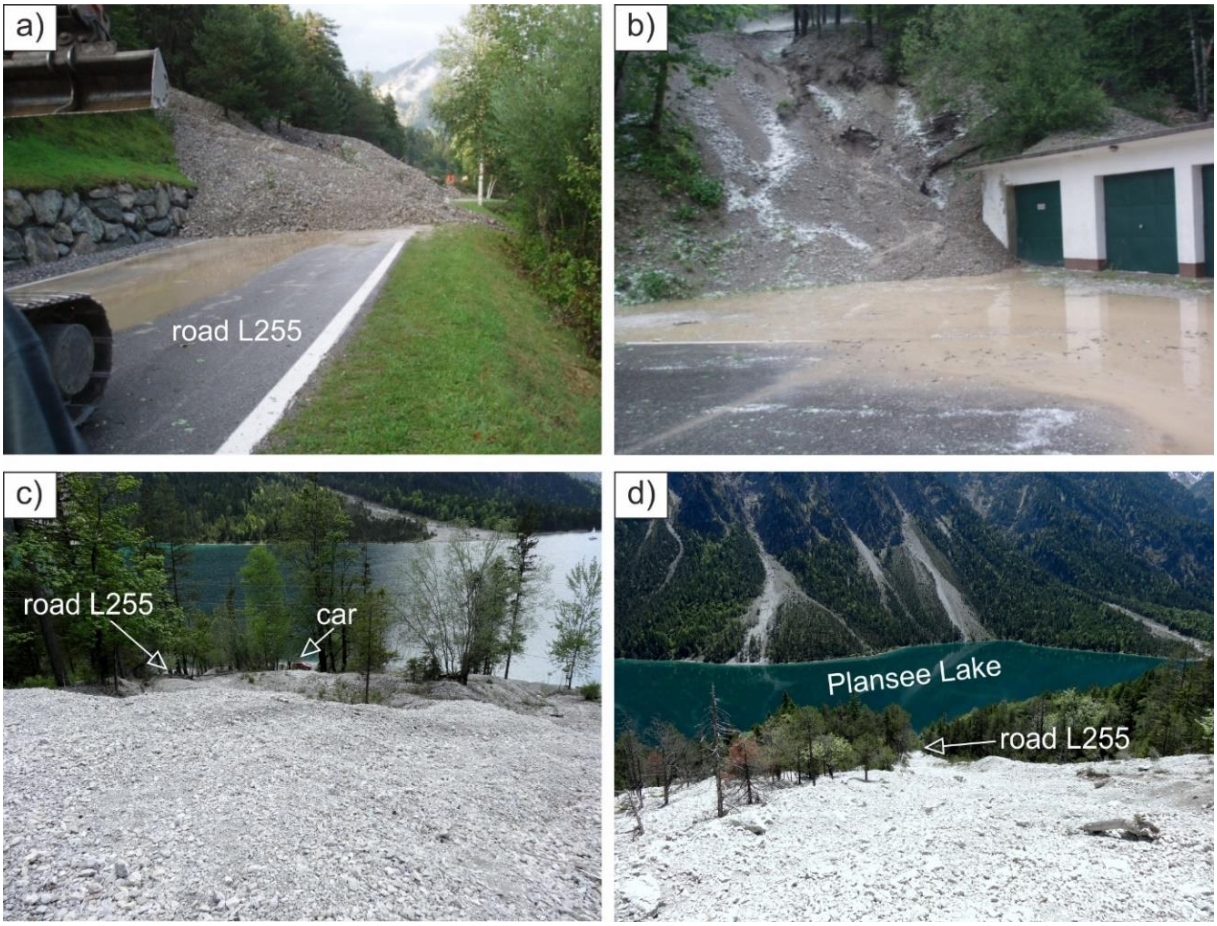

Figure 2: a) and b): Debris flows at the north side of the Plansee Lake on 4th of July 2012. With kind permission of Feuerwehr Breitenwang (2012). c) and d): Photos taken during field work in summer 2014.

The site at the Plansee Lake was chosen as (i) complete debris-flow fans can be studied, (ii) the system is transport-limited (large amounts of dolomite debris in the channels and catchments available) and (iii) daily precipitation values exist since 1921.

2.2 Syn-depositional: Meaningful control factors for debris-flow erosion

2.2.1 Problem and background

In June 2015, a debris-flow event occurred in Oberstdorf, Germany (Figure 3). The debris flow caused costs of several millions of Euros and hundreds of people had to be evacuated (Mayer, 2015). Except from minor landslides, initiated by intense rainfall (Figure 3b), the transported debris-flow material originated mainly from channel-bed erosion (Figure 3c-d). The volumetric growth of a debris flow by material entrainment can frequently be observed in nature (Berti and Simoni, 2005). However, the volume of the debris flow affects runout distances and impact pressures significantly. Consequently, previous research has focused on different approaches to anticipate potential debris-flow magnitudes. Dong *et al.* (2009) used simple empirical formulas to predict debris-flow volumes, while others applied more sophisticated methods, such as magnitude-frequency relationships (Riley *et al.*, 2013, Stoffel, 2010) or geomorphological field assessment guidelines (Gertsch, 2009). Although their research contains novel data and advanced methods, their approaches partially lack physical justification, are

limited by subjective application or lack data for a meaningful statistical analysis. Physical-based approaches are rare and are – if applied – limited to laboratory settings or small-scale test sites.

2.2.2 Aims and key questions

Considering the background and problems mentioned in Chapter 2.2.1, the following questions arise:

1. How can we estimate potential future debris-flow volumes more reliably compared to other recent approaches?
2. How can we precisely quantify erosion rates of recent debris flows?
3. Which influence does lithology have on these erosion rates?
4. Can we relate these erosion rates to physical flow properties of a debris flow?

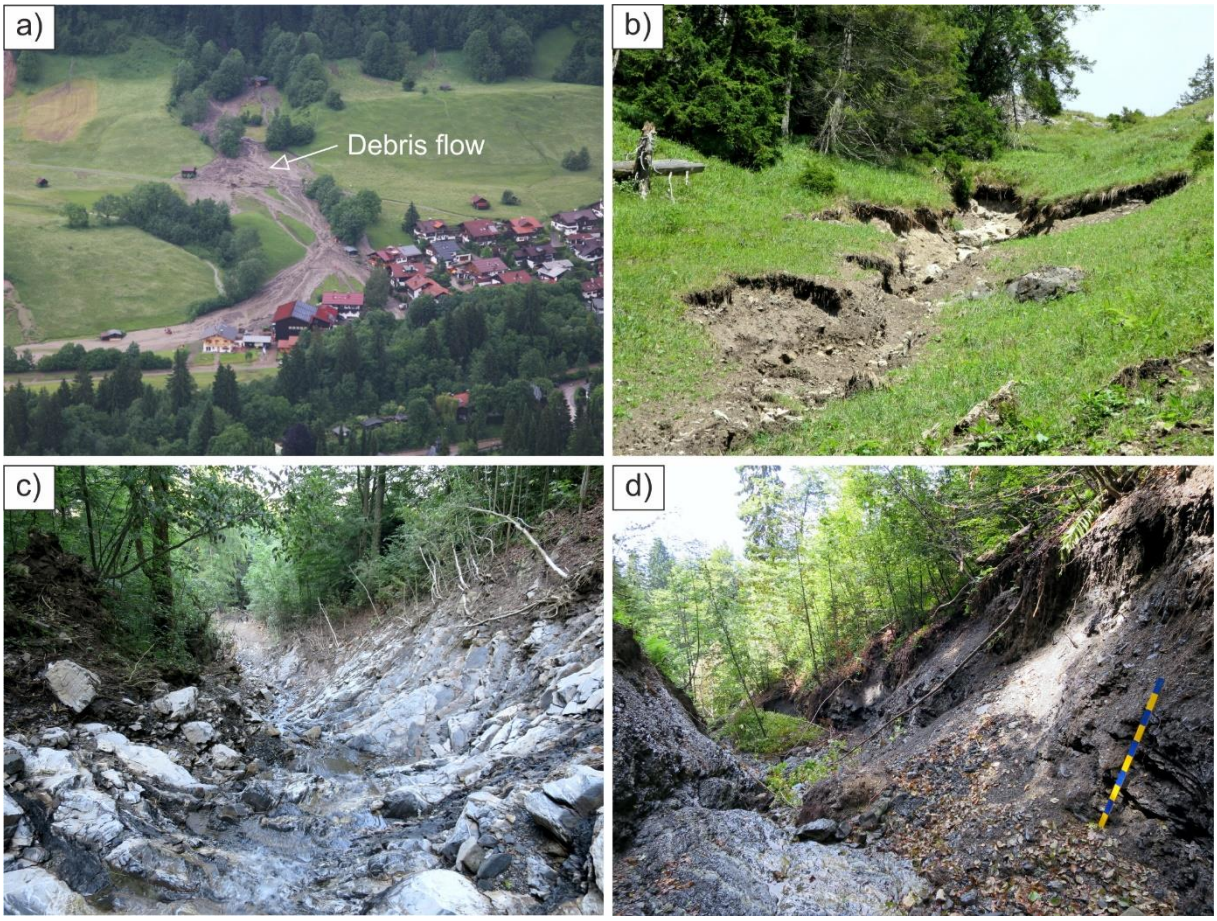

Figure 3: a): Police helicopter picture of the debris-flow extent in Oberstdorf (Germany) in June 2015. With kind permission of the police headquarter Swabia South/West, Oberstdorf. b): Most upper parts of the Roßbichelgraben torrent show landslide features. c) and d): Scoured channel bed. Scale in d) is 1 m. b)-d) Photos taken during field work in summer 2015.

The study site at the Roßbichelbach (Figure 3) was chosen, as (i) the study site is accessible from top to bottom and (ii) the height difference, induced by the debris-flow event, can be measured by means of a pre-event and a post-event DEM. In contrast to 2.1, the studied system is – in parts – sediment limited, as the incision into the substrate reaches bedrock (Figure 3c).

2.3 Post-depositional: Monitoring of post debris-flow sediment redistribution

2.3.1 Problem and background

On the same date, when the event mentioned in Chapter 2.2.1 occurred, another debris flow was observed in an adjacent torrent (Figure 4). Luckily, no buildings were destroyed, as the debris flow left the channel bed and stopped in a meadow before it reached inhabited areas. However, potential future debris flows will not necessarily leave the channel bed and may hit the city downstream. To know, whether a similar event could happen in future, it is substantial to estimate potential erodible sediment volumes in the channel (Figure 4d-e). Consequently, different approaches and methods have been applied in previous studies to investigate channel scour and fill including total stations surveys (Theule *et al.*, 2012), terrestrial laser scanning (Blasone *et al.*, 2015, Staley *et al.*, 2014, Theule *et al.*, 2015), airborne laser scanning (Cavalli *et al.*, 2017) or UAV surveys using RTK-GNSS ground control points (Fonstad *et al.*, 2013, Javemick *et al.*, 2014, Kenner *et al.*, 2014). Some of these studies provide simplified fixed (Glade, 2005) or more sophisticated recharge rates (Jakob *et al.*, 2005) over time and area and are often – when using high areal and temporal resolution methods – limited to small study sites (Bezak *et al.*, 2017, Theule *et al.*, 2015) or are not performed directly after debris-flow events. In addition, explicit controls – such as rainfall intensity – on geomorphic changes and their annual and seasonal variability are still not well understood (Berger *et al.*, 2011b, Fuller and Marden, 2011).

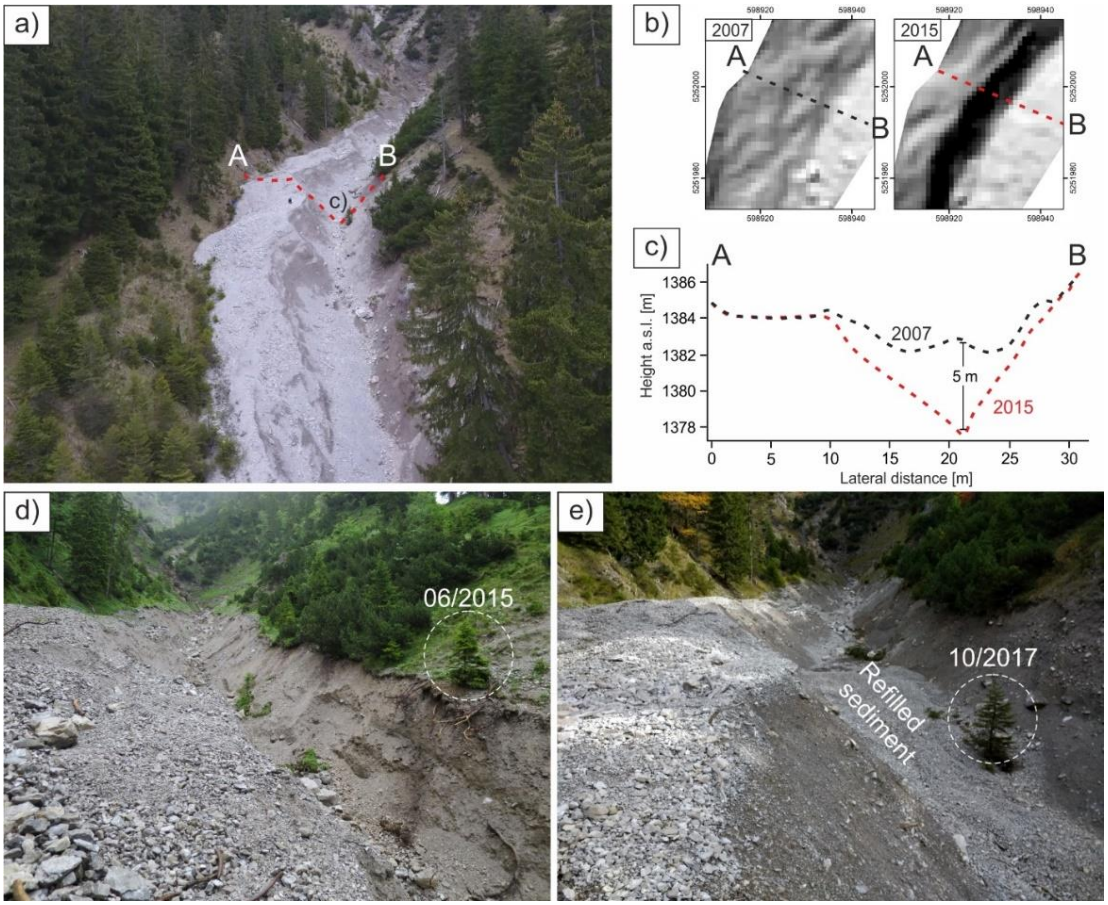

Figure 4: a) UAV photograph of the Roßbichelgraben torrent after the debris-flow event in June 2015. b) Top view of an area showing debris-flow incision. The torrent was evenly filled up with sediments prior to the event. c) Comparison of profiles prior to the event (black dashed line) and after the event (red dashed line). Highest elevation changes reach more than 5 m.

2.3.2 Aims and key questions

Considering the background and problems mentioned in Chapter 2.3.1, the following questions arise:

1. How can we reveal the post debris-flow sediment redistribution and the channel refill shortly after an event with high temporal and areal resolution?
2. Can we link the sediment redistribution to temporal and meteorological controls?

The study site at the Roßbichelgraben (Figure 4) was chosen as (i) measurements could be carried out straight after the debris-flow event in June 2015, (ii) the study site is easy accessible and (iii) the sediment production in this lithology is relatively high (transport-limited system) and, thus, can be measured in a short period of time.

2.4 Thesis organisation

This thesis is organised into 8 Chapters. Chapters 1 and 2 introduce the problem, research gaps and objectives of the thesis. Chapter 3 seeks to present the state of the art in debris-flow research related to the topic of this thesis and the applied methods in both collecting field data and their processing. Chapters 4 to 6 are stand-alone contributions related to each research gap presented in Chapter 2. The presented approaches in Chapter 4 give a straightforward guidance to analyse the activity of debris flows over a larger period of time (Figure 1 → ① pre-depositional). The methodology presented in Chapter 5 provides a strategy to reveal meaningful controlling factors for debris-flow erosion processes (Figure 1 → ② syn-depositional). Chapter 6 seeks to decipher the sediment dynamic and channel refill with material after an event (Figure 1 → ③ post-depositional). In Chapter 7 the main findings of Chapters 4 to 6 are briefly synthesised and discussed in a broader context. Chapter 8 gives a short outlook on future developments and research objectives.

3 State of the art

3.1 Debris-flow definition

A variety of terms and definitions can be found in literature, which try to characterise debris flows as a type of gravitational mass movement (Costa and Wieczorek, 1987, Crozier, 1986, Hungr *et al.*, 2014, Hutchinson, 1968, Johnson and Rodine, 1984, Stiny, 1910, Zaruba and Mencl, 1982). In this thesis the term "debris flow" refers to the definition of Hungr *et al.* (2014), which is an updated version of the Varnes (1978) classification:

"Debris flow: Very rapid to extremely rapid surging flow of saturated debris in a steep channel. Strong entrainment of material and water from the flow path." (Hungr *et al.*, 2014)

Some of the terms in this definition need clarification:

For a simplified field description the term "**debris**" means unsorted and mixed sand, gravel, cobbles, boulders and a varying content of silt and clay with, crucially, low plasticity (Hungr *et al.*, 2014). In contrast, "mud" may also have coarse components, but has a significantly higher silt and clay content to produce plasticity and cohesiveness (Table 1). Thus, the corresponding soil classes for "mud" contains often low plastic clays (CL) or high plastic clays (CH), while "debris" usually corresponds to coarse grained soils from clayey sand (SC) to well graded gravel (GW) (Table 1).

Table 1: Distinction of the terms "mud" and "debris". Modified from Hungr *et al.* (2014).

Material name	*Simplified field description*	*Laboratory indices (if available)*
Mud	Plastic, unsorted and close to liquid limit, often fine-grained	Placiticity Index > 0.05 Liquidity Index > 0.5
Debris	Low plasticity, unsorted and mixed, often coarse-grained	Placiticity Index < 0.05

"**Very rapid to extremely rapid**" means that the flowing mass reaches velocities of several metres per second, which corresponds to velocity classes 6 and 7 in the Cruden and Varnes (1996) classification (Table 2).

The occurrence of debris flows is limited to "**steep channels",** mainly first-order or second-order drainage systems. The minimum slope angle to initiate debris flows in these channels is not exactly specified in Hungr *et al.* (2014), but the values of other authors range from 23% to 65% (13°-33°) (D'Agostino, 2013, Spreafico *et al.*, 1996, Takahashi, 2009).

The rapid moving sediment mass causes an undrained loading of the channel bed. This results in "**strong entrainment"** of channel-bed material, as the pore water pressure increases significantly due to un-drained loading. Thus, debris-flow volumes can increase by orders of magnitudes during an event (Reid *et al.*, 2016).

Table 2: Velocity classes for landslides. Modified from Cruden and Varnes (1996).

Velocity class	Description	Velocity (mm/s)	Typical velocity
7	Extremely rapid	$5 \cdot 10^{3}$	5 m/s
6	Very rapid	$5 \cdot 10^{1}$	3 m/min
5	Rapid	$5 \cdot 10^{-1}$	1.8 m/hr
4	Moderate	$5 \cdot 10^{-3}$	13 m/month
3	Slow	$5 \cdot 10^{-5}$	1.6 m/year
2	Very slow	$5 \cdot 10^{-7}$	16 mm/year
1	Extremely slow		

3.2 Debris-flow processes and mechanics

3.2.1 Preconditioning factors for debris flows

As mentioned in the previous section, the occurrence of debris flows is limited to specific locations. Thus, the susceptibility of a system to debris flows is influenced by factors that hardly change over long periods of time (Figure 5), such as topography. However, other factors that influence susceptibility show strong temporal (and spatial) dependencies (Figure 5). On the one hand, the time-independent basic susceptibility, which does not significantly change in hundreds and thousands of years, consists of factors like type of lithology in an area, exposition, steep torrents and a high relief (Kaitna *et al.*, 2013):

- *Lithology*

  The lithological setting in an area only changes in very large time scales (which would usually coincidently lead to a change in surface topography). The lithology controls material properties, such as the angle of friction and cohesive properties, which both strongly influence the mobility and runout of debris flows (Christen *et al.*, 2010, Frank *et al.*, 2017). Additionally, the production of scree and loose debris (sediment supply), caused by weathering, depends on lithological material and rock mass properties in the catchment area (Krautblatter and Dikau, 2007).

- *Exposition*

  Authors showed that the exposition of a catchment area influences rates of rockwall retreat. North-exposed rock faces have significantly higher frost-shattering rate compared to south-exposed sites (Sass, 2005a). Hence, the exposition of has an impact on the sediment supply.

- *High relief and steep torrents*

  Steep torrents increase the long-term susceptibility in a mountainous region. A slope angle of at least 23% is needed to initiate debris flows (D'Agostino, 2013, Takahashi, 2009). High slope angles in the catchment enhance material transport into the debris-flow channel.

These factors lead to a continuously low, medium or high susceptibility (Figure 5). On the other hand, the presence and type of vegetation, type of land use, current season, the existence of loose debris and intensity and amount of pre-event precipitation cause a highly temporally variable susceptibility to debris-flow events (Figure 5). Consequently, the same event power, e.g. rainfall in a specific period of time, may once lead to a debris flow and once not, depending on the respective current total susceptibility of the system at each time.

- *Presence and type of vegetation; type of land use*

  The absence of vegetation in a catchment area significantly enhances material erosion and transport into the debris-flow channel and, thus, can increase debris-flow activity in a catchment (Dietrich and Krautblatter, 2017). In wildfire-affected areas, debris flows are triggered at significantly lower thresholds compared to non-burned areas (Cannon *et al.*, 2008).
- *Current season and amount of pre-event precipitation*

  The amount and intensity of rainfall is not equally distributed during a year. In the Northern Alps a pronounced summer precipitation with increased rainstorm frequencies can be observed, compared to spring, autumn and winter. Pre-event rainfalls saturate soils and increase pore-water pressures, leading to a lowered triggering threshold to initiate debris flows (Kaitna *et al.*, 2013). In addition, the season affects the sediment production, as the rate of rockwall retreat is influenced by e.g. freeze-thaw cycles in spring (Sass, 2005b).
- *Presence of mobilisable loose debris*

  Some of the above mentioned factors lead to a variable availability of mobilisable loose debris. Besides, glaciers can influence the presence of debris over longer time scales, as they are able to transport and deposit large amounts of sediments at specific locations. The thawing permafrost and the continuing glacier retreat in higher altitudes release formerly ice-covered or frozen sediments and lead to oversteepened slopes (Lugon and Stoffel, 2010). The increased availability of mobilisable debris increases the susceptibility (Figure 5).

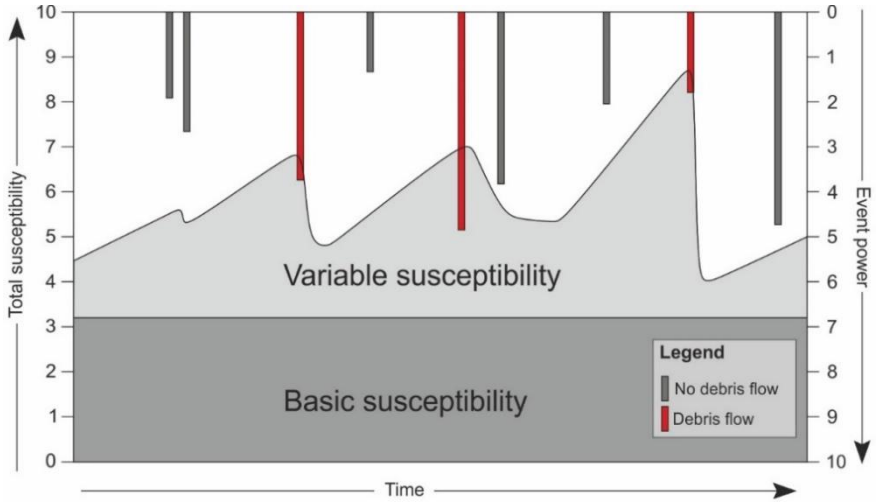

Figure 5: The total susceptibility consists of a basic and a variable susceptibility. The event power (e.g. of a heavy rainfall event) is proportional to the length of the bars from top to bottom. Grey bars mean no debris-flow event, red bars represent debris-flow events. Adapted from Zimmermann *et al.* (1997).

3.2.2 Triggering factors and debris-flow initiation

Debris flows are initiated by mainly two different mechanisms: (i) Progressive transition of a landslide into a debris flow and (ii) generalised erosion and instability of the stream bed (Coussot and Meunier, 1996, Hungr *et al.*, 2014). Both initiation mechanisms, described more precisely later, are almost always triggered, in tectonically less active regions, by (heavy) rainfall events in a given time span. A simultaneously occurring snow melt additionally increases water supply (Coussot and Meunier, 1996, Palacios *et al.*, 1998). General triggers for landslides, e.g. earth quakes in tectonically active counties (Fu *et al.*, 2009, Keefer, 2002, Ma *et al.*, 2013), can be studied in Brunsden and Prior (1984) and Iverson (2000) and are not further discussed in this thesis.

In literature, authors often suggest thresholds for shallow landslides and debris flows (often not clearly distinguished) by introducing a relationship between rainfall intensity and duration (Figure 6). The minimum power (threshold) of a trigger, which is needed to cause a debris flow, varies with the present total susceptibility in the study area (Figure 5).

Caine (1980) was one of the first researches, who described a limiting curve for the minimum intensity of a rainfall in a given time span (10 minutes to 10 days), which potentially initiates a debris flow. The large scatter in this relationship (Figure 6) originates of the variable total susceptibility of the investigated study areas. Other authors updated this rainfall intensity-duration relationship (Guzzetti *et al.*, 2008) and established regional thresholds (Gregoretti and Dalla Fontana, 2007, Staley *et al.*, 2013, Tiranti and Rabuffetti, 2010, Wieczorek and Glade, 2005). However, all rainfall data were measured at the spatially next raingauge, which is often kilometres away from the debris-flow initiation zone. Thus, a large uncertainty in the intensity data is present (Nikolopoulos *et al.*, 2014), as thunderstorms often are locally limited. Besides, Brayshaw and Hassan (2009) suggest that a threshold should be also based on the sediment recharge rate and the time since the last debris flow in a channel. Contrary to other studies (Glade, 2005, Kaitna *et al.*, 2013, Zimmermann *et al.*, 1997), they suggest that each debris flow resets the threshold to a lower value. Thus, a low volume of ICSS is related to a lower intensity-duration threshold for debris-flow initiation (Brayshaw and Hassan, 2009).

The specific process, to get large amounts of material in suspension, depends on the above mentioned initiation mechanisms:

- Sudden increase in pore water pressure and liquefaction of sediments (Figure 7). This increase in pore water pressure can either originate from a landslide failure (Figure 8) with a following impact on the water-saturated channel bed, resulting in an undrained loading (Brayshaw and Hassan, 2009, Gabet and Mudd, 2006, Iverson *et al.*, 1997, Malet *et al.*, 2005, Sassa *et al.*, 2007) or from more rare types like dam breaks (Takahashi, 1981) or ice avalanches (Plafker *et al.*, 1971). The undrained loading causes a destruction of the granular skeleton and thus liquefies the mass.

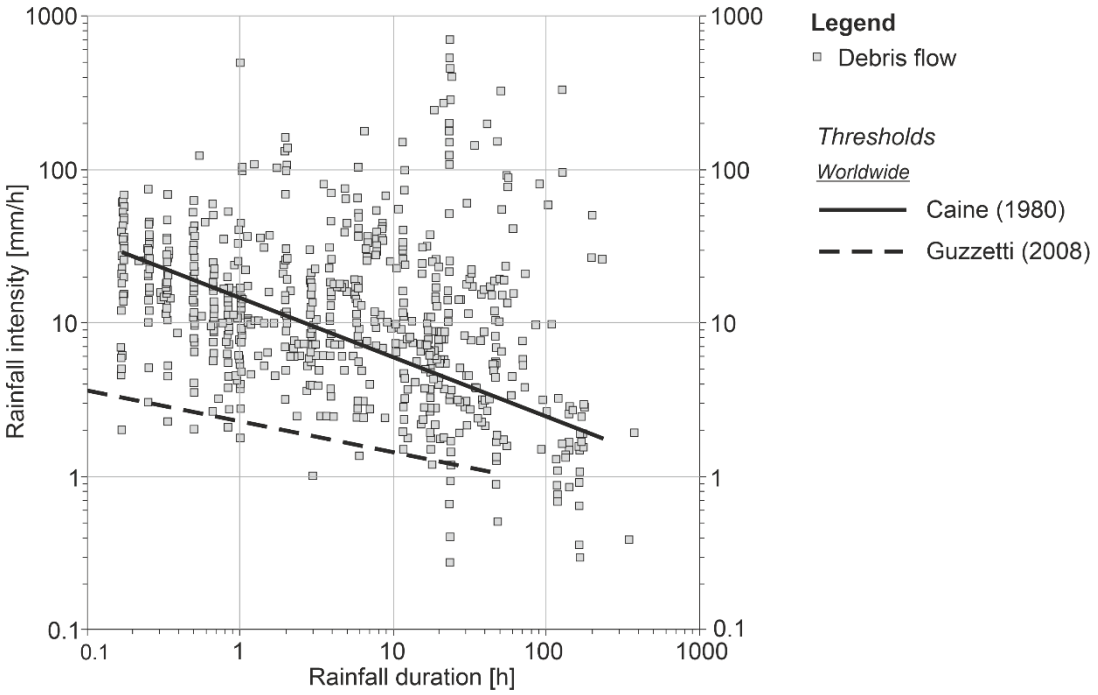

Figure 6: Intensity-duration relationships for the initiation of debris flows. Adapted from Guzzetti *et al.* (2008).

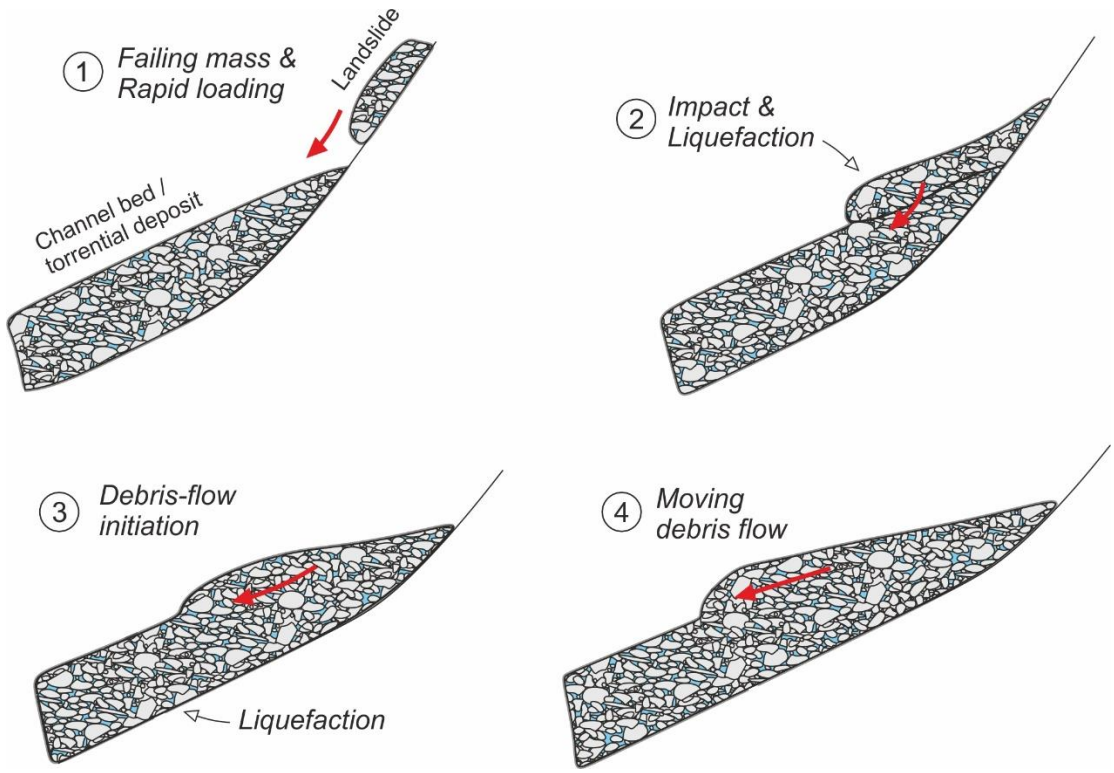

Figure 7: Landslide failure (1) with following impact on the water-saturated channel bed (2) results in an undrained loading and initiates a debris flow (3), (4). Adapted from Sassa *et al.* (2007).

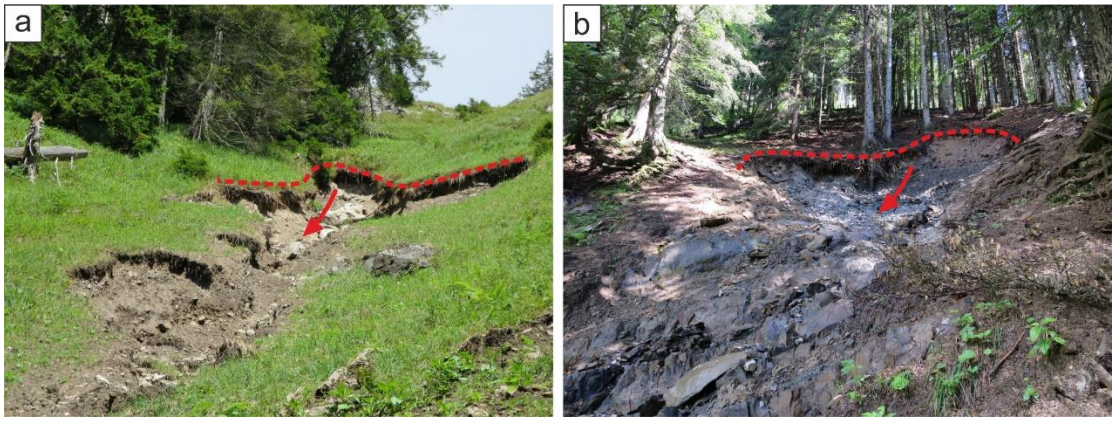

Figure 8: Slides as potential initiation mechanisms.

- Successive erosion and instability of the stream bed (Figure 9 and Figure 10). The successive erosion causes a step-by-step growth of the transported sediment volume (Coe *et al.*, 2008, Kean *et al.*, 2013, Legg *et al.*, 2014). Example: Surficial water (depth h) flows on top of a saturated, cohesionless granular debris layer on an inclined slope (angle θ). The lower limit of layer a is the intersection of the shear stress and resisting stress line. Layer a will become unstable when the following simplified equation is satisfied (Takahashi, 2009):

Equation 1:

$$\tan\theta \geq \left\{\frac{C_*(\sigma-\rho)}{C_*(\sigma-\rho)+\rho(1+\frac{h}{a})}\right\}\tan\varphi$$

C_* is the volumetric grain concentration, σ is the density of the grains, ρ the density of the fluid, φ is the internal friction angle of the material. The gravitational flow of layer a leads to an increase in the density of the fluid and in a shear stress acting on the static bed, which results in a self-enforcing process. Further mathematical model descriptions are given in Takahashi (2009) and Kean *et al.* (2013).

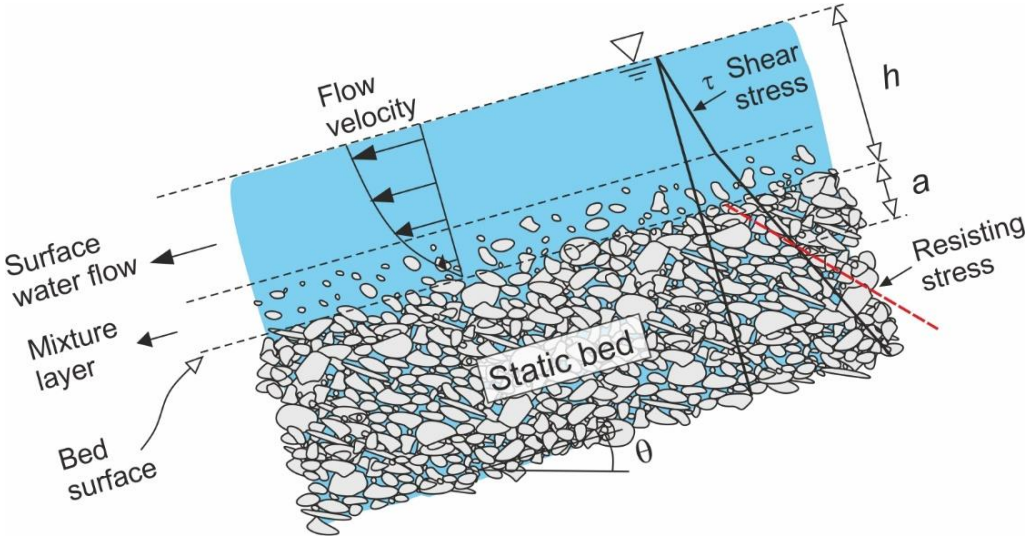

Figure 9: Stress distributions and successive erosion and instability of a stream bed under the effects of surficial water flow. Simplified stresses are assumed to increase linearly with depth and density. Adapted from Takahashi (2009).

3.2.3 Debris-flow acceleration and material erosion

Once a debris flow has been initiated by one of the above explained mechanisms, the flowing mass accelerates and decelerates depending on the present topography and lithology. During transport, the components of the flowing mass (water, debris, organic matter and air) interact with the substrate, which is normally the channel bed or the debris fan (Figure 10a-b). These shear stresses induce an acceleration of the upper most layer of the erodible bed (e.g. debris). Due to particle collisions, material is released from the substrate and gets entrained in the flowing mass (Figure 10c). Analogue forces and stresses act on banks and slopes of the channel. The erosion and entrainment of ICSS can reach up to several metres in depth (Figure 11). Dependent on the lithology, the bedrock can be exposed and prevent a deeper incision (Figure 11a).

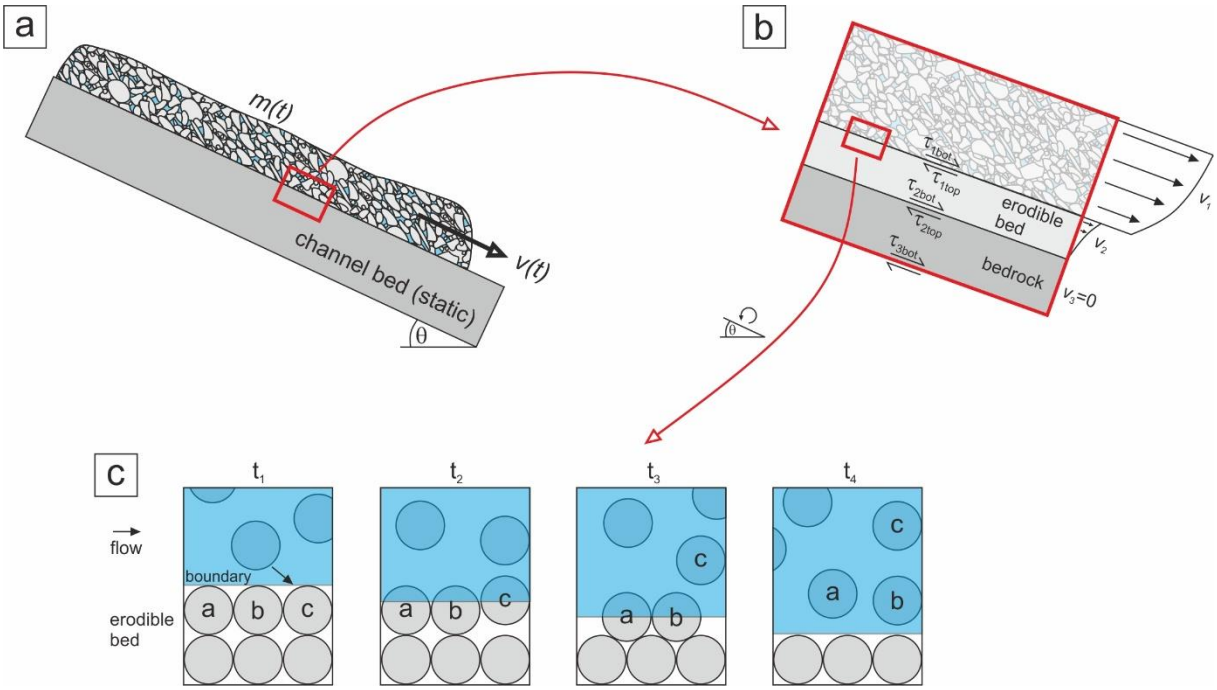

Figure 10: Simplified sketch for material erosion and entrainment at the bottom of the debris flow. a) Flowing mass on an inclined plane. b) Velocity profiles of the flow and erodible beds in a simplified 3-layer model with acting shear stresses. c) Grain-scale sketch for particle entrainment. Adapted from Iverson and Ouyang (2015) and Iverson (2012).

When the material is transported its pathway downstream and the debris flow grows in magnitude by erosional processes, it may leave the channel at some locations. Trees, which get hit by the flowing mass, suffer shear and normal stresses acting on the stem, which leads to a removal of the bark (Figure 12a-c). Hence, after an event, the maximum flow height can be reconstructed by investigating hit trees near and in the channel. Additionally, some of the stems get partly buried with sediments (Figure 12a). As a consequence, researchers use this information in dendrochronology to date debris flows and to determine their extents (Bollschweiler *et al.*, 2007, D'Agostino, 2013, Stoffel, 2010, Stoffel *et al.*, 2008).

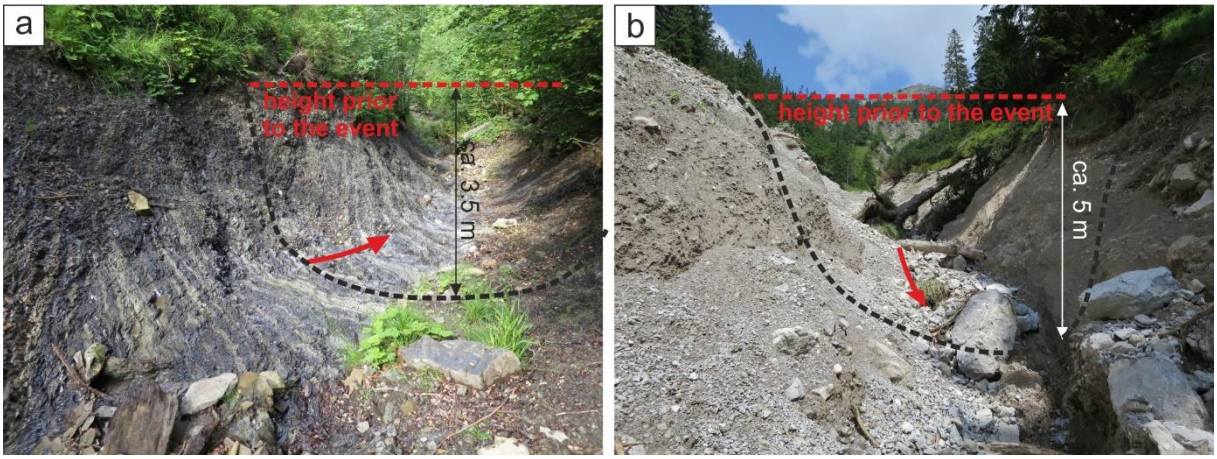

Figure 11: Steeply incised channels as a result of material erosion and entrainment. a) Bedrock prevented deeper erosion. b) Channel bed consists still of lose debris and boulders after an event.

This allows to estimate the magnitude and frequency of former debris flows, which helps to analyse and assess hazard and risk in threatened areas (Mayer *et al.*, 2010, Saez *et al.*, 2011). Apart from the bark removal, complete trees can be destroyed, snapped off and fall into the channel. These trees or parts of these trees can be transported over long distances and increase the risks through log jams. Nevertheless, most of the eroded and transported material consists of loose debris. To derive controlling factors for these erosion processes, two data sets have to be available: (i) High-resolution data deciphering erosion and deposition volumes induced by a recent debris-flow event and (ii) information about physical flow properties on the pathway, or similar, to which these erosion and entrainment volumes can be linked. Regarding (i), erosion and deposition volumes of debris flows have been revealed by using pre- and post-event data sets. For this purpose, LiDAR and photogrammetry (Tsutsui *et al.*, 2007, Veyrat-Charvillon and Memier, 2006) are key techniques to acquire high-resolution data sets. Due to the oblique line of sight, TLS (Perroy *et al.*, 2010, Theule *et al.*, 2015) is less often used than ALS (Bremer and Sass, 2012, Cavalli *et al.*, 2017, Scheidl *et al.*, 2008) except for densely vegetated areas. Although these data sets provide insights into spatial information, regarding debris-flow erosion and deposition, authors relate this information rarely to meaningful controlling factors. Only few researchers gathered data on physical flow properties in spatially limited sections, as continuous measurements of debris-flow properties are not available. These data sets include ground-vibration measurements with geophones (Kean *et al.*, 2015), pressure fluctuations (e.g., Berger *et al.*, 2011a, McArdell, 2016), pore fluid pressures and normal forces to decipher erosion induced by debris flows (McCoy *et al.*, 2010, McCoy *et al.*, 2013). Thus, most published literature deals with theoretical ideas and assumptions concerning material entrainment (Iverson, 2012, Iverson and Ouyang, 2015, Iverson *et al.*, 2010). First rough implementations in numerical simulation software consider user-defined erosion layers (e.g., Begueria *et al.*, 2009, Hussin *et al.*, 2012), flow velocity (Takahashi *et al.*, 1992) or shear stresses (Chen and Zhang, 2015, Frank *et al.*, 2015), but the suggested approaches are, if at all, sparsely validated by real events. For a mathematical description of material entrainment I refer to Iverson and Ouyang (2015).

The erosion is typically described as a growth in volume per reference unit. This reference unit is often represented by a normalisation of the erosion volume to an area [m³/m²] (Dietrich and Krautblatter, 2019, Reid *et al.*, 2016), or to the flow path [m³/m] (Gertsch, 2009, Hungr *et al.*, 1984). This value can also be seen as a kind of rate, as the growth in volume applies to the length of the event (minutes). However, this time component does not show up in the reference unit, as the erosion is determined by one specific short-lived event and not by long-lasting processes over years or decades.

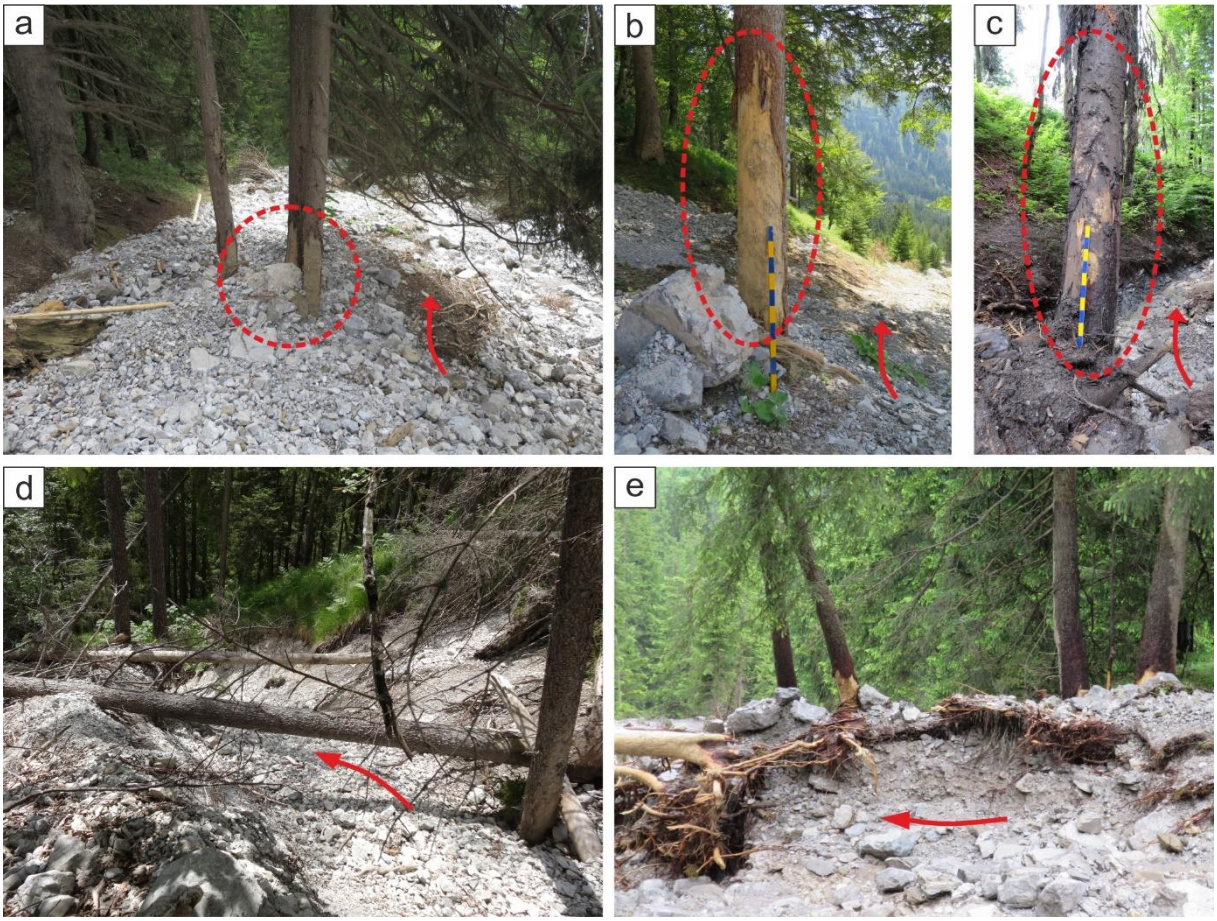

Figure 12: Debris-flow characteristics in field. a-c: Destroyed and torn down trees and roots. d-e: Flow marks at trees. The bark has been removed.

3.2.4 Depositional characteristics

During the movement downstream, some of the transported material can be heaped at one or both sides of the channel and build lateral levees (Figure 13a-b). Figure 13c shows a mathematical description of a levee. Using the curve radius of the channel (r_b), the slope of the channel (β), the slope angle between both sides of the levee (δ_b) and the gravitational acceleration (g), the velocity (v) of the debris flow can be estimated by a formula of Costa (1984):

Equation 2:

$$v = \sqrt{g \cdot r_b \cdot cos\beta \cdot tan\delta_b}$$

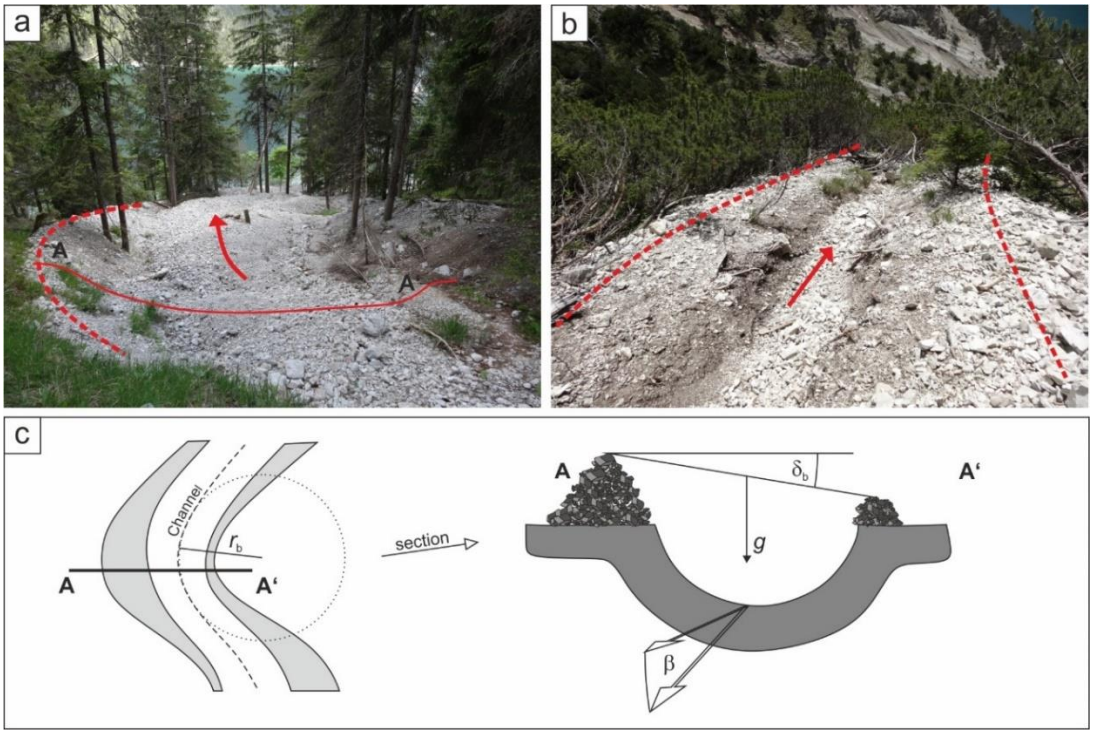

Figure 13: a-b: Field evidences for lateral levees. c: Mathematical description of levees in order to estimate the velocity. Adapted from Johnson and Rodine (1984).

Debris flows have a relatively high viscosity and the materials in the flowing mass are highly mixed and sheared. Due to the turbulent manner and the high density of the flow, even large boulders may undergo buoyancy and can be uplifted to the top of the flow (Figure 14).

Thus, deposits usually show no or negligible grain sieving (Costa, 1984, Friedman *et al.*, 1992). Nevertheless, some authors emphasise that large boulders often accumulate at the debris-flow front during transportation (Pierson, 1986). The grain size distribution of the deposits varies depending on the respective lithological setting. In debris-flow deposits of clay-rich Flysch turbidites, the sediment components are often smaller than in deposits of dolomites or limestone-formations (Figure 15c-d). Generally, the material is often deposited on well-established debris fans or debris cones with a typical debris-flow head (Figure 15a-b). The transition from a steep channel to a debris fan causes a loss of confinement and often co-occurs with a reduction of the slope angle (Hungr, 2005). This leads to a sudden decrease in pore-water pressure and water content. Other debris-flow characteristics are steep incisions into the channel-bed substrate (Figure 11) and destroyed or flow-marked trees (Figure 12).

Depositional characteristics also depend on the involved material in the process. Debris flows, which consists mainly of coarse grained sediments, e.g. dolomites or limestones, often provide clearly delimited deposition zones, as the water content in the flowing mass rapidly decreases (large pores) and the flow suddenly stops. In absence of a large amount of fine components, the extents of the newly deposited material are well defined (Figure 15a-c). The delimitation of flow deposits with a larger share of silty or clayey components can be more difficult. The type of material also affects the frictional processes within the flowing mass and thus dominates mobility and runout of the debris flow (see Chapter 3.3.2).

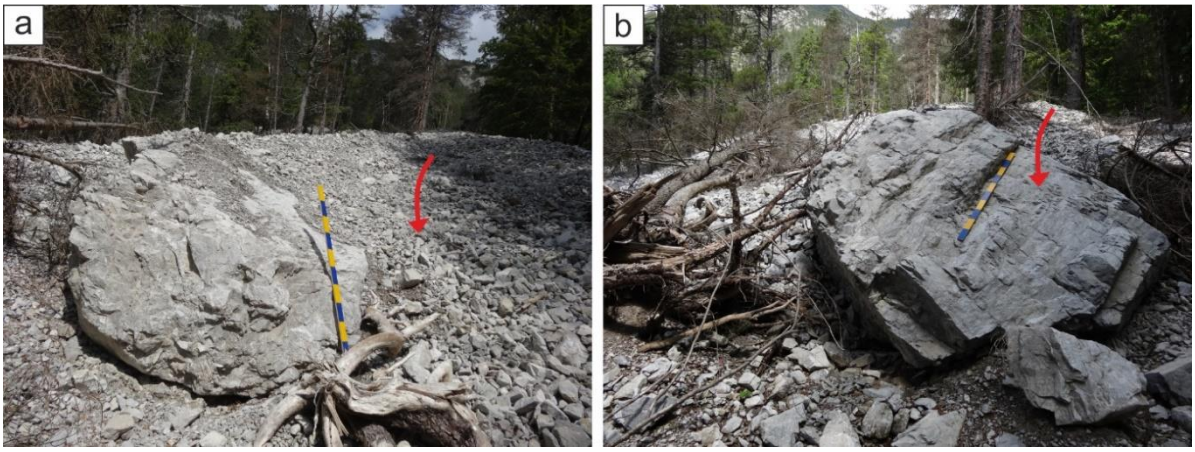

Figure 14: Debris-flow deposition of large boulders. Scale bar is 1 m. Red arrows represent the flow direction.

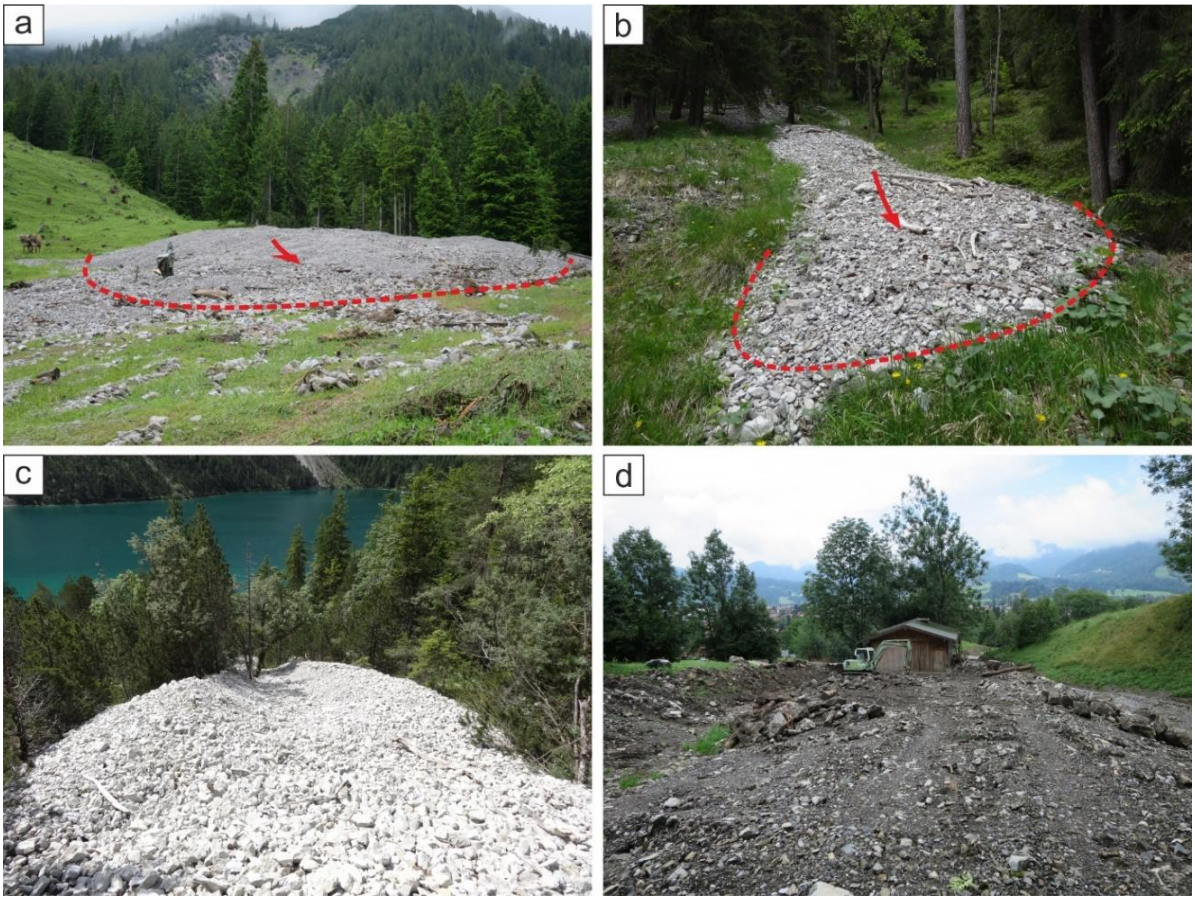

Figure 15: Field evidences for debris-flow characteristics. a-b: Typical debris-flow heads in small (b) and large scale (a). c-d: Debris-flow deposits, which consist of nearly exclusively coarse dolomitic clasts (c) and deposits with a significant amount of fine sediments of Flysch formations (d).

3.2.5 Summary

Most debris flows are initiated by either a landslide failure or a successive erosion and instability of the stream bed. Both mechanisms usually cause a step-by-step growth in volume by entraining sediments from the channel bed. Normal forces, acting on the channel bed, induce shear stresses, which lead to an acceleration of the uppermost layer of the erodible substrate. Due to particle collisions, material gets released from the substrate and is entrained in the flowing mass. Although high-resolution data sets on these erosion processes exist, reproducible links to meaningful and reliable controlling factors are rare.

3.3 Numerical modelling of debris flows

A variety of models has been developed to predict and simulate debris flows in endangered areas. The following subchapters introduce simplified rheological models for fluids (Chapter 3.3.1) and their implementation in different numerical debris-flow models (Chapter 3.3.2).

3.3.1 Rheological models for fluids

All models simplify a debris flow as a fluid with specific flow properties. These flow properties are represented by a more or less sophisticated rheological model. However, direct measurements of rheological properties of real-scale debris flows are – up to date – nearly impossible. Even large rotationnal rheometers in laboratories suffer non-reproducibility (Ancey, 2007). They cannot fully characterise properties of large debris flows (Coussot and Meunier, 1996) and, thus, their results have to be extrapolated with caution. Hence, none of the following models is able to completely describe the complex behaviour and the changing properties of debris flows by a simplified function (Iverson, 2003). Nevertheless, the approximation of flow properties allows for numerical models, which in turn have to be validated by field data.

3.3.1.1 Bingham

The model from Bingham and Green (1919), initially derived from paint colour, was adapted for debris flows by Johnson (1970) and was for a long time the most often used one. In this model, the shear stress (τ) is linearly related to the shear rate ($\dot{\gamma}$) and depends on the (constant) Bingham viscosity (η) and a yield stress (τ_B):

Equation 3:

$$\tau = \tau_B + \eta\dot{\gamma}$$

Hence, the shear stress linearly increases with shear rate (Figure 16). The unknowns in this formula are both Bingham viscosity and yield stress, which are estimated by the grain size distribution and the sediment concentration of the flowing mass or are measured in laboratory (Kaitna *et al.*, 2007). Depending on the material composition and the water content, the results show a broad range of values from 5 to 75 Pa·s for η and 450 to 3,000 Pa for τ_B (Boniello *et al.*, 2010, Kaitna *et al.*, 2007, Parsons *et al.*, 2001).

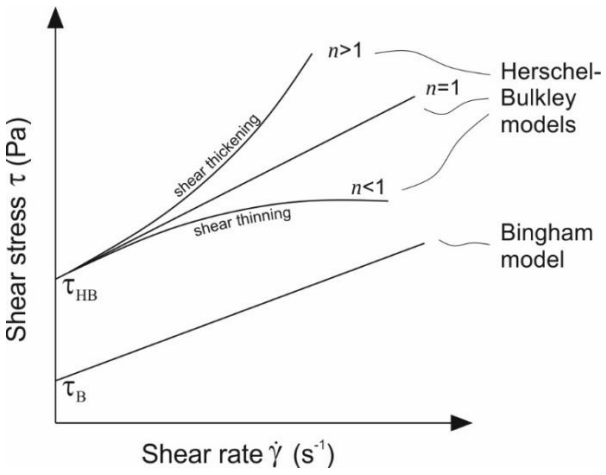

Figure 16: Relationship between shear rate and shear stress for different rheological models.

3.3.1.2 Herschel-Bulkley

A similar, but more generalised model, was developed by Herschel and Bulkley (1926):

Equation 4:

$$\tau = \tau_{HB} + K\dot{\gamma}^n$$

Shear stress is gained by a function of a yield stress (τ_{HB}) and a product of a consistency index (K) and the shear rate ($\dot{\gamma}$) with an exponent (n). For $n = 1$ the function represents a linear model (similar to the Bingham model), for $n > 1$ the shear rate exponentially increases and for $n < 1$ the shear rate exponentially decreases. Clay-rich suspensions in laboratory often show values for $n < 1$ (often $n \approx 0.3$) and, thus, they are characterized by shear thinning (Kaitna *et al.*, 2007). Values for $n > 1$ are rarely reported in literature, as conventional rheometers are limited to fine grained materials.

3.3.1.3 Power law

Julien and Lan (1991) and O'Brien *et al.* (1993) used a power-law (quadratic) rheological model to describe a relationship between shear rate and shear stress (τ) and incorporated a dynamic viscosity (η_d):

Equation 5:

$$\tau = \tau_y + \eta_d \left(\frac{d_v}{d_y}\right) + C \left(\frac{d_v}{d_y}\right)^2$$

C represents the inertial shear stress coefficient, $\left(\frac{d_v}{d_y}\right)$ is the shear rate and τ_y is a sum of a cohesive yield stress τ_c and a Mohr Coulomb shear τ_{MC} (Julien and Lan, 1991, O'Brien *et al.*, 1993).

3.3.1.4 Voellmy-Salm

The model was introduced by Voellmy (1955) and Salm (1966) and was adapted by Bartelt *et al.* (1999). Christen *et al.* (2010) modified the model for mass flows in three dimensional terrain. Initially, the model had been developed for avalanche simulations and was then adapted for debris-flow modelling. In a Voellmy fluid no shearing occurs within the fluid. However, active and passive earth pressures govern the longitudinal straining of the flowing mass (Bartelt *et al.*, 1999). Friction – at the base of the flow – is incorporated by a modified Coulomb friction law

Equation 6:

$$\tau_{MC} = \mu \cdot \rho \cdot H \cdot g \cdot cos(\varphi)$$

and velocity-dependent friction term (Bartelt *et al.*, 1999):

Equation 7:

$$\tau_v = \frac{\rho \cdot g \cdot v^2}{\xi}$$

The Mohr Coulomb-based shear stress τ_{MC} depends on the friction coefficient μ, the density of the flowing mass ρ, the flow height H, the gravitational acceleration g and the slope angle φ. The velocity-dependent friction τ_v additionally depends on the velocity v and a (turbulent) friction coefficient ξ.

3.3.1.5 Bagnold

Another model was developed by Bagnold (1954). Although it was widely used by geophysicists in the past, it is limited to extremely rapid flows of dry masses of cohesionless particles and should not be considered for mixtures of water and debris (Coussot and Meunier, 1996).

3.3.2 Numerical debris-flow models

The most frequently applied debris-flow models are shortly described in the following subchapters.

3.3.2.1 RAMMS Debris Flow

RAMMS Debris Flow is based on the Voellmy-Salm rheological approach and solves the depth-averaged shallow water equations conserving mass and momentum. RAMMS Debris Flow uses the total diminishing finite volume scheme and an Eulerian framework as reference system (Christen *et al.*, 2010). In the past, the one-phase model has been used by researchers as well as by experts for debris-flow hazard mapping (e.g., Bertoldi *et al.*, 2012, Hussin *et al.*, 2012, Schraml *et al.*, 2015b). Frictional deceleration (S_f) – others call it friction slope or total resistance – is calculated by:

Equation 8:

$$S_f = \mu \cdot \rho \cdot H \cdot g \cdot cos(\varphi) + \frac{\rho \cdot g \cdot v^2}{\xi}$$

The individual parameters have been introduced in Chapter 3.3.1.4. At slow velocities the Coulomb-type friction coefficient μ dominates frictional deceleration, at higher velocities the (turbulent) friction coefficient ξ dominates (Bertoldi *et al.*, 2012). Suggested friction values for solid-dominated, granular debris flows are $\xi \approx$ 100-200 m/s² and for fluid-like, muddy debris flows $\xi \approx$ 200-1,000 m/s² (Bartelt *et al.*, 2017). For further model descriptions I refer to Chapter 5.4.4.

3.3.2.2 FLO-2D

FLO-2D is a model with two uncoupled phases. It uses a finite difference method to solve the governing equations. The friction slope S_f is given by:

Equation 9:

$$S_f = \frac{\tau_B}{\gamma_m h} + \frac{R\eta_d V}{8\gamma_m h^2} + \frac{n^2 v^2}{h^{4/3}}$$

In addition to the mentioned parameters in Chapter 3.3.1, this formula uses the specific weight of the sediment-water-mixture γ_m, the resistance parameter R, which depends on geometry and roughness of the channel bed, the depth-averaged velocity v, the Manning value n, the dynamic viscosity η_d and the flow depth h (O'Brien *et al.*, 1993). FLO-2D has also been widely used in research and practice (Bertoldi *et al.*, 2012, Bertolo and Wieczorek, 2005, Hübl and Steinwendtner, 2001, Jakob *et al.*, 2012, Rickenmann *et al.*, 2006, Sosio *et al.*, 2007).

3.3.2.3 DAN3D

DAN3D was introduced by Hungr (1995) and modified for three-dimensional modelling by Hungr and McDougall (2009). It is – similar to RAMMS Debris Flow – based on the Voellmy-Salm rheological model and solves the depth-averaged shallow water equations conserving mass and momentum. In contrast to RAMMS Debris Flow, DAN3D uses smoothed particle hydrodynamics as numerical solution scheme and a Lagrangian framework as reference system (Hungr and McDougall, 2009). It has also successfully been applied to model runout patterns of debris flows (Bossi *et al.*, 2015, Schraml *et al.*, 2015b).

3.4 Debris-flow volume quantification

All above mentioned models need a specification of the transported debris-flow volume. However, the determination of this crucial value is not straightforward, especially for future events. Thus, the volumes of recent events have often been used as indicators and reference values for potentially upcoming debris flows. For this purpose, different approaches have been carried out to estimate recent volumes. In Chapter 3.4.1 different techniques for data acquisition are shortly described. The workflow for a reproducible geomorphic change detection and volume computation, based on the collected data, is presented in Chapter 3.4.2.

The following Subchapters 3.4.1.3 and 3.4.2 contain, inter alia, contents of Dietrich and Krautblatter (2019), but were significantly revised and extended.

3.4.1 Methods for data collection

3.4.1.1 Formula-based methods

In the past, researchers have tried to link (maximal) debris-flow magnitudes with different catchment-specific parameters. D'Agostino et al. (1996), Kronfellner-Kraus (1984) or Rickenmann (1995) suggested to use the mean slope angle of the torrent to derive debris-flow magnitudes. Others related the size of the catchment area (Franzi and Bianco, 2001, Zeller, 1985) or lithological factors (Bianco et al., 2001) to debris-flow volumes. Although some of these approaches seem to be able to explain at least a share of factors controlling the total debris-flow magnitude, they are not suitable to back-calculate volumes of recently occurred events, as these formulae often provide maximum volumes for potentially occurring events. Additionally, many of these formulae suffer bias due their local derivation (Marchi and D'Agostino, 2004). Therefore, Scheidl and Rickenmann (2010) proposed an empirical-based approach using the deposition area of recently occurred debris flows. They related the area of a deposition (B) to its volume (V) based on a large number of field observations. Deposition areas are approximated by a circular sector (Scheidl and Rickenmann, 2010):

Equation 10:

$$B\ [\mathrm{m^2}] = L_f^2 \cdot \pi \cdot \psi \cdot 1/360°$$

In this formula, L_f [m] is the radius and ψ [°] is the angle of the circular sector. The empiric mobility coefficient k_b [-] is derived by:

Equation 11:

$$k_b = 5.07 \cdot y_d^{-0.1} \cdot y_c^{-1.68}$$

k_b depends on the mean channel slope y_c [-] (typically 10°-35°) and the mean slope of the debris-flow fan y_d [-] (typically 5°-25°). Thus, the volume V [m³] of the debris-flow deposition can be calculated by:

Equation 12:

$$V = B^{3/2} \cdot k_b^{-3/2}$$

Less mobile materials with a small amount of fine-grained sediments (e.g. main dolomite) usually show small k_b values (due to steep fans and steep channels) and vice versa. If we presume two identical deposition areas – one consisting of coarse grained material and the other of fine-grained material – the coarse-grained deposition typically has a larger height and, thus, a larger volume. The method has been successfully applied in literature (Dietrich and Krautblatter, 2017, Scheidl and Rickenmann, 2010).

3.4.1.2 Geophysical methods

Electrical resistivity tomography (ERT)

Geophysical methods can be used to estimate recent debris-flow volumes in a more transparent way. ERT uses the varying ability of materials to conduct electrical current (Figure 17). By changing the electrodes, in which the current (DC) is injected, and the electrodes, which are used to obtain the difference in potential, an image of the resistivity distribution of the substrate can be achieved.

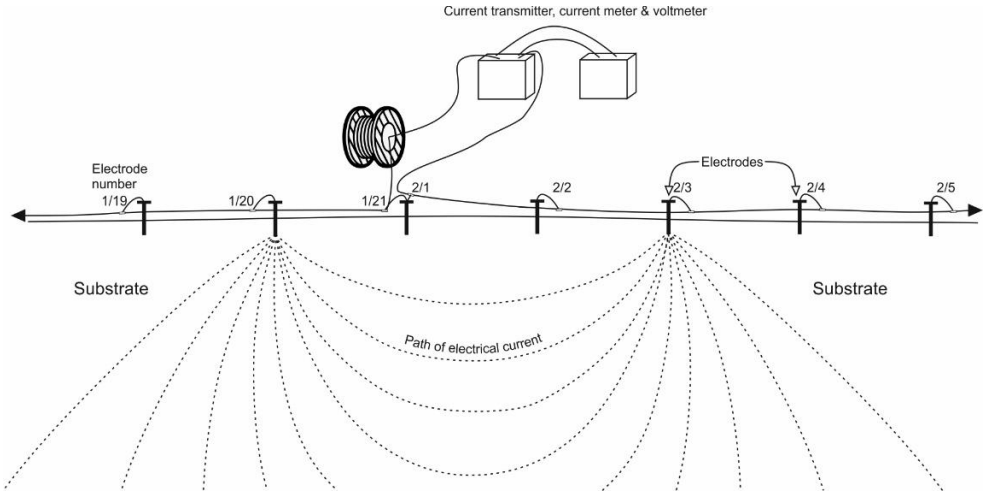

Figure 17: Measurement setup for an electrical resistivity tomography with two cables. In this example the current (DC) is injected between electrode 1/20 and 2/3. The difference in potential (voltage) is measured between electrode 2/1 and 2/2.

As deposits of debris flows in an area usually consist of similar lithological components and, thus, have similar resistivity values, the differentiation of successively, but individually occurred events is challenging. However, the method is able to provide insights into fan evolution, as postglacial basal tills, large boulders or bedrock can be delimited from overlying debris. Sass (2006) linked different alpine talus accumulations, deciphered by a combination of ERT, SRS and GPR, to different processes, such as rock falls or debris flows and basal moraines beneath the talus. Similar surveys were conducted by Senderak *et al.* (2017) in Spitsbergen (Norway) or by Barski and Mieszkowski (2014), who tried to link resistivity values, derived by ERT measurements, to debris-flow deposits in Poland.

Reflection and refraction seismic

Both reflection and refraction seismic use travel times of seismic energy detected by geophones. As the seismic velocities vary for different materials (e.g. slower in debris than in bedrock), the seismic energy gets refracted and partly reflected at material boundaries. Maraio et al. (2018) used a combination of reflection and refraction seismic to reveal deposits of debris flows, alluvial valley fills and hosting bedrock in the Eastern Italian Alps. Schrott et al. (2003) deciphered sediment storage types and quantified valley fill deposits in an alpine basin in Germany by refraction seismic. Similar surveys, applying refraction seismic, were carried out in different geomorphological settings (Haeberli *et al.*, 2001, Mauritsch *et al.*, 2000, Prekopova *et al.*, 2017, Sass, 2006, Winkler *et al.*, 2016). Although these methods allow a delimitation of different material types, especially due to their varying densities, these approaches do usually not allow for a volume quantification of an individual recent debris-flow event.

Ground-penetrating radar (GPR)

Ground-penetrating radar uses electromagnetic wave pulses with radio spectrum wavelength. These pulses get reflected at discontinuities in the sub-surface. Travel times are recorded by a receiving antenna. Reflections can be produced by a sudden change in moisture, grain size or shape (Starheim *et al.*, 2013). The non-invasive method has been widely applied in geosciences. Depositions of debris flows have been detected by Sass and Krautblatter (2007), Sass (2006), Clague *et al.* (2003) or Pelpola and Hickin (2004) using GPR. Starheim *et al.* (2013) even tried do delimit the internal structure of a debris-flow deposit in Cass, New Zealand. Their results provide insights into the thickness of the debris flow at different locations, however, the underlying material is not another debris flow, but grassland. Although this method is labour-intensive, especially when spatially large deposits shall be recorded in 3D, GPR is able to detect individual debris flows under specific conditions.

3.4.1.3 Geodetic methods - airborne laser scanning and terrestrial laser scanning

Laser scanners emit electromagnetic pulses. These pulses are reflected at objects in the line of sight. In comparison to ground-penetrating radar, the wavelength of the emitted energy often lies in the infrared range and is emitted from an airplane, UAV or helicopter (airborne) or, alternatively, from a tripod up to 2 m above ground (terrestrial). Depending on the measurement system, the used wavelength and the type of object, the laser pulse is able detect multiple targets, as a proportion of the pulse is refracted at a boundary surface of an object and moves further to the next one (e.g. leaves, Figure 18). The aim of TLS and ALS is to produce high-resolution point clouds, which can be processed to digital elevation models. Airborne LiDAR data have been widely used in different disciplines in the geosciences and environmental sciences. Authors used ALS to extract forest inventory data (Hyyppa *et al.*, 2008, Kaartinen *et al.*, 2012, White *et al.*, 2013), to measure snow depth for snow hydrology and avalanche applications (Deems *et al.*, 2013), to classify land cover (Yan *et al.*, 2015) and to detect landslide features in field (Chigira *et al.*, 2004, Jebur *et al.*, 2014, Sekiguchi and Sato, 2004).

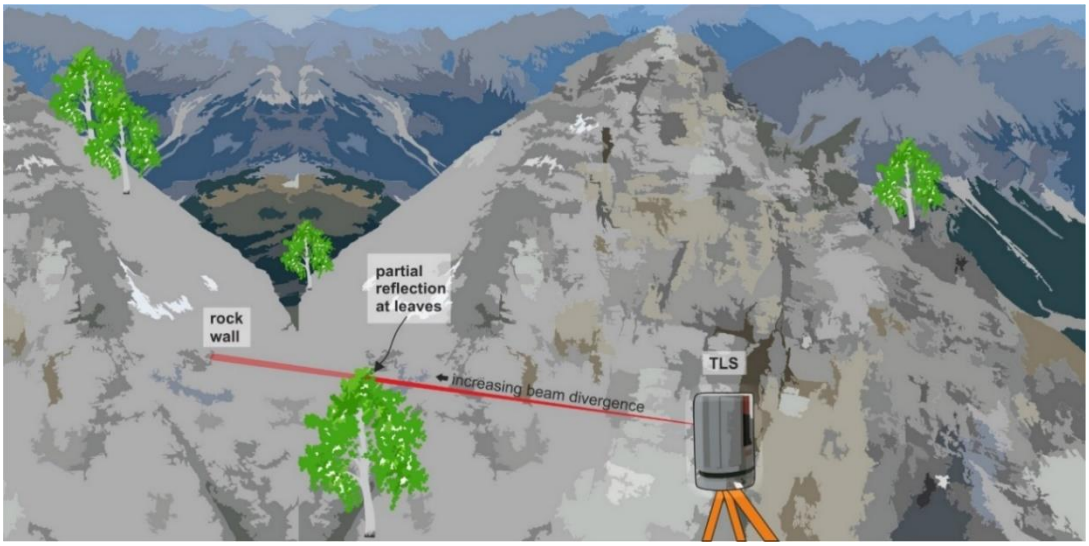

Figure 18: Application of terrestrial laser scanning in field. The laser beam diverges with increasing travel distance and is able to detect multiple targets.

Other researchers used ALS data to detect geomorphic changes induced by debris flows as well as to calculate their volumes (e.g., Breien *et al.*, 2008, Bremer and Sass, 2012, Cavalli *et al.*, 2017, Cavalli and Marchi, 2008, Goodwin *et al.*, 2016, Scheidl *et al.*, 2008). Recently, terrestrial laser scanning gained more and more attraction due to its possibility to produce DEMs in cm-scale. Thus, TLS was used to budget debris flows more precisely and to monitor sediment fluxes in highly dynamic fluvial systems (e.g., Baewert and Morche, 2014, Bimböse *et al.*, 2011, Blasone *et al.*, 2015, Bühler and Graf, 2013, Carrivick *et al.*, 2013, Perroy *et al.*, 2010, Staley *et al.*, 2014, Theule *et al.*, 2015, Theule *et al.*, 2012, Wheaton *et al.*, 2010b). Airborne laser scanning gained popularity since the late 1990s and has found to be the appropriate method to gather data sets for large areas with a relatively low point density (0.5-5 points/m²). In Bavaria, Germany, the first flights have been carried out in 1996. Terrestrial laser scanning has been applied since the early 2000s, but most studies have been carried out particularly in the last decade. On the one hand, the advantages of TLS are a much higher spatial resolution, a smaller beam divergence on short distances, the possibility to carry the equipment in a backpack in field and lower capital investment costs compared to ALS. On the other hand, the low incidence angle of a terrestrial laser scanner on oblique targets causes a larger deviation of the laser pulse and an inhomogeneous coverage due to obstacle-related shadowed areas in scans (Perroy *et al.*, 2010). Thus, each of these platform systems has its own preconditions, advantages and limitations, but they also provide a useful overlap, where both methods complement each other. However, researchers rarely made use of the possibility to combine measurements of these different platforms to take up different geoscientific challenges. Perroy *et al.* (2010) quantified soil loss due to gully erosion in a heavily degraded watershed on Santa Cruz Island, California, while Young *et al.* (2010) used both data sets to reveal seacliff erosion in Del Mar, California. Others used both platform data sets to delineate landslide boundaries (Wang *et al.*, 2013) or to measure displacement vectors of landslides (Corsini *et al.*, 2013, Ghuffar *et al.*, 2013, Stewart *et al.*, 2009). Bremer and Sass (2012) used TLS and ALS data in the Halltal, Austria, to quantify the volume of a recent debris flow.

3.4.1.4 Structure-from-Motion photogrammetry

Although high-resolution data sets can be achieved with TLS quiet easily, the method is limited to accessible areas, has relatively high capital investment costs and has often an oblique line of sight. All these limitations can be turned into advantages of photogrammetry. Consequently, SfM photogrammetry is nowadays widely used in geoscience applications. Its beginning reaches back to the 1980s, when Harris and Stephens (1988) developed their first edge detector for images and Förstner (1986) established a feature-based algorithm for image matching. Szeliski and Kang (1994) recovered their first 3D shapes from image alignment. Early approaches used only two photos of a calibrated camera, a stereo-pair, to extract 3D terrain data (Chandler, 1999). To date, hundreds and thousands of photos can be processed to derive highly accurate spatial data, if the high hardware requirements can be satisfied. Surveys are often carried out using UAVs with an integrated camera, as they are able to take perpendicular-oriented photos of an object (Figure 19). Although many UAVs have a relatively accurate GNSS, the produced point clouds (and photos) have to be georeferenced carefully by means of precise GCPs to avoid systematic errors in the final models (James and Robson, 2014). These GCPs have to be laid out prior to the survey and they have to be measured exactly with RTK-GNSS (global coordinates), a total station (local coordinates) or by means of terrestrial laser scanning (local coordinates). Pre- and post-event surveys deliver high-resolution point clouds and DEMs in less time and at lower costs compared to TLS surveys (James and Robson, 2012, Westoby *et al.*, 2012), especially in areas with no or little vegetation (Berger *et al.*, 2011b, Cucchiaro *et al.*, 2018, Fonstad *et al.*, 2013, Javemick *et al.*, 2014, Kenner *et al.*, 2014, Westoby *et al.*, 2012). Thus, researchers analyse debris-flow volumes and rates more frequently with SfM photogrammetry (Tsutsui *et al.*, 2007).

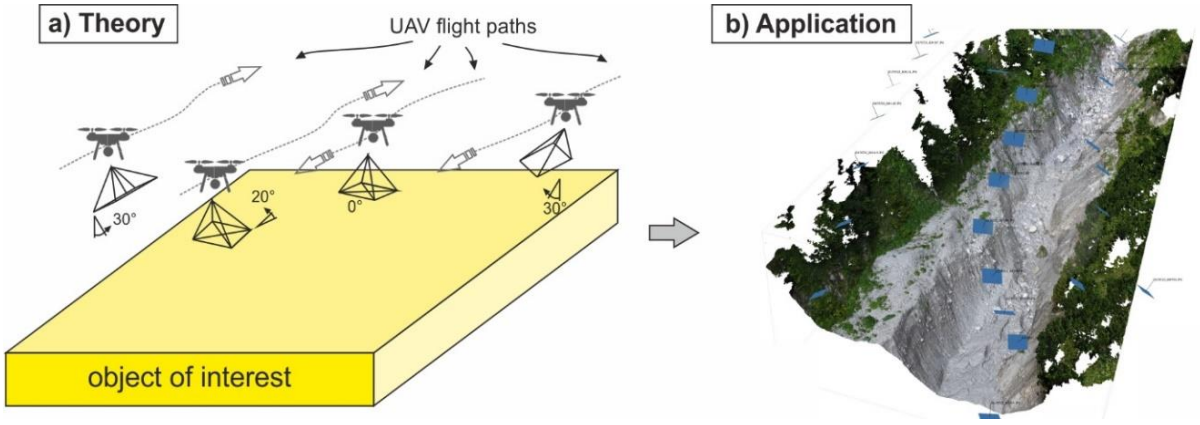

Figure 19: a) Theoretical approach for Structure-from-Motion photogrammetry. Photos have to be taken of multiple camera positions, best with a slightly varying camera angle. b) Processed images with Agisoft Photoscan. All camera positions are estimated and aligned based on common key points in different images. A reconstructed dense point cloud is displayed.

3.4.2 Change detection

By means of the above mentioned methods, pre- and post-event DEMs can be produced with a centimetre-scale resolution. Geoscientific challenges often deal with geomorphic changes in a given time span, such as sediment dynamic and transport in a fluvial system (Bezak *et al.*, 2017, Javemick *et al.*, 2014, Schürch *et al.*, 2011a), rockfall activity in a study area (Abellan *et al.*, 2011, Rabatel *et al.*, 2008, Rosser *et al.*, 2005) or characterisation and quantification of erosion and deposition areas of a landslide (Gatter *et al.*, 2018, Rossi *et al.*, 2018, van Westen and Getahun, 2003). The easiest way to detect these geomorphic changes between temporally consecutive surveys is to subtract the height values of the associated DEMs, e.g. new DEM minus old DEM (Figure 20). Although this approach seems to be straightforward, the results will often show a large amount of errors, provided that the analysis suffers insufficient error treatment. These errors arise from inaccuracies of the measurement system, from the imprecise co-registration of individual laser scan point clouds, from errors produced during point-cloud processing (e.g. vegetation removal) and depends on the used DEM interpolation method (Williams, 2012). Consequently, the subtraction of the DEMs often results in erroneous DoDs. Therefore, different approaches have been developed in the past to account for these errors in geomorphic change detections. Fuller *et al.* (2003) used a simple constant minimum level of detection ($_{min}$LoD) independent of the spatially variable DEM quality. All surface height changes smaller than a user-defined $_{min}$LoD are not considered as true elevation changes.

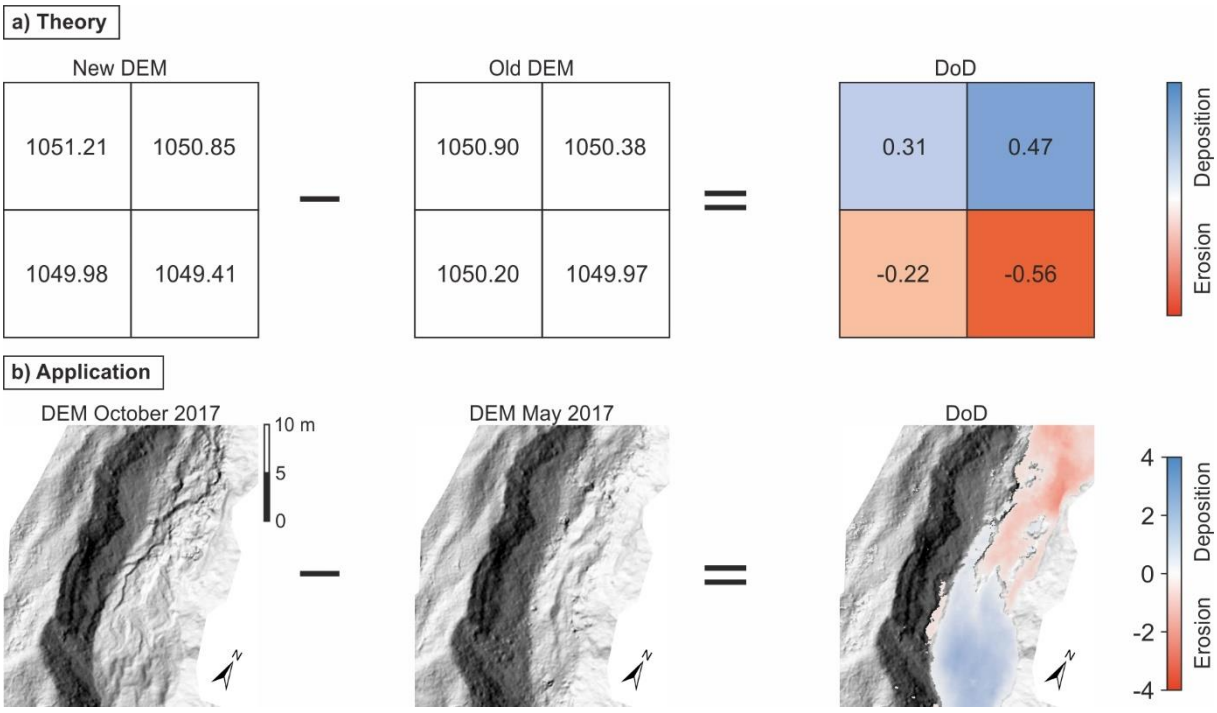

Figure 20: Theory (a) and application (b) of a geomorphic change detection. The older DEM is subtracted from the more recent one resulting in a DEM of Difference (DoD). Numbers in (a) correspond to elevation heights. It is assumed that the old and new DEMs have the same spatial extent, cell size and projected coordinate system. DEMs in (b) are displayed as hillshades. A hillshade of the new DEM underlays the DoD in (b) for better visibility.

However, this method cannot distinguish between small elevation changes, which are real and small elevation changes, produced by different sources of errors, which are not real. Wheaton *et al.* (2010b) improved the methodology by considering DEM precision and quality. He derived a spatial variable DEM uncertainty and included probability-based thresholds and spatial coherence of erosion and deposition in the change detection. This approach has been widely used in recent literature and has found application in different geomorphological settings (Bangen *et al.*, 2016, Kasprak *et al.*, 2015, Le Mauff *et al.*, 2018, Norman *et al.*, 2017, Prosdocimi *et al.*, 2017, Schaffrath *et al.*, 2015, Wiggins *et al.*, 2019). The workflow of this approach has been implemented in ArcGIS by an Add-On called "Geomorphic Change Detection". The workflow is shown in Figure 21and is described in the following section.

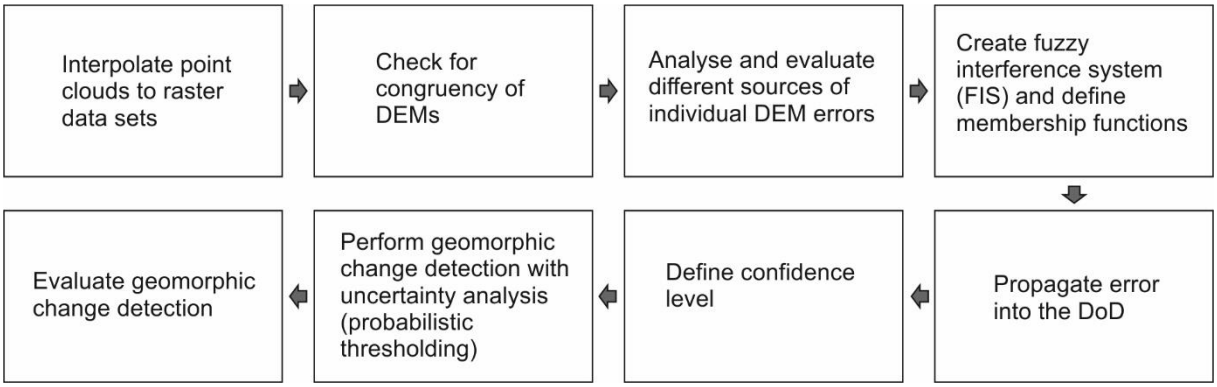

Figure 21: Workflow of a geomorphic change detection. The Add-On for ArcGIS was developed by Wheaton *et al.* (2010b).

The raster data sets – derived by interpolated point clouds – can be clipped to the same spatial extents to reach congruent DEMs. Subsequently, individual DEM parameters, quality and precision can be derived on a cell-by-cell basis (Figure 22) considering (i) the roughness of the DEM (Brasington *et al.*, 2012, Rychkov *et al.*, 2012), (ii) bootstrapping experiments (Wheaton, 2008), (iii) DEM parameters like slope angle (Wheaton *et al.*, 2010a) or interpolation errors (Bangen *et al.*, 2016), (iv) other user-defined data sets like vegetation indices (Schaffrath *et al.*, 2015) and (v) the point density of the initial point cloud (Blasone *et al.*, 2014). These data sets, representing different sources of individual DEM errors, are combined to an DEM uncertainty on a cell-by-cell basis using fuzzy set theory (Gottwald and Bandemer, 1995, Klir and Yuan, 1995). This DEM elevation uncertainty (δz), calculated by the associated membership functions, has to be calibrated to field settings. For this calibration, it has to be checked iteratively, whether the calculated erosion and deposition areas and depths match with observations during field surveys for specific areas. The DEM uncertainty of each of the DEMs (old and new, e.g. Figure 22) is then propagated into the DoD by taking the square root of the squared individual elevation uncertainties (Brasington *et al.*, 2003). Bedsides the usage of this propagated error as a minimum level of detection, the software allows for probabilistic thresholding regarding different t-scores and confidence limits (Wheaton *et al.*, 2010b).

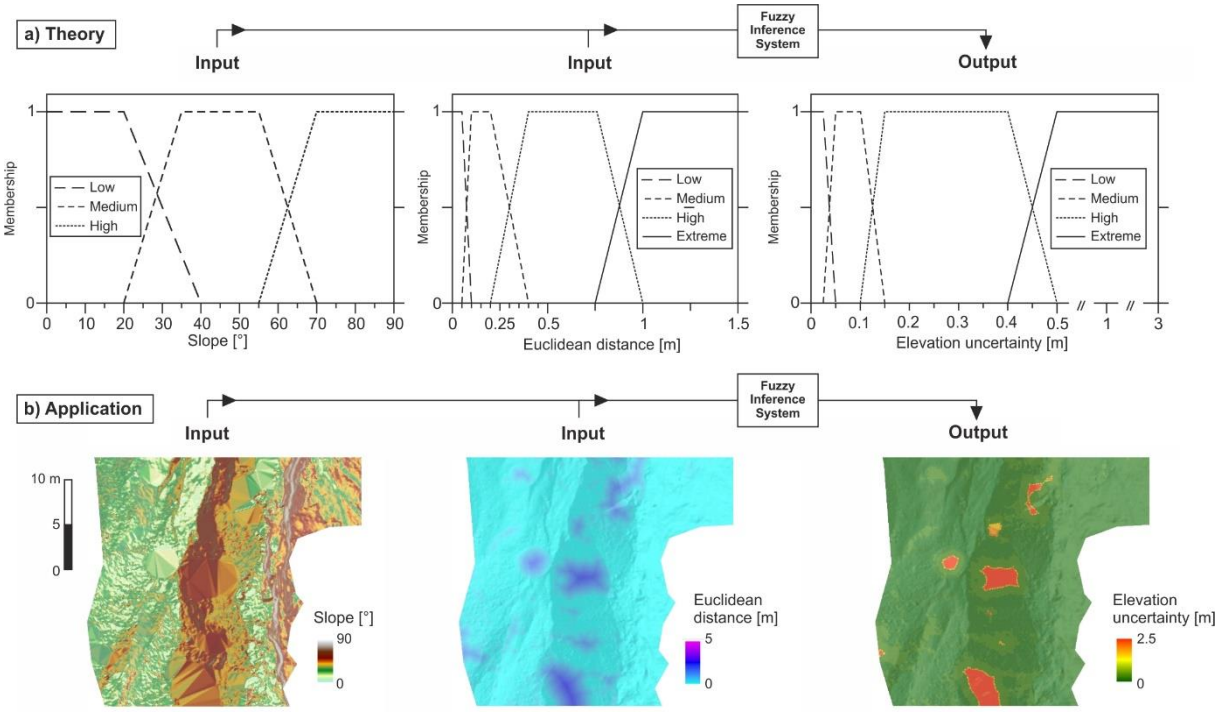

Figure 22: Theory (a) and application (b) of a FIS. Quality parameters of the DEMs (inputs), e.g. slope angle and Euclidean distance to the next data point, are used to define an elevation uncertainty (output) of each DEM.

Thus, a measured elevation difference and an elevation uncertainty value is reported for each individual cell of the DoD, e.g. 0.5 ± 0.1 m (Figure 23b). If the measured elevation difference (e.g. 0.5 m) is higher than the elevation uncertainty value (e.g. ± 0.1 m), the resulting volume (considering cell size) is added to an erosion or deposition volume, respectively. In the opposite case, the volume is added to an error volume (Figure 23c).

The change detection can be performed with DEMs from variable sources, even for the same project area. However, multi-temporal survey campaigns often aim to produce DEMs of a study area with the same method multiple times, e.g. with total stations (Bangen *et al.*, 2016), terrestrial laser scanning (Abellan *et al.*, 2009, Theule *et al.*, 2015, Wheaton *et al.*, 2010b, Williams *et al.*, 2018), airborne laser scanning (Thoma *et al.*, 2005, Woolard and Colby, 2002) or photogrammetry (Cucchiaro *et al.*, 2018, Javemick *et al.*, 2014). Change detections with DEMs derived by different methodological approaches are performed quiet rarely (Bremer and Sass, 2012, Kenner *et al.*, 2014, Lane *et al.*, 2003), although they usually provide at least equivalent informational content.

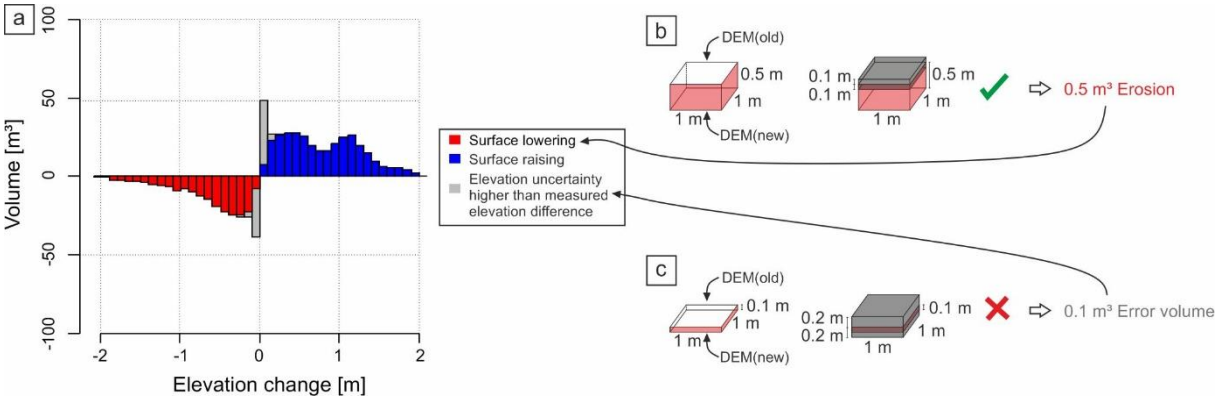

Figure 23: Volume calculation by the GCD. The volumetric changes (a) comprise of elevation differences, which exceed the elevation uncertainty value (b, shown in red and blue colour in a) and error volumes (c, shown in grey colour in a). In (b) the elevation difference of a raster cell is 0.5 m and the elevation uncertainty ± 0.1 m, in (c) the elevation difference is 0.1 m and the elevation uncertainty ± 0.2 m.

3.5 Impacts of climate change on debris-flow activity

The following Chapters 3.5.1 and 3.5.2 contain, inter alia, revised and significantly extended contents of Dietrich and Krautblatter (2017).

3.5.1 Quantification of debris-flow activity

In this thesis debris-flow activity is defined as a combination of debris-flow frequency and magnitude and is controlled by the number of events in a given time span and their transported sediment volumes. The approximation of recent debris-flow volumes has been discussed in Chapter 3.4.1. To receive values for debris-flow frequency, the correct age of recent and historical debris-flow events has to be determined. For this, different approaches have been carried out. For recent decades, some researchers analysed historical data of archives (D'Agostino and Marchi, 2001, Marchi and Cavalli, 2007, Marchi and Tecca, 2006, Melis *et al.*, 1995, Tropeano and Turconi, 2004) and aerial photographs from different dates to decipher phases of higher und lower debris-flow activity (D'Agostino, 2013, Dietrich and Krautblatter, 2017, Procter *et al.*, 2011, Procter *et al.*, 2012, Šilhán and Tichavský, 2016). However, sufficient amount and quality of photographs are available only since the 1940s for parts of the European Alps. Historical data are often biased, as the population has moved more closely to debris-flow endangered areas in the last decades and more effort is recently put into a full recording of events. For longer time scales authors have used tree rings as indicators for debris-flow events, as the contact of solids with trees leads to growth disturbances (Bollschweiler and Stoffel, 2010b, Bollschweiler *et al.*, 2007, Mayer *et al.*, 2010, Procter *et al.*, 2011, Saez *et al.*, 2011, Schraml *et al.*, 2015a, Stoffel and Beniston, 2006, Stoffel *et al.*, 2013). Long-term fan developments can be investigated by specific isotopes, like ^{14}C, but the identification and delimitation of individual events is often difficult (Clague *et al.*, 2003, Matthews *et al.*, 1997, Matthews *et al.*, 2009, Schürch *et al.*, 2016).

By means of these methods, the debris-flow activity can be revealed qualitatively and sometimes even quantitatively. As triggers for debris flows are well known, the discussion about the impacts of a changing climate on the debris-flow activity has experienced increased attention in the last years and decades.

3.5.2 Climate forcing and climate change

As mentioned in Chapter 3.2.2, debris flows are usually initiated by intense rainstorm events. Thus, the question arises, whether the climate change results in an increased frequency of heavy rainfall events and – if so – whether these rainfall events lead to an enhanced debris-flow frequency and activity in different alpine regions over the world. At the end of the last century Rebetez *et al.* (1997) showed that the world is faced a more frequent occurrence of extreme events, including different types of events with different impacts on the earth itself and on human beings. Cubasch *et al.* (1995) forecasted for the next 30 years an increase in intense precipitation events in some parts of the world, while Fuhrer *et al.* (2006) even predicted a three-fold increase in intense precipitation events by the end of the 21st century for Switzerland. For susceptible systems (see Chapter 3.2.1) this increase in heavy rainfall events should theoretically lead to an increase in debris-flow frequency and activity (Sewell *et al.*, 2015). However, this conclusion is discussed contrarily. Some authors described such an increase in debris-flow activity in some parts of the European Alps (Dietrich and Krautblatter, 2017, Pavlova *et al.*, 2014, Šilhán and Tichavský, 2016). Especially the results of tree-ring analyses often seem to suggest an increase in debris-flow events in the last decades (Bollschweiler and Stoffel, 2010a, Mayer *et al.*, 2010, Procter *et al.*, 2012, Schraml *et al.*, 2015a), but are often systematically biased as recent events are often more likely to be detected, especially when a tree population has (re-)grown in recent decades (Silhan *et al.*, 2015). Thus, other researchers cannot observe a significant increase (Jomelli *et al.*, 2003, Kaitna and Huber, 2017). One reason for different outcomes, regarding this discussion, is that the sediment supply varies both temporally and spatially (e.g. lithologically) over short distances in the Alps (Schürch *et al.*, 2016). A low sediment recharge rate results in a supply-limited system. Thus, not every highly intense rainstorm causes a debris flow, as the limited sediment supply governs the frequency of debris flows (Brayshaw and Hassan, 2009, Glade, 2005). Hence, a direct correlation between intense rainfall events and debris-flow activity is complicated and regional setting have to be considered when making general statements. In addition, seismic events in some areas of the world may also increase the debris-flow activity without a direct link to climate change. Zhang and Zhang (2017) showed that the rainfall threshold to initiate debris flows dropped directly after the Wenchuan Earthquake in 2008 to one thirds of the pre-earthquake level in that region.

4 Pre-depositional: Debris-flow activity in the last decades in the Northern Calcareous Alps

Parts of this chapter originate from the master thesis of Dietrich (2014) but have been completely rewritten and substantially extended for the paper of Dietrich and Krautblatter (2017). The following text is the accepted version of the following article:

Dietrich A, Krautblatter M. 2017. Evidence for enhanced debris-flow activity in the Northern Calcareous Alps since the 1980s (Plansee, Austria). Geomorphology 287: 144-158.

The final version has been published at http://dx.doi.org/10.1016/j.geomorph.2016.01.013

The following changes have been made to the accepted version:

- ⇨ The numbering of each figure, table and equation has changed
- ⇨ The captions of Chapters 4.3.3, 4.5.3, 4.5.4, 4.6.2 and 4.6.3 have slightly changed

4.1 Abstract

Debris flows are among the most important natural hazards. The Northern Calcareous Alps with their susceptible lithology are especially affected by a double digit number of major hazard events per year. It is hypothesised that debris-flow intensity has increased significantly in the last decades in the Northern Calcareous Alps coincident to increased rainstorm frequencies, but yet there is only limited evidence. The Plansee catchment exposes extreme debris-flow activity due to the intensely jointed Upper Triassic Hauptdolomit lithology, being responsible for most of the debris-flow activity in the Northern Calcareous Alps. The debris flows feed into a closed sediment system, the Plansee Lake, where Holocene/Lateglacial sedimentation rates, rates since the late 1940s and recent rates can be inferred accurately. Using aerial photos and field mapping, the temporal and spatial development of eight active debris-flow fans is reconstructed in six time intervals from 1947, 1952, 1971, 1979, 1987, 2000 and 2010 and mean annual debris-flow volumes are calculated. These are compared with mean Holocene/Lateglacial debris-flow volumes derived from the most prominent cone, whose contact with the underlying till is revealed by electrical resistivity tomography (ERT). Debris-flow activity there increased by a factor of 10 from 1947-1952 (0.23 ± 0.07 $10^3 m^3/yr$) to 1987-2000 (2.41 ± 0.66 $10^3 m^3/yr$). Mean post-1980 rates from all eight fans exceed pre-1980 rates by a factor of more than three coinciding with an enhanced rainstorm activity recorded at meteorological stations in the Northern Calcareous Alps. The frequency of rain storms (def. 35 mm/d) has increased in the study area on average by 10% per decade and has nearly doubled since 1921. Recent debris-flow activity is also 2-3 times higher than mean Holocene/Lateglacial rates. The strong correlation between the non-vegetated catchment area and the annual debris-flow volume might indicate a decadal positive feedback between enhanced rainstorm activity and debris flows. Here we investigate the temporal and spatial development of debris-flow fans to better understand the sensitivity of alpine catchments to heavy rainfall events in the context of climate change.

4.2 Introduction

Debris flows are continuously deforming, fast moving landslides of predominantly coarse loose material on slopes and in steep channelized torrents (Varnes, 1978). They occur in all alpine regions due to intensive rainstorms and mobilisable loose debris. From 1950 to 2011 almost 80.000 people lost their lives through the occurrence of debris-flow events (Dowling and Santi, 2014). Consequently, many countries are faced with the construction of appropriate countermeasures. As debris-flow fans store a record of recent and past events, their history is a key requirement for hazard management. Most case studies have concentrated on the potential mobilisable sediment volume for a single event, but they often ignore the long term dynamics of fans and sediment supply. Debris-flow magnitudes correlate generally with the size of the catchment area (Franzi and Bianco, 2001, Takei, 1984, Zeller, 1985), the slope angle of the torrent (D'Agostino *et al.*, 1996, Kronfellner-Kraus, 1984, Rickenmann, 1995, Rickenmann and Koschni, 2010) or geologically (lithologically) related factors (Bianco *et al.*, 2001, D'Agostino *et al.*, 1996, Rickenmann and Koschni, 2010), as the erodibility as well as the availability and production of loose debris varies in different lithologies. Publications suggest simple relationships but their explanatory power and accuracy is limited as they are strongly biased by the environment in which they were derived (Marchi and D'Agostino, 2004).

Besides the analysis of historical records (Marchi and Cavalli, 2007, Marchi and Tecca, 2006), a variety of methods has been used to investigate the temporal development of debris-flow activity. For dating debris flows on larger time scales, ^{14}C dating of organic matter involved in the process is applied (Matthews *et al.*, 2009) and rarely ^{3}He (Cerling *et al.*, 1999). For more recent debris flows, growth disturbances in century-old trees (Bollschweiler and Stoffel, 2010b, Bollschweiler *et al.*, 2007, Saez *et al.*, 2011, Schraml *et al.*, 2013, Stoffel, 2010, Stoffel *et al.*, 2008), orthophoto reconnaissance (D'Agostino, 2013, Helsen *et al.*, 2002, Lang *et al.*, 1999, Procter *et al.*, 2011, Procter *et al.*, 2012) or lichenometric dating is applied (Helsen *et al.*, 2002, Winchester and Harrison, 1994). However, most of these studies rather target debris-flow recurrence rates, whereas this study quantifies the volume of mean annual debris-flow transport and compares it on different time scales.

Some authors have related the global climatic change to a rise of the global temperature with a more frequent occurrence of extreme events in general (Easterling, 2000, Knight and Harrison, 2009, Rebetez *et al.*, 1997, Rosenzweig *et al.*, 2008). In particular, this rise of the temperature causes the melting of glaciers and permafrost in high alpine regions, which can be connected to an increase in debris-flow frequency (Evans and Clague, 1994, Haeberli and Beniston, 1998, Haeberli *et al.*, 1993, Zimmermann *et al.*, 1997). The more frequent occurrence of extreme rainfall events in the 20th century (Cubasch *et al.*, 1995, Frei and Schar, 1998, Fuhrer *et al.*, 2006) may lead to an enhanced frequency of landslides in general (Beniston and Douglas, 1996) and debris flows in particular (Pelfini and Santilli, 2008). Sass *et al.* (2007) reported a five-fold increase in debris-flow transport from the 19th century 103 (±87) m³/yr to 20th century 489 (±87) m³/yr in the Reintal (Northern Calcareous Alps). In contrast, some authors hold the opinion that debris-flow activity has decreased in parts of the Alps since 1980, especially in areas

below the permafrost zone (Jomelli *et al.*, 2003, Jomelli *et al.*, 2007, Jomelli *et al.*, 2004). Regarding this discussion, the study will contribute to a better understanding of the activity of debris flows by presenting a case study from the Austrian Alps.

This article investigates debris-flow activity in the very well constrained and highly active Plansee area to answer the following questions. (i) How can we interpret air photography time series in terms of mean annual debris-flow activity? (ii) How did mean annual debris-flow transport change from 1947 to 2014? (iii) How do present rates relate to mean Holocene/Lateglacial debris-flow transport rates? (iv) Can we see a significant increase in debris-flow activity coincident with the enhanced rainstorm frequency?

4.3 Methodology

4.3.1 Orthophoto analysis

Official archives contained areal orthophotos for the dates from 13.09.1947, 01.07.1952, 10.07.1971, 17.09.1979, 31.08.1987, 24.08.2000 and 01.08.2010 with a varying raster resolution (Table 3). For the analysis of the photos, ArcMap 10.1 was used. We examined (i) on which parts of the fans new debris-flow deposits could be identified for each time period; (ii) the extent of new debris-flow deposition areas; (iii) the decrease or increase in vegetation on fans and catchments. For (iii) we conducted an image classification in ArcMap 10.1 with two classes (vegetated and non-vegetated area) for the classification. For each of the two classes several training samples in a photo were chosen. This ensured capture of all possible colour variations within each class. ArcMap detected the colour-values of each pixel of the training samples on each band of the photo (each photo is a 3-band raster image). The software automatically classified each pixel into one of the two classes by a maximum likelihood classification. Areas with shadows were assigned manually into one of the classes, as the software could not distinguish whether a shadowed area was vegetated or not. As the colour varies in the seven photos, this classification was done for each orthophoto separately. With the help of the orthophotos, the investigated depositions in the field could be matched into specific time intervals for dating.

Table 3: Raster resolution (cell size) of each orthophoto.

Date of the orthophoto	Cell size of raster (x;y) [m]
1947	0.75; 0.75
1952	1.61; 1.61
1971	1.54; 1.57
1979	2.34; 2.34
1987	2.43; 2.43
2000	1.20; 1.20
2010	0.50; 0.50

4.3.2 Geomorphological mapping of debris flows and associated phenomena

Figure 24: a) Differentiation of debris flows bye the colour of the debris. The younger debris flow shows a lighter colour than the older one. b) Close-up of an age-induced colour break of Hauptdolomit debris-flow sediments (left: event between 1988 and 2000; right: event between 2001 and 2014). c) Plan curvature map indicates debris-flow channels (dashed lines).

In the field, evidence for recent debris flows was examined in the channels and on the fans. A detailed field map (scale 1:1000) with the following features was created, to identify sediments as debris-flow deposits: (i) scarps, (ii) levees in the channel and on the fan, (iii) damaged vegetation, (iv) lobate margins, (v) accumulation of coarse clasts at the margins, (vi) poorly sorted, randomly oriented sediments with wood fragments, (vii) convex surface morphology and (viii) steep incised channels. The channels were investigated uphill as far as possible. Field mapping was supported with a 1 m resolution digital terrain model (Land Tirol, 2006), georeferenced photos and historical postcards.

Besides the historic aerial photos mentioned in Chapter 3.1, the colour of the sediments and the intensity of vegetation cover were qualitative indications in the field of their age. A few years after debris-flow sedimentation, the colour of the sediment darkens (i.e. Hauptdolomit turns grey a few years after deposition (Friedel, 1935)) and plant succession and tree growth set in (Figure 24a,b). Levees and lobate margins of older events could be preliminarily identified by using the plan curvature of the terrain in ArcMap 10.1 (Figure 24c). All deposits were compiled into a digital map of the study area.

4.3.3 Quantification of sediment budgets of debris flows using empiric formulas and geophysics

4.3.3.1 Quantification of the Holocene/Lateglacial debris-flow volume supported by ERT

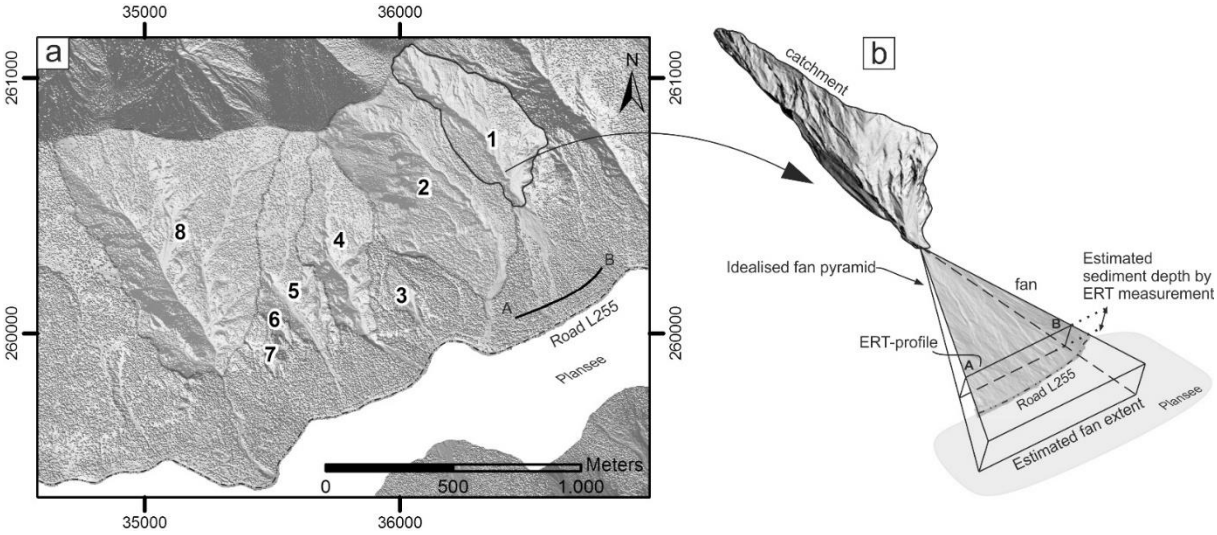

Figure 25: a) Location of the electrical resistivity tomography profile on Fan 1 shown on a DTM. Length of the profile is 400 m with ends A and B. b) Visual plot of the Holocene/Lateglacial debris-flow volume of Fan 1 by a pyramid. The sediment depth is interpreted by the ERT results. Data basis: Region of the Tyrol (2006).

In order to quantify the entire Holocene/Lateglacial debris-flow volume of Fan 1, an electrical resistivity tomography (ERT) was carried out (Figure 25a) to delimit the basal contact of a debris flow with the underlying till. ERT was measured with an ABEM SAS 1000 with 81 electrodes and equal spacings of 5 m, resulting in a total profile length of 400 m. Data were processed using Res2DInv using mesh refinement and robust inversion to allow a better inversion progress in view of the material boundary between high resistivity debris-flow material and low-resistivity underlying material. The inversion process was controlled using uncertainty plots based on a model covariance matrix (Alumbaugh and Newman, 2000). Comparing Wenner and Schlumberger arrays we yielded an ERT with high resolution of more than 850 apparent resistivity datums with a sharp (>4 fold) resistivity transition at the inferred transition between moraine and debris-flow material. The measured sediment depth of the ERT was translated into a pyramid to estimate the entire sediment volume of Fan 1 (Figure 25b) (Siewert *et al.*, 2012). The extent of the fan was extrapolated into the Plansee based on bathymetric data by Hibler (1921).

4.3.3.2 Quantification of recent debris-flow volumes with empiric formulas

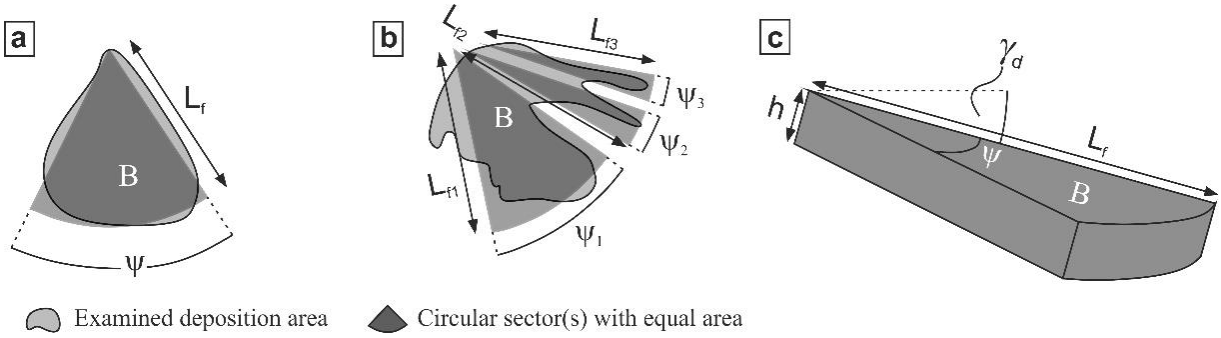

Figure 26: Applied method for calculating recent debris-flow volumes. a) The deposition area is approached by a circular sector. b) Characterisation of smaller debris-flow trajectories leaving the cone (lobes). c) 3D-view; the deposition height is a function of the deposition area and slope of the torrent and fan (modified from Rickenmann and Scheidl (2013)).

While other authors have tried to estimate recent debris-flow volumes by laser scanning (Bremer and Sass, 2012, Jaboyedoff *et al.*, 2012) or photogrammetry (Schwab *et al.*, 2008), we applied the method from Scheidl and Rickenmann (2010). The parameterization of the model used is based on 126 past events in Austria, Italy and Switzerland. We approximated the area of each debris-flow deposit lobe by a circular sector (Figure 26a-c). The deposition area B [m²] was calculated as

Equation 13:

$$B = L_f^2 \cdot \pi \cdot \psi \cdot 1/360°$$

where L_f [m] is the radius and ψ [°] is the angle of the sector.

The empiric mobility coefficient k_b [-]

Equation 14:

$$k_b = 5.07 \cdot y_d^{-0.1} \cdot y_c^{-1.68}$$

is a function of the slope of the channel y_c [-] and the slope of debris-flow fan y_d [-].

The volume V [m³] was calculated as follows:

Equation 15:

$$V = B^{3/2} \cdot k_b^{-3/2}$$

The average depth h [m]

Equation 16:

$$h = V/B$$

could then be calculated from the volume (V) and the deposition area (B).

The method was modified, as smaller debris-flow trajectories leaving the cone (outliers) were described with extra circular sectors, which result in lower height values (see Figure 26b). These estimated height values were proofed in field work where possible and seem to better match reality. In the given times intervals (e.g. in 1947-1952, 1953-1971, 1971-1979), we could only estimate the mean annual transport, because the differentiation into single events within one time period was not always possible. Thus, the method was applied to quantify the volume of the deposits of one complete time interval. For the

computation of the volumes, the slopes of channels and fans were assumed to be constant over recent decades. The slope of the fan γ_d was determined by using the highest point of the fan and a point at road level, as specific information for the deepest point below water surface of the Plansee were not available. The slope of the torrent γ_c was defined by a point in the catchment, at which a channelised flow could be firstly observed, and the lowest point of the fan (Schraml *et al.*, 2013). For an error calculation the slopes of both fans and channels were varied by ± 3° in each time interval.

4.4 Study site

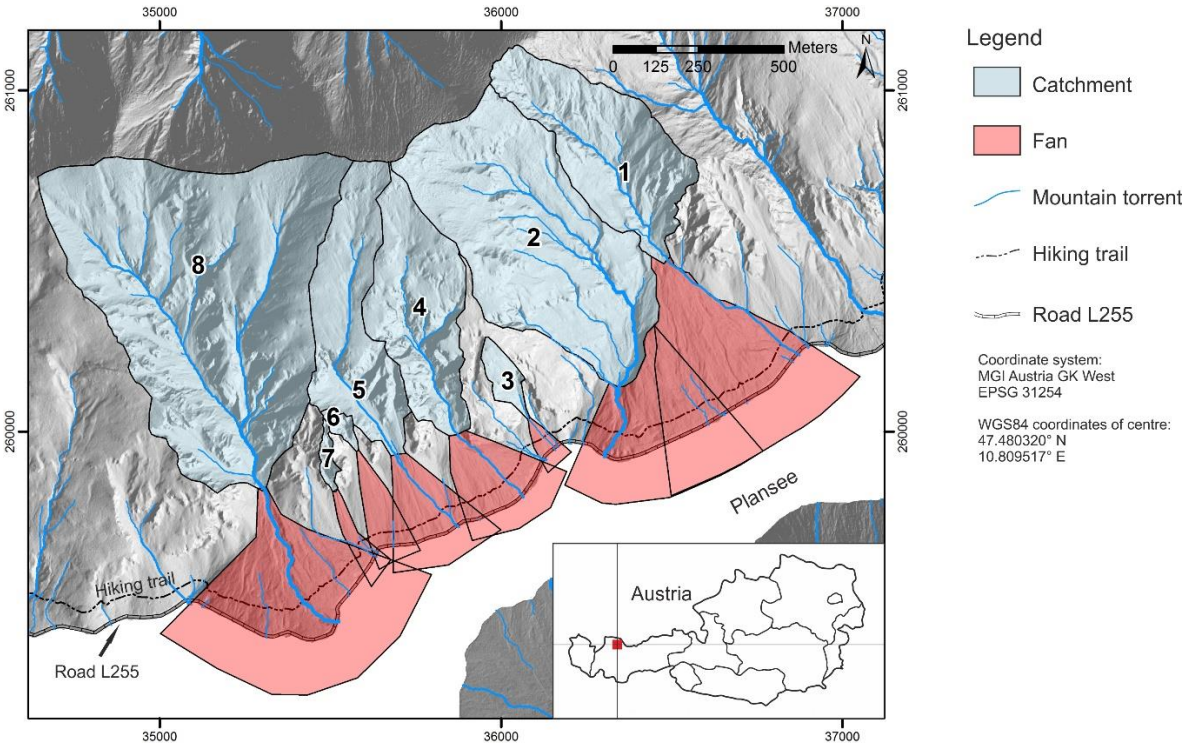

Figure 27: Debris-flow fans and corresponding catchments (Nr. 1 to 8) on the north side of the Plansee. Catchments are highlighted in blue, fans in red colour. The road L255 leads along the north side of the lake, the hiking trail lies about 50 m above. Data basis: DEM for hillshade provided by Region of the Tyrol (2006).

The investigated debris-flow fans and their catchments are located on the north side of the Plansee in the federal state Tyrol in western Austria (Figure 27). The catchments shown (1-8) are delineated automatically from the digital elevation model. The fans are extrapolated manually into the Plansee, based on depth-profiles from Hibler (1921). The road L255 and a hiking trail lead along the north side of the lake (Figure 27) and are therefore endangered by gravitational natural hazards. In recent decades, the road has been blocked several times by debris flows. The bedrock of the examined catchments in the Northern Calcareous Alps consists exclusively of Upper Triassic so-called “Hauptdolomit” (i.e. Main Dolomite) with varying content of organic matter (Ampferer, 1924, Ampferer and Ohnesorg, 1924) and is the most important source of massive debris flows in the Northern Calcareous Alps. The fine-crystalline dolomite was deposited in shallow water facies and lagoons in the Norian (225-206 myr). During the orogenesis of the Alps, the Hauptdolomit was mechanically stressed and intensely jointed at a cm-dm-scale resulting in a massive creation of Quaternary dolomite detritus (Bayerisches Geologisches Landesamt, 1996).

The catchments and their corresponding fans are located at heights between 975 m and 1740 m asl. Fan areas range from 0.01 - 0.17 km² (projected area) with average slopes from 15° to 35° (Table 4). Catchment areas vary from 0.01 - 0.57 km² (projected area) with average channel slopes from 26° to 39° over channel lengths from 100 to 1000 m. The annual precipitation reaches 1700 mm with a pronounced summer rainstorm precipitation maximum (BMLFUW, 2011).

Table 4: Basic parameters of the investigated torrents and fans. Areas are given as projected areas.

Parameter	Unit	Catchment/Fan							
		1	2	3	4	5	6	7	8
Slope of the fan	°	23	15	35	28	26	32	25	16
Slope of the channel	°	30	30	38	31	33	39	38	26
Fan area	km²	0.17	0.1	0.01	0.05	0.05	0.03	0.01	0.12
Catchment area	km²	0.16	0.34	0.02	0.15	0.15	0.01	0.01	0.57
Channel length	m	1000	1000	150	600	400	100	130	800

4.5 Results

4.5.1 Orthophoto analysis

The ArcMap image classification concerning vegetation loss and increase in the entire project area of all seven orthophotos is shown in Figure 29. The relative proportion of the vegetated and non-vegetated areas was computed (Table 5). The vegetated area increases from 1947 to 1952, followed by a slight decrease until 1987 and heavily decreases between 1987 and 2000. From 2000 to 2010 the vegetation increases by 10.8%.

Table 5: Change in vegetation cover (entire project area). Positive values show an increase in vegetation, negative values a decrease in vegetation.

	1947*	1952	1971*	1979	1987	2000	2010
Vegetated area [10^3 m²]	1,822	1,827	1,798	1,779	1,736	1,493	1,710
Non-vegetated area [10^3 m²]	185	181	209	228	271	515	298
Change in vegetation cover to previous photo (whole project area) [%]		+1.5	-1.4	-1.0	-2.2	-12.1	+10.8

* The area with no data was added to the vegetated area (as it is mostly vegetated in the previous and following photo)

Due to the great extent of the entire project area, a detailed orthophoto analysis is shown on Fan 1 (Figure 28 and Table 6). On all other fans the analysis was performed in the same way. The orthophotos show the results of the processes on Fan 1 from 1947-2010. The extent of the debris-flow deposition areas was identified and the increase or decrease was assessed. From 1947 to 1987 only two debris-flow channels (DFC1&2) existed (Figure 28). From 1987 to 2000 a new channel (DFC3) formed in the north-east of Fan 1. In the time between 2000 and 2010 another new channel (DFC4) developed between DFC 2 and DFC 3.

Table 6: Chronology of the geomorphological development concerning debris-flow activity on Fan 1.

Debris-flow channel (DFC)	Time interval					
	1947-1952	1953-1971	1972-1979	1980-1987	1988-2000	2000-2010
DFC1	decreasing deposition area, increasing vegetation	decreasing deposition area, increasing vegetation	increasing deposition area in upper areas, decreasing in lower areas	increasing deposition area, decreasing vegetation	increasing deposition area, decreasing vegetation	decreasing deposition area, increasing vegetation
DFC2	increasing deposition area in upper areas, decreasing in lower areas	increasing deposition area in upper areas, decreasing in lower areas	increasing deposition area, decreasing vegetation	± unchanged deposition area and vegetation	± unchanged deposition area and vegetation	slightly increasing deposition area*
DFC3					**Newly formed**	decreasing deposition area, increasing vegetation
DFC4						**Newly formed**

* after field surveys a reactivation of DFC2 between 2010 and 2014 has been additionally observed

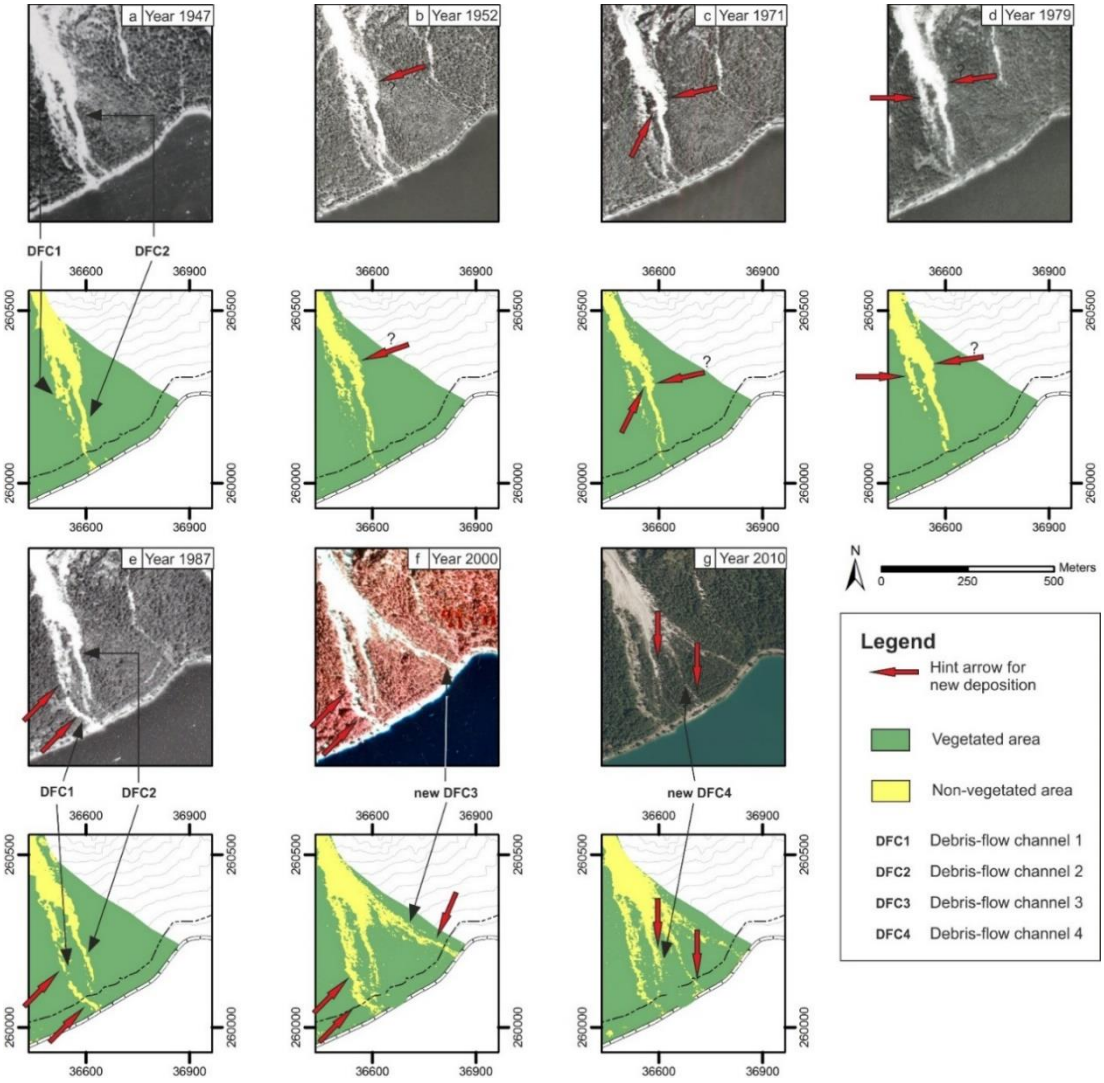

Figure 28: Chronology of the geomorphological development concerning debris-flow activity on Fan 1.

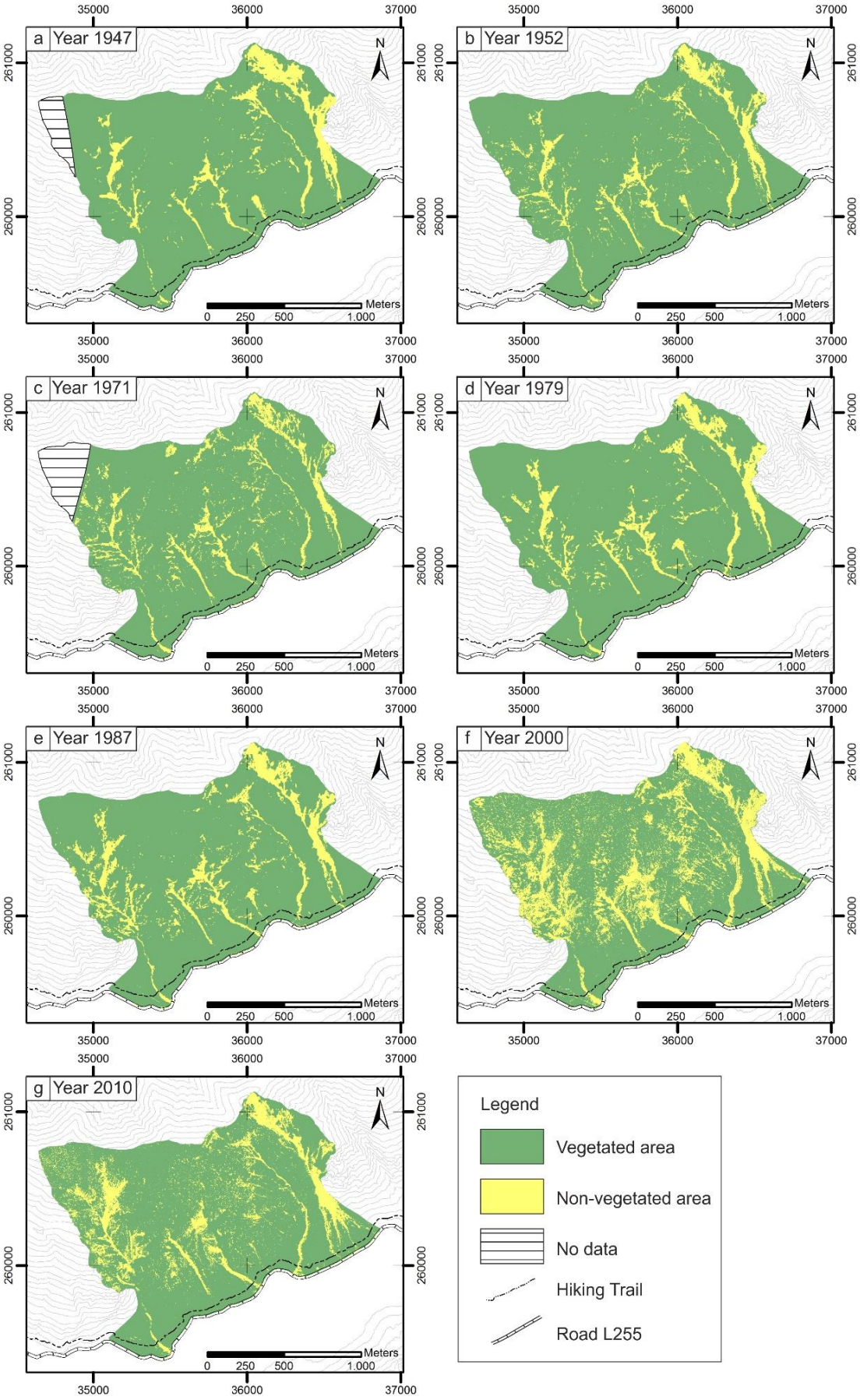

Figure 29: Results of the Interactive Supervised Classification. The highest decrease in the vegetated area (-12%) can be recognised between 1987 and 2000. Green colour indicates vegetated area, yellow colour shows non-vegetated area. For lined areas no data were available.

4.5.2 Mapped debris flows with respect to their period of occurrence

All indices for debris flows, mentioned in Chapter 3.2., were recorded in field (Figure 30). The mapped debris-flow deposits were matched in the field into the time intervals between successive orthophotos. The spatial and temporal appearance of the debris flows is shown in Figure 31. We could observe debris-flow deposits of the last 60 years in all investigated catchments and fans. The most extensive deposits occurred in the time intervals from 1980-1987, 1988-2000 and 2001-2014, with a peak at 1988-2000, especially on Fan 1 and 2.

Figure 30: Field evidence for debris flows. a) Steeply incised channels. b) Levees in a channel (red dashes lines). c) Large boulder. Scale bar is 1 m. Photos: June and July 2014.

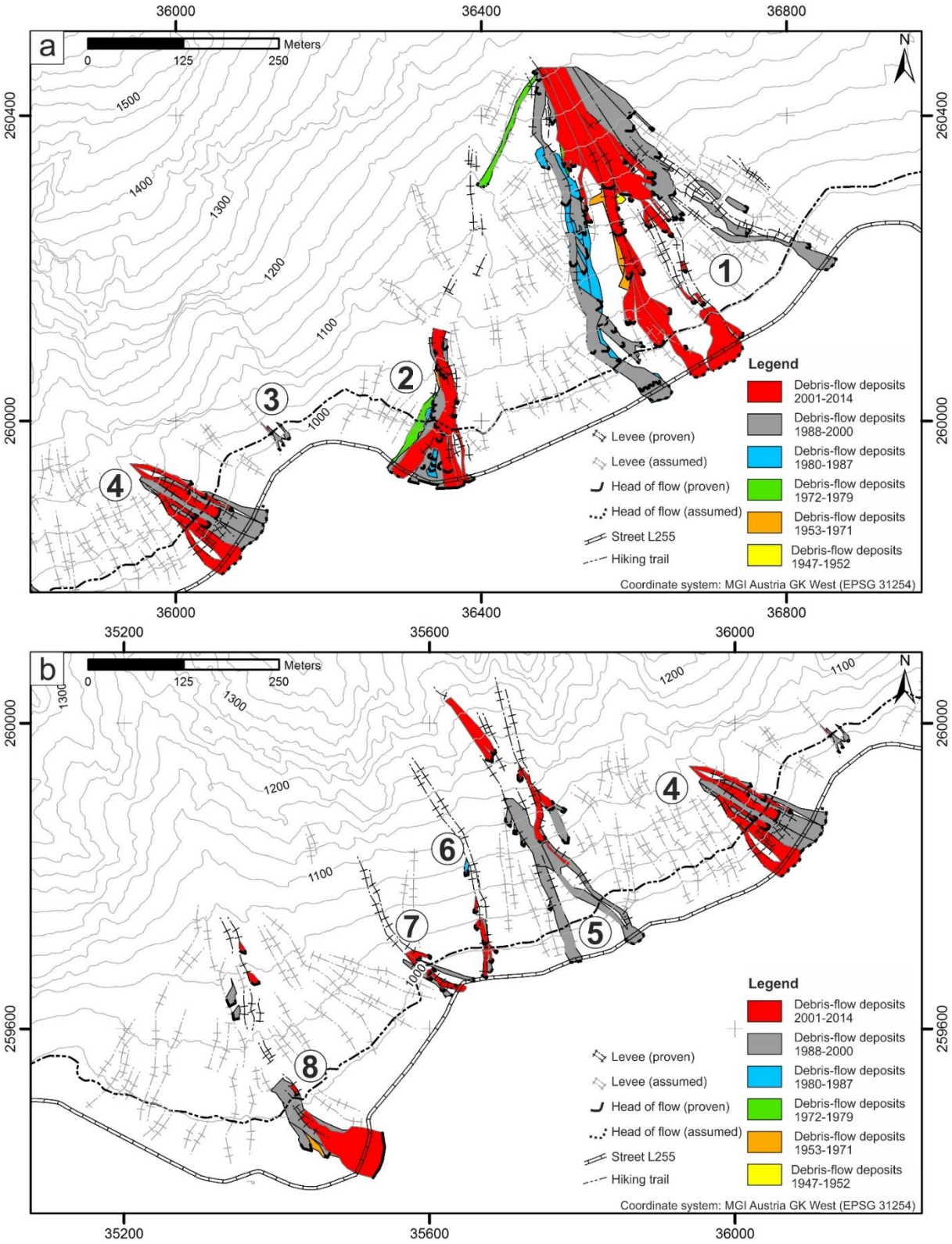

Figure 31: Mapped debris flows with respect to their period of occurrence from 1947-2014. a) Debris flows on Fan 1-4. b) Debris flows on Fan 4-8. Data basis: Region of the Tyrol (2006).

4.5.3 Quantified debris-flow volumes for each time interval using empiric formulas

The quantified volumes are shown in Figure 32. The average thickness of the debris flows (Equation 16) ranges from 0.1 to 1.1 m. All fans show a similar trend: the volume increases until the time interval 1988-2000, followed by a slight decrease in 2001-2014. According to the volumetric equations (Equation 13-Equation 15), the debris-flow volume is directly proportional to its covering area B. This area was approximated by a sector by using the georeferenced field maps and ArcMap 10.1. As slopes vary in space and time, an error of 3° (~5%) for the slopes of channels and fans was assessed. The resulting mobility coefficient k_b ranges from 7.4 ($k_{b\,min}$ Fan 7) to 31.6 ($k_{b\,max}$ Fan 8) (Table 7).

Table 7: Parameters for the volume calculation for all eight fans. $k_{b\,min}$ is gained by using 3° lower slopes for channels and fans, for $k_{b\,max}$ 3° higher slopes.

Parameter	Fan 1	Fan 2	Fan 3	Fan 4	Fan 5	Fan 6	Fan 7	Fan 8
Slope of the fan [-]	0.42 ± 0.05	0.31 ± 0.05	0.7 ± 0.05	0.49 ± 0.05	0.49 ± 0.05	0.62 ± 0.05	0.47 ± 0.05	0.28 ± 0.05
Slope of the torrent [-]	0.51 ± 0.05	0.44 ± 0.05	0.75 ± 0.05	0.55 ± 0.05	0.62 ± 0.05	0.7 ± 0.05	0.78 ± 0.05	0.42 ± 0.05
$k_{b\,min}$ [-]	14.4	18.4	7.6	12.6	10.5	8.5	7.4	20.0
$k_{b\,avarage}$ [-]	17.1	22.6	8.5	14.9	12.2	9.7	8.3	24.7
$k_{b\,max}$ [-]	20.8	28.5	9.7	17.8	14.3	11.1	9.4	31.6

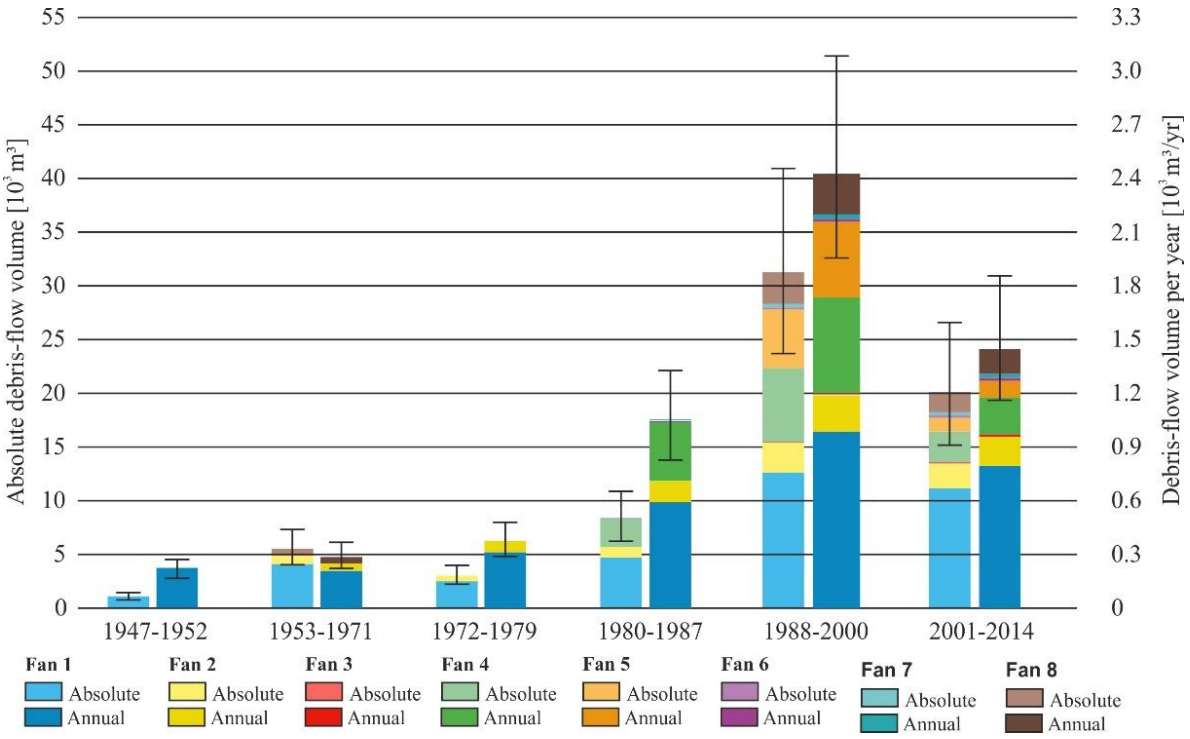

Figure 32: Absolute (left column) and annual (right column) debris-flow volumes for each fan and each time interval (summed up). Both increase until 2000, followed by a decrease. Fan 1 is contributing a major part to the total volume.

In Figure 32, the absolute and annual debris-flow volumes from all eight fans are summed up for the six time intervals. The annual debris-flow transport is quasi-constant or increases slightly from 1947 (0.2 ± 0.07 $10^3 m^3/yr$) to 1979 (0.4 ± 0.1 $10^3 m^3/yr$). During the years 1980 to 2000 a heavy increase from 1.1 ± 0.3 $10^3 m^3/yr$ to 2.4 ± 0.7 $10^3 m^3/yr$ can be observed. Afterwards the annual volume per year decreases to 1.4 ± 0.4 $10^3 m^3/yr$. While rates before 1980 range between 0.2-0.4·10^3 m^3/yr, rates after 1980 range between 1.1-2.4·10^3 m^3/yr, on a more than three-fold elevated level.

These results coincide with the data on the non-vegetated part in the catchment area (Figure 33). The higher the annual debris-flow volume per year in a time interval the larger is the non-vegetated area in the catchment at the endpoint of the period.

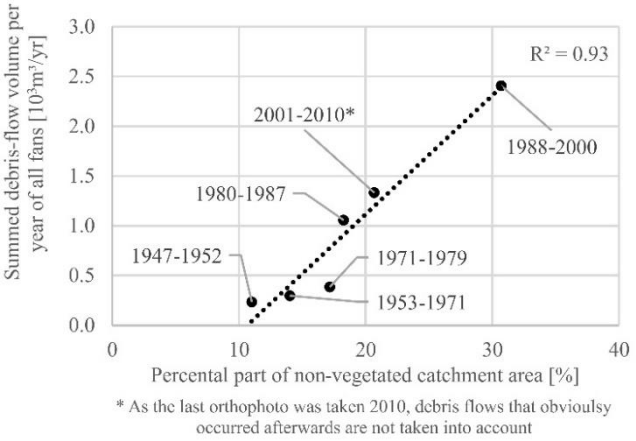

Figure 33: Relationship between annual debris-flow volume (of all eight fans, summed up) and non-vegetated catchment area (at the end of each time interval).

4.5.4 Holocene/Lateglacial debris-flow volume of Fan 1 quantified with ERT

The Holocene/Lateglacial debris-flow volume of Fan 1 was approximated by a geometric approximation of its surface shape, its bathymetry and a delineation of the contact with the underlying morainic till using electrical resistivity tomography (Figure 34a,b). At a depth of 5 to 20-30 m, the electrical resistivity ranges from 1,000 to 4,000 Ωm in debris-flow material. Below 20-30 m, the values suddenly decline by a factor of four or more to 200 to 800 Ωm. Analysing Min and Max-Plots of the ERT uncertainty based on a model covariance matrix (Alumbaugh and Newman, 2000) indicates that this transition depth is only subject to small changes due to the high amount of resistivity datums indicating this transition (Figure 34b).

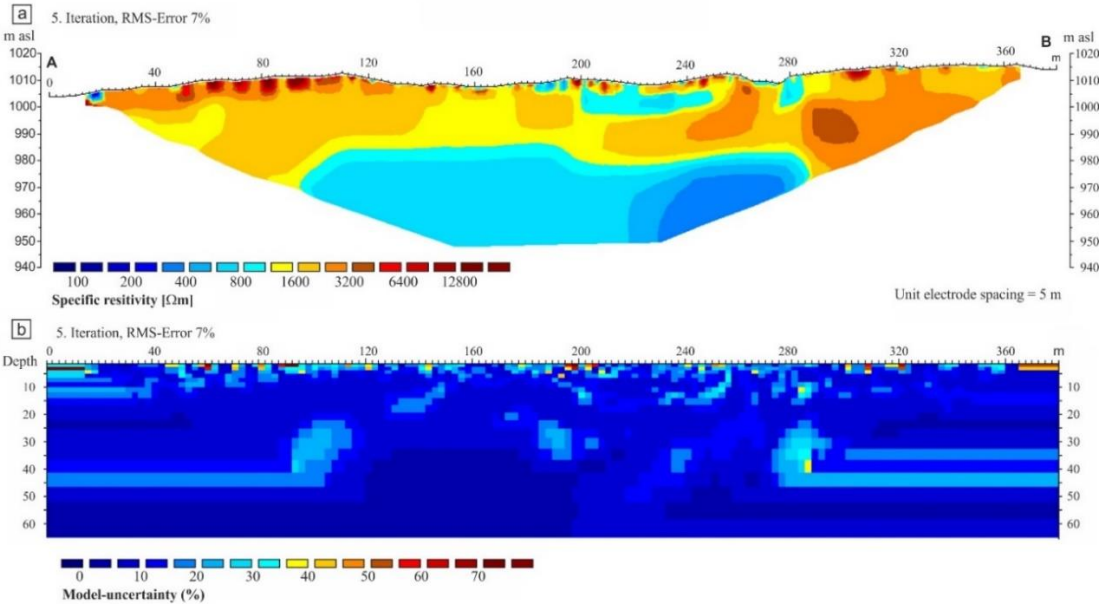

Figure 34: a) ERT of Fan 1 indicating a transition of resistivity values of 1,000-4,000 Ωm above 980 m asl to 200-800 Ωm below interpreted as the transition to local basal till. b) The model uncertainty is mostly below 10% especially at the inferred transition.

We interpret the results as follows. The sediments with a high resistivity in the upper 25 meters are debris-flow dolomite material. At depths greater than 25 m (below 985 m asl), we infer basal local till containing also carbonates but a much higher share of fine materials. The measurement coincides with additional long ERT transects we have performed outside the study site at the opposite lake side of the Plansee and the descriptions of Ampferer (1907) and Hibler (1921).

To estimate the Holocene/Lateglacial debris-flow volume, an idealised pyramid was built using the information of the ERT (Figure 35). The depth of the debris-flow sediments was inter- and extrapolated with the mean dolomitic detritus depth in the ERT (Figure 34). The Holocene/Lateglacial time period available for debris-flow sedimentation is approximated with 14,000 ± 1,000 years (Prager *et al.*, 2008). The mean Holocene volume $V_{Mean\ (Holocene)}$ is 0.35 (±0.03)·10^3 m^3/yr. This value rather overestimates Holocene rates as Lateglacial rates are included (Krautblatter *et al.*, 2012, Sass and Krautblatter, 2007).

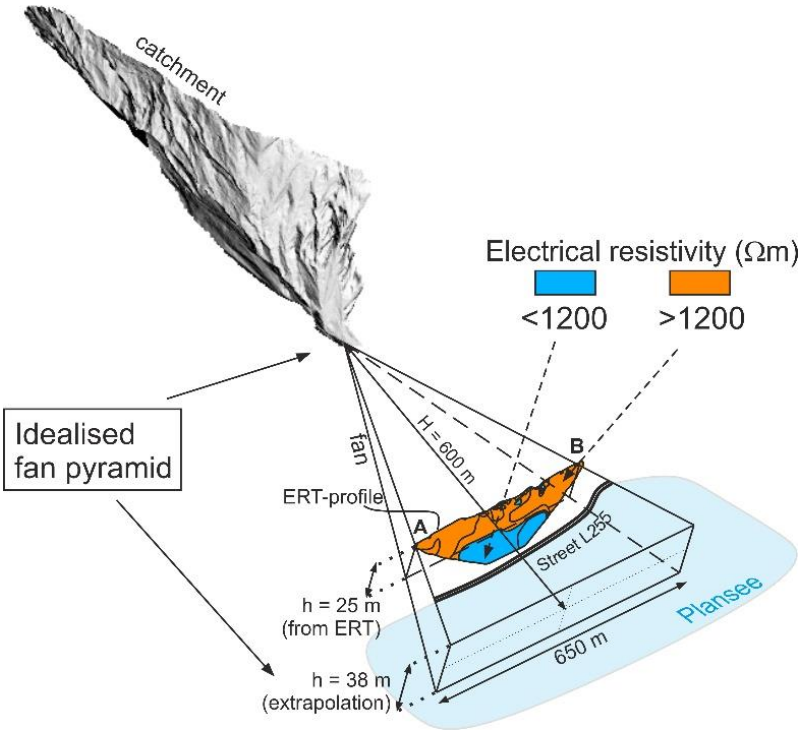

Figure 35: Volume assumption of the Holocene/Lateglacial debris-flow fan using the depth information of the ERT. For the calculation of the depth, the resistivity higher than 1,200 Ωm was taken into account. Values <1,200 Ωm were interpreted as till. Data basis for the catchment: Region of the Tyrol (2006).

4.5.5 Comparison of recent and Holocene/Lateglacial mean debris-flow volumes

The estimated mean annual Holocene/Lateglacial debris-flow volume is about 0.35·10^3 m^3/yr on Fan 1. In Figure 36 the minimum and maximum values of the mean annual Holocene/Lateglacial volume is compared to the mean annual debris-flow volumes of recent decades. From 1947-1979 the estimated volume in the time periods lies below or near that interval, from 1980 to 2014 considerably above the range of the mean annual Holocene/Lateglacial volume.

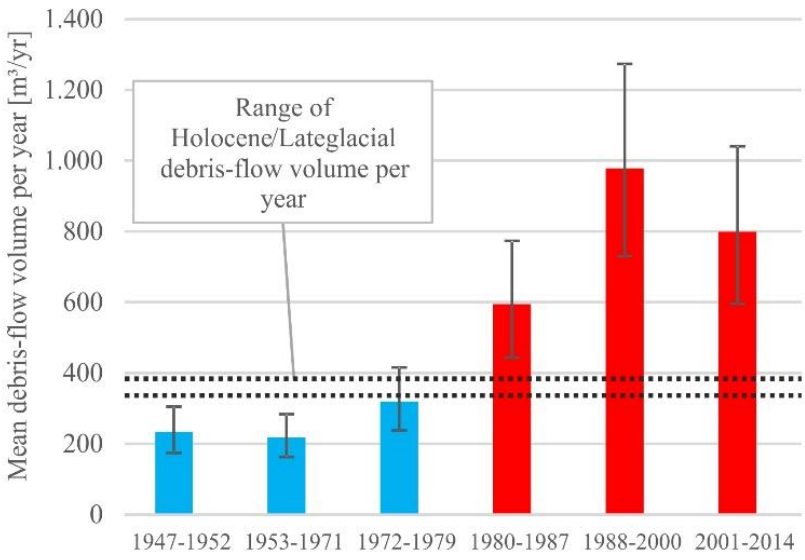

Figure 36: Comparison of the range of the mean annual Holocene/Lateglacial debris-flow volume and the annual volumes of the recent decades on Fan 1. The dashed lines represent the range of the annual Holocene/Lateglacial volume. Before 1980 (blue bars) the annual volume is lower than the annual Lateglacial volume. Since 1980 (red bars) the annual volumes exceed the annual Lateglacial volume.

4.6 Discussion

4.6.1 Historic orthophoto analysis and geomorphological mapping

Detailed mapping of the catchments and fans is a prerequisite for making reliable statements in terms of debris-flow ability, activity and risk assessment (Hearn and Hart, 2011, Theler *et al.*, 2010). Due to the orthophotos, the active parts of the project area could be preliminary identified by field work, although the resolution and contrast of the photos caused some problems. The image classification concerning vegetated and non-vegetated areas (Figure 29 and Figure 28) was run several times with different brightness, contrast and gamma values to get reliable results. Nevertheless, the interpretation of the activity was not completely clear on some orthophotos (e.g. Figure 28). But the long-term activity of all fans concerning larger events in space and time could be reconstructed.

The estimation of the areal extent of former debris flows by orthophoto analysis caused certain challenges: i) Minor flows that affected only ground near vegetation but no larger trees caused no obvious change in two successive orthophotos but probably have small volumes. (ii) Small flows that did not manage to leave pre-existing channels or did not change the colour of the sediments in them, were hard to identify but probably also have small volumes. Consequently, our database contains events larger than few tens of m³ and represents a minimum mean rate. This underestimation of high-frequency and low-volume events is also postulated by other authors (Bollschweiler and Stoffel, 2010a, Helsen *et al.*, 2002, Mayer *et al.*, 2010, Stoffel *et al.*, 2013). Information on former flows that could not be seen on the photos was in most cases obtained by field survey and then checked against the orthophotos. In this way, we support the hypothesis of Procter *et al.* (2011) and (Procter *et al.*, 2012) that carefully analysed and validated air photography is a valuable source for the historic interpretation of former debris-flow activity.

4.6.2 Quantified debris-flow volumes in the time periods using empiric formulas

4.6.2.1 Parameters for the semi-empirical volume estimation

The mean coefficient k_b ranges in this study from 8.3 to 24.7 (Table 7). The steeper the slope of the torrent and fan, the smaller is the value for k_b. Thus, k_b is a function of the friction angle, as material with a higher friction angle can develop steeper fans, as well as a function of activity, as the gradient of a fan gets normally lower with each event. The mean for k_b for all fans is 14.8. Table 8 compares the gained k_b with other authors (Crosta *et al.*, 2003, Griswold, 2004, Iverson *et al.*, 1998, Scheidl and Rickenmann, 2010). Granular debris flows normally show a k_b in the range of 6-30 (Table 8). Thus, the calculated k_b values in this study ranging from 8.3 to 24.7 are representative.

Table 8: Calculated values for the factor k_b for different regions and flow types (adapted from Scheidl and Rickenmann (2010)). The values in this study are in the range of previous studies.

Author	Process	Region	N	$k_{b\ (avarage)}$
Crosta *et al.* (2003)	Granular debris flow	Alps, Northern Italy	91	6.2
This study	Granular debris flow	Alps, Tyrol	8	14.8
Scheidl and Rickenmann (2010)	Granular debris flow	Alps, South Tyrol	44	17.3
Griswold (2004)	Debris flow	Worldwide	44	19.9
Scheidl and Rickenmann (2010)	Granular debris flow	Alps, Switzerland	34	28.1
Iverson *et al.* (1998)	Lahar	USA, Columbia, Philippine	27	200

4.6.2.2 Comparison of annual debris-flow volumes among the different fans

By comparing the annual debris-flow volumes of all fans, it shows that the activity of Fan 1 is considerably higher than the other fans and represents almost half of the summed up volume (Figure 32). The reasons for larger debris-flow volumes can be connected with a larger catchment area (Franzi and Bianco, 2001, Takei, 1984, Zeller, 1985), a higher slope angle of the torrent (D'Agostino *et al.*, 1996, Kronfellner-Kraus, 1984, Rickenmann, 1995, Rickenmann and Koschni, 2010) or geological-ly/lithologically induced factors (Bianco *et al.*, 2001, D'Agostino *et al.*, 1996, Rickenmann and Koschni, 2010). But neither the catchment area nor the torrent slope angle are obviously larger or higher than in the adjacent similar catchments (Figure 37a,b). A better correlation can be seen with the channel length, slope of the fan and slope of the torrent (Figure 37c). But for Fan 1 the ratio of non-vegetated area and the total area of the catchment (*R*) is clearly higher than in the other catchments. This ratio increases due to (shallow) landslides or extensive erosion of areas with low plant cover. This is again based on geological factors, like joint spacing, glacial fillings with Quaternary deposits, slope of hillsides, etc. So, the ratio (*R*) results in combination with the channel length in the best explanation for higher annual debris-flow volumes (Figure 37d). Furthermore, the local variability of rainfall intensity in the project area and the exposure of the catchments to rainfall contributes also to an enhanced debris-flow occurrence in the catchments.

Similar results with respect to the correlation between *R* and annual debris-flow volume per year also apply for the entire project area (Figure 33) for the same reasons. Following this result, we constitute, that geological factors and the channel length are not sufficiently considered in formula-based estimations of debris-flow volumes for a study area, both for a single event and regarding mean annual volumes and should be addressed in future research in other areas.

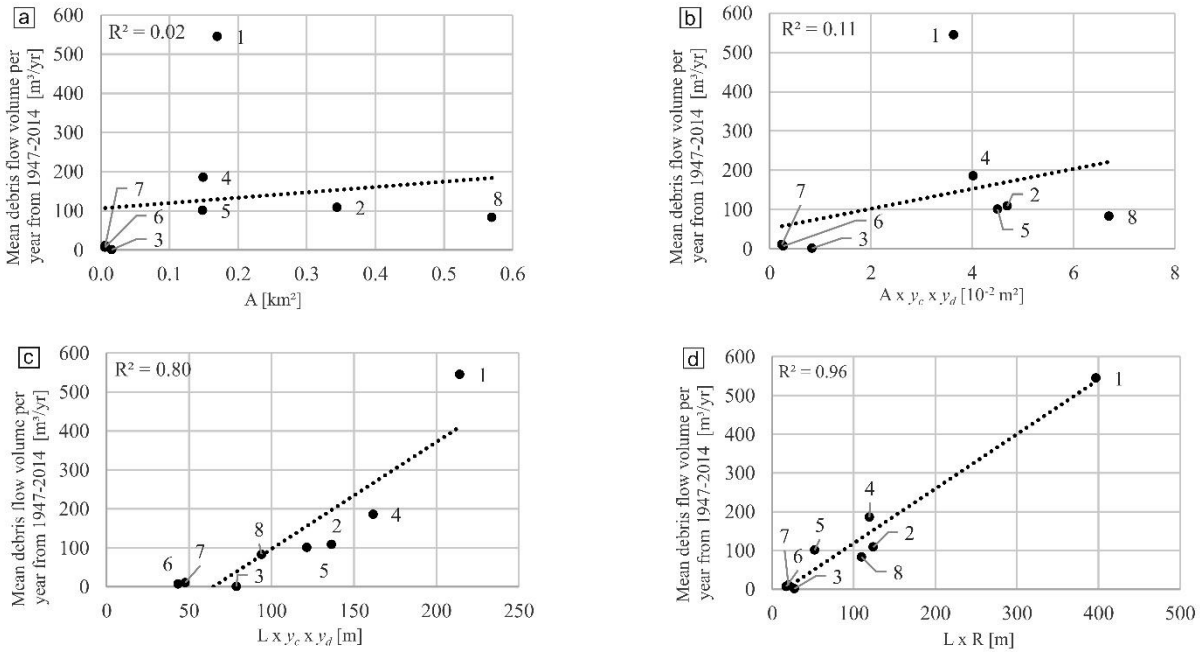

Figure 37: Relationship between annual debris-flow volume per year (1947-2014) of all fans (numbered 1 to 8) and different catchment parameters. The best correlation can be achieved by relating the mean annual debris-flow volume per year and the ratio of non-vegetated area and the total area of the catchment times the channel length (d). The mean debris-flow volume per year from 1947-2010 is plotted: a) vs. catchment area (*A*), b) vs. catchment area (*A*) x slope of fan (y_d) x slope of torrent (y_c), c) vs. channel length (*L*) x slope of fan (y_d) x slope of torrent (y_c), d) vs. channel length (*L*) x ratio of non-vegetated area and total area of the catchment, averaged from 1947-2010 (*R*).

4.6.2.3 Comparison of the total volumes in the time intervals

The results presented in Figure 32 show an increase in absolute and annual debris-flow volumes and an enhanced frequency since the 1980s on all eight fans. Analogous results, with event peaks between the years 1990 and 2000, are documented in other parts of the European Alps (Pavlova *et al.*, 2014, Procter *et al.*, 2011, Schraml *et al.*, 2013). Bollschweiler and Stoffel (2010a) show in the Zermatt valley also an increase since 1950 until 2000 and a following reduction of debris-flow activity until today using dendrogeomorphological analysis. In these studies, there will be a bias, as events prior to 1980 are not well documented and smaller events can hardly be seen by an orthophoto analysis and also in field, if the deposits have been buried by later debris flows. But all large and relevant events are taken into account in this study.

Debris flows are often triggered by intensive rainfalls within a few minutes to a few hours (Caine, 1980, Guzzetti *et al.*, 2008, Johnson and Rodine, 1984, Kaitna *et al.*, 2013). However, most intense summer precipitation in the last decades has often coincided with certain weather patterns and storm trajectories like the Vb (according to the van Bebber classification) bringing wet air from the Mediterranean Sea to the Northern Alps causing some of the most intense debris-flow seasons such as in 2002 and 2005

(Krautblatter and Moser, 2009, Morche and Schmidt, 2012). Figure 38a shows the daily precipitation sums of the nearest meteorological station (Berwang, distance 8 km) from 01.01.1921 to 31.12.2010. There were two outstanding rainfall events in recent decades. The first one occurred on the 21.05.1999 (which developed into the so-called Whitsun-flood, 180 mm/d) and the second on the 22.08.2005 (131 mm/d). On both dates, the occurrence of large debris flows in the Plansee area is confirmed. This might be a reason why we estimate higher debris-flow volumes from 1988-2000 and 2001-2014. Besides these two extreme events we can also see a general trend in the time series (Figure 38b). The occurrence of heavy rainfall events at ten year intervals shows an increase in their relative frequency. While the daily mean precipitation also increases in the time intervals (Figure 38c, black bars), the relative frequency of days with precipitation (> 0.05) mm decreases (Figure 38c, grey bars). If we take this development into consideration, the higher frequency of extreme rainfall events may have caused the increase in mean annual debris-flow volumes.

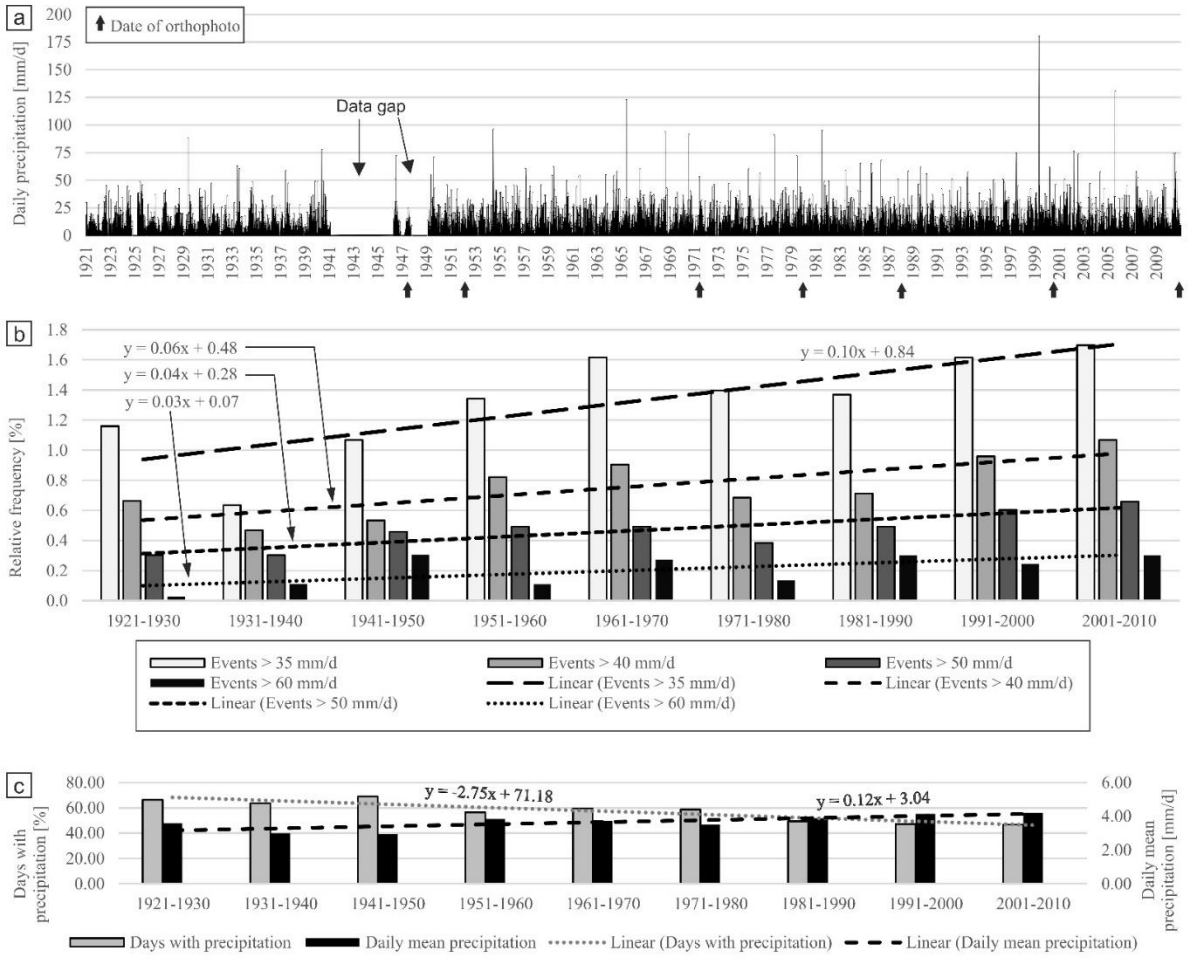

Figure 38: a) Daily precipitation sums of the nearest meteorological station "Berwang" (Hydrographischer Dienst Tirol, 2014). Black arrows indicate the dates of the orthophotos. b) Relative frequency of heavy rainfall events in ten year intervals with different intensities. All linear regression models have a positive slope and indicate an increasing frequency of heavy rainfall events. c) Relative frequency of days with precipitation > 0.05 mm (grey bars) and daily mean precipitation (black bars).

Consequently, the question arises, whether these extreme rainfall events can be linked to climate change. It is beyond all doubt that climate change affects different parts of the Alpine mountain regions in different ways (Beniston *et al.*, 2011, Bohm *et al.*, 2001, Zimmermann *et al.*, 1997) as well as all other parts of the world (Easterling, 2000, Keiler *et al.*, 2010, Knight and Harrison, 2009, Rebetez *et al.*, 1997, Rosenzweig *et al.*, 2008). Besides, an increase in so called Vb-weather conditions, especially since the 1970s, in most alpine parts in Austria can be revealed (Formayer, 2009, Fricke, 2002). These Vb weather conditions often cause circulating intense rainstorms over several days and lead to extreme debris flows, floods and outburst floods. As in the study area the number of days with precipitation decreases but the daily mean precipitation as well as the relative frequency of heavy rainfall events increases from 1921 to 2010, a link to climate change in this area might be indicated.

In a similar steep catchment in the Northern Calcareous Alps Reintal (10 km southern Garmisch-Partenkirchen, Germany) the 2005 Vb rainstorm released a debris-flow volume of >5,300 m³, which infilled a lake and equals the 10 year mean debris-flow activity of the late 20th century at this site (Morche and Schmidt, 2012, Sass *et al.*, 2007). While Sass *et al.* (2007) could show the long-term trend of increasing debris-flow activity since the Little Ice Age and the decadal impact of single rainstorms, the sharp increase since the 1980s could not be demonstrated clearly before in other areas.

4.6.3 Holocene/Lateglacial debris-flow volume of Fan 1 quantified with ERT

For the calculated annual Holocene/Lateglacial debris-flow volume, four basic assumptions have been made. (i) The approach of the debris-flow fan in nature by an imaginary pyramid is sufficiently accurate, (ii) the material building Fan 1 originates only from Catchment 1 and (iii) the material was moved there only by debris flows and (iv) the time-dependent development of the fan is neglected. So, the estimation results of the Holocene/Lateglacial mean of 0.35 (±0.03)·10^3 m^3/yr show a maximum value as a result of assumptions (ii) and (iii) as Fan 2 contributes a minor share per year and an insignificant share of material has been moved there also by rockfalls and fluvial transport. Considering assumption (iv), normally an exponential decline in postglacial sediment accumulation is assumed (Curry and Morris, 2004). But as no measurements for a parametrization of the negative exponential model are available, we assumed a constant sediment rate contributing to the development of Fan 1. Thus, the calculated rate of 0.35 (±0.03)·10^3 m^3/yr for the Holocene/Lateglacial debris-flow activity is a maximum estimate and quite likely Holocene mean rates would be lower. Remarkably, the mean annual debris-flow rates for the last three time intervals are 2-3 times higher than mean Holocene/Lateglacial debris-flow activity (Figure 36). Therefore, we postulate enhanced debris-flow activity during the last 2-3 decades coinciding with enhanced rainstorm activity. Vegetation and tree clearance in the catchment implies that elevated rates will relax only over decades with slow vegetation succession.

The approach for debris-flow volume estimation allows an approximation of recent event frequency and magnitude of the Plansee area, despite the limitations inherent to orthophoto analysis. The results contribute to a better understanding of the activity on debris-flow fans with respect to climatic change and are helpful for future calculations in hazard and risk assessment in the project area.

Future research on geomorphic processes on active debris-flow fans is needed to get a reliable link between more intensive rain storms or a higher frequency of intense rain storms due to climate change and the sensitivity of alpine catchments with an increased regularity of debris-flow occurrences, especially in transport limited systems. Moreover, the long term sediment recharge of torrents regarding hillslope-channel-coupling has to be more intensely examined. With a rising population in alpine regions, this research has a direct use for human beings as more and more frequently infrastructure is affected by debris-flow events.

4.7 Conclusions

The temporal and spatial development of eight debris-flow fans could be reconstructed for the last 60 years by a series of aerial photos and field reconnaissance. Due to the orthophotos and the areal extent of vegetation, a temporal classification of occurred debris flows was possible. Thus, we could show in this study:

1. Debris-flow activity has increased by a factor of more than three in eight debris-flow catchments since the 1980s in comparison to the 1940s to 1970s reference period.
2. The mean annual debris-flow activity on Fan 1 also exceeds the Holocene/Lateglacial activity by factor of 2-3.
3. We relate this enhanced debris-flow activity to an enhanced rainstorm frequency in the study area.
4. A strong correlation between non-vegetated area in the debris-flow catchments and annual debris-flow volumes indicates that enhanced activity might persist for decades until vegetation recovers.

Acknowledgements

The authors thank the department for geoinformation of Tyrol for providing the digital elevation model and the orthophotos of the project area. Besides, our thank goes to the Torrent and Avalanche Control Tyrol (Außerfern), the department for Traffic and Infrastructure Tyrol and the District Commission Reutte for the permission to use their forest roads. We thank the department for water management in Vienna for providing the rainfall data. The authors appreciate the comments and suggestions of two anonymous reviewers who helped to improve the quality of the paper.

5 Syn-depositional: Meaningful factors controlling debris-flow erosion

The following text is the accepted version of the following article:

Dietrich A, Krautblatter M. 2019. Deciphering controls for debris-flow erosion derived from a LiDAR-recorded extreme event and a calibrated numerical model (Roßbichelbach, Germany). Earth Surface Processes and Landforms 44: 1346-1361.

The final version has been published at https://doi.org/10.1002/esp.4578

The following changes have been made to the accepted version:

- ⇨ The numbering of each figure, table and equation has changed
- ⇨ The captions of Chapters 5.4.4, 5.5.2, 5.6.2 and 5.6.4 have slightly changed

5.1 Abstract

Debris flows are among the most destructive and hazardous mass movements on steep mountains. An understanding of debris-flow erosion, entrainment and resulting volumes is a key requirement for modelling debris-flow propagation and impact, as well as analysing the associated risks. As quantitative controls of erosion and entrainment are not well understood, total volume, runout and impact energies of debris flows are often significantly underestimated. Here, we present an analysis of geomorphic change induced by an erosive debris-flow event in the German Alps in June 2015. More than 50 terrestrial laser scans (TLS) of a 1.2 km long mountain torrent recorded geomorphic change in comparison to an airborne laser scan (ALS) performed in 2007. Errors were calculated using a spatial variable threshold based on the point density of ALS and TLS and the slope of the digital elevation models. Highest erosion rates approach 5.0 m^3/m^2 (mean 0.6 m^3/m^2). During the event 9,550 ± 1,550 m^3 was eroded whereas only 650 ± 150 m^3 was deposited in the channel. Velocity, flow pressure, momentum and shear stress were calculated using a carefully calibrated RAMMS Debris-Flow model including material entrainment. Here we present a linear regression model relating debris-flow erosion rates to momentum and shear stress with an R^2 up to 68%. Channel transitions from bedrock to loose debris sections cause excessive erosion up to 1 m^3/m^2 due to previously unreleased random kinetic energy now available for erosion.

5.2 Introduction

Debris flows occur in all alpine regions subject to intense rainstorms and mobilisable loose debris. Globally, a total of more than 80,000 destructive and life-threatening debris flows have caused more than 75,000 fatalities in the last six decades (Dowling and Santi, 2014). Recent studies provide quantitative evidence for increasing frequencies of debris flows in the last few decades due to increased rainstorm frequencies, e.g. in the Northern Calcareous Alps (Dietrich and Krautblatter, 2017) in the Carpathian Mountains (Šilhán and Tichavský, 2016), the Italian Alps (Pelfini and Santilli, 2008) and parts of the Rocky Mountains (Rathburn *et al.*, 2013, Rubin *et al.*, 2012). Most debris flows are either initiated as landslides by widespread Coulomb failure within a sloping soil mass (e.g., Gabet and Mudd,

2006, Iverson, 1997) or, alternatively, by a critical runoff in a stream (Berti *et al.*, 2000, Berti and Simoni, 2005). To reduce the rising risk of susceptible economic values and threatened human life, implementing appropriate countermeasures is vital. The size of hazard zones and the size and site of countermeasures strongly depend on the debris-flow runout and flow height. Among other things, these parameters are governed by the debris-flow volume, which cannot be easily estimated, as the entrainment of material leads to an increasing volume during an event (Abanco and Hurlimann, 2014, Frank *et al.*, 2015). Therefore, the spatial variable erosion and entrainment and their geomorphological and lithological dependencies should be of broad interest for both researchers and practitioners.

Nevertheless, few attempts have been made to anticipate debris-flow volumes and debris-flow erosion rates. Potential debris-flow volumes have either been estimated with straightforward empirical formulae (e.g., D'Agostino *et al.*, 1996, Dong *et al.*, 2009, Franzi and Bianco, 2001, Rickenmann and Koschni, 2010), magnitude-frequency relationships (e.g., Riley *et al.*, 2013, Stoffel, 2010, van Steijn, 1996), geomorphological field assessment guidelines (Gertsch, 2009, Hungr *et al.*, 1984) or physically-based methods (e.g., Li *et al.*, 2017, Pudasaini, 2012). Empirically derived equations mostly account for catchment area and the angle of the torrent thalweg (Guthrie *et al.*, 2010). Some also include lithological factors, but their explanatory power is regionally limited. Geomorphological field assessments focus on channel width and length, river slope and banks and composition of the riverbed. However they somehow depend on the experience of the employed expert.

Recent advances in survey technology have facilitated post-event budgeting of debris-flow volumes and erosion rates by detecting geomorphic change with different methods on multiple scales (Turowski and Cook, 2017). Whenever we use the term "erosion rate" in the paper, we refer to a value with the unit volume related to an area. As debris flows are always short-lived processes, the term erosion rate applies to the length of the event, typically shorter than one hour (Warburton, 1993). Debris-flow volumes and rates are often assessed with photogrammetry (Tsutsui *et al.*, 2007), airborne laser scanning (ALS) (e.g., Cavalli *et al.*, 2017, Cavalli and Marchi, 2008, Scheidl *et al.*, 2008), terrestrial laser scanning (TLS) (Perroy *et al.*, 2010, Theule *et al.*, 2015) and combinations of all of these (Blasone *et al.*, 2015). TLS in particular has recently been used to monitor and budget sediment fluxes in highly dynamic fluvial systems (e.g., Baewert and Morche, 2014, Bimböse *et al.*, 2011, Bühler and Graf, 2013, Carrivick *et al.*, 2013, Theule *et al.*, 2015, Theule *et al.*, 2012). After recent debris-flow events, multi-temporal TLS can be used to identify source regions of debris-flow material (e.g., Blasone *et al.*, 2014, Bremer and Sass, 2012, McCoy *et al.*, 2010, Schürch *et al.*, 2011a, Staley *et al.*, 2014, Wasklewicz and Hattanji, 2009). TLS is, due to the high resolution, also applied for small scale debris-flow laboratory experiments (Hung and Capart, 2013). However, TLS has rarely been used in combination with ALS to calculate debris-flow volumes and their source regions (Bremer and Sass, 2012), as the point density of past ALS surveys was considered insufficient. Furthermore, the co-registration of individual TLS positions to one connected point cloud has often caused an unacceptable amount of errors. Recently, the ALS survey

point densities have increased significantly and facilitate accurate co-registration of TLS and ALS if errors are considered carefully.

High-resolution multi-temporal laser scans before and after a debris-flow event open up the opportunity to explain erosion depths by topographical data and physical properties of the debris flow. Whipple and Tucker (1999) related stream power to erosion in fluvial systems, but the concept has neither been extended to steep slopes nor to debris-supported slopes (Stock and Dietrich, 2003). Alternative concepts for quantifying erosion rates in steep channels include channel gradient (Abanco and Hurlimann, 2014) and discharge (Weichert *et al.*, 2009). Schürch *et al.* (2011b) identified flow depth as an important factor governing the location and magnitude of erosion. Recent research also includes ground-vibration measurements with geophones (Kean *et al.*, 2015), measured pressure fluctuations (e.g., Berger *et al.*, 2011a, McArdell, 2016), pore fluid pressures and normal forces to delimit the erosivity of debris flows (McCoy *et al.*, 2010, McCoy *et al.*, 2013).

In spite of the increasing amount of information on debris-flow erosion and on controlling processes (Iverson *et al.*, 2010, Mangeney, 2011), few simulation models are capable of predicting entrainment (Hungr and McDougall, 2009) and thus they systematically underestimate debris-flow propagation or employ user-defined erosion layers (e.g., Begueria *et al.*, 2009, Hussin *et al.*, 2012). The explanatory power of physical debris-flow properties has been implemented in predictive models using flow velocity (Takahashi *et al.*, 1992) and shear stresses (Chen and Zhang, 2015, Frank *et al.*, 2015), but these are rarely validated by real events. A momentum-dependent erosion rate has been described for ice-rock avalanches (Schneider *et al.*, 2010), but the transfer to debris-flow erosion processes is not straightforward.

The goal of this paper is (i) to develop a combined ALS and TLS analysis strategy to reliably quantify source regions of mobilised material and related erosion rates of recent debris flows as well as (ii) to develop a statistical model relating debris-flow erosion rates to velocity, flow pressure, momentum and shear stress. As a consequence of the results of these two research questions, we (iii) quantify erosion peaks along bedrock - loose debris transitions as a potential measure of the excessive random kinetic energy available for erosion. The key findings of this paper have broader implications for excess erosion at bedrock - loose debris transitions and thus might also affect long-term channel profile development in mountain regions. Deciphering controls for debris-flow erosion advances a reasonable and reproducible prediction of potential future debris-flows volumes.

5.3 Study site

The investigated “Roßbichelbach” torrent is located in southern Bavaria at the eastern municipal border of Oberstdorf (Figure 39). The torrent rises in the Hauptdolomit lithology (Norian, 225-206 myr) near the crest of the Gaisalphorn mountain (1953 m.a.s.l.). Further downstream, the torrent crosses a softer, densely fractured Flysch sequence including intercalated quartz-graywackes and different mudstones, marls and limestones, all deposited in the Lower Cretaceous (145-100.5 myr). The bed thickness ranges

from millimetres to decimetres, representing typical turbidites with graded Bouma sequences (Bouma, 1962). These formations are partially covered by moraine material, mostly originating from the Würmian Pleniglacial to Late Glacial, as well as scree. The catchment area delineated on the digital elevation model (DEM) of 2007 (Bavarian Surveying and Mapping Authority, 2007) is 0.29 km² (Figure 39). The mean torrent slope is 25.2° (47%) with a length of approx. 1.2 km and a height difference of about 565 m. The yearly mean precipitation is about 1800 mm with a pronounced summer rainstorm precipitation maximum (DWD Climate Data Center, 2015).

On 14 June 2015, an extreme rainfall event with approximately 90-120 mm in 45 minutes recorded by local residents occurred in this region (the next official weather station 2 km away recorded 35 mm/h). As a result, a debris flow damaged several buildings located on the fan, a road and areas of land used for agricultural purposes (Bavarian Environment Agency, 2015).

To check how much material could still be mobilised by a potentially occurring future event, we mapped the substrate of the river bed shortly after the debris-flow event and were able to distinguish between sections consisting of bedrock and loose debris (Gertsch, 2009).

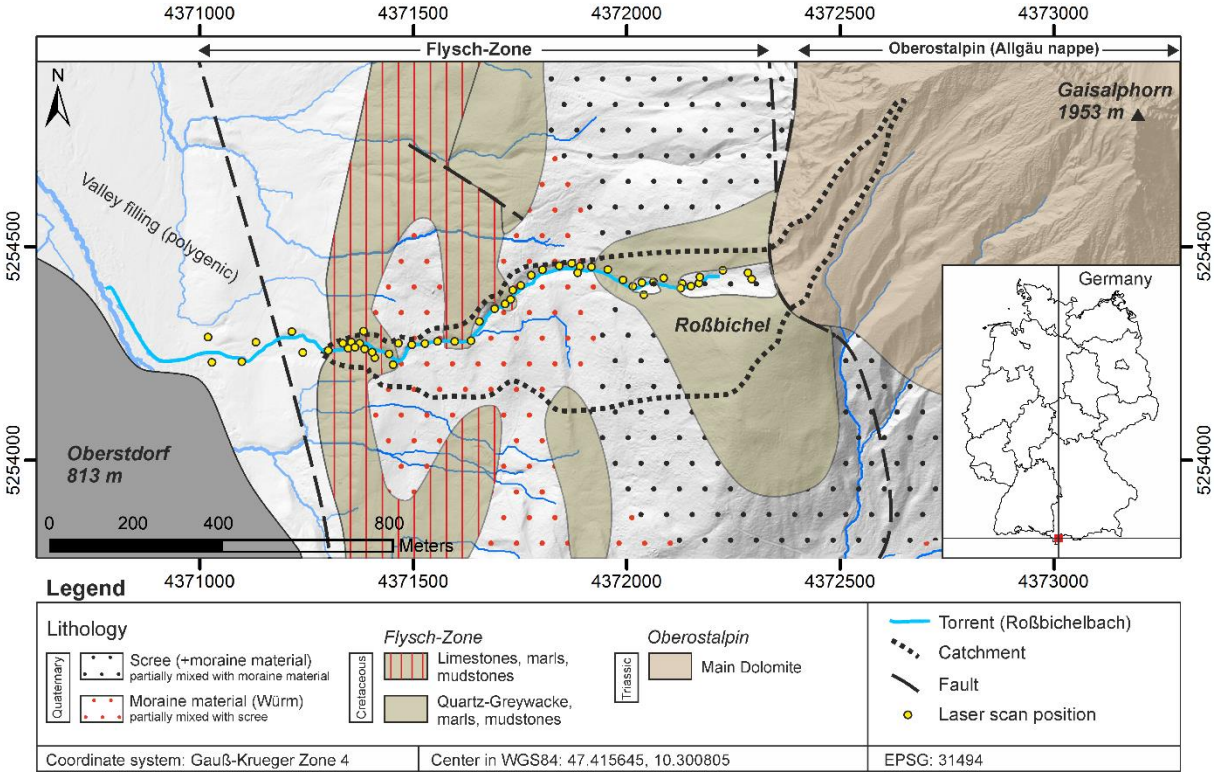

Figure 39: Geological setting of the torrent catchment (Bavarian Environment Agency, 2015, Zacher, 1985). The torrent stream originates in Triassic dolomites before it flows across softer Flysch mudstones, marls and Quaternary sediments. Yellow dots represent laser scan positions performed in summer 2015 in the channel and adjacent slopes. Source of underlying DEM: Bavarian Surveying and Mapping Authority (2007).

5.4 Data and Methods

5.4.1 Airborne laser scan

The airborne laser scan was carried out between 19 April 2007 and 19 June 2007 and has been made available by the Bavarian Topographic Survey (Bavarian Surveying and Mapping Authority, 2007). The height accuracy is better than 0.2 m and the positional accuracy is better than 0.5 m. The resulting unfiltered point density of the airborne laser scan in the catchment varies between 1.4 and 15 points/m². In the torrent and on the adjacent slopes, the density lies mostly between 3 and 10 points/m² (mean 5.5 points/m²). The ALS point cloud was filtered to eliminate vegetation using RiSCAN Pro (Figure 40). The point cloud was filtered using an octree algorithm with an edge length of 0.5 m (Girardeau-Montaut *et al.*, 2005). The linearly interpolated raster of this point cloud has a cell size of 0.5 m. We checked whether the ALS raster shares the exact same extent as the raster generated of the terrestrial laser scans to have congruent data sets.

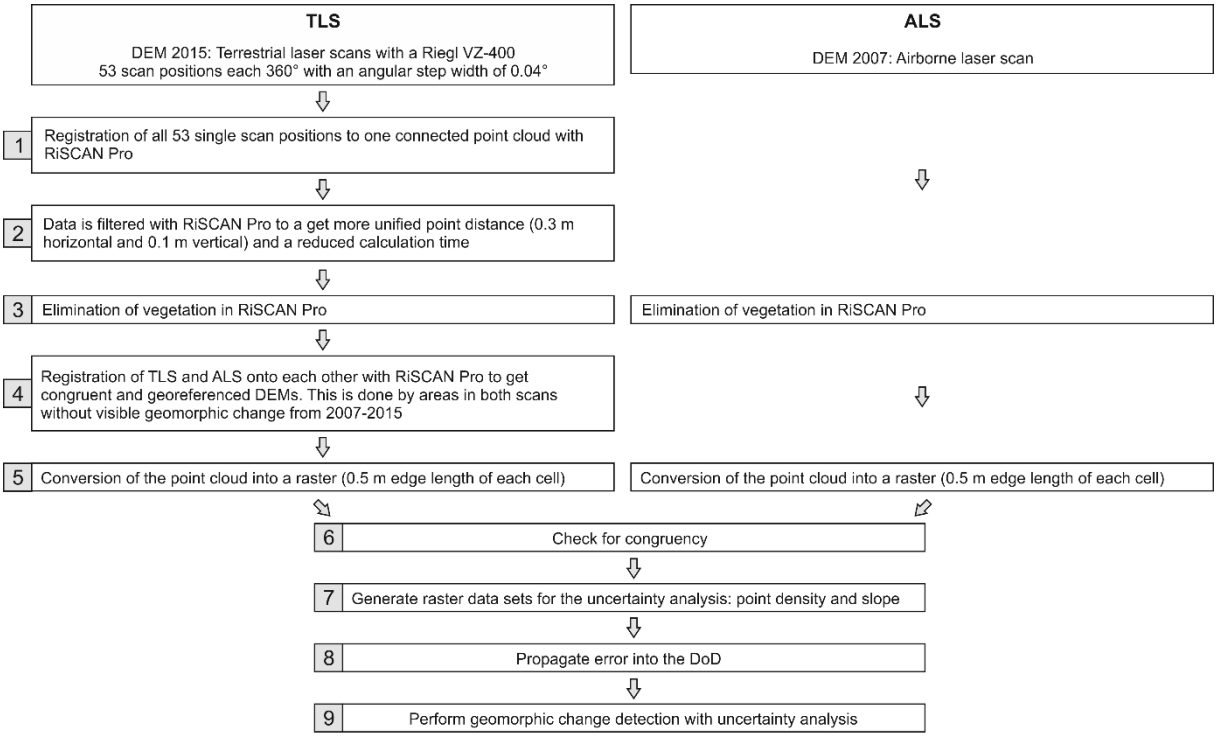

Figure 40: Processing workflow for terrestrial laser scans (TLS), the airborne laser scan (ALS) and the resulting geomorphic change detection. Steps 1-5 were performed with RiSCAN Pro, steps 6-9 with ESRI ArcMap 10.5.1.

5.4.2 Terrestrial laser scan

The terrestrial laser scan was carried out shortly after the event using a RIEGL VZ-400 mid-range laser scanner. For each 360° scan, an angular step of the rotating scanner of 0.04° was chosen with an angle measurement resolution < 0.0005° (Riegl LMS, 2013). With this adjustment, the point spacing is 7 cm at a shot distance of 100 m. The laser pulse repetition rate was 300 kHz with an effective measurement rate of 122,000 measurements per second. According to the manufacturer's specifications, the horizontal and vertical accuracy, describing the conformity of a measured quantity to its actual (true) value, is 5 mm at 100 m. The precision (reproducibility) is 3 mm at 100 m. The laser shows a beam divergence

of 0.35 mrad using a near infrared wavelength (Riegl LMS, 2013). The measurements were carried out during dry weather conditions without any surficial water flow in the torrent in order to avoid surface height errors.

All 53 scans were coarse-registered in RiSCAN Pro by defining at least 4 corresponding points in two consecutive scans and were then fine-registered by a multi-station adjustment (MSA) (Figure 40). For the MSA, both point clouds were filtered for characteristic plane segments. This was done by a so-called plane patch filter. An algorithm searched for plane segments within each scan from which normal vectors were created (Riegl LMS, 2013). Subsequently, the distances of these normal vectors in both scans were minimised by an iterative closest point algorithm (Besl and McKay, 1992, Rusinkiewicz and Levoy, 2001).

The vegetation was automatically eliminated by filtering the point cloud with a multidimensional algorithm in RiSCAN Pro (Riegl LMS, 2013). As the software did not completely detect all vegetation types, the remaining points were deleted manually. Subsequently, the TLS point cloud was filtered to 0.3 m in the x-y-direction and 0.1 m in the z-direction (Figure 40). The thinned point cloud of all TLS positions was registered onto the ALS point cloud by an MSA. Therefore, areas of the point clouds were selected that had definitely remained stable from 2007 to 2015. These “stable areas” were carefully chosen during field surveys in the study area. The multi-station adjustment provides metrics on how well the two disparate data sets could be co-registered. The residues of the corresponding planes showed a Gaussian distribution. The overall standard deviation of the normal distances (> 370 plane patches) was 15 cm. The TLS point cloud was then filtered using an octree algorithm with an edge length of 0.5 m (Girardeau-Montaut *et al.*, 2005) and linearly interpolated to obtain a raster with a cell size of 0.5 m. We checked whether the raster was congruent with the raster derived from the ALS point cloud.

5.4.3 Change detection and error analysis

Point clouds of both ALS and TLS provide point information of the surface. However, the produced raster data sets do not represent the real shape of the surface. Inaccuracies of DEMs arise from (i) measuring errors and inaccuracies of the sampling systems, (ii) errors in the co-registration of scans, (iii) vegetation, which is erroneously taken into account for the DEM-interpolation and (iv) the chosen interpolation method itself (Williams, 2012). The subtraction of two DEMs, taken at different times, produces a DEM of differences (DoD) showing geomorphic height changes between the two data sets. For this, different error sources should be considered in geomorphic change detection. They can be expressed by a simple user-defined constant minimum level of detection ($_{min}$LoD) (Fuller *et al.*, 2003), by a probabilistic threshold using a user-defined confidence limit or by a spatial variable threshold based on spatial variable uncertainties in repeated scans or by spatial coherence of erosion and deposition (Wheaton *et al.*, 2010b, Williams, 2012).

The geomorphic change detection was performed with the ArcGIS Add-On “Geomorphic Change Detection 7” introduced by Wheaton *et al.* (2010b). Both DEMs were subtracted and a DoD was built with a cell size of 0.5 m. The uncertainty of the DEMs was taken into account using a morphological

method established by Brasington *et al.* (2000) and Lane *et al.* (2003), and extended by Wheaton *et al.* (2010b) using fuzzy set theory. At first, the individual elevation uncertainties of the two raster data sets were estimated on a cell-by-cell basis. For this, our approach uses the point density of ALS and TLS and the slope of the DEMs as parameters relating to different degrees of DEM elevation uncertainty (Figure 41). The adjectives 'high', 'medium' and 'low' were chosen to describe slope angle and point density. Subsequently, membership functions were defined by specifying the range of values covered by each adjective. The elevation uncertainty (δz) was then calculated on a cell-by-cell basis for each DEM using a fuzzy interference system, which was calibrated to field settings. For this calibration, we iteratively checked whether the calculated erosion and deposition extents and depths match with our observations during field surveys and then adjusted the value ranges for slope angle and point density for the membership function. The output of this membership function is an elevation uncertainty and represents a spatially variable noise in each DEM (Figure 41). These individual DEM elevation uncertainties were propagated into the DoD on a cell-by-cell basis (Brasington *et al.*, 2003, Wheaton, 2008):

Equation 17:

$$\delta u_{DoD} = \sqrt{(\delta z_{new})^2 + (\delta z_{old})^2}$$

The heterogeneous estimate of DoD uncertainty δu_{DoD} for each raster cell in the DoD represents the square root of the squared individual elevation uncertainties of the new and old DEM. A t-score was derived from the DoD value and the DoD elevation uncertainty δu_{DoD} (Wheaton *et al.*, 2010b):

Equation 18:

$$t = \frac{|z_{new} - z_{old}|}{\delta u_{DoD}}$$

We used a confidence limit of 95% (t = 1.96), assuming a two-tailed test. All changes with probability values less than the chosen threshold were discarded, as they could not be distinguished from noise, otherwise the change was assumed to be real. For a more detailed methodological description, we refer to Wheaton *et al.* (2010b).

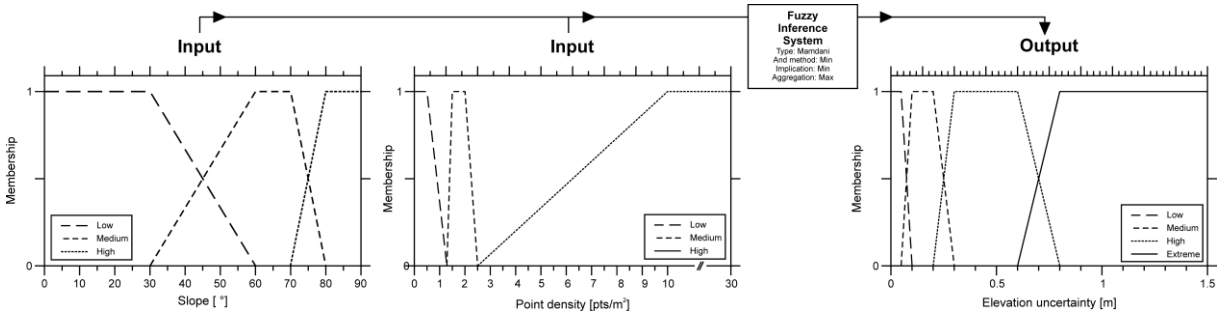

Figure 41: Input and output membership functions. Values of slope angle (input) and point density (input) are converted into an elevation uncertainty (output).

5.4.4 Debris-flow modelling

RAMMS Debris Flow is a widely used simulation software in both research and practice (e.g., Bertoldi *et al.*, 2012, Rickenmann *et al.*, 2006, Schraml *et al.*, 2015b). In this software, debris flows are incorporated as non-Newtonian fluids (Bertoldi *et al.*, 2012). The model is based on the solution of the depth-averaged shallow water equations. The deceleration due to friction (S_f) is calculated by the resistance law of Voellmy-Salm (Salm, 1966, Voellmy, 1955):

Equation 19:

$$S_f = \mu \cdot \rho \cdot H \cdot g \cdot cos(\varphi) + \frac{\rho \cdot g \cdot v^2}{\xi}$$

The total resistance S_f is determined by the Coulomb-type friction value μ, the turbulent friction value ξ, the density of the debris flow ρ, the debris-flow height H, the slope angle φ of the terrain, the gravitational acceleration g and the velocity of the debris flow v. The Coulomb-type friction value μ dominates the total resistance when the debris flow is relatively slow (e.g. stopping) while ξ dominates at higher velocities (Bertoldi *et al.*, 2012). Mass balance is given by

Equation 20:

$$\dot{Q}(\mathrm{x},\mathrm{y},\mathrm{t}) = \partial_t + \partial_x(Hv_x) + \partial_y(Hv_y)$$

where $\dot{Q}(\mathrm{x},\mathrm{y},\mathrm{t})$ is the source term (mass production), $H(\mathrm{x},\mathrm{y},\mathrm{t})$ is the flow height and $v(\mathrm{x},\mathrm{y},\mathrm{t})$ represents velocity. Since late 2017, an entrainment module has been implemented to predict erosion depth by the moving debris flow (Frank *et al.*, 2015, 2017). The entrainment rate is a function of the local shear stress (τ) acting on the channel bed, which is given by

Equation 21:

$$\tau\ [\mathrm{kPa}] = \rho\ \cdot\ g \cdot H \cdot\ \varphi$$

Pressure (p) is given by

Equation 22:

$$p\ [\mathrm{kPa}] =\ \rho \cdot\ v^2$$

and momentum (m) by

Equation 23:

$$m\ \left[\frac{\mathrm{m}^2}{\mathrm{s}}\right] =\ H \cdot\ v$$

For further model descriptions we refer to Christen *et al.* (2010), Christen *et al.* (2011) and Frank *et al.* (2017).

To calibrate the RAMMS Debris-Flow model accurately, we used the entrainment information given by the performed change detection. Therefore, we identified nine simplified sections in the DoD, which

showed similar erosion patterns (Figure 42). These areas were implemented in RAMMS Debris Flow using ESRI shapefiles. Within the sections, we adjusted the entrainment parameters during the calibration until the modelled entrainment volume was the same as the entrainment volume found by change detection (Figure 42). For this, RAMMS Debris Flow offers the opportunity to set erosion rate, critical shear stress and maximum erosion depth for each shapefile separately. With this dynamic material intake we assured that flow volume and discharge at every location of the channel coincides with flow marks gathered during field surveys. Rather than a simplified landslide initiation, we used a more realistic three-point discharge hydrograph as the initial condition for the debris flow. To account for the water content in the flowing mass, an initial water volume of 2,800 m³ (=30% of the entrained sediment volume, ρ = 1,100 kg/m³) was injected into the channel. The percental water content was estimated by literature values from Coussot and Meunier (1996) and Hungr *et al.* (2014). The maximum initial discharge of 15 m³/s was gathered during calibration to match flow marks recorded by field surveys.

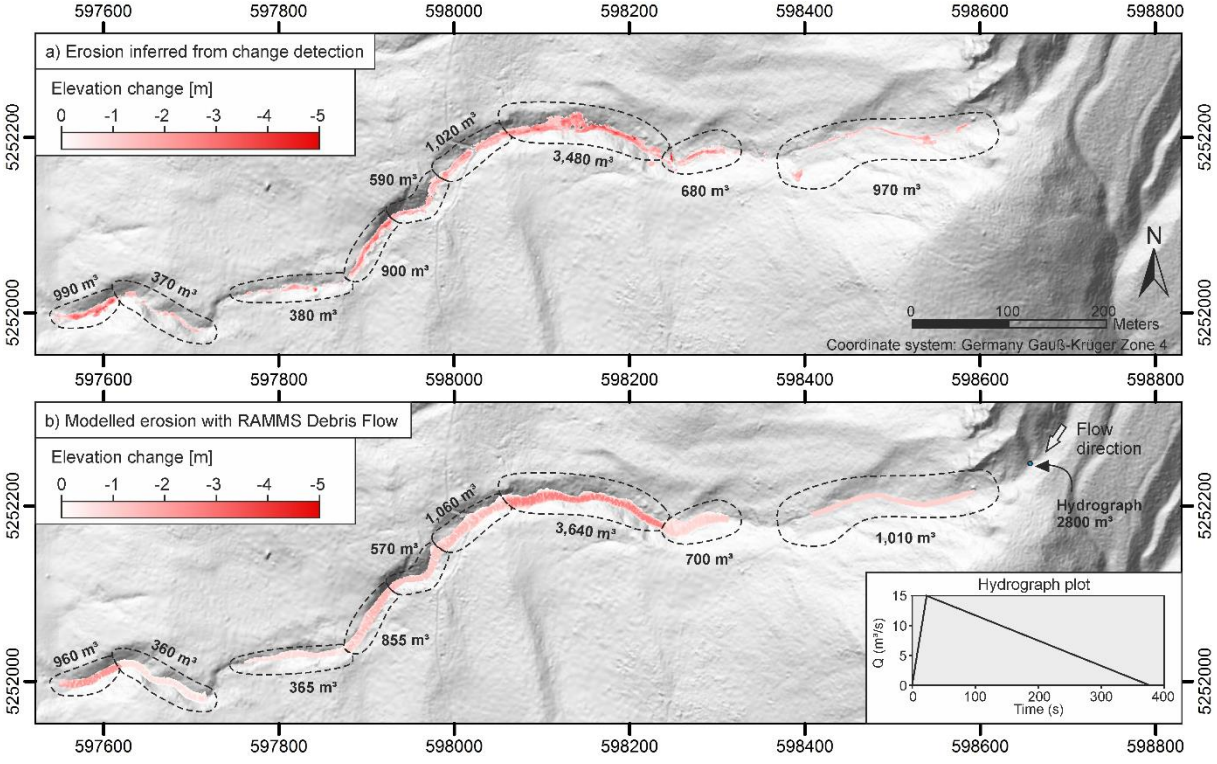

Figure 42: Comparison between observed (a) and modelled erosion (b). The error is less than 5% for each of the shown areas.

As, obviously, no direct measurements of the velocity during movement at the cross-sections were possible, the mean velocity of the debris flow was calculated by an h²S method (Prochaska *et al.*, 2008) at different locations in the channel and was checked for plausibility with reference to observations by Coussot and Meunier (1996). The flow height h was measured by flow marks in field with a yardstick and in the laser scans by means of photographs. The slope S was measured in the laser scans averaged over distances of 5-10 m. The following empirical relation for the h²S method (Prochaska *et al.*, 2008) was used to estimate velocity:

Equation 24:

$$v = 0.35h^2S + 5.36$$

The density of the entrained material was estimated at 2,100 kg/m³. The simulation was based on a 1 m DEM from the ALS in 2007. Obstacles, such as buildings, were considered by assigning no-flux cells to the model. The friction parameters μ and ξ were gained by a careful calibration of the recent event (see Results). The best-fit simulation for the runout and the flow pattern were used for further calculations. The simulation results are velocity [m/s], pressure [kPa], flow momentum [m²/s] (as a product of velocity and flow depth) and shear stress [kPa]. To analyse these results more effectively, we divided the torrent into averaged cross-sections of 5 m and repeated the analysis with segment length of 10 and 20 m. For each analysis the section length was kept constant. Within these sections, the mean velocity, pressure, flow momentum and shear stress were calculated to compare the data to mean erosion rates better and to level out small-scale effects.

5.5 Results

5.5.1 Change detection and error analysis

The difference of the DEMs of 2007 and 2015 accurately shows the areas in which material was eroded and deposited during the debris-flow event (Figure 43). The calculated height differences (DoDs) of the two DEMs ignore morphodynamics in the channel by e.g. earlier heavy rainfall events. The total erosion volume amounts to 9,550 ± 1,550 m³ (Table 9) and preferably originates from the riverbed (Figure 43a, c, d) with a maximum erosion depth of 5.0 m. A minor portion of the material originates from slopes (e.g. Figure 43e, f and 100 m west of the place Pic. d was taken). About 650 ± 150 m³ were deposited during the debris-flow event (Pic. b in Figure 43). Some smaller translational and rotational slides can be seen in the upper region of the catchment (Pic. E, F in Figure 43).

Table 9: Calculated volumes by the difference of the DEMs. The erosion volume is shown in red in Figure 44, the deposition volume in green. The net volume describes the difference of erosion volume and deposition volume and was not covered by the TLS survey.

	Volume [m³]		± Error [m³]	Error [%]
Total erosion volume	9,550	±	1,550	17
Total deposition volume	650	±	150	23
Total difference volume	10,200	±	1,700	17
Total net volume	-8,900	±	1,500	-17

Naturally, the largest part of the investigated area does not show any significant elevation change (Figure 44a), as the calculated DoD error often exceeds small elevation changes. This especially applies to areas with steep slope angles and low point densities in the ALS, like most of the riverbanks and the upper catchment area (Figure 43). Consequently, these large parts of the study area, showing no significant elevation change (Figure 44a), contribute only a little to the overall volumetric change (Figure 44b). Conversely, the comparatively small area with a significant height change (Figure 44a) contributes the largest proportion of volumetric change (Figure 44b).

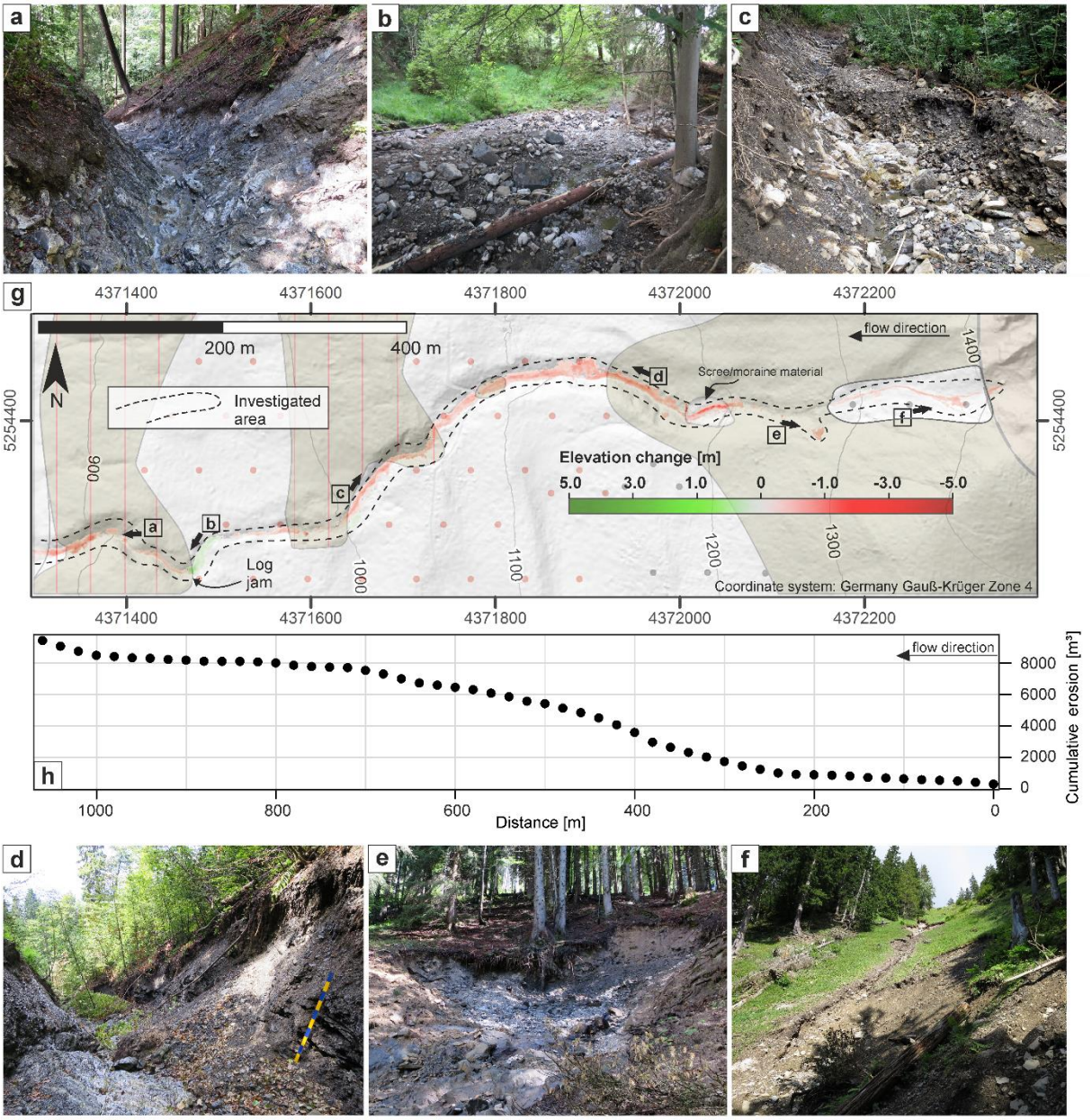

Figure 43: Photographs of channel erosion or deposition (a-f) and surface difference (g) of the ALS 2007 and TLS 2015. Green positive values show deposition, red negative values show erosion of material. Pictures a) to f) show the situation in the torrent after the event. The arrows indicate the directions in which the photo was taken. (a) Erosion of approx. 1 to 2 m. (b) Deposition at the log jam up to 3 m. (c) Erosion of approx. 2 to 2.5 m. (d) Erosion of approx. 2 to 3.5 m. (e) Erosion of approx. 1.5 m. (f) Erosion of approx. 1 to 1.5 m. (h) Cumulative erosion volume along the travel path. Source of underlying DEM in (g): Bavarian Surveying and Mapping Authority (2007).

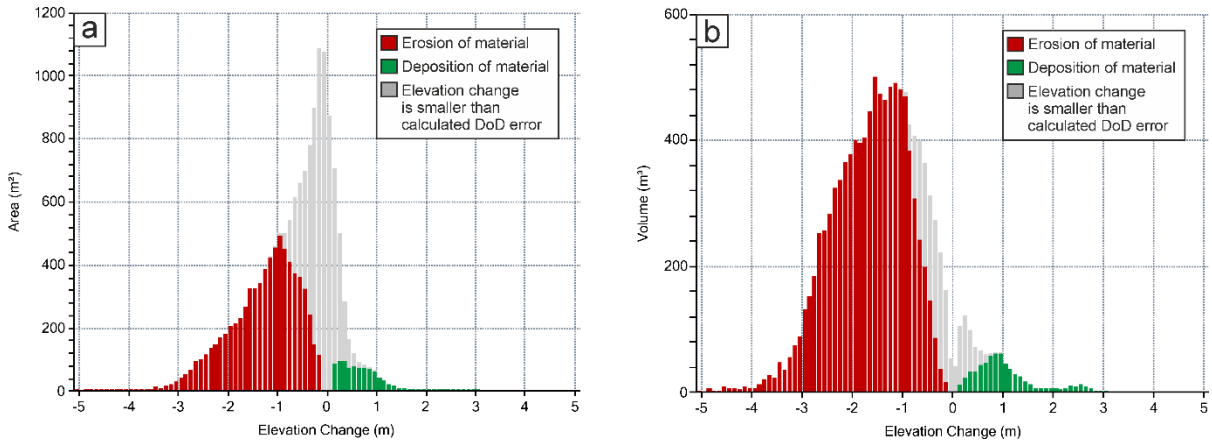

Figure 44: Histograms of the DEM of difference. Each bar represents a 10 cm interval in elevation change. a) Histogram of the elevation change of the investigated area. b) Elevation change expressed as a volumetric change. Red and green bars represent areas (a) and volumes (b) that show a significant change. For gray areas the elevation change is smaller than the error in the DoD.

5.5.2 Explaining erosion rates with momentum and shear stress

With our careful calibration, we ensured that the model correctly reproduced the measured properties of the real event. Thus, we hypothesise that the model also gives correct values for properties of the real event that could not be observed, measured or estimated in all portions of its pathway. The calibrated model shows that the deposition areas can be accurately reproduced by the simulation (Figure 45). The modelled heights of the deposition range from 5 cm to 2.5 m. These heights were checked in the field by a careful survey with photographic data of the event and an assessment by the Bavarian Environment Agency immediately after the event. We also checked whether the flow heights at different cross-sections in the torrent coincide with data on the real event (debris-flow marks) and the simulation. The best-fit simulation is obtained with an input peak discharge of 15 m³/s, injected at the top of the channel (Figure 47). The Coulomb-type friction value μ is 0.16 and the turbulent friction value ξ is 200 m/s², which are typical values for mud-rich debris flows, consistent with the Flysch stream bed lithology of intercalated mudstones and graywackes (Bartelt *et al.*, 2017).

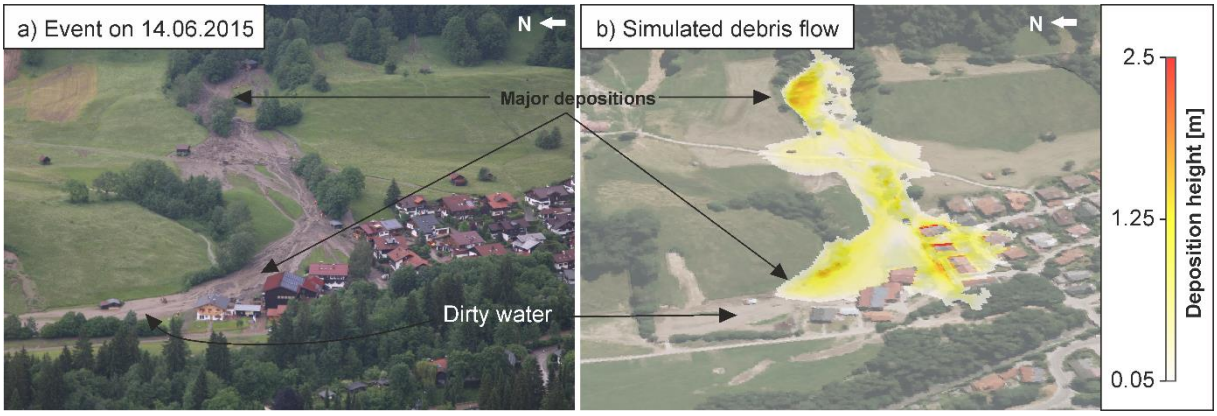

Figure 45: Comparison between the extent of the real event on 14 June 2015 (a) and the simulated extent and deposition heights with RAMMS Debris Flow as a result of the calibration (b). Source of a): Police helicopter picture from the police headquarters Swabia South/West, Oberstdorf. Background picture in b): Google Maps.

We implemented entrainment information, gathered by the change detection, in the model calibration. Nine erosion sections, representing areas with similar erosion patterns, were used during the model calibration to match field data (Figure 42).

Besides the deposition height, the simulation gives information about velocity, flow pressure, momentum and shear stress of the debris flow in each raster cell of the torrent (Figure 47b-e). Velocities range up to 14 m/s, with pressures up to 225 kPa, momenta to 65 m²/s and shear stresses up to 50 kPa. By comparing the modelled parameters with the elevation changes (Figure 47a), the largest values of the modelled parameters match well sectionally with the observed highest negative elevation changes. However, in some parts, the modelled parameters show large values, while only a small amount of erosion occurred. To compare the simulation results more easily with significant elevation changes, we divided the torrent into sections of 5, 10 and 20 m each from top to bottom. In these sections, the mean velocity, pressure, momentum, shear stress and erosion rates originating from the river bed were calculated. We could therefore transfer the visual simulation results to specific data points. Length profiles for 5, 10 and 20 metre sections of mean shear stresses versus elevation changes show that shear stresses in loose debris sections are in most cases lower than in bedrock sections, as the steepest parts in the torrent consist of bedrock (Figure 46a, b and c). Large erosion rates can be observed in both loose debris and previously sediment covered bedrock. Surprisingly (and not explained by the model), real observed erosion peaks occur systematically shortly after transitions from bedrock to loose debris.

To statistically derive control factors for erosion, we constructed scatter plots of modelled flow properties against erosion in 5 m, 10 m, and 20 m sections (Figure 46d-f). The mean erosion rate was calculated by summing up all the height changes within a section (5, 10 or 20 m) divided by the area that the modelled debris flow covered. This erosion rate in m³/m² – other authors call it area growth factor (Reid *et al.*, 2016) – indicates how much material is eroded per square metre of river bed. It shows that mean erosion can be predicted by the shear stress in sections consisting of loose debris with a coefficient of determination of between 48% (5 m sections) and 65% (20 m sections). In contrast, the data points for sections consisting of bedrock show a greater scatter. Large erosion values would have probably occurred in these sections if the bedrock had been covered by a thick sediment layer before the event. The coefficient of determination in these previously sediment-covered bedrock sections is between 6 and 11% and has a distinctly lower slope.

To explain mean erosion rates, we split up the data points to continue the analysis only where erosion did not exceed sediment availability and conditions were limited by transport rather than by supply (Figure 48). These remaining data points were plotted against the corresponding mean velocity, pressure, momentum and shear stress of the flow (Figure 48a-l). Mean velocities range from 6 to 12 m/s, pressures from 40 to 150 kPa, momenta from 3 to 38 m/s² and shear stresses from 3 to 14 kPa, which explains the mean erosion rates from 0 to 2.5 m³/m². The empirically derived linear regression models (Table 10) show similar slopes for all section lengths for velocity (Figure 48a-c), pressure (Figure 48d-f), momentum (Figure 48g-i) and shear stress (Figure 48j-l). Higher values of these parameters are

associated with higher mean erosion rates. The regression model for velocity explains, depending on section length, up to 29-41% of the observed erosion, for pressure 29-42%, for momentum 50-68% and for shear stress 48-65%, respectively. While the linear regression models, describing mean erosion, do not change with longer sections, the coefficients of determination increase, especially in relation to momentum and shear stress. Based on the linear regression models and the 95% confidence limit, these two parameters explain erosion rates best.

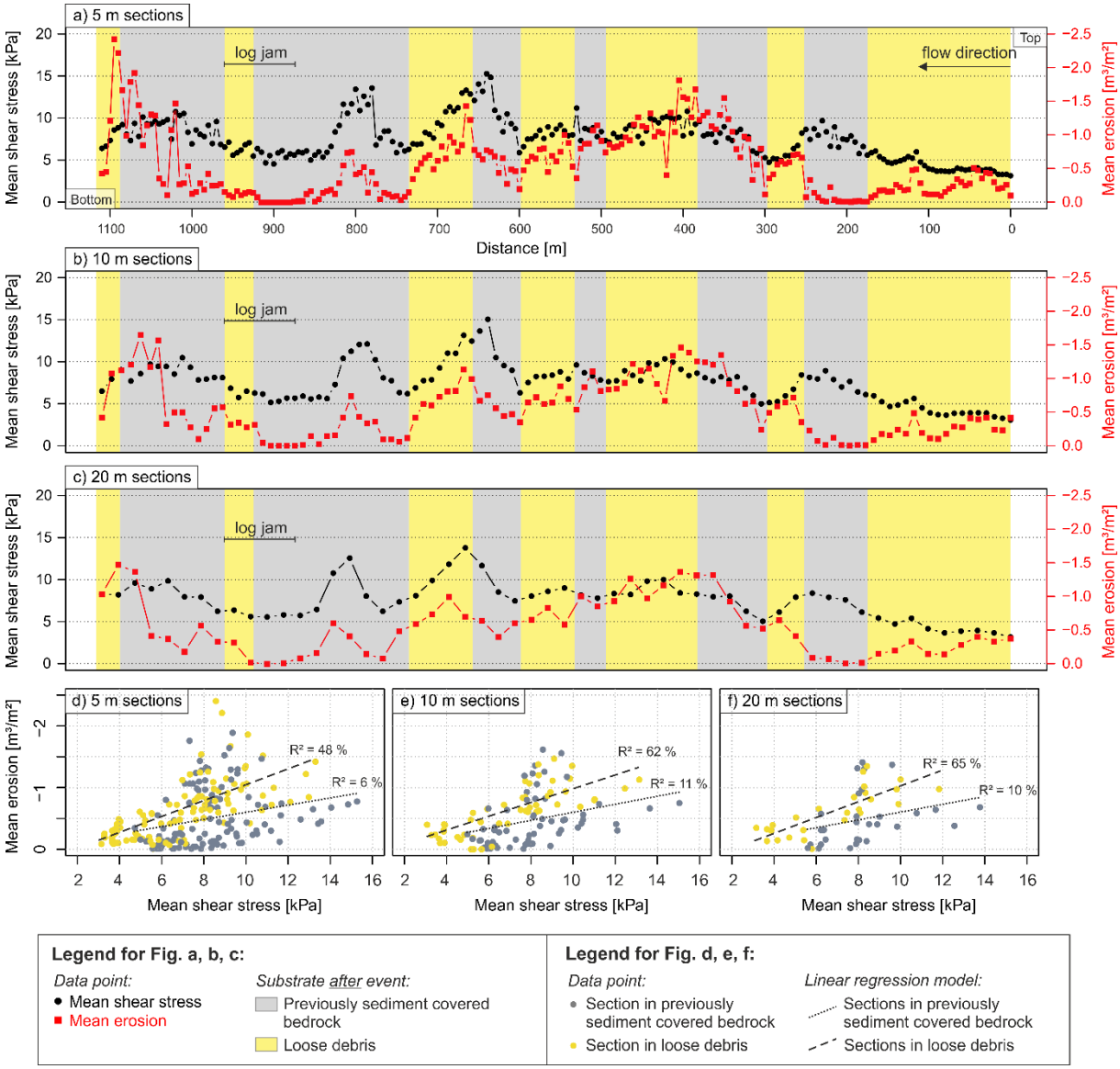

Figure 46: Modelled mean shear stress (black) and LiDAR-derived mean erosion (red) along the channel shown in Figure 47. The background colour indicates the kind of underlying substrate in the riverbed: grey = previously sediment covered bedrock, yellow = loose debris. d-f: Corresponding scatter plots for a-c of the modelled mean shear stress and mean elevation change. The data points influenced by a log jam were not considered for the linear regression analysis. The flow direction is from right to left to be consistent with Figure 43.

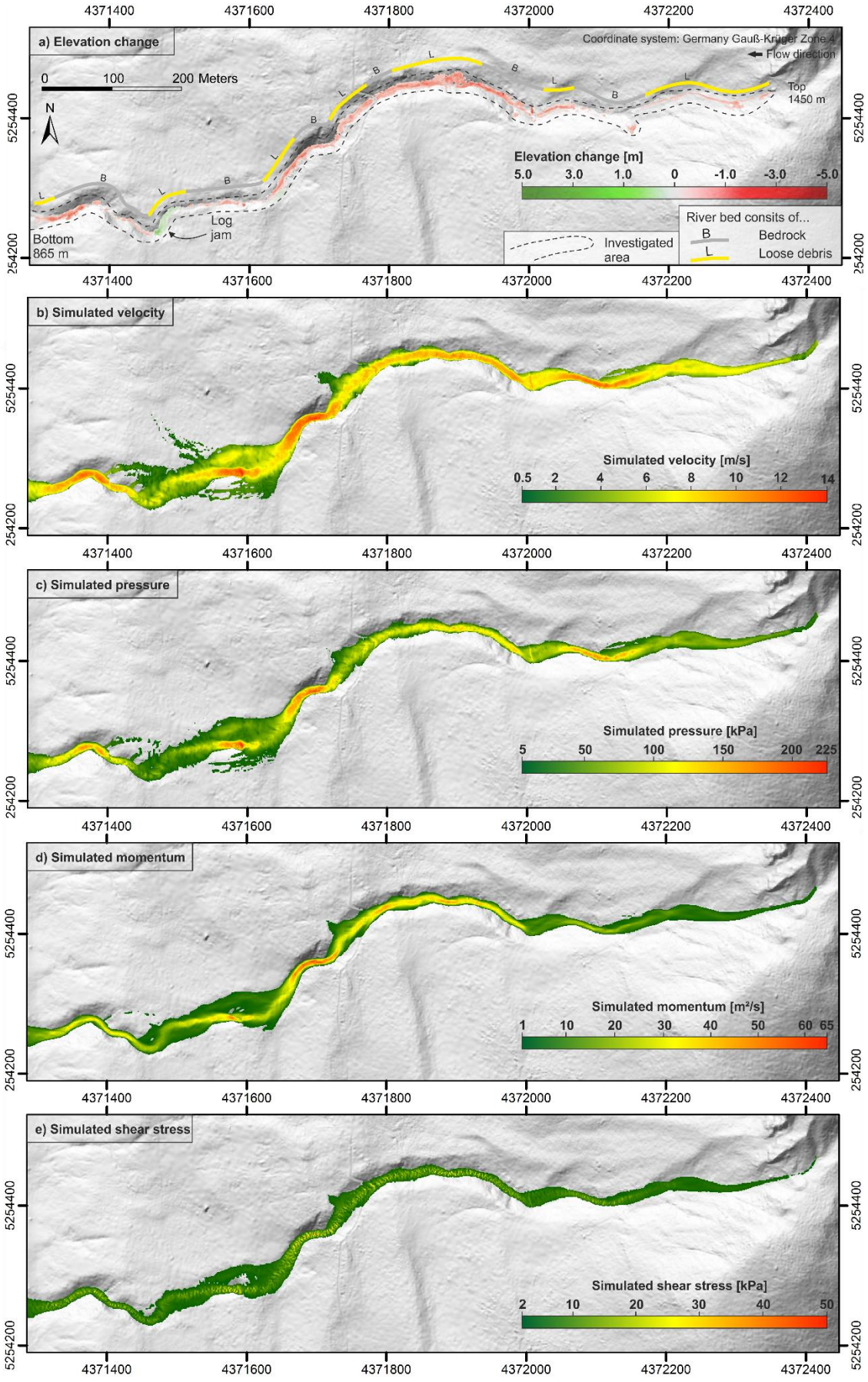

Figure 47: Comparison of the elevation changes (a) to velocity (b), pressure (c), momentum (d) and shear stress (e) of the debris flow simulated with RAMMS Debris Flow. Source of underlying DEM: Bavarian Surveying and Mapping Authority (2007).

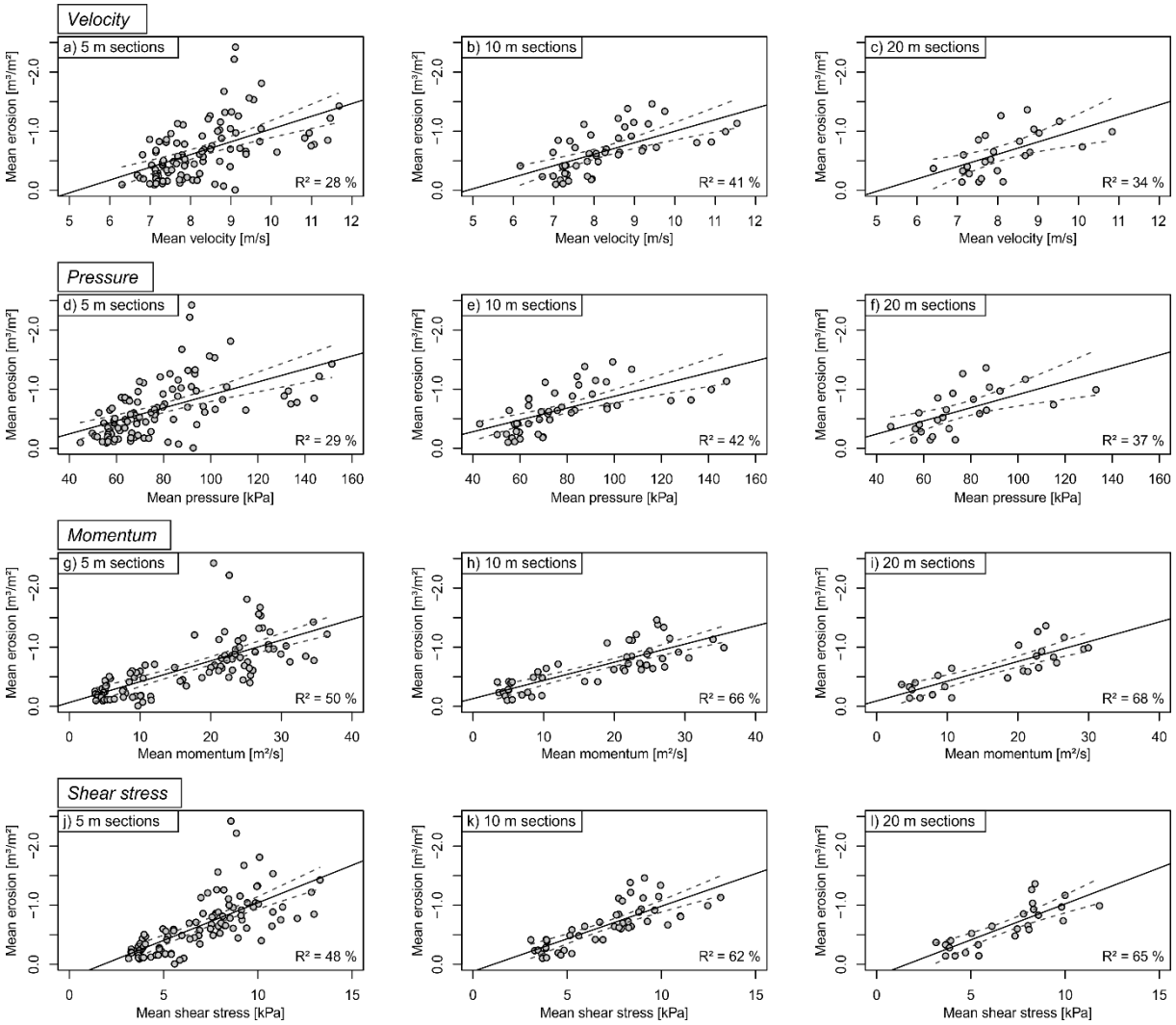

Figure 48: Scatter plots of modelled mean velocity (a-c), pressure (d-f), momentum (g-i) and shear stress (j-l) of the debris flow versus mean erosion rate for all sections consisting of loose debris (grey dots). Left to right show different section lengths (5, 10, 20 m). The black lines are linear regression models with given R^2. Dashed lines represent the 95% confidence interval.

Table 10: Derived linear regression models, which explain erosion by modelled flow properties. Formulae are given for each section length (5, 10, 20 m) and show only small variations. Erosion rates are given in m^3/m^2.

	Section length			
	5 m	10 m	20 m	R^2 [%]
Velocity v (m/s)	$e = 1.122 - 0.216v$	$e = 0.949 - 0.195v$	$e = 1.064 - 0.209v$	28-41
Pressure p (kPa)	$e = 0.195 - 0.011p$	$e = 0.119 - 0.010p$	$e = 0.205 - 0.011p$	29-42
Momentum m (m^2/s)	$e = 0.064 - 0.035m$	$e = -0.130 - 0.031m$	$e = -0.090 - 0.033m$	50-68
Shear stress τ (kPa)	$e = 0.230 - 0.127\tau$	$e = 0.120 - 0.110\tau$	$e = 0.196 - 0.122\tau$	48-65

5.6 Discussion

5.6.1 Change detection

If the system were closed, the erosion and deposition volume should be equivalent, assuming no changes in bulk density. In our study area, the erosion volume is significantly larger than the deposition volume (Figure 43, Figure 44). On the one hand, the survey did not cover the whole deposition area, on the other hand part of the material was excavated and taken away shortly after the event, as several houses were partly buried or threatened. Thus, the erosion and deposition volumes do not balance out.

Looking at the DoD of the compared surfaces, the errors concerning the elevation change show a Gaussian-like distribution (Figure 44a). So, for very small height changes, the spatially variable $_{min}$LoD, often exceeds these small elevation changes and the volumes are added to an error volume (Figure 44b, Table 9). Nevertheless, in contrast to calculations with a constant $_{min}$LoD, some low magnitude geomorphic changes are not discarded a priori and are taken into account for the erosion or deposition volume. Another advantage compared with a spatially constant $_{min}$LoD is the possibility that pixels with a higher elevation change can also be discarded, if a low point density (often a consequence of dense vegetation) of the ALS concurred with steep slopes, as the vertical values can vary heavily over a short distances (Figure 43). Thus, the applied method using a more sophisticated spatial variable threshold significantly enhances the volume calculation in terms of reliability and robust uncertainty analysis (Wheaton *et al.*, 2010b). The calculated volumetric error of the combined ALS-TLS analysis of 17-25% (Table 9) is slightly larger than other recent studies have shown (Bremer and Sass, 2012, Scheidl *et al.*, 2008) and, therefore, represents a more conservative calibration of the model given in (Wheaton, *et al.*, 2010).

With advances in the construction of unmanned aerial vehicles (UAV) and their cameras, recent research focuses more and more on the opportunities of photogrammetry in debris-flow catchment monitoring (e.g., Blasone *et al.*, 2015, James and Robson, 2012, Westoby *et al.*, 2012). Although this method is low-cost, easy to use and surveys can be conducted in less time than with laser scanning, the accuracy of photogrammetric studies is limited by the resolution of the pictures and the software algorithms used to eliminate the distortions of the camera lens. Additionally, photogrammetry is not effective in vegetated areas, as it may lead to erroneous DEMs incorporating trees, grass or other non-ground points. Therefore, we think ALS and TLS are the state-of-the-art methods for acquiring high-quality terrain models in slightly vegetated areas and complex terrain (Perroy *et al.*, 2010). Limitations are set to large areas, to portability in challenging terrain or to high capital investment costs (Westoby *et al.*, 2012). Besides, flat terrain is more complex to survey from the ground due to the oblique line of sight.

5.6.2 Explaining erosion rates with momentum and shear stress

The results show that the parameters modelled with RAMMS Debris Flow explain a majority of the erosion occurring in sections consisting of loose debris (Figure 47, Figure 46, Figure 48). Nevertheless, about 30-40% of the observed variance cannot be explained by the simulated flow velocity, flow pressure, momentum or shear stress of the debris flow. Therefore, we consider the following causes:

5.6.2.1 Errors inherent to the change detection

We compared the digital elevation models of 2015 and 2007. The DEM of difference represents the sum of all morphological changes in the inter-survey period. Thus, it might contain changes that can be attributed to different processes and events other than the 2015 debris flow, but cannot be temporally resolved in this study. Therefore, the calculated height differences (DoDs) of the two DEMs might not be exactly true, as some material will have been transported in the channel by e.g. earlier heavy rainfall events. Nevertheless, we know from previous observations and photography that by far the greatest proportion of the material has been eroded and transported during the debris-flow event in an otherwise non-active and partly vegetation-covered channel bed. No rainfall event since 2007 recorded at a rainfall station 2 km away had an intensity as large as the one on 14 June 2015 (DWD Climate Data Center, 2016). Unofficial measurements by people living close to the torrent show an even more remarkable rainfall intensity of 90-120 mm/45 min. Thus, we think that only a minor part of the explanation for the residuals shown in Figure 48 can be traced back to morphologic changes in the inter-survey period.

5.6.2.2 Errors caused by model parameters

A further possible explanation for the discrepancy of the simulation results and real erosion includes (i) the simplification of the real event by a single triangular hydrograph. The discharge, which was injected at the top of the torrent, had a peak discharge of 15 m^3/s. This discharge could not be measured in the field, but was derived from field surveys and empirical relationships (Prochaska *et al.*, 2008). The simulated flow height seems to reproduce the real observed event quite well, as small overflows of the channel could be reconstructed in the model (Figure 47). (ii) We used a 1 m DEM for the simulation to strike a balance between topographic accuracy, calculation time and the numerical stability of the model. Therefore, small topographic features could not be considered in the simulation. (iii) The bulk density of the flowing material was estimated at a literature value of 1900-2000 kg/m^3 (Iverson, 1997), as it was not possible to measure the density in the event. (iv) We could not directly measure the velocity of the flow. But the results of the approach from Prochaska *et al.* (2008) showed very reasonable values (Figure 47), which coincide with observed typical velocities of debris flows from 3-13 m/s reported by Coussot and Meunier (1996). (v) A jam caused by logs was observed (Figure 43). This obstacle could not be considered in the simulations. Therefore, this area was excluded for the linear regression models. We think another minor explanation for the residuals shown in Figure 48 can be traced back to erroneous and simplified model input data.

5.6.2.3 Errors caused by the incomplete physical model

The model is based on the Voellmy-Salm resistance law, which requires few variables for calibration, is widely used, and reproduces debris flows well (Salm, 1966, Voellmy, 1955). Both scientists and practitioners have found good results in the back analysis of debris-flow events (e.g., Hürlimann *et al.*, 2003, Pirulli and Sorbino, 2008, Rickenmann *et al.*, 2006), although some physical properties are not sufficiently considered. Consequently, we think another minor explanation for the residuals shown in Figure 48 can be traced back to the simplified physical description of flow and material properties in RAMMS Debris Flow.

5.6.2.4 Sediment availability and size effect of riverbed components

Our analysis includes sections in which sediment availability is unlimited (Figure 48). Nevertheless, sediments might be unequally eroded over the total length of the channel as the composition of loose debris will vary spatially and the size of the components can change. This size effect of riverbed components can be studied at several locations in the channel in which the riverbed includes large boulders (Figure 49). Although the modelled flow properties in this areas reach relatively high values, the erosion rate is remarkably lower than we would expect from the linear regression models. Thus, we follow the hypothesis of Johnson and Whipple (2007) and Yager *et al.* (2007), who postulate that erosion is less effective as the diameter of the riverbed components increases. We therefore consider an additional explanation for the residuals shown in Figure 48 can be traced back to causes inherent to changes in lithology and the size of riverbed material.

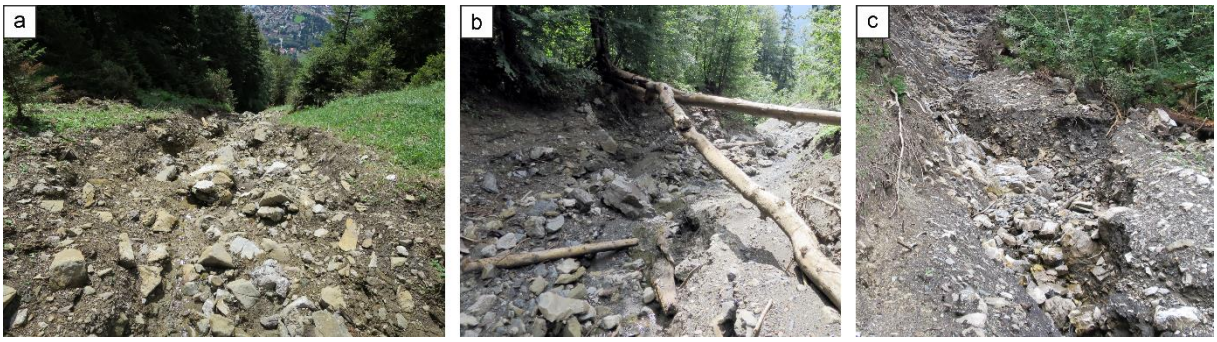

Figure 49: Sections showing a rough riverbed including large boulders. a) 150-180 m downstream in Figure 46, b) 560-600 m downstream in Figure 46, c) 680-700 m downstream in Figure 46.

5.6.3 Massive erosion at riverbed transitions from bedrock to loose debris

Erosion generally occurs in loose debris if shear forces of the debris flow exceed shear resistances of the riverbed (Hungr *et al.*, 2005). The resulting elevated pore pressures in the riverbed lead to liquefaction of the material, especially at the debris-flow front (e.g., Berger *et al.*, 2011a, Iverson *et al.*, 2010, McArdell, 2016). As the momentum of the debris flow grows with increasing vectorial velocity in ground direction and with flow depth, our simulation results are able to explain a significant portion of the entrainment of material.

After the event, the riverbed consists of alternating bedrock and loose debris. Taking a closer look at the transitions between bedrock and loose debris, we observed a distance lag between sections with high momenta and sections with large erosion rates (Figure 50). While high momenta occur in bedrock sections, the largest erosion rates are often observed at transitions from bedrock to loose debris. This mostly coincides with changes in lithology (Figure 39, Figure 46).

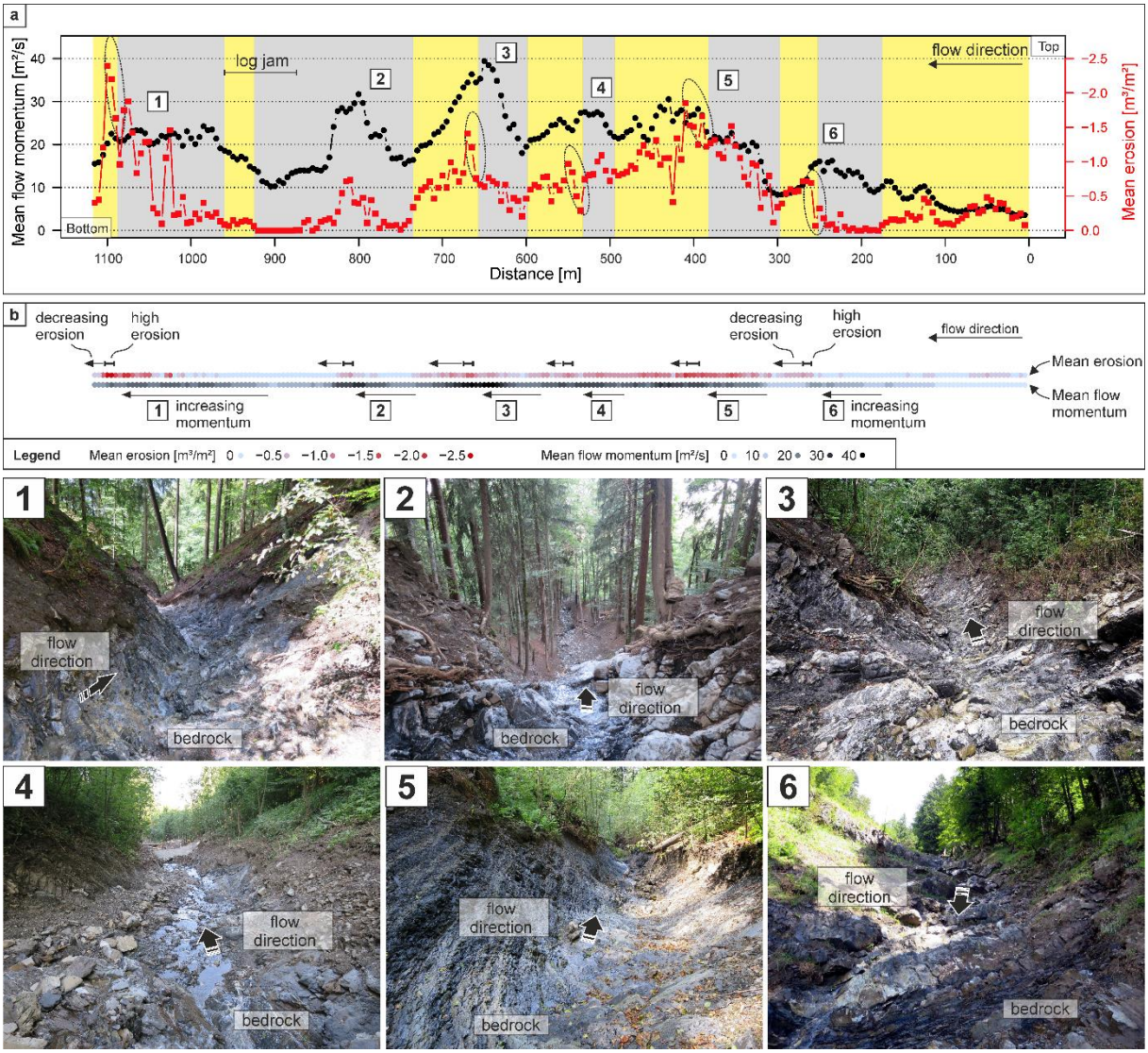

Figure 50: Calculated mean erosion rate vs. simulated mean flow momentum in sections of 5 m. The dashed ellipses indicate the steep increase in mean erosion rate shortly after bedrock sections. The underlying colours in (a) refer to the lithological setting in the project area (legend shown in Figure 39). Mean flow momentum and mean erosion rate are shown in (b) as colour-graded values. A lag distance between high momenta and large erosion rates can be observed. While high momenta occur in sections consisting of bedrock, the deepest erosion can be often observed in the subsequent loose debris section. Pictures 1 to 6 correspond to high momenta bedrock sections shown in (a) and (b).

The underlying bedrock, involving layered limestones, marls and mudstones, prevented deeper erosion (Figure 50) and the flow obviously did not lose momentum in these sections. Less friction occurred at the debris-flow channel-bed interface compared to sections consisting of loose debris. Thus, the accelerated flow was suddenly able to release the retained momentum at transitions from bedrock to loose debris and incise more deeply, which can be seen in erosion rate peaks (Figure 50a, b). As the newly entrained material had to be accelerated, the flow lost velocity (and momentum) at that point. As a result,

erosion rates decrease shortly after the erosion rate peaks. Thus, the regression analysis is negatively influenced by the lagged erosion of material at transitions from bedrock to loose debris. Upslope developing debris-flow properties, e.g. acceleration in steep bedrock sections, cannot be directly linked in the regression analysis (Figure 48) with deep incisions in the following loose debris sections (Figure 50).

5.6.4 A novel approach to estimate erosivity and sediment entrainment

Our results reveal key factors controlling debris-flow channel-bed erosion in the studied area using a combination of field work and numerical modelling (Figure 47 to Figure 50). The calculation of physical flow parameters of the debris flow by a simulation software seems to predict erosion rates in unconsolidated rock well, if the underlying model is accurately calibrated by field surveys. In our study, we find debris-flow momentum and shear stress to be the best-fitted controlling factors for erosion rates as these two parameters also take – besides other factors – flow depth into account (Figure 48g-l). The significance of flow depth for debris-flow erosion has also been shown by Hungr and McDougall (2009) and Frank *et al.* (2015). This coincides with our observations regarding the lower coefficients of determination for velocity and flow pressure (Figure 48a-f). Analogue results for a momentum-dependent erosion rate have been shown by Schneider *et al.* (2010) for ice-rock avalanches. The erosion considered along a travel path in our simulation greatly modifies debris-flow parameters such as momentum or shear stress, as shown by Iverson (2012) and Iverson and Ouyang (2015).

Anticipating debris-flow erosion rates is key requirement for predicting reach, deposition, impact and the resulting hazard potential of debris flows. However, previous models often do not take the erosion capacity of debris flows into account and, thus, would heavily misjudge runout, impact and the resulting risk. Here we present empirically derived formulae that help to anticipate erosion rates based on the forward simulation of potential future events. The results displayed provide a relatively robust relationship of shear stress or momentum and erosion rate in the area studied. Hence, new and future debris-flow simulation software should take these two parameters into account rather than flow velocity or flow pressure as causes of erosion. Further research should now point to the verification of the linear regression models and the newly postulated formulae (Table 10) by comparing recent debris-flow erosion rates to modeled debris-flow properties in complementary settings and lithologies. As the new approach was developed using a debris-flow sediment volume of 9,550 m^3, possible limitations for significantly larger volumes (e.g. hundreds of thousands of cubic metres) have to be tested. These investigations will show whether the regression model can be linearly extended for higher and lower parameter ranges (Figure 48). Based on the findings relating to severe erosion at bedrock-loose debris transitions, future research needs to investigate these processes more precisely.

5.7 Synopsis and conclusions

The knowledge of recent and historic debris-flow volumes is essential in order to reliably design debris-flow mitigation measures. We therefore detected the geomorphic change of a mountain torrent after a debris-flow event using a combination of airborne and terrestrial laser scanning. Based on hydrological and geological conditions and the recorded runout of the debris flow, a model was calibrated with RAMMS Debris Flow. We compared erosion rates with output parameters of the model such as velocity, flow pressure, momentum and shear stress. In this paper we show:

1. The possibilities and limitations of a combined ALS/TLS geomorphic change detection of a complete mountain torrent in challenging terrain.
2. The identification of erosion and deposition areas with a spatially variable uncertainty of the change detection. The results were accurately checked during field surveys.
3. How to develop a well-calibrated numerical Voellmy-Salm model, reproducing plausible ranges for velocity, flow pressure, momentum and shear stress, which is in turn carefully validated by field record.
4. Modelled momentum and shear stresses explain erosion induced by a debris flow by 50-68%.
5. We show the importance of bedrock-loose debris transitions in the channel, which produce local erosion maxima, presumably due to excessive unbalanced drag forces at the base of the flow subsequent to low-friction bedrock channels.

The results contribute to a better understanding of the spatial variable erosion rates of debris flows. The calibrated model was used to predict the runout of potential future events and to establish an appropriate countermeasure in the study area. The method of explaining erosion rate by numerical model outputs should be tested in other catchments, lithologies and with other debris-flow magnitudes. Thus, the relationships determined between simulated flow properties and erosion rate might be applicable in future debris-flow erosion estimations. A prediction of the volumetric debris-flow growth is essential for analysing associated risks and designing reliable mitigation measures. Furthermore, the excess erosion at bedrock - loose debris transitions might even have broader implications for the long-term channel profile development in alpine regions.

Acknowledgments

The authors would like to thank the Bavarian State Office for Digitization, Broadband and Surveying for providing us with the orthophotos and the airborne laser scan data. The data used is listed in the references, figures and tables. This work was financially supported by the Bavarian Environment Agency (Granting No: AZ: 61-0270-19559/2016). We thank Karl Mayer and Andreas Rimböck from the Bavarian Environment Agency for their useful comments on the design of the project. We also thank Georg Dietrich who supported the laser scan field trips in the challenging mountain environment. The authors thank Brian McArdell, anonymous reviewers and the editors for their constructive feedback on the manuscript.

6 Post-depositional: Monitoring of post debris-flow sediment redistribution

Journal article to be submitted (title can change):

Dietrich, A., Keilig, K., Stammberger, V., Krautblatter, M.: A 4-D reconstruction of post debris-flow sediment redistribution inferred from multi-temporal terrestrial laser scanning and photogrammetry (Roßbichelgraben, Germany).

6.1 Abstract

Most debris flows occur in steep debris-rich mountain channels subject to heavy rainstorm events in a short time. However, the amount of entrained material depends largely on the mobilisable loose debris available for transport, which in turn controls the debris-flow mobility and runout. After a debris-flow event, a system usually recharges with sediments originating from nearby slopes or with material of the above lying catchment. But still very limited data exists regarding the sediment recharge rates and, crucially, which factors control these rates. For this purpose, we investigated the Roßbichelgraben torrent (Oberstdorf, Germany), in which a debris-flow event occurred in June 2015. Ten terrestrial laser scan campaigns, consisting of more than 360 single scan positions, were carried out between June 2015 and October 2018. Additionally, nine temporally synchronised UAV surveys provide more than 7,000 photos, which were used for SfM-based photogrammetry. A 400-metre-long section of the torrent was investigated to reveal the temporal, spatial and seasonal sediment dynamic and channel recharge. Controlling factors were deciphered by means of a nearby meteorological station, delivering high-resolution precipitation values. The results show that both terrestrial laser scanning and SfM-based photogrammetry provide equivalent erosion and deposition volumes (difference < 5%). The channel recharged with 1,150 m³ of sediments between June 2015 and October 2018 (≈ 1 m³/d). The redistribution of sediments is more active in the summer than in winter. The erosion, deposition and net volumes were compared to different rainfall intensities (mm/10 min to mm/72 h) to examine potential links between rainfall pattern and sediment dynamic. The novel approach shows that the post-event sediment dynamic can best be explained (R^2 up to 0.9) by short intense rainstorm events. Additionally, the elapsed time since the last debris flow influences the channel refill significantly, as most over-steepened river banks failed shortly after the event.

6.2 Introduction

Debris flows are destructive mass movements in alpine environments. They occur in steep channelised torrents and are able to transport large amounts of sediments and water at high velocities (Hungr *et al.*, 2014, Varnes, 1978). Their ability to cause loss of agricultural land, economic goods and, crucially, threaten the lives of human beings, makes them one of the riskiest natural hazards. Debris flows can be triggered by both landslide failure (Brayshaw and Hassan, 2009, Iverson *et al.*, 1997) and progressive runoff mobilisation of in-channel stored sediments (Coe *et al.*, 2008, Kean *et al.*, 2013). Their

destructive power largely depends on their impact pressures, which is, among other things, related to the amount of transported material. Consequently, previous research has investigated the growth of debris flows by entraining sediments during flow (Frank *et al.*, 2017, Iverson and Ouyang, 2015, Reid *et al.*, 2016) and the prediction of their potential trajectories (Jakob *et al.*, 2012, Mergili *et al.*, 2017, Schraml *et al.*, 2015b). In addition, the frequency and activity of debris flows has to be known in order to plan countermeasures economically, especially in times of climate change. Authors have shown that the changing climate affects mountain regions in different ways. Some results suggest a decrease in debris-flow activity below the permafrost zone in some areas in the French Alps over the last few decades (Jomelli *et al.*, 2004) while others state an increase in debris-flow activity coincidental with an enhanced rainstorm frequency in parts of the Northern Alps (Dietrich and Krautblatter, 2017), French Alps (Pavlova *et al.*, 2014) and Slovakia Alps (Šilhán and Tichavský, 2016), especially since the 1980s. But the increase in debris-flow activity is restricted by the availability of sediments to be transported. An enhanced debris-flow activity can result in a sediment-limited system, as the recharge of the torrent with sediments is slower than the potential frequency of debris flows (Bovis and Jakob, 1999, Brayshaw and Hassan, 2009, Glade, 2005, Jakob *et al.*, 2005).

In previous studies, a number of different approaches and methods have been applied in order to investigate sediment scour and recharge. Ballantyne (2002) proposed a general model of long-term landscape response to external triggers. He hypothesised that sediment release can be generally displayed by a negative exponential function after a triggering event has occurred (long-term: e.g. deglaciation; short-term: e.g. slope failures after a heavy rainstorm event), but the suggested models are hardly validated by real data. As high quality monitoring data sets are hard to acquire for large study areas and a long time span, most research is based on catchment-scale surveys. Jakob *et al.* (2005) approximated post-debris-flow channel recharge in completely scoured bedrock channels using geometric approximations of newly deposited sediments. Glade (2005) showed that rockfall and solifluction are the most relevant processes for sediment recharge in gullies in Iceland using field mapping and simplified literature retreat rates. Semi-empirical formulas used by Ballio *et al.* (2010) depend on a set of parameters, which are difficult to determine and thus show a large variability in estimated sediment yields. More recent studies monitored geomorphic changes in torrents with total station surveys of cross sections (Theule *et al.*, 2012), terrestrial laser scanning (Blasone *et al.*, 2015, Goodwin *et al.*, 2016, Staley *et al.*, 2014, Theule *et al.*, 2015, Wheaton *et al.*, 2010b) and airborne laser scanning (Cavalli *et al.*, 2017, Goodwin *et al.*, 2017). In areas with no or little vegetation, photogrammetric analyses of UAV surveys, using RTK-GNSS ground control points, also delivered high-resolution field records in less time and at lower costs than TLS surveys (Berger *et al.*, 2011b, Cucchiaro *et al.*, 2018, Fonstad *et al.*, 2013, Javemick *et al.*, 2014, Kenner *et al.*, 2014, Westoby *et al.*, 2012). These studies provided unprecedented high spatial and temporal resolution in relation to channel scour and fill. However, explicit controls on geomorphic changes and their annual and seasonal variability are still not well understood (Berger *et al.*, 2011b, Fuller and Marden, 2011, Veyrat-Charvillon and Memier, 2006). Fuller and

Marden (2011) tried to link rainfall data to geomorphic changes in Waipaoa catchment, New Zealand, but could not decipher clear relationships between normalised cumulated daily rainfall intensities and geomorphic work. Previous studies provided both simplified fixed (Glade, 2005) and more sophisticated changing recharge rates (Jakob *et al.*, 2005) over time and area and are often – when using high-resolution methods – limited to small areal study site extents (Bezak *et al.*, 2017, Theule *et al.*, 2015) or were not performed directly after debris-flow events.

The aim of this paper is to provide a transition from the methodological application of terrestrial laser scanning and photogrammetry to novel geomorphological insights in regard to the post debris-flow sediment dynamic in a mountain torrent. We show that (i) the combination of these two methods can result in a highly reproducible and reliable record of sediment volume changes in the channel by using temporal and spatial variable uncertainties. (ii) Data sets of 13 surveys in the last 3.5 years indicate quantitatively that short and highly intense rainstorms best explain the recorded sediment dynamic (R^2 up to 0.9) resulting in a channel refill (net) of 1,150 m^3 ($\approx$ 1 m^3/d). (iii) We find that the activity of the sediment dynamic in the study area exponentially decreases with elapsed time since the last debris flow, as most over-steepened river banks failed shortly after the event.

6.3 Study site

The study site is located in southern Bavaria, Germany, near the city of Oberstdorf (Figure 51). The catchment area, automatically delineated with ArcGIS 10.5.1, represents an area of 165,330 m^2. The highest elevation in the catchment area represents the Gaisalphorn Mountain with a height of 1953 m a.s.l. The height of the study area (red rectangle in Figure 51) ranges from 1170 m to 1420 m a.s.l. The torrent originates in Upper-Triassic (225-206 myr) Main Dolomite lithology. The fine-crystalline dolomite was intensely jointed in course of the orogenesis of the Alps. The torrent crosses downstream mixed Quaternary scree and moraine material from the last glaciation resting on Cretaceous limestones, marls and mudstones from the Flysch formation. The two nearest rainfall stations recorded an annual mean precipitation from 1981-2010 between 1835 and 2340 mm (DWD Climate Data Center, 2015).

In June 2015 a debris-flow event occurred in the torrent. Most of the transported material was eroded in the channel bed and was deposited a few hundred metres downstream (Figure 52a). The debris flow incised more than 5 m into the underlying substrate (Figure 52b-d).

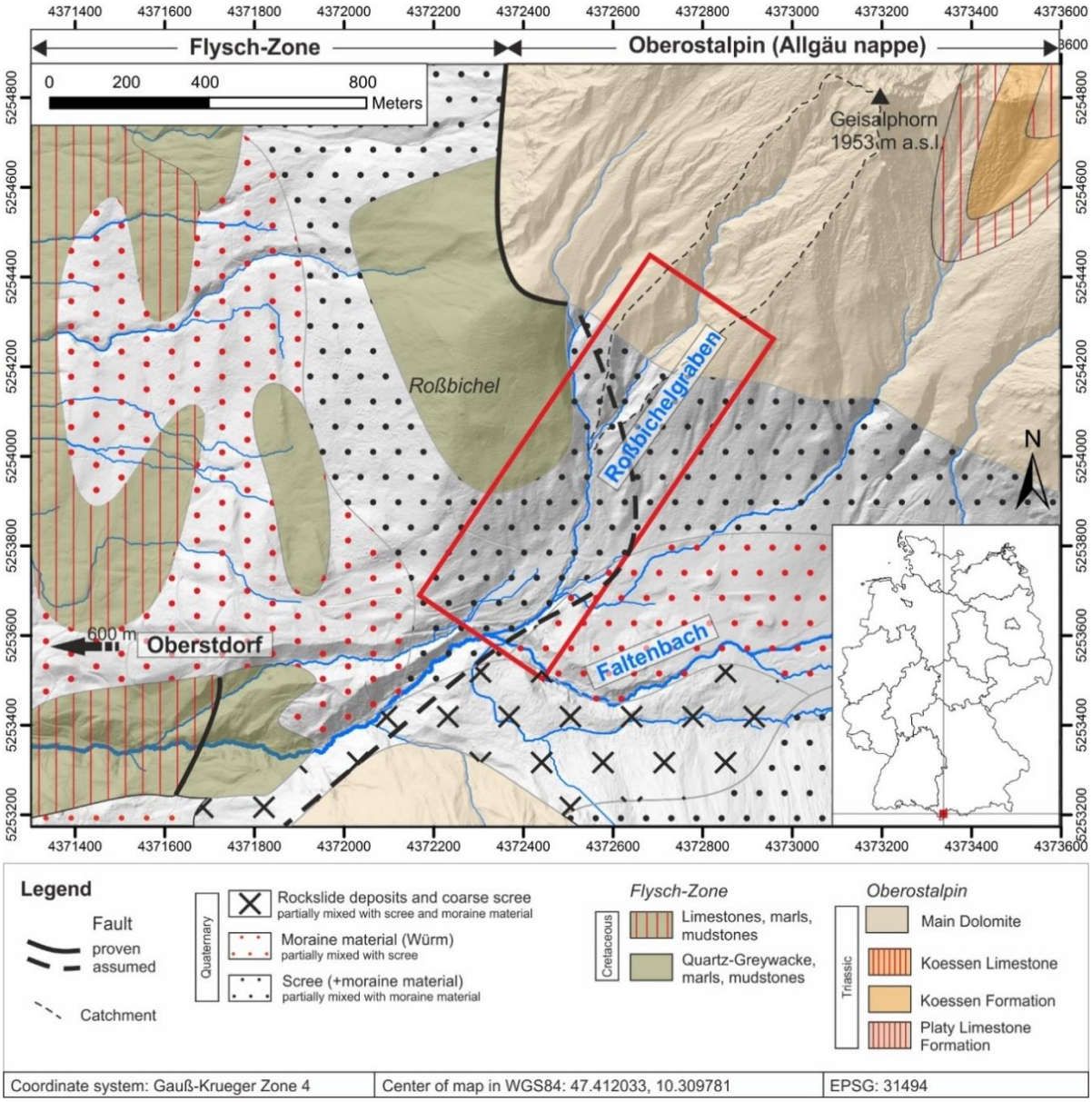

Figure 51: Geological setting of the study site (Zacher, 1985). The torrent "Roßbichelgraben" originates in Triassic dolomites and crosses downstream Quaternary deposits, which mainly consist of dolomites, too. Source of the underlying DEM: Bavarian Surveying and Mapping Authority (2007).

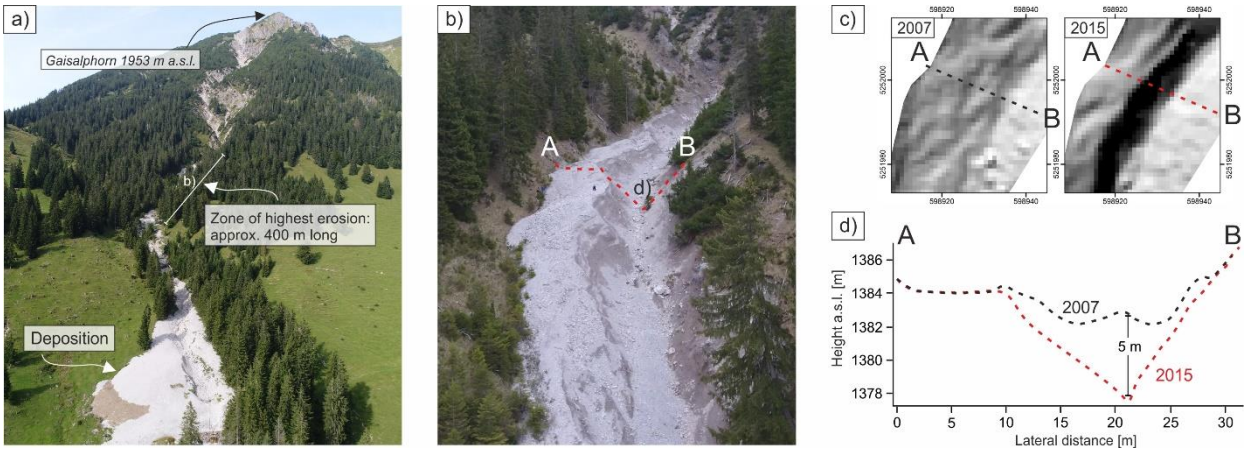

Figure 52: a) Erosion and deposition area of the debris flow. The deposition has been humanly modified. b) and c) Zone of large material entrainment. The torrent was evenly filled up with sediments prior to the event. Erosion heights reach 5 m and more (d).

6.4 Data and methods

6.4.1 Airborne laser scanning

The airborne laser scan of the study area was carried out between 19 April 2007 and 19 June 2007. The metrics, given for this flight, are a height accuracy better than 0.2 m and a positional accuracy better than 0.5 m. As the study area is hardly vegetated (Figure 54b), just little vegetation had to be eliminated using RiSCAN Pro 2.5.1 (Figure 53 middle). The resulting point density is in average 2.7 p/m² (± 1.2 p/m²). Vegetation was eliminated by both a multidimensional filter algorithm and by hand. The point cloud was then linearly interpolated to receive a grid with a cell size of 1 m in X and Y direction. The extents of the data set were set equal to the extents of the SfM and TLS data.

The airborne laser scan data was used – in combination with TLS data from 2015 – to compute the debris-flow volume from the event in June 2015.

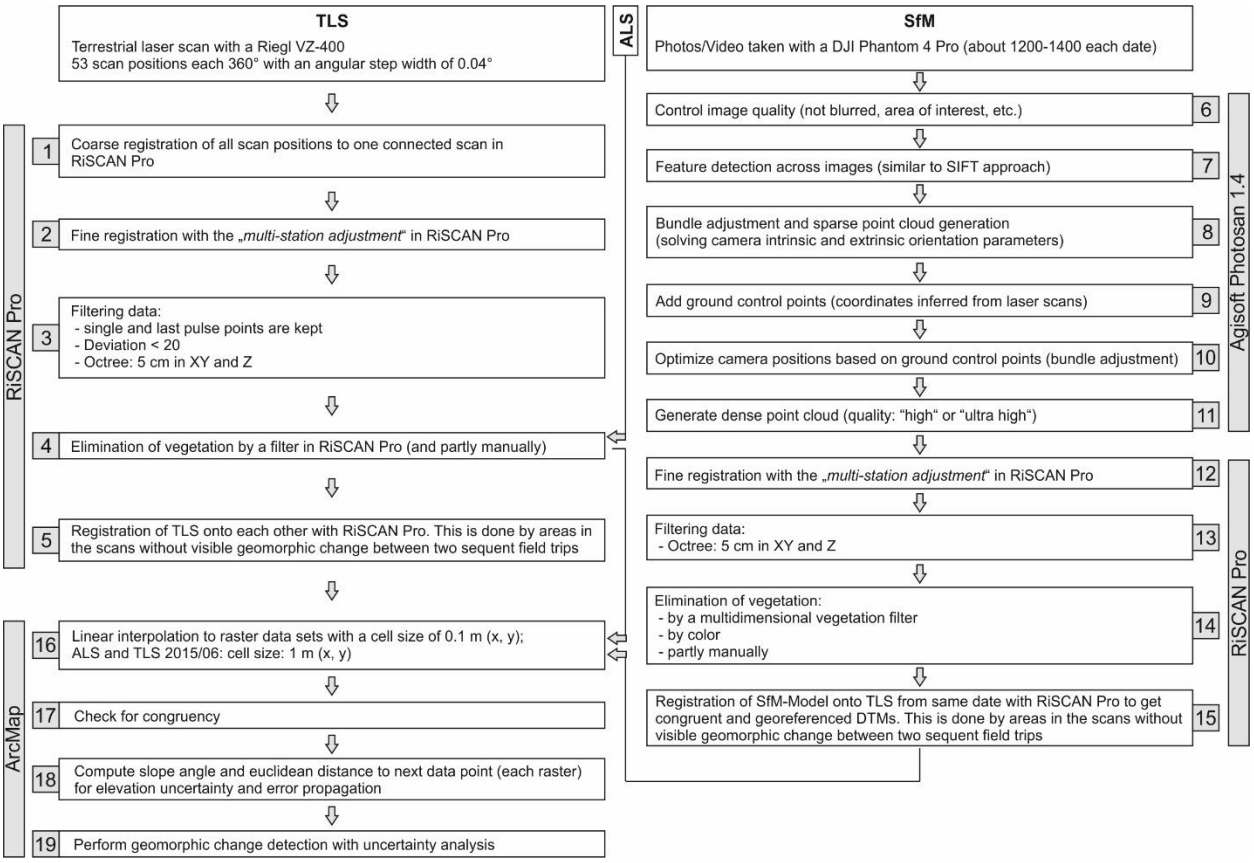

Figure 53: Workflow for the processing of the terrestrial laser scans (TLS), the airborne laser scan (ALS), the processing of the photos for photogrammetric purposes and the resulting geomorphic change detection.

6.4.2 Terrestrial laser scanning

Terrestrial laser scanners produce spatially distributed data points of a surface. To avoid errors, caused by flowing water in the channel bed, we carried out the laser scan campaigns during dry weather conditions without any surficial water flow. We performed the first terrestrial laser scan survey seven days after the event using a RIEGL VZ-400 mid-range laser scanner. Except for the first survey, the number of single laser scans varies between 65 and 80 for the complete torrent (Figure 54a) and between 38 and 40 laser scans for the extent of the UAV surveys (Table 11 and Figure 54a). Scans were performed approx. every 20 m on both sides of the curved channel to avoid shadowed areas in the co-registered point cloud (Figure 54b). The angular step of the laser scanner was chosen of at least 0.06°. The angle measurement resolution was < 0.0005°. The distance between two adjacent data points is approx. 1.5 cm at a distance of 20 m, assuming a vertical-oriented obstacle. The laser pulse of the near infrared wavelength (0.3 mrad beam divergence) was repeated with an effective measurement rate of 122,000 measurements per second. The manufacturer's metrics for the horizontal and vertical accuracy are 5 mm at 100 m. The precision is 3 mm at 100 m.

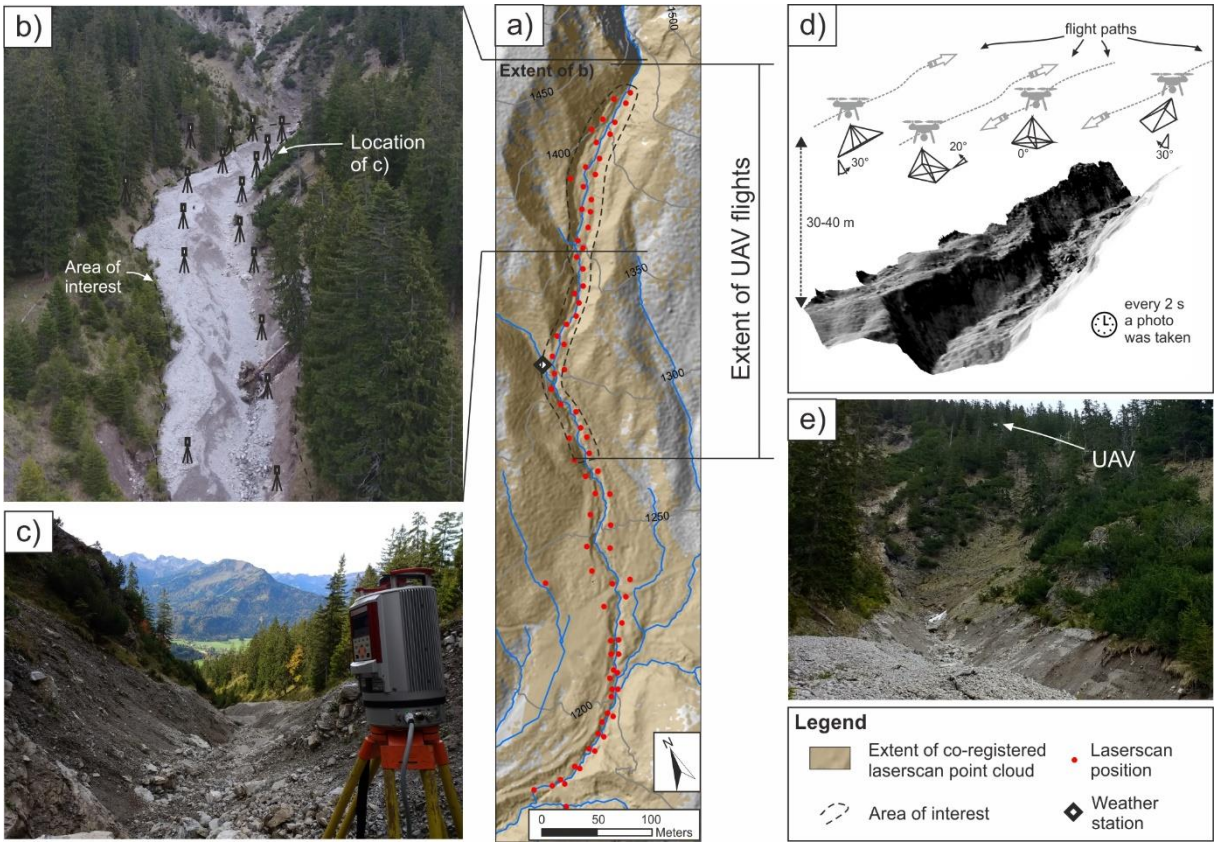

Figure 54: a) Locations of the scan positions in the study area. The area of interest is about 20,000 m². The extent of a) corresponds to the red rectangle shown in Figure 51. b) UAV photograph with approximate positions of laser scans (Photo taken by Florian Konrad). c) In-field application of the laser scanner. d) Sketched flight paths of the UAV with camera orientations. e) In-field application of the UAV.

The co-registration of all scans of one campaign was conducted in RiSCAN Pro (Figure 53, left). At least four corresponding points had to be identified in two consecutive point clouds. To fine-register all scans, the so-called multi-station adjustment was applied (Riegl LMS, 2013). Thus, an algorithm

identified plane segments in each point cloud. An ICP algorithm (Besl and McKay, 1992) iteratively minimised the distances of normal vectors of these plane areas between two scan positions. Afterwards, the data of each survey was filtered by a deviation gate < 20 (Williams *et al.*, 2018), limiting the change in shape of the received waveform to eliminate erroneous data points. Additionally, just single and last pulse points were kept. The point cloud was then filtered to 5 cm in all three dimensions (XYZ) and vegetation was both automatically and manually eliminated in RiSCAN Pro. The combined point cloud of each TLS survey was in turn registered onto the previous survey by identifying stable areas between two consecutive surveys (Table 12). The standard deviations of these co-registrations showed error values less than 2.5 cm (Table 12), except for the ALS-TLS co-registration (25.4 cm), due to the significantly lower resolution. Finally, the TLS point clouds were filtered to cells with an edge length of 0.1 m and were linearly interpolated to raster data sets with a cell size of 0.1 m. All data sets were checked for congruency.

Table 11: Number of laser scan positions and number of UAV photos used to derive the corresponding point clouds and DEMs.

	Laser scanning			UAV				
Survey date	No. of laser scans	Points (unfiltered)		No. of UAV Photos	Photo Quality [MP]	Dense points (unfiltered)	GCPs	Total Error GCPs [m]
2015/06	14	297,950,423		-		-	-	-
2016/06	39	769,602,413		-		-	-	-
2016/09	40	420,364,909		-		-	-	-
2017/05	39	424,005,539		744	8	370,685,445	21	0.010
2017/06	40	408,373,386		-		-	-	-
2017/07	40	433,756,758		551	20	508,130,045	21	0.012
2017/08	39	419,384,584		634	20	574,587,380	20	0.012
2017/10	38	407,113,668		640	20	507,804,609	21	0.010
2018/05	39	442,370,066		747	20	600,838,744	37	0.031
2018/06	-	-		988	20	176,269,601	37	0.036
2018/07	-	-		928	20	205,572,702	37	0.036
2018/08	-	-		952	20	181,715,636	37	0.033
2018/09	37	434,608,079		917	20	184,686,931	37	0.026

Table 12: Standard deviations (cm) between two consecutive point clouds as a result of the multi-station adjustment (MSA) in RiSCAN Pro.

			Long time intervals					
	Compared point clouds	DF 2015/06-2007	TI-1 (2016/06-2015/06)	TI-2 2016/09-2016/06	TI-3 2017/05-2016/09	TI-4 2017/10-2017/05	TI-5 2018/05-2017/10	TI-6 2018/08-2018/05
Std. dev. [cm]	ALS-TLS	25.4	-	-	-	-	-	-
	TLS-TLS	-	2.1	1.0	1.4	1.1	0.8	-
	SfM-SfM	-	-	-	-	2.0	2.5	2.0

		Short time intervals							
	Compared point clouds	TI-4.1 2017/06-2017/05	TI-4.2 2017/07-2017/06	TI-4.3 2017/08-2017/07	TI-4.4 2017/10-2017/08	TI-6.1 2018/06-2018/05	TI-6.2 2018/07-2018/06	TI-6.3 2018/08-2018/07	DF 2018/09-2018/08
Std. dev. [cm]	TLS-TLS	0.5	0.8	0.6	0.6	-	-	-	-
	SfM-SfM	1.7		0.9	0.9	1.4	1.3	1.6	2.0

6.4.3 SfM photogrammetry

The number of processed photos of each UAV survey ranges from 551 to 988 (Table 11). The photos were taken during constant light conditions with high fog or clouds to avoid overexposure and partly shadowed areas. In May 2017, the DJI Phantom 4 captured a 4K video, on all other dates a Phantom 4 Pro was used, capturing photographs every 2 seconds. Four flight paths were flown for each survey (Figure 54) with a varying orientation of the camera to minimise systematic errors in the topographic models derived from the images (James and Robson, 2014).

The images have a resolution of 8 MP (May 2017) to 20 MP (all other surveys). The UAV speed was approx. 1 m/s at a height of 30-40 metres above ground surface, which results in an imagery ground sample distance of approx. 1 cm. Depending on the light conditions, the shutter speed ranged between 1/240 s and 1/400 s to avoid blur in the images. All images were taken with at least 80% forward and 60% side overlap (Colomina and Molina, 2014).

All photos were processed with Agisoft PhotoScan Pro (v.1.4.4). This included feature detection across images by a similar approach to the well-established Scale Invariant Feature Transform (SIFT) algorithm (Lowe, 1999, Lowe, 2004). Afterwards, a bundle adjustment resolved the camera's intrinsic and extrinsic orientation parameters and a sparse point cloud was generated. All the point clouds were georeferenced by ground control points (GCPs) based on objects that could be clearly recognised in both TLS data and images. All coordinates were extracted from TLS data and implemented in the UAV-based point clouds (Martínez-Espejo Zaragoza *et al.*, 2017). The dense cloud was generated by a multi-view stereo reconstruction (Figure 53). The reconstruction parameter for the dense cloud generation was set to "ultra high" (original photo size was processed) for data sets from May 2017 to May 2018 and reduced to "high" (downscaling by factor of four) for data sets from June 2018 to September 2018 to save processing time (Table 13). The resulting point clouds were further processed similarly to the TLS data in RiSCAN Pro (Figure 53). Vegetation was additionally filtered by RGB colour values (green and

brown). All filtered UAV-derived point clouds were then co-registered with the temporarily synchronised recorded TLS point clouds or, if not available, with stable areas of the point cloud of the respective last survey (Table 12).

Table 13: Chosen values for feature detection, image alignment, bundle adjustment and dense cloud generation in Agisoft PhotoScan Pro.

Feature detection and image alignment			Bundle adjustment			Dense cloud generation	
Accuracy	Highest		Image Count	2		Quality	Ultra high (05/2017-05/2018) High (06/2018-09/2018)
Reference preselection	Yes		Reprojection error	0.2		Depth filtering	Aggressive
Key point limit	unlimited		Projection accuracy	5			
Tie point limit	unlimited		Reconstruction uncertainty	25			

6.4.4 Change detection and uncertainty analysis

All the DEMs suffer from imprecise survey planning, diverse inaccuracies of the measurement system used and processing errors, such as inaccurate image matching, residual vegetation and erroneous interpolation between adjacent data points. As a result, studies have suggested different approaches for error treatment in repeated scan and UAV surveys. Some authors account for errors in DEM differencing by using a general detection threshold ($_{min}$LoD) (Brasington *et al.*, 2000, Fuller *et al.*, 2003). Although this technique is straightforward and easy to apply, the method is unable to distinguish more or less erroneous raster cells. Therefore, more recent studies provide procedures to specify and derive typical and spatially variable errors, representing uncertainties of the measurement system used and errors inherent to the object or area being studied (Bangen *et al.*, 2016, James *et al.*, 2017, Schaffrath *et al.*, 2015). In our study, topographic errors were mainly determined by two factors: (i) boulders of different size caused a high roughness of the riverbed and (ii) shadowed areas in the TLS surveys caused interpolated areas, whose uncertainty increases with the distance to the nearest data point measured.

All point clouds since 2015 have been rasterised and interpolated linearly to DEMs of 10 cm cell size in the X and Y direction. The ALS data and the first TLS survey of May 2015 were rasterised to 1 m DEMs, as the point density of the ALS data set was significantly lower than all following TLS data sets. We used the ArcGIS Add-In "Geomorphic change detection" (v. 7.4) of Wheaton *et al.* (2010b). Within this tool, the user can specify and quantify different sources of errors, which occur by rasterising and interpolating a point cloud to a raster. To account for the riverbed roughness, we used the slope angle of the DEMs and related the value to three different levels of uncertainty (Figure 55). Additionally, the Euclidean distance to the next neighbouring data point was considered to represent different degrees of interpolation errors. We used a fuzzy interference system to avoid hard limits of each group. The combination of different degrees of uncertainty (inputs) results – using membership functions – in an elevation uncertainty (output) for each individual DEM on a cell by-cell basis (Figure 55), and thus

varies spatially. These individual DEM uncertainties were propagated cell-wise into the DEM of Difference (DoD) using the square root of the squared individual elevation uncertainties of the new and old DEM (Brasington *et al.*, 2003). Considering a t-score, derived from the DoD value and the DoD elevation uncertainty (Wheaton *et al.*, 2010b), all elevation changes with a probability of less than 95% (t=1.96, two tailed test) were thresholded out. All other elevation changes were assumed to be significant and real. For a more detailed methodological description we refer to Wheaton *et al.* (2010b).

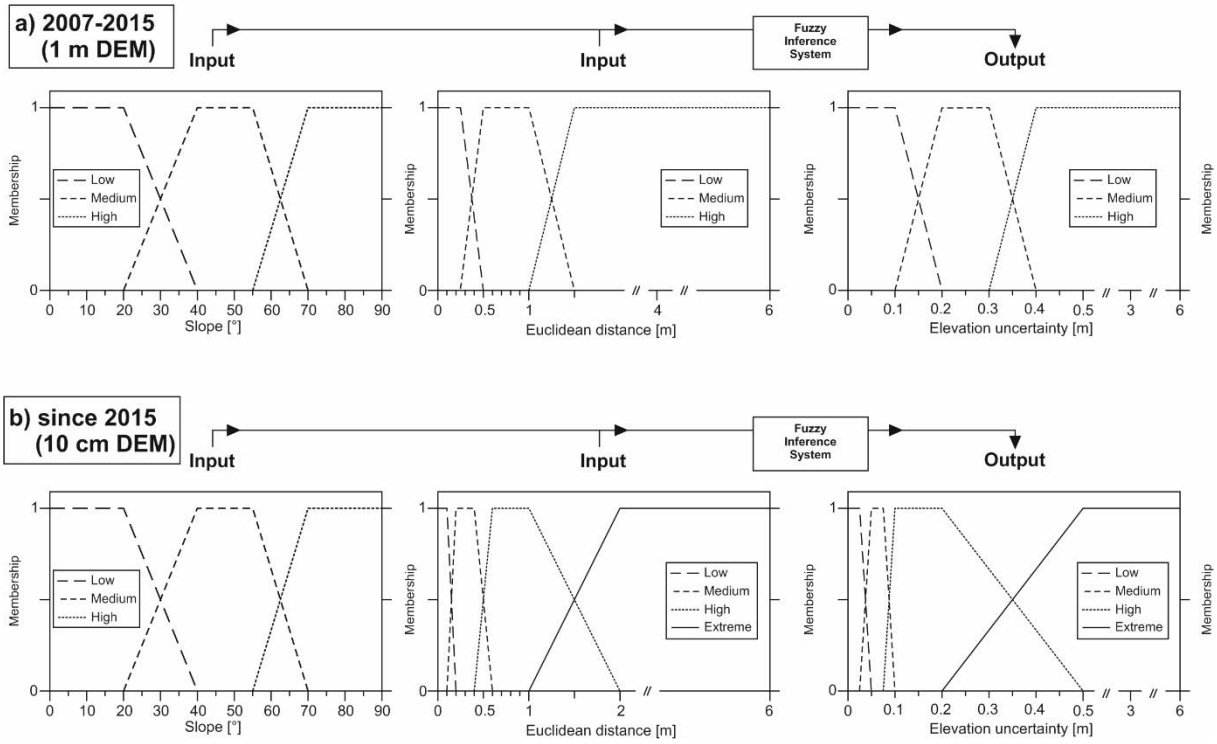

Figure 55: Applied fuzzy interference systems to account for uncertainties in DEM generation and change detection. Input values are slope raster data sets of the DEMs and the Euclidean distance of a data point to the spatially next data point. In b) an additional uncertainty class ("extreme") was introduced for raster cells that were linearly interpolated over a large distance and, thus, were subject to high elevation errors.

6.4.5 Rainfall data

To investigate potential relations between sediment dynamic and rainfall, we used rainfall intensities ranging from mm/10 min, mm/1 h, mm/6 h, mm/24 h to mm/72 h. The rainfall station is located in the catchment area next to the torrent (Figure 54). As the station is unable to measure snow fall intensity (approx. December-March), the data on these months were substituted by data from the nearest DWD station in Oberstdorf, which is 2.5 km away from the torrent (Figure 56). Both stations have a logging interval of 10 minutes.

Figure 56 gives an overview of the occurred rainfall intensities in mm/h and the dates, on which the laser scan and UAV surveys were conducted. The time intervals are named TI-1 to TI-6 (long time intervals). Time intervals between higher frequently performed surveys in summer 2017 and 2018 are named 4.1 to 4.4 and 6.1 to 6.3 (short time intervals).

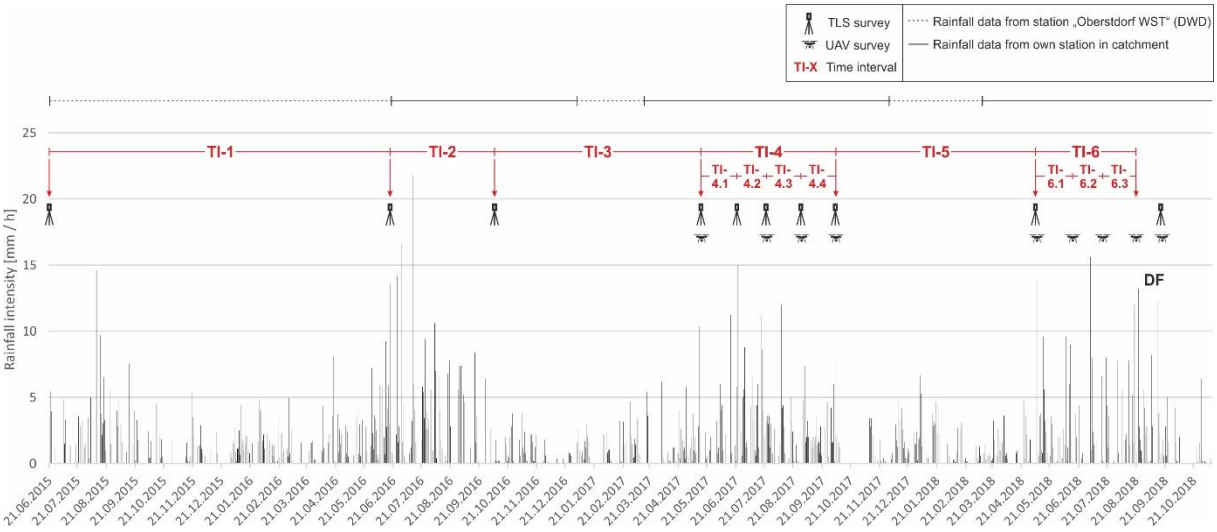

Figure 56: Rainfall intensities from 06/2015 to 10/2018. The lines on top of the figure indicate the source of the data. TI-# refers to the number of the time interval.

6.5 Results

6.5.1 Change detection

6.5.1.1 Debris-flow event (ALS and TLS data)

The geomorphic change detection of the ALS-derived DEM from 2007 and the first TLS-derived DEM from June 2015 accurately reveals the erosion and deposition areas of the debris-flow event in June 2015 (Figure 57). It shows that a volume of more than 12,600 m³ has been eroded, mainly from the upper part of the channel (Figure 57a-c, Table 14). This material mostly originates from channel-bed entrained sediments with incision depths up to 6 m. A larger proportion (approx. 7,000 m³) of the transported flow volume was deposited a few hundred metres downstream, which was then excavated and moved next to the torrent a few weeks after the event. A volume of more than 5,500 m³ was transported into the receiving channel “Faltenbach”. Typical indications of a debris flow could be observed in and along the channel (Figure 57d-g), including debris-flow marks on trees, levees on both sides of the channel, deep incisions in the channel bed and a debris-flow head in the deposition zone.

Subsequent to the event, the questions arose of whether (and if so, then how fast) this torrent will be refilled with sediments and which factors control these processes.

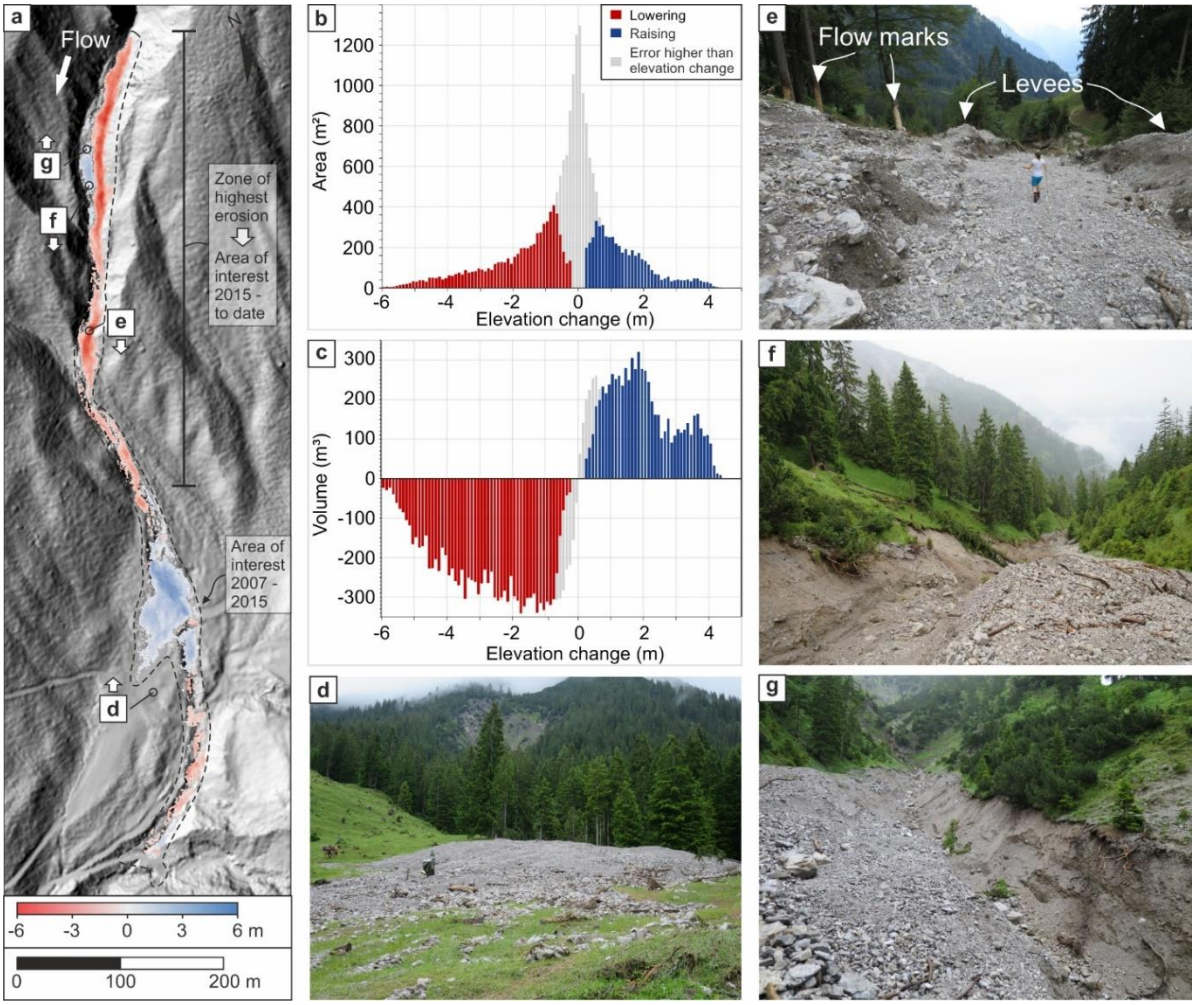

Figure 57: a) Erosion and deposition areas of the debris-flow event in June 2015 in the Roßbichelgraben torrent. b) Areal elevation changes in the area of interest. c) Volumetric elevation changes in the area of interest. d)-g): Photographs of debris-flow characteristics shortly after the event. Their location is shown in a). The arrows indicate the direction in which the photographs were taken. Source of underlying DEM: Bavarian Surveying and Mapping Authority (2007).

Table 14: Volumetric changes from 2007 to June 2015 mainly caused by the debris-flow event in June 2015. Raster cell size for the calculation is 1 m.

	Volume [m³]		± Error [m³]	% Error
Total volume of surface lowering [m³]	12,610	±	1,660	13
Total volume of surface raising [m³]	7,080	±	940	13
Total volume of difference [m³]	19,690	±	2,600	13
Total net volume difference [m³]	-5,530	±	1,900	34

6.5.1.2 Sediment redistribution from 2015 to date (TLS data only)

To investigate the post-depositional debris-flow material dynamic in the torrent, TLS surveys over the same range as shown in Figure 57a were performed. These TLS surveys showed that sediment redistribution is clearly more active in the upper part of the torrent. In some periods practically no changes could be observed in the lower parts, as many drop structures were implemented in the channel after the event, functioning as sediment traps. Hence, the UAV surveys were only conducted in the upper part of the torrent (approx. 400 m long, see Figure 54a). All following change detections (TLS and UAV) and volume calculations relate to this upper part of the channel.

6.5.1.2.1 Long time intervals

The change detections reveal that most material (in absolute numbers) was redistributed in the first time interval (TI-1) after the debris-flow event, from June 2015 to June 2016 (Figure 58 and Table 15). Due to the deep incision of the debris flow, many slopes partly collapsed shortly after the event (Figure 58a). The eroded material was deposited nearby or tens of metres downstream. However, the time-normalised values for erosion, deposition and net volume increased from TI-1 to TI-2 (June to September 2016) and decreased in the winter months from October 2016 to May 2017 (TI-3) (Figure 58d, g and Table 15). The activity increased again in summer 2017 (TI-4) and summer 2018 (TI-6), interrupted by a period of reduced sediment dynamic in winter 2017/2018 (TI-5). Elevation changes in the study area reach a maximum of 4 m (Figure 58b and c), but lie often in range from -2 to 2 m (Figure 58f,i,l,o and r). The resulting normalised volumetric changes range from 0.24 m³/d to 4.28 m³/d for surface lowering, 0.54 m³/d to 4.45 m³/d for surface raising and -0.48 m³/d to 0.76 m³/d for net volume difference (Table 15). With the exception of the first value from June 2015 to June 2016, all the net volume differences for these time intervals (TI-2 to TI-6) show positive values, representing channel refill with sediments.

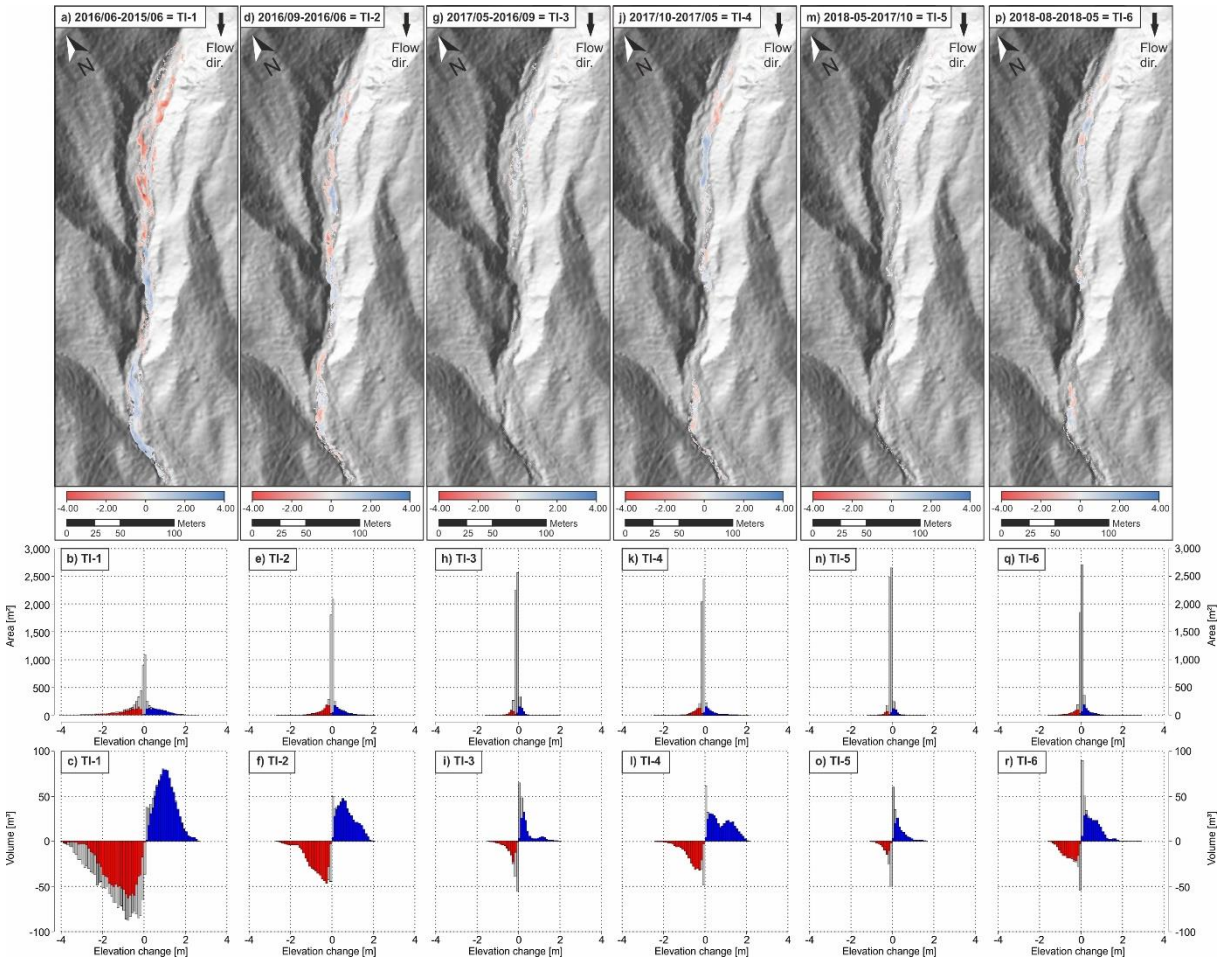

Figure 58: Sediment dynamic after the debris-flow event in 2015. A-c: June 2015-June 2016. D-f: June 2016-September 2016. G-i: September 2016-May 2017. J-l: May 2017-October 2017. M-o: October 2017-May 2018. P-r: May 2018-August 2018.

Table 15: Total and normalised volumes for surface lowering, surface raising and net volume difference for each time interval. Normalised volumes are given in cubic metres per day.

	TI-1 2016/06- 2015/06	TI-2 2016/09- 2016/06	TI-3 2017/05- 2016/09	TI-4 2017/10- 2017/05	TI-5 2018/05- 2017/10	TI-6 2018/08- 2018/05
Total volume of surface lowering [m³]	1,100±160	450±60	90±20	250±40	50±10	180±30
Total volume of surface raising [m³]	930±100	470±50	140±30	370±40	120±30	260±40
Total net volume difference [m³]	-170±190	20±80	50±40	120±50	70±30	80±40
Normalised volume of surface lowering [m³/d]	3.06±0.44	4.28±0.55	0.38±0.10	1.74±0.25	0.24±0.07	1.70±0.24
Normalised volume of surface raising [m³/d]	2.58±0.28	4.45±0.46	0.61±0.14	2.50±0.26	0.54±0.11	2.43±0.34
Normalised net volume difference [m³/d]	-0.48±0.60	0.17±0.79	0.23±0.20	0.76±0.38	0.29±0.14	0.73±0.33

To conclude: The normalised values (Table 15) suggest (i) a seasonal varying sediment dynamic (summer vs. winter), (ii) a decreasing activity with time (except for the first interval, which represents one complete year and, thus, the activity cannot be distinguished for summer and winter) and (iii) a slightly increasing net volume with time (also with an seasonal variation).

6.5.1.2.2 Short time intervals in summer 2017 and 2018

We also analysed the sediment redistribution in summer 2017 and 2018 at a higher temporal resolution (Table 16). The change detections show that a highly variable amount of material is moved in each month. The values range for erosion between 0.1 m³/d and 5.1 m³/d, for deposition between 0.2 m³/d and 8.4 m³/d and for the net volume difference between -1.0 m³/d and 3.3 m³/d. Except for the period between August and October 2017, all the time intervals show positive net volume differences. No general trends can be seen in these short-term data.

Table 16: Total and normalised volumes for surface lowering, surface raising and net volume difference for each time interval in summer 2017 and 2018. Volumes for TI-4.1 to TI-4.4 are derived from TLS data, for TI-6.1 to TI-6.3 from UAV data. Normalised volumes are given in cubic metres per day.

	TI-4.1 2017/06- 2017/05	TI-4.2 2017/07- 2017/06	TI-4.3 2017/08- 2017/07	TI-4.4 2017/10- 2017/08	TI-6.1 2018/06- 2018/05	TI-6.2 2018/07- 2018/06	TI-6.3 2018/08- 2018/07
Total volume of surface lowering [m³]	2±1	198±29	20±4	91±15	174±24	45±10	8±2
Total volume of surface raising [m³]	6±2	329±34	30±5	55±10	215±30	63±18	15±4
Total net volume difference [m³]	4±2	130±45	10±7	-37±18	41±39	18±16	8±5
Normalised volume of surface lowering [m³/d]	0.07±0.02	5.09±0.75	0.11±0.03	2.61±0.43	4.46±0.63	1.28±0.27	0.23±0.07
Normalised volume of surface raising [m³/d]	0.19±0.07	8.42±0.88	0.52±0.14	1.56±0.29	5.51±0.77	1.91±0.37	0.35±0.10
Normalised net volume difference [m³/d]	0.12±0.07	3.33±1.22	1.07±0.23	-1.04±0.52	1.05±1.00	0.63±0.46	0.12±0.16

6.5.1.3 Comparison of TLS data and SfM data sets

The change detection analyses with DEMs, derived from temporally synchronised UAV surveys, show equivalent results compared to change detections performed with TLS data sets. Both raw and thresholded volumes lie in a very similar range with almost equal error values (Table 17 and Figure 59).

Table 17: Total volumes for surface lowering, surface raising and net volume difference for temporally synchronised TLS and UAV surveys.

		TI-4 2017/10-2017/05	TI-4.1 + TI-4.2 2017/07-2017/05	TI-4.3 2017/08-2017/07	TI-4.4 2017/10-2017/08
TLS	Total volume of surface lowering [m³]	254±36	196±29	20±4	91±15
	Total volume of surface raising [m³]	365±39	338±37	30±5	55±10
	Total net volume difference [m³]	111±53	142±47	10±7	-37±18
SfM	Total volume of surface lowering [m³]	250±36	194±29	21±5	90±15
	Total volume of surface raising [m³]	376±40	340±37	32±6	57±11
	Total net volume difference [m³]	125±54	146±47	11±7	-33±18

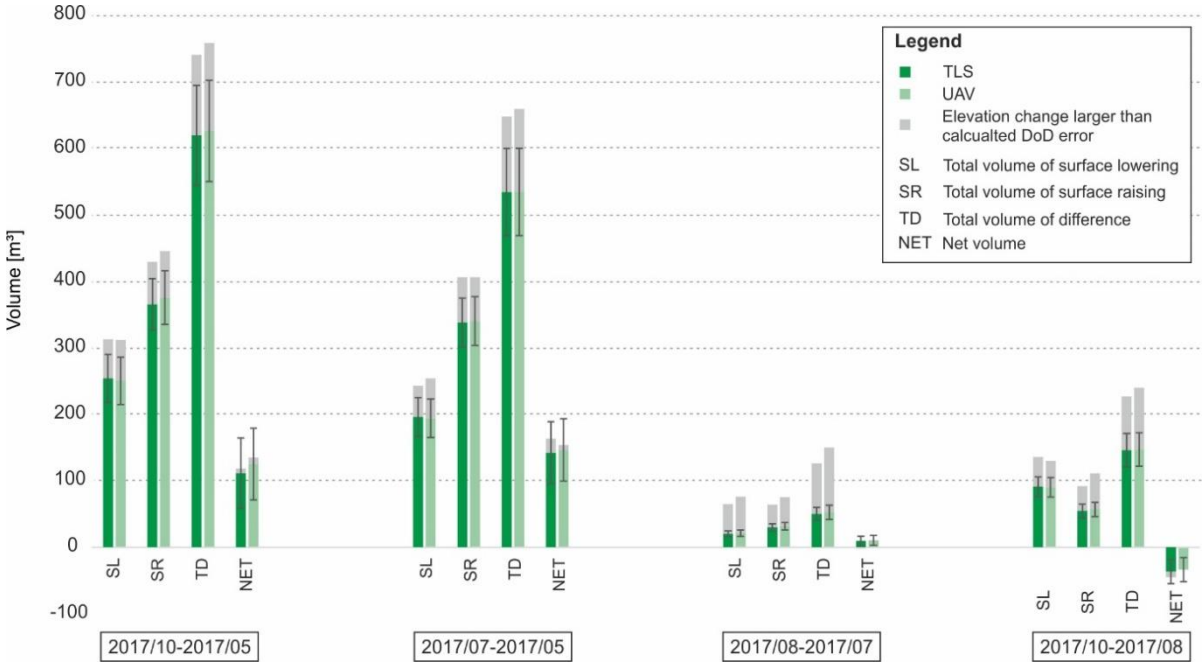

Figure 59: Comparison of the calculated volumes derived from temporally synchronised TLS (dark green) and the UAV (light green) surveys.

6.5.2 Rainfall as controlling factor

To check whether channel scour and fill can be related to rainfall events, we used rainfall intensities (named as mm/time in the following formula) ranging from mm/10 min, mm/1 h, mm/6 h to mm/24 h and mm/72 h. We also examined whether an exponential weighting factor (x) of these rainfall events provides improved correlations for channel scour and fill. Our hypothesis was that the sediment volume moved (erosion, deposition and net) in a given time span is proportional to the sum of the weighted rainfall events in the same time span, respectively:

Equation 25:

$$\text{Sediment volume moved [m}^3\text{/d]} \sim \Sigma(\text{mm/time})^x$$

The value range of the exponent *x* was chosen from 1 to 4 in 0.2 intervals. We also set intensity thresholds to discard low-intensity rainfall events (see legend in e.g. Figure 60). Accordingly, we investigated, which rainfall intensities – weighted differently – have the largest impact on sediment fluxes in the torrent.

6.5.2.1 Complete study area

The term "complete study area" refers to both channel bed, adjacent river banks and all other areas, which were recorded by TLS and UAV surveys. We analysed the data sets for long time intervals (TI-1 to TI.6, Figure 60a-o) and short summer intervals (TI-4.1 to TI-6.3, Figure 60p-ad) separately. Each individual graph in Figure 60 represents 96 colour-coded R^2 values of linear regression analyses based on different intensity thresholds (colour) and weighting factors (x-axis).

It shows that the erosion of sediments in the area studied can best be explained for the longer time intervals (TI-1 to TI-6) by rainfall intensities from mm/10 min to mm/6 h with a coefficient of correlation up to 70% (Figure 60b-c). The exponential weighting of rainfall events marginally influences the results (Figure 60a-e). The coefficient of correlation increases slightly with an increased weighting exponent (larger value of the exponent *x*), except for 3-day rainfall intensities (Figure 60e). Deposition of sediments are largely controlled (R^2 up to 0.9) by short and highly intense rainstorms (Figure 60f-h), representing rainfall durations from 10 min to 6 h, hardly influenced by the weighting factor. Longer rainfall events (24 h to 72 h) show a considerably lower correlation. Although both erosion and deposition of sediments in the studied area can be explained by a large portion by short and heavy rainstorm events, the total net volume shows low coefficients of correlation (up to 25%), especially for longer rainfall durations (Figure 60k-o). For each investigated rainfall duration, the R^2 value converges with an increasing weighing exponent in relation to different intensity thresholds.

Looking at shorter time intervals in summer (Figure 60p-ad), we can see that R^2 values are significantly higher for rainfall intensities between mm/10 min and mm/1 h than for all longer rainfall intensities, in relation to erosion, deposition and net volume in the study area. Up to 95% of the total eroded sediment volume can be explained by these short rainfall events (mm/10 min mm/1 h), especially with weighting factors between 1.5 and 2.5, without or with low thresholds (Figure 60p-q). We obtained similar results in regard to the coefficients of correlation for the deposition volumes (Figure 60u-v). Low-intensity rainfall events do not explain erosion and deposition of sediments in the study area. The R^2 increases (Figure 60p, q, u, v, z and aa) when these rainfall events are either thresholded out or have less influence due to the higher exponential weighting.

Some of the graphs, representing individual R^2 values (dots) in Figure 60, are shown as examples for both long (Figure 61a-c) and short time intervals (Figure 61g-i) with corresponding residuals (Figure 61d-f and j-l, respectively) for the applied linear regression analyses.

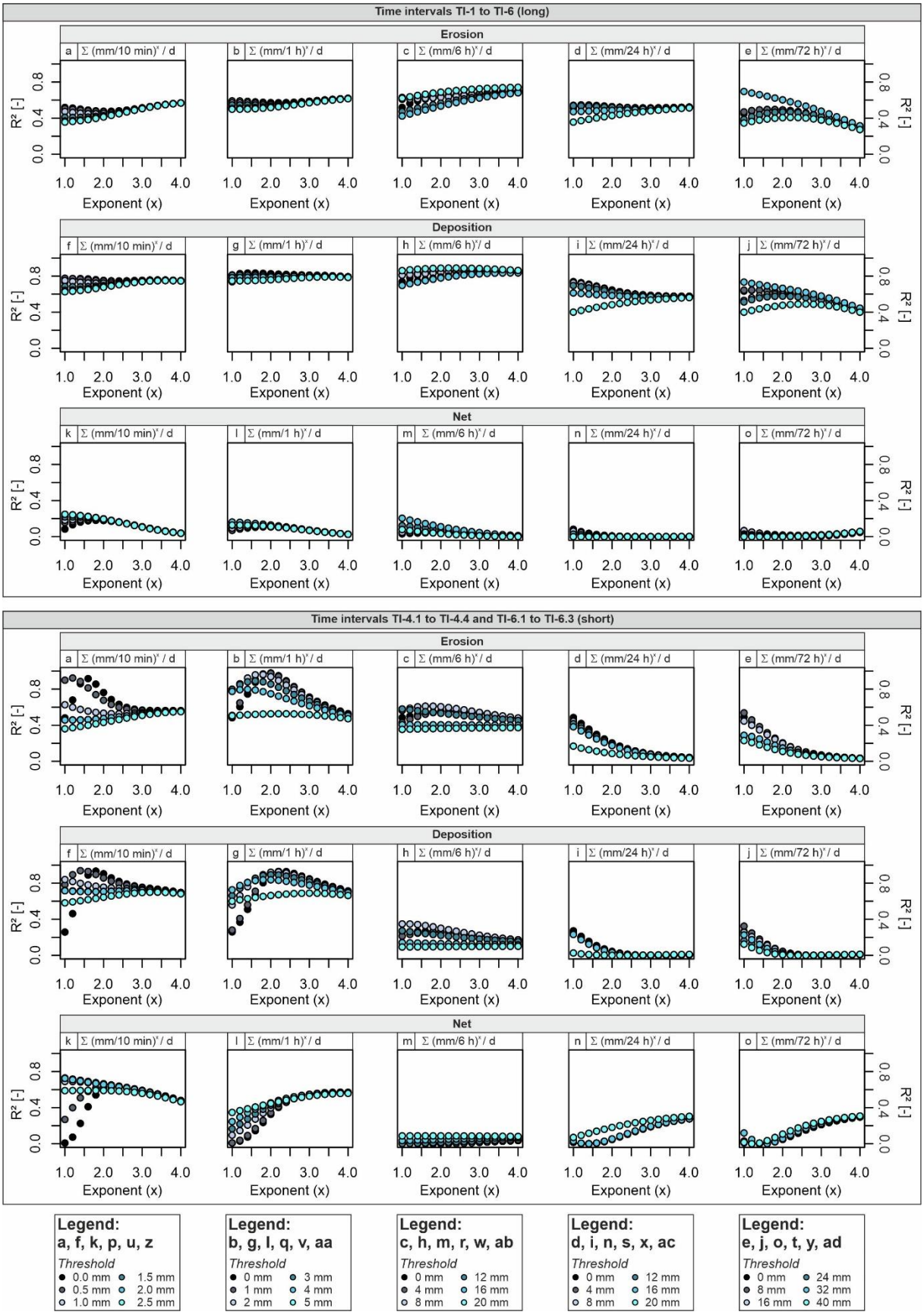

Figure 60: Sediment redistribution in the *complete study area* is taken into account. Relationship between R², exponent (x) and rainfall intensity duration. Different colours refer to different intensity thresholds from mm/10 min to mm/72 h. Values lower than the threshold values shown were not considered in the analysis.

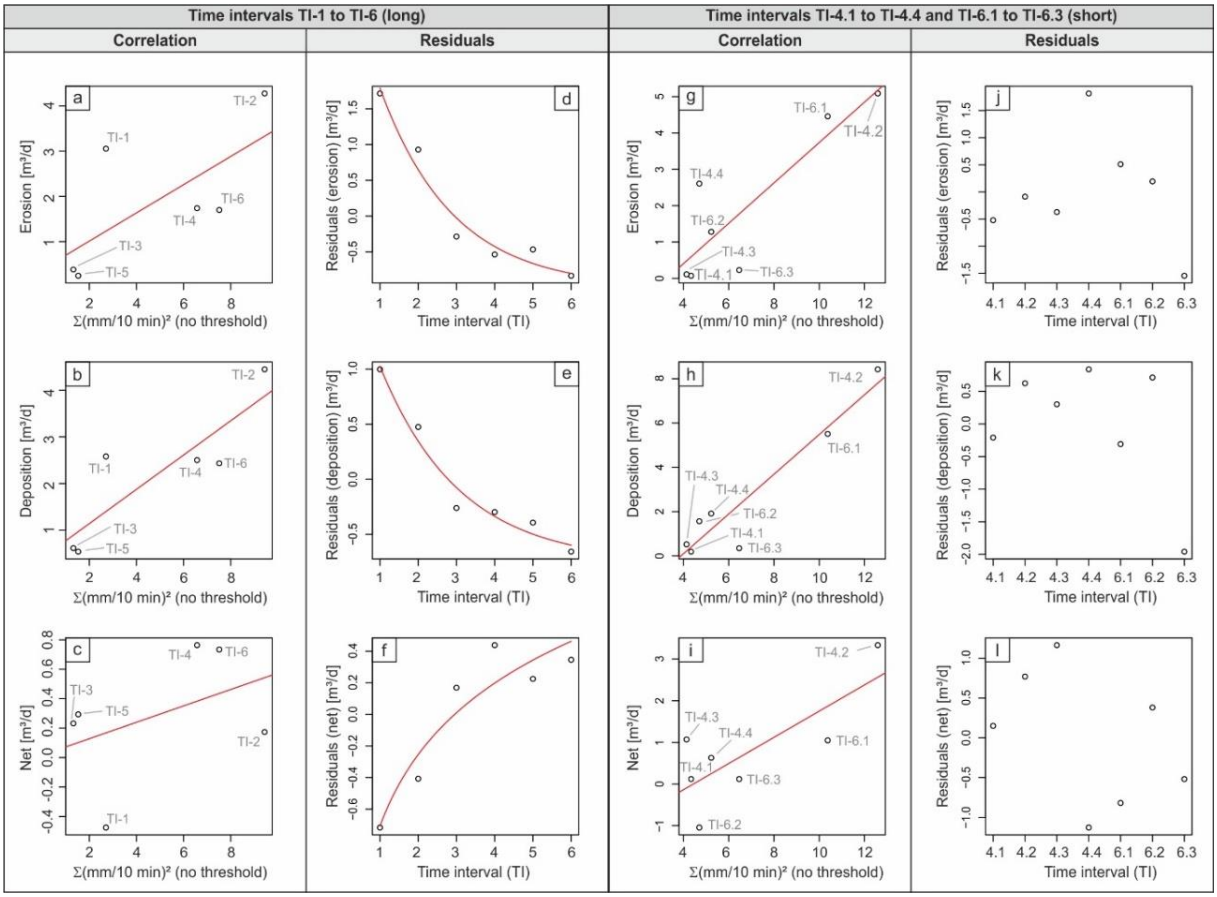

Figure 61: Relationships between summed weighted (exponent = 2) rainfall intensity (mm/10 min) and sediment dynamic in the long time intervals TI-1 to TI-6 (a-c) and short summer time intervals TI-4.1 to TI-6.3 (g-i). Corresponding residuals of the data points in a-c are shown separately in d-f and the residuals in g-i are displayed separately in j-l. In this figure the sediment dynamic in the *complete study site* is displayed.

Lining up the residuals according to the elapsed time since the debris-flow event in June 2015, it shows that they depict an exponential decline in sediment erosion (Figure 61d) and deposition volumes (Figure 61e). Simultaneously, the variance of the residuals decreases with time. In contrast, the net volume increases with time (Figure 61f), also with a decreasing variance of the residuals. The residuals within the summer of 2017 and 2018 (Figure 61j-i) scatter with no general trend.

6.5.2.2 Channel bed

We performed the same analysis (as is Chapter 6.5.1.2) for the channel bed solely, neglecting all adjacent river banks and slopes (Figure 62, Table 18 and Table 19). Hence, we were able to analyse the refill of the channel bed with sediments, which are available for potential future debris-flow events. A net volume of more than 1,150 m³ was deposited, representing an average refill rate of about 1 m³/d in relation to the complete time span. However, this rate varies for the individual time intervals from 0.26±0.05 m³/d (TI-5) to 2.12±0.52 m³/d (TI-2).

Table 18: Total and normalised volumes in regard to the *channel bed solely* for surface lowering, surface raising and net volume difference for each time interval. Normalised volumes are given in cubic metres per day.

	TI-1 2016/06- 2015/06	TI-2 2016/09- 2016/06	TI-3 2017/05- 2016/09	TI-4 2017/10- 2017/05	TI-5 2018/05- 2017/10	TI-6 2018/08- 2018/05
Total volume of surface lowering [m³]	300±50	240±30	10±1	190±20	10±3	150±20
Total volume of surface raising [m³]	900±90	460±50	110±20	360±40	70±10	230±30
Total net volume difference [m³]	600±100	220±50	100±20	170±40	60±10	80±30
Normalised volume of surface lowering [m³/d]	0.81±0.14	2.22±0.29	0.01±0.00	1.26±0.17	0.05±0.01	1.41±0.18
Normalised volume of surface raising [m³/d]	2.47±0.25	4.34±0.43	0.46±0.09	2.44±0.25	0.31±0.06	2.20±0.28
Normalised net volume difference [m³/d]	1.66±0.29	2.12±0.52	0.45±0.09	1.18±0.30	0.26±0.05	0.79±0.33

Table 19: Total and normalised volumes in regard to the *channel bed solely* for surface lowering, surface raising and net volume difference for each time interval in summer months of 2017 and 2018. Volumes for TI-4.1 to TI-4.4 are derived from TLS data, for TI-6.1 to TI-6.3 from UAV data. Normalised volumes are given in cubic metres per day.

	TI-4.1 2017/06- 2017/05	TI-4.2 2017/07- 2017/06	TI-4.3 2017/08- 2017/07	TI-4.4 2017/10- 2017/08	TI-6.1 2018/06- 2018/05	TI-6.2 2018/07- 2018/06	TI-6.3 2018/08- 2018/07
Total volume of surface lowering [m³]	1±0	145±20	16±3	83±12	138±17	31±7	3±1
Total volume of surface raising [m³]	2±1	322±32	26±4	53±10	198±25	55±10	7±2
Total net volume difference [m³]	1±1	177±38	10±5	-29±16	60±31	24±12	3±3
Normalised volume of surface lowering [m³/d]	0.04±0.01	3.72±0.50	0.41±0.08	2.36±0.36	3.54±0.45	0.93±0.20	0.10±0.03
Normalised volume of surface raising [m³/d]	0.05±0.02	8.26±0.83	0.66±0.11	1.52±0.27	5.07±0.65	1.66±0.30	0.20±0.05
Normalised net volume difference [m³/d]	0.01±0.01	4.54±0.97	0.25±0.13	-0.84±0.45	1.53±0.79	072±0.36	0.09±0.09

The explanation of sediment erosion, deposition and net volume for the longer time intervals is even higher compared to the analysis of the complete study site (Figure 62a-o). The analyses for the shorter intervals in summer 2017 and 2018 show very similar results (Figure 62p-ad). We, again, plotted individual graphs for both long (Figure 63a-c) and short time intervals (Figure 63g-i) with corresponding residuals (Figure 63d-f and j-l, respectively) for the applied linear regression analyses. The temporally lined up residuals now describe exponentially declining functions for sediment erosion (Figure 63d), deposition (Figure 63e) *and* net volume (Figure 63f). The residuals within the summer month of 2017 and 2018 (Figure 63j-i) scatter with no general trend.

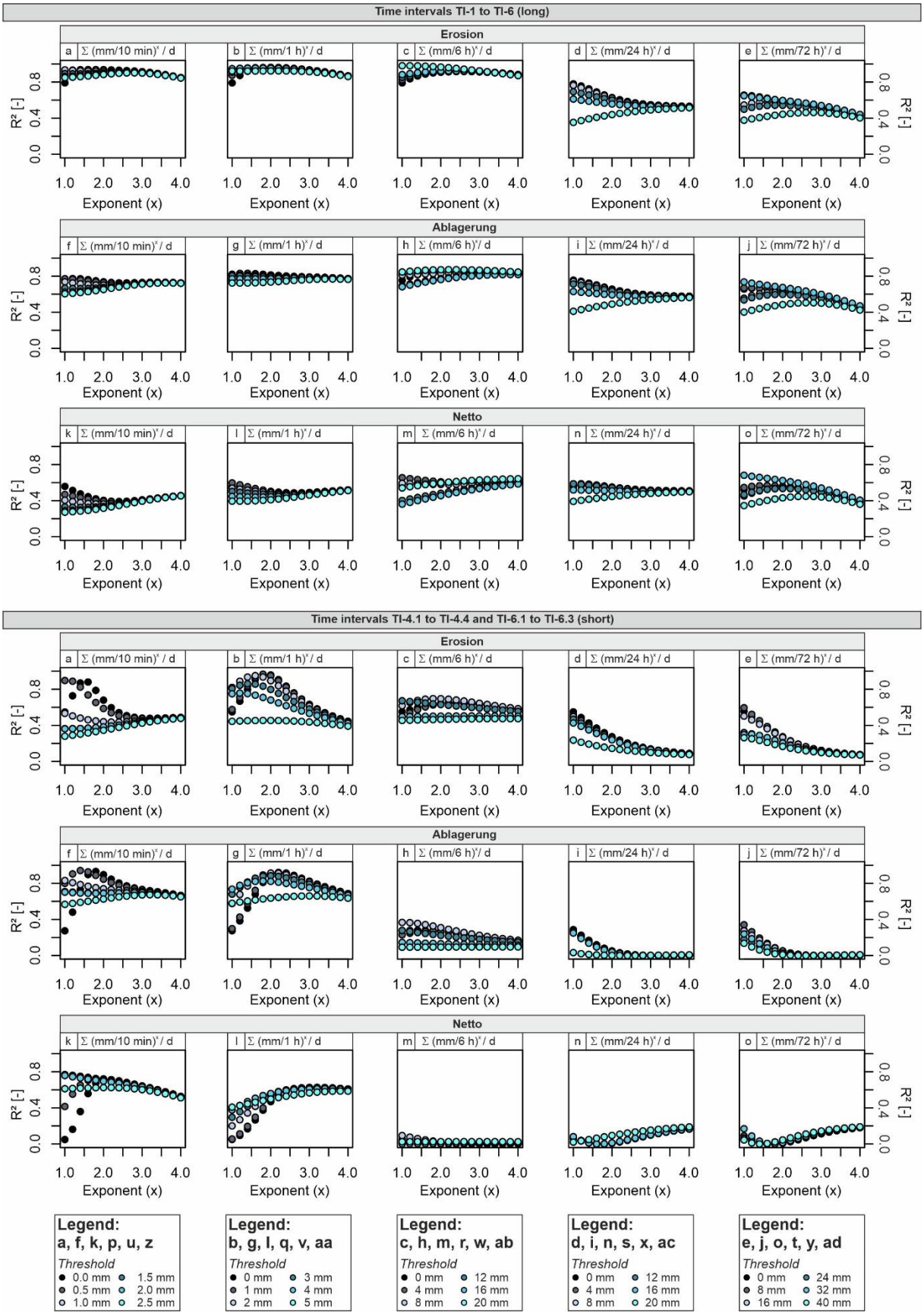

Figure 62: Sediment redistribution *solely in the channel* is taken into account. Relationship between R^2, exponent (x) and rainfall intensity duration. Different colours refer to different intensity thresholds for mm/10 min to mm/72 h. Values lower than the threshold values shown were not considered in the analysis.

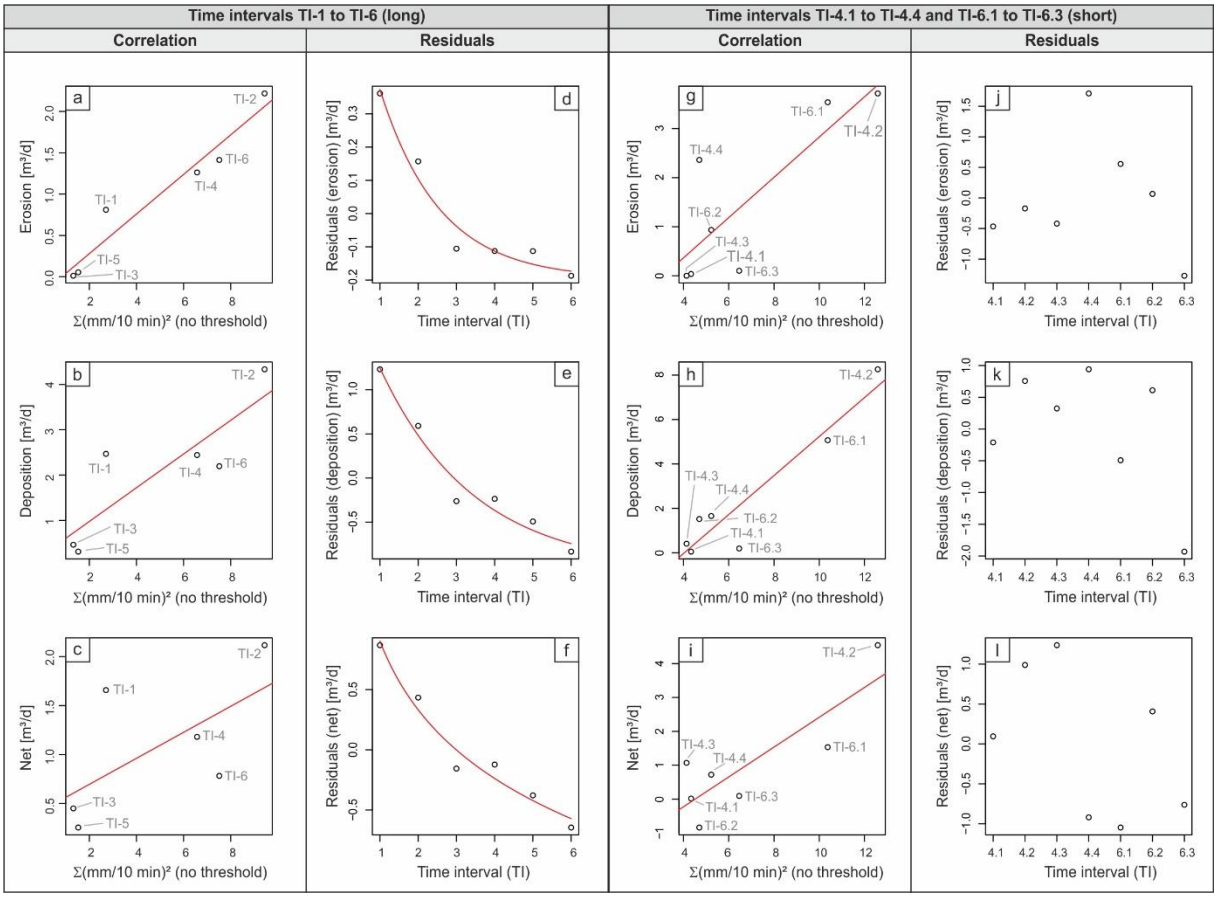

Figure 63: Relationships between summed weighted (exponent = 2) rainfall intensity (mm/10 min) and sediment dynamic in longer time intervals TI-1 to TI-6 (a-c) and shorter summer time intervals TI-4.1 to TI-6.3 (g-i). Corresponding residuals of the data points in a-c are shown separately in d-f and residuals in g-i are displayed separately in j-l. In this figure only the sediment dynamic within the *channel* is displayed (without slopes or river banks).

6.5.3 Debris-flow event(s) between August and September 2018

Between the surveys in August and September 2018, another debris flow (or more) occurred in the torrent (Figure 64). The change detection analysis between the DEM of August (Figure 64b) and the DEM of September (Figure 64c) shows that a volume of about 550 ± 65 m³ was eroded and a volume of 800 ± 65 m³ was deposited in the channel, resulting in approx. 250 ± 90 m³ net volume (Figure 64a and j). The largest erosion values reach 3.5 m, the largest deposition height is 2.8 m. The hourly rainfall intensities reveal two heavy events during this time interval (Figure 56), on 23 October 2018 (13.2 mm/h) and on 13 September 2018 (12.2 mm/h). Although these two rainfall events did not have intensities as high as prior events in the timeline (e.g. Figure 56, 21.8 mm/h on 12 July 2016), a debris flow was triggered.

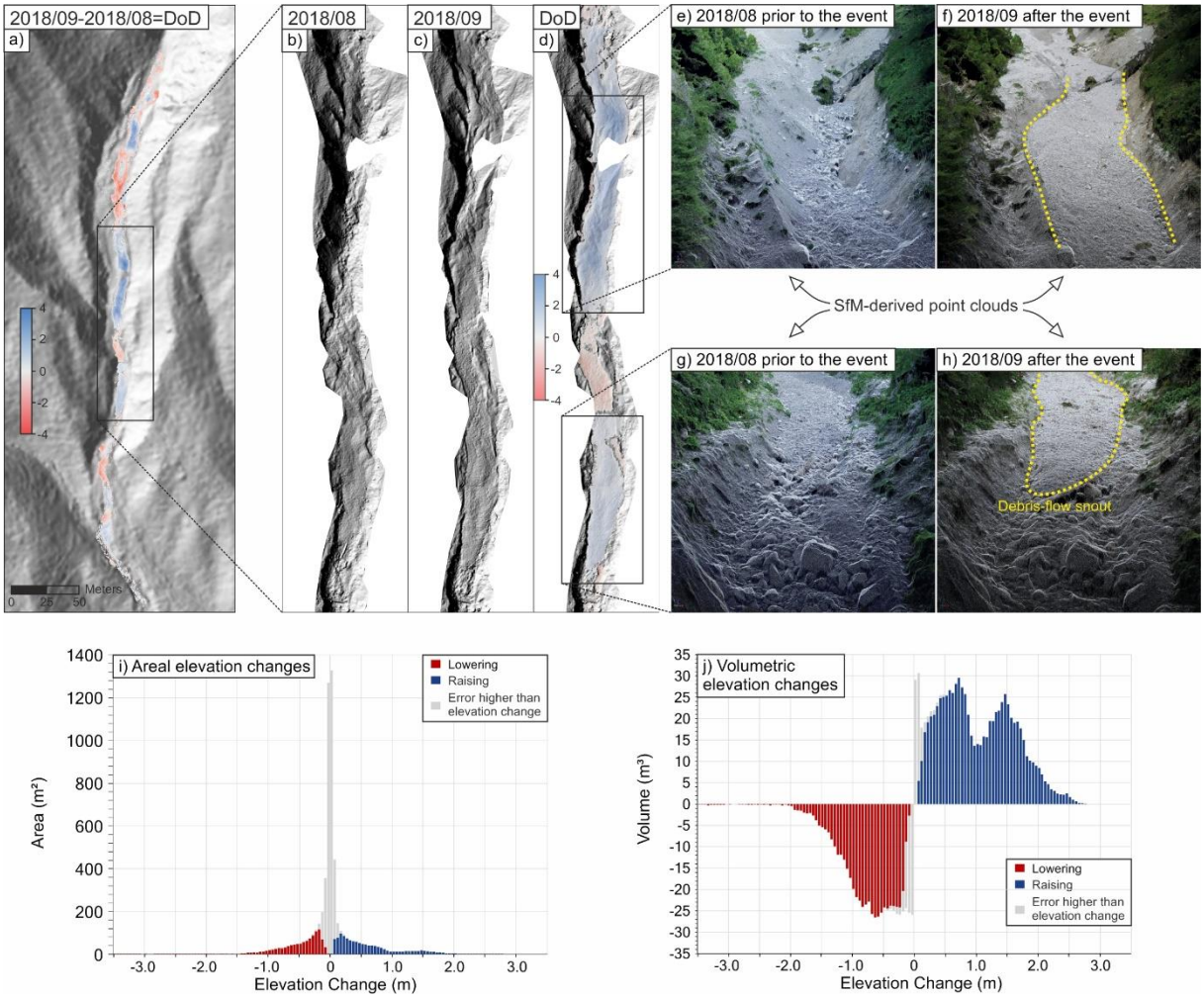

Figure 64: Debris-flow event(s) between field surveys of August and September 2018. a-d: The difference of the pre-event and post-event DEM results in a DoD. e-h: Comparisons of pre- and post-event point clouds derived from SfM analyses. i-j: Areal and volumetric elevation changes.

6.6 Discussion

6.6.1 Change detection

6.6.1.1 Sediment redistribution from 2015 to date (TLS data only)

Assuming a totally closed system, only positive net volume differences should occur. However two change detections reveal negative net volumes from June 2015 to June 2016 (Table 15) and from August to October 2017 (Table 16). With regard to the period from June 2015 to June 2016, the small amount of laser scans in 2015 (Table 11) with resulting large DEM interpolation errors, for which the uncertainty analysis probably did not fully account for, might have caused negative net volumes. The second interval with negative net volumes (August to October 2017), is the only period with a very intense rainfall event over a longer period of time (120 mm in three days). This continuous precipitation might have caused sediment transport out of the study area. All other net volume differences are positive and the study area contains several sediment traps, especially at the bottom of the surveyed area. We therefore consider that only a small amount of material was transported out of the study area compared to the total sediment volume moved within the study area.

Table 15 shows a significantly lower volumetric sediment redistribution in winter than in summer. On the one hand, this region has its largest precipitation values in summer, including a pronounced rainstorm maximum from June to August (DWD Climate Data Center, 2016), one the other hand, precipitation in winter months typically falls as snow. Falling snow has less kinetic energy than falling rain drops and often has no direct impact on sediment movement as it remains on the surface until the temperature rises or it is melted by warmer rain.

Although we tried to monitor the study area at similar time intervals, the length of the intervals (Table 11) varies between four months (second interval) and one year (first interval). In particular, the first interval from June 2015 to June 2016 includes both winter and summer months and therefore represents averaged volumes over this period. Assuming a more active phase in the summer months, the normalised volumes relating to surface lowering and surface raising should be even higher in summer than the averaged volumes given in Table 15.

6.6.1.2 Comparison of TLS data and SfM data sets

The comparison of detected volumetric change by TLS und UAV data (Figure 59 and Table 17) shows very similar results, with a discrepancy of 2.2 ± 1.4% for erosion, 3.5 ± 1.7% for deposition and 9.4 ± 3.3% for net volume (on average 5% in total). These slightly different values arise from both difficulties in TLS and SfM data processing, resulting in (i) errors inherent to the co-registration of TLS scans, (ii) incomplete vegetation removal in both TLS and SfM point clouds, (iii), errors produced by the limited accuracy of GCPs points used in the SfM procedure and (iv) the effects of differently smooth point clouds.

- *Errors inherent to the co-registration of individual TLS scan positions (relates to TLS data only)*
  All individual laser scans have to be co-registered to receive one connected point cloud. Although the procedure used is state-of-the-art and tens of thousands of plane normals have been used for each co-registration, a small amount of error still remains. To minimise the erroneous identification of plane normal, we filtered the point cloud by a deviation gate < 20, as suggested by Williams *et al.* (2018).
- *Errors inherent to the co-registration of filtered, aligned point clouds (relates to both TLS and SfM data)*

  All aligned and filtered point clouds were co-registered with the point cloud of the respective previous field survey. Although thousands of plane normals have been taken into account for each co-registration (Rusinkiewicz and Levoy, 2001), a small amount of error still remains, especially if the co-registration of individual scan positions was not accurate (Table 12 and Table 20). To minimise this kind of error, we aligned all the positions carefully and checked whether the stand deviation between two co-registered point clouds reached a value below 2 to 3 cm (Table 20).

Table 20: Standard deviations (cm) between a TLS and SfM point cloud of the same survey date computed in RiSCAN Pro.

	2017/05	2017/07	2017/08	2017/10	2018/05	2018/09
Std. dev. [cm]	1.2	0.8	0.9	0.8	1.4	1.7

- *Errors caused by incomplete data acquisition (relates to both TLS and SfM data)*

  Both techniques, TLS and SfM, are capable of gathering very large data sets in a short time. However, due to the laser scanner's oblique line of sight and the relatively low survey height of approx. 2 m above ground, a curvilinear channel with steep river banks is difficult to record in its entirety. Hence, a few small "shadowed areas" could be observed during data processing.

  In contrast, the UAV with a flight height of 30-40 m and nadir-oriented camera is capable of acquiring a full record of the channel, as it takes enough overlapping photographs for the SfM workflow. Nevertheless, photographs have just one element of colour information per pixel and are – in contrast to TLS – unable to detect multiple elements of information in the line of sight. Consequently, SfM-derived point clouds do not bear any additional information on what is beneath the vegetation and, therefore, they have some small data gaps following vegetation removal.

  We tried to take this error into account by detecting geomorphic change based on a spatially variable uncertainty, which increases along with the distance to the next data point (Euclidean distance) based on a cell-by-cell basis (Wheaton *et al.*, 2010b).

- *Errors due to an incomplete removal of vegetation from all point clouds (relates to both TLS and SfM data)*

  The parameters for the automatic vegetation removal were chosen carefully and applied multiple times in a row to eliminate as much vegetation as possible. However, not all forms of vegetation were recognised by the software and were thus eliminated manually. But still after the time-consuming manual removal of vegetation, the point cloud was not 100% free of vegetation. These erroneous data points influenced the DEM generation and may have led to errors in the elevation height of some raster cells.

- *Errors produced by the limited accuracy of GCPs used in the SfM procedure (relates to SfM data only)*

  All GCPs, used in the generation of the SfM point cloud, were derived from temporally synchronised TLS surveys (Martínez-Espejo Zaragoza *et al.*, 2017). However, the position of these control points, measured in the laser scan point clouds, does also have a limited accuracy. Additionally, the identification of these control points in all the photographs of the UAV survey is challenging. To minimise this kind of error, we thoroughly selected control points, which were clearly visible in both laser scan point clouds and on the corresponding photographs.

- *Effects of differently smoothed point clouds (relates to both TLS and SfM data)*
  The laser beam has a width of approx. 3 mm on exit and diverges in the atmosphere with 0.3 mrad. Due to the near scan distances, the laser beam often has a small diameter – from 5 mm to 10 mm (7 to 25 m shot distance). Consequently, small or rough features on the surface can be captured. In contrast, the resolution of the SfM-derived point cloud depends on the resolution of the images, the flight height and the focal length of the used camera lens. The resulting "ground sample distance" at a flight height of 30 m is approx. (8 mm) for 20 MP (5,472x3,648) images and 11 mm for 8 MP (4,096x2,160) video frames. If all the pixels are used for the dense point cloud generation in the SfM workflow (Figure 53), this ground sample distance should be equal to the point distance in the dense cloud produced for a nadir and plane object. However, for data sets since June 2018, all the images were downscaled by factor of four (twice for each side) for the dense point cloud generation in order to reduce processing time, resulting in a resolution that was four times lower. Rough objects therefore appear smoother than they actually are (Nouwakpo *et al.*, 2016). This effect slightly affects the metrics of the co-registration with temporally synchronised TLS surveys (Table 20).

6.6.2 Rainfall as controlling factor

Previous research has shown that the mobilised sediment volume for different processes is – among other things – a function of a given rainfall intensity in different alpine environments (Angulo-Martinez *et al.*, 2012, Krautblatter and Moser, 2009, Parsons and Stone, 2006). This function is often described as a nonlinear interaction between rainfall and the mobilisation of material (Parsons and Stone, 2006). However, these relationships are often gained by small-size experiments under laboratory conditions with steady rainfall and limited drop size variation (Navas *et al.*, 1990) or gained from small study areas. In addition, very limited data exists regarding the temporally and seasonally controlled development of sediment recharge in debris-flow channels after a debris-flow event (Jakob *et al.*, 2005), although sediment supply is known to be time-dependent (Bovis and Jakob, 1999).

We initially suggested a linear relationship between summed weighted rainfall events and eroded and deposited sediment volumes (Figure 61 and Figure 63). However, some conditions for a linear regression analysis are not fully met, such as normally distributed residuals or the constant variance of residuals. However, the analysis with its residual plots reveals why the linearly related variables do not match perfectly.

6.6.2.1 Complete study area

Assuming an unlimited sediment availability in the catchment and adjacent slopes, an exponential decrease in sediment recharge in the channel should be assumed (Jakob *et al.*, 2005). Accordingly, the normalised erosion and deposition volumes trace such an exponential function in the first 3.5 years after the debris-flow event (Figure 61d-e). However, the real net sediment recharge appears quite the opposite (Figure 61f). Beginning with negative residuals (less material is net deposited than predicted by the linear model in Figure 61c), the net volume difference reaches positive values after 1.5 years. The heavy

rainfall event including the debris flow in June 2015 (Figure 57) may have depleted the sediment storages in the catchment area. In the following months, rainfall events transported material, originating from unstable channel banks, out of the surveyed area. At the same time, the production of new material was not fast enough to refill the sediment storages in the catchment area (sediment limited), resulting in a negative net value in the study area. As time progresses, the continuing sediment production increases sediment availability and, thus, the deposition of these has been accompanied with a positive net value since September 2016 (Figure 61f).

6.6.2.2 Channel bed

Highest sediment redistribution activity was found during rainstorm events in summer (Table 18 and Table 19), which is also reported by Theule *et al.* (2012) in the Manival Torrent in France. The small, but constant increase in stored sediment in the channel during the winter months was also found by Fuller and Marden (2010) in the Waipaoa catchment in New Zealand and by Berger *et al.* (2011b) in the Illgraben Catchment in Switzerland.

We correlated time-normalised transported sediment volumes solely in the channel bed with exponentially weighted rainfall events (Figure 63). A larger proportion of the sediment dynamic can be explained by this approach, especially in regard to eroded and deposited sediment volumes (Figure 63a-c). The temporally lined up residuals (Figure 63d-f) trace exponential functions for erosion, deposition and net volume differences. The declining residuals over time can be linked to a decreasing activity of sediment dynamic in the channel bed, as most over-steepened slopes failed shortly after the event (Figure 58), leading to an over-proportional deposition and net volume in the channel bed at the beginning of the investigated time span. As a result, it is vital not only to take the intensity and frequency of heavy rainfall events into account, but also the elapsed time since the last triggering event. This coincides with observations of Jakob *et al.* (2005) for debris-flow channels in British Columbia and with more general geomorphological concepts of Ballantyne (2002).

6.6.3 Debris-flow event(s) between August and September 2018

Although more intense rainfall events had occurred before, no debris flow had previously been triggered. In contrast to Brayshaw and Hassan (2009), who linked a smaller amount of sediment volume stored in a channel to a higher probability of debris-flow initiation, we find that an increasing volume of in-channel stored sediment increases the susceptibility of the system similar to Bovis and Jakob (1999), Glade (2005), Jakob *et al.* (2005) and Kaitna *et al.* (2013). A long-term investigation of the study area can give indications, whether a following slower refill of the channel bed is now taking place, as the catchment area is probably again partly depleted, similar to Figure 61f.

6.7 Synopsis and conclusion

The TLS and UAV surveys decipher the temporal, spatial and seasonal variability of erosion and deposition in the study area. The high-resolution data sets reveal a rainstorm-driven activity of sediment dynamics. Best results are achieved using short (mm/10 min or mm/1 h), intense rainfall events, while

long, low-intensity precipitation events explain variances less well. The unexplained variances of the regression analyses indicate a logarithmic increase in sediment supply in the *catchment* with increasing time being elapsed since the debris-flow event. Simultaneously, residuals derived from linear regression analyses using precipitation-normalised values show an exponential decline in sediment recharge rate in the *channel bed*, as unstable banks collapsed shortly after the event. This led to an over-proportional deposition and net volume in the channel bed at the beginning of the investigated time span.

The debris-flow event between August and September 2018 shows that the conceptual model of Bovis and Jakob (1999) for weathering limited (supply-limited) systems is applicable. The increasing sediment volume in the channel increased the susceptibility of the system. An intense (but not extreme) rainfall event resulted in the release of a debris flow.

In this paper we show that:

1. The post debris-flow sediment dynamic in a torrent can be revealed by a high number of terrestrial laser scans, including temporal and spatial variable uncertainties
2. Time-expensive TLS surveys can be substituted by photogrammetric analysis of UAV surveys with a similar accuracy and in less time
3. About 1,150 m³ of material is stored in the channel bed within 3.5 years after the event, which corresponds an average refill rate of about 1 m³/d in relation to the complete time span
4. Short and highly intense rainstorm events explain a large proportion of the post-event sediment dynamic
5. The unexplained variances of the regression analyses suggest a logarithmic increase in sediment supply in the *catchment* over time
6. At the same time, an exponential decline in sediment recharge rates can be observed in the *channel bed*, as unstable banks collapsed shortly after the event, leading to an over-proportional sediment recharge in the channel bed at the beginning of the time span

This paper helps to better understand the time and precipitation-dependent pattern of sediment delivery at the top of the sediment cascade. The suggested relationships (Figure 61 and Figure 63) should be verified by a long-term survey of the study area. The results contribute to a more reliable assessment of debris-flow related hazards in alpine regions.

Acknowledgements

The authors would like to thank the Bavarian State Office for Digitization, Broadband and Surveying for providing us with the orthophotos and the airborne laser scan data. This work was partly financed by the Bavarian Environment Agency (Granting No: AZ: 61-0270-19559/2016). We thank Karl Mayer and Andreas Rimböck from the Bavarian Environment Agency for their ideas on the design of the project.

7 Main findings and short synoptic discussion

The following subchapters contain, inter alia, contents of Dietrich and Krautblatter (2017) and Dietrich and Krautblatter (2019), but were significantly revised and extended.

7.1 How can we reveal long-term debris-flow activity?

The activity of debris flows varies considerably in both space and time. The activity has a significant relevance for the construction of properly dimensioned countermeasures at an appropriate site. Previous research has shown that tree-ring analysis of debris-flow fans can provide information regarding debris-flow activity in the last decades and centuries (Bollschweiler and Stoffel, 2010b, Šilhán and Tichavský, 2016, Stoffel, 2010). Procter *et al.* (2011) used additional data of air photographs to better analyse the spatial extents of debris-flow events on an alpine fan. However, these studies have concentrated rather on computing debris-flow frequencies in the last decades than on absolute volumes and are often methodologically biased. For this purpose, Scheidl and Rickenmann (2010) and Schraml *et al.* (2013) analysed air photographs for single debris-flow events. The approach shown in this thesis and Dietrich and Krautblatter (2017) reveals that the methodology can be applied to long time series of air photographs – in this thesis back to the 1940s (Figure 31). The accuracy of the orthophoto analysis increases significantly by using additional information of field mapping. Thus, mean annual debris-flow transport rates could be calculated over the last decades and related to climate (e.g. rainstorm frequency) and geomorphological controls (e.g. non-vegetated catchment area). In non-vegetated regions, photogrammetry of old aerial photographs can be an alternative approach to quantify historic debris-flow volumes (Nunez-Andres *et al.*, 2019). In addition, the analysis of drill cores in lakes is also a promising approach, but has rarely been applied in past research (Irmler *et al.*, 2006, Kotarba, 1997, Yang *et al.*, 2014). Due to frequent and high-resolution airborne laser scanning campaigns, the identification and quantification of debris-flow events and activity will be more straightforward in future.

7.2 Did mean annual debris-flow transport change in the last decades?

To date, studies targeting debris-flow recurrence rates have often shown an increase in debris-flow events in the last century or decades (Pelfini and Santilli, 2008). In contrast, other authors have described a decrease in debris-flow frequency in some parts of the French Alps in the last decades (Jomelli *et al.*, 2007, Jomelli *et al.*, 2004). However, most of these studies did not provide information about the absolute volumes and, thus, do not give mean debris-flow transport rates or similar numbers. Using air photography time series and field data, the results in this thesis provide specific decadal data regarding mean debris-flow transport rates (Figure 32). It shows that mean transport rates have increased by a factor of more than three in the study area since the 1980s compared to the 1940s to 1970s reference period. This sharp increase since the 1980s could not be demonstrated clearly before in other study areas. The increase in debris-flow activity in the last decades was also observed by Frank *et al.* (2019) in six individual catchments in Switzerland. Looking at a longer period of time, Sass *et al.* (2007) deciphered

a five-fold increase in mean debris-flow transport from the 19th century to 20th century in the Reintal in Germany using ground penetrating radar. However, these rates will probably not continuously increase in future, as many catchment will – or do already – suffer limited sediment supply and additional time has to elapse before the next debris flow can occur (Bovis and Jakob, 1999).

Recent debris-flow rates have rarely been related to Holocene/Lateglacial debris-flow transport rates in literature. Explicit dating of Holocene debris flows has been carried out by Matthews *et al.* (1997) using ^{14}C, Cerling *et al.* (1999) and Marchetti and Cerling (2005) used ^{3}He. As the volume calculations for individual Holocene events is quiet challenging (especially in the young Northern Calcareous Alps seen from a geologic point of view), I made a more general approximation using a complete debris-flow fan. Although some assumption concerning Holocene fan evolution (Curry and Morris, 2004) had to be made (see Chapter 4.6.3), the Holocene debris-flow fan volume represents a rough maximum estimate (Figure 35). The results in this thesis show for the first time, that the recent debris-flow activity exceeds the Holocene/Lateglacial activity by factor of two to three (Figure 36).

7.3 Can we link debris-flow activity to rainstorm frequency?

Debris flows are often triggered by heavy rainstorm events (Caine, 1980, Guzzetti *et al.*, 2008). Authors have shown that an increased global air temperature leads to an increased occurrence of extreme events (Easterling, 2000, Rosenzweig *et al.*, 2008) and to a more frequent occurrence of heavy rainstorm events in alpine regions (Rebetez *et al.*, 1997). Thus, a higher frequency and activity of debris-flow events should be expected in recent decades. In contrast, some studies have provided data that partially contradict this line of thought (Bollschweiler and Stoffel, 2010a). They have stated no significant trend in parts of the Swiss Alps in the last decades due to short-term changes in triggering rainfall (Bollschweiler and Stoffel, 2010a) or due to supply-limited systems. Otherwise, in some regions of the Alps, the number of debris-flow events has significantly increased (Procter *et al.*, 2011) or even doubled over the last 35 years (Pavlova *et al.*, 2014). In this thesis, orthophoto reconnaissance, validated by field mapping, indicates a relationship between rainstorm frequency and debris-flow activity (Dietrich and Krautblatter, 2017). Similar to other studies (Procter *et al.*, 2011), highest activity was observed from 1980-2000 (Figure 32 and Figure 38). The following decrease in debris-flow activity since 2000 – also observed by Bollschweiler and Stoffel (2010a) and Stoffel *et al.* (2008) – might be caused by (i) limited sediment supply in the catchment areas and, especially, (ii) an over-proportional number of extreme events in 1999. Additionally, the study reveals a strong correlation between non-vegetated area in the debris-flow catchments and annual debris-flow volumes. This indicates that enhanced activity might persist for decades until vegetation recovers (Figure 37), similar to a long-term increase in debris-flow activity in recently burned mountain areas (Cannon and DeGraff, 2009, Nyman *et al.*, 2019, Riley *et al.*, 2013).

7.4 Which factors control debris-flow erosion?

The size of hazard zones and the dimensioning of countermeasures strongly depend on the debris-flow runout and flow height. Among other things, these parameters are governed by the debris-flow volume, which often increases significantly during an event due to erosion of channel-bed material (Abanco and Hurlimann, 2014, Frank *et al.*, 2015). The importance to consider erosion along a travel path – modifying flow properties – has also been described insistently by Iverson (2012) and Iverson and Ouyang (2015). Recent studies suggested that flow velocity (Takahashi *et al.*, 1992), discharge (Gregoretti *et al.*, 2019) or shear stresses (Chen and Zhang, 2015, Frank *et al.*, 2015) may induce erosion of material, but these hypotheses often lack sufficient real-scale validation data or relate to different landslide processes (Schneider *et al.*, 2010). The used combination of field work and numerical modelling in this thesis suggests that flow momentum and shear stress are the best-fitted (R^2 up to 0.7) controlling factors for debris-flow erosion (Figure 47 to Figure 50). Latest research with particle flow codes support this hypothesis (Kang and Chan, 2018). Moreover, the data in this thesis reveal the importance of bedrock-loose debris transitions in the channel, which produce local erosion maxima subsequent to low-friction bedrock channels (Figure 50). This might generally affect the long-term channel profile development in alpine regions. The findings in this thesis are applicable in future debris-flow erosion estimations and will enhance existing numerical models (Begueria *et al.*, 2009, Hungr and McDougall, 2009, Hussin *et al.*, 2012).

7.5 How can we reveal the post debris-flow sediment redistribution with high temporal and areal resolution?

For a long time, terrestrial LiDAR was the dominating method to acquire high-resolution data sets in different geomorphological settings (Abellan *et al.*, 2009, Lefsky *et al.*, 2002, Monserrat and Crosetto, 2008). However, in the last decade, photogrammetric analyses of UAV surveys have gained more and more attention, as they also provide georeferenced, high-resolution field records in less time and at lower costs compared to TLS surveys (Berger *et al.*, 2011b, Fonstad *et al.*, 2013, Javemick *et al.*, 2014, Kenner *et al.*, 2014, Westoby *et al.*, 2012). In this thesis, the change detection analyses with DEMs, derived from temporally synchronised UAV and TLS surveys, show a highly reproducible and reliable record of the changing sediment budget over time. Both, raw and thresholded volumes computed with each method, lie in a very similar range with almost equal error values (Figure 59). Thus, the photogrammetric analysis of UAV surveys is – regarding costs, time and logistics – a major development for many geoscientific challenges. The increasing importance and relevance of SfM-based photogrammetry also show up in the number of publications per year (Figure 65). While the trend is increasing for SfM photogrammetry, the number of publications, related to TLS studies, stagnates in the last years (Figure 65a). Looking at the percentage of yearly published articles related to the total number of publications within each research field, this trend can be seen even more clearly, e.g. 25% of all articles (ISI-listed), dealing with SfM photogrammetry, were published in 2018, whereas this value is only 13% for TLS studies.

Nevertheless, for specific fields of application, TLS is still the state-of-the-art method to gather unique data sets in vegetated areas (multiple echoes), in no-fly zones for UAVs or in areas without the possibility to precisely measure ground control points (Blasone *et al.*, 2015, Goodwin *et al.*, 2016, Staley *et al.*, 2014, Theule *et al.*, 2015, Wheaton *et al.*, 2010b).

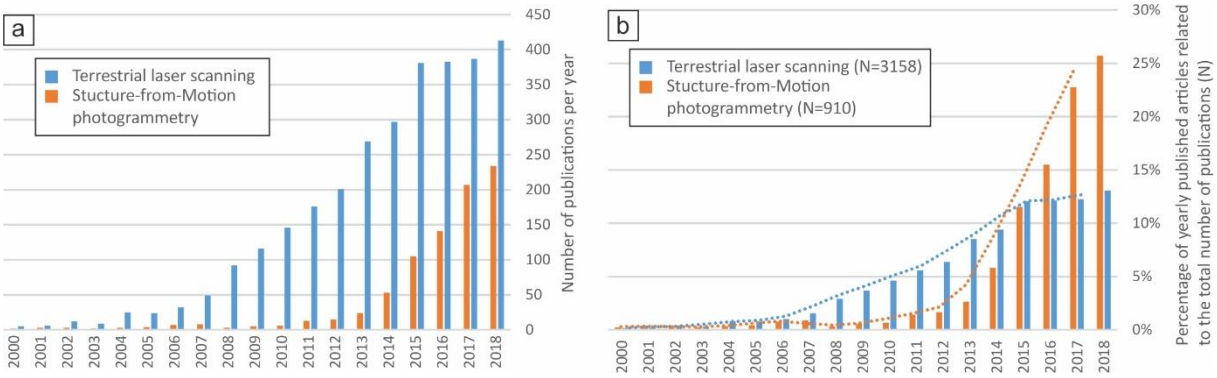

Figure 65: (a) Number of publications per year dealing with the topic of "terrestrial laser scanning" or "structure-from-motion photogrammetry" (ISI-listed). (b) Percentage of yearly published articles related to the total number of publications within each research field. The dashed lines in (b) represent a moving average (2 year). Data source: Web of Science.

7.6 Can we link post-event sediment dynamics to temporal and meteorological controls?

Studies from Bovis and Jakob (1999) and Glade (2005) suggest that the susceptibility of a system depends, among other things, on the sediment supply in the catchment and in the channel. A high sediment supply is usually related with an increased susceptibility, leading to a potentially higher activity of debris flows (Bovis and Jakob, 1999). However, explicit controls on the temporal and seasonal variability of sediment dynamics are still poorly understood (Berger *et al.*, 2011b, Fuller and Marden, 2011). To date, studies have provided both simplified fixed recharge rates considering time and area (Glade, 2005) and more sophisticated models (Jakob *et al.*, 2005). However, most of them are – when using high-resolution methods – limited to small areal study site extents (Bezak *et al.*, 2017, Theule *et al.*, 2015). The high-resolution data sets in this thesis reveal a rainstorm-driven activity of sediment dynamics and channel refill. Variances are best explained by short, intense rainfall events (mm/10 min or mm/1 h). Similarly, Badoux *et al.* (2012) proposed rainfall intensity-duration thresholds for bedload transport initiation in small alpine catchments.

The residuals of the regression analysis (Chapter 6.5.2) suggest a logarithmic increase in sediment supply in the *catchment* with time since the debris-flow event. This could be linked to newly produced material in the catchment due to weathering (Figure 61) or changes in connectivity. At the same time, the residuals derived from the linear regression analysis, using precipitation-normalised values, show an exponential decline in sediment recharge in relation to the *channel bed*, as unstable banks collapsed shortly after the event (Figure 63) and slowly stabilise subsequently.

7.7 Does uncertainty scale with the applied methodological approaches?

For the three main objectives (see Chapter 2 and Figure 66b), different methods with varying accuracy and uncertainty have been applied to decipher erosion and deposition volumes at different study sites. The calculations with ERT data, which were used to approximate the Holocene/Lateglacial debris-flow volume of a fan, have the largest uncertainties considering the made assumptions (Figure 66). Only one profile was used to delimit the basal contact of a debris-flow fan with the underlying till, although the contact surface will certainly vary in height. Additionally, the fan geometry was idealised by a pyramid and some simplified assumptions regarding fan development have been made (Curry and Morris, 2004). However, the methodological mix allows for a first sophisticated estimate of a Lateglacial debris-flow fan volume. The ERT profile shows a sharp transition to underlying materials and has a low inversion error (Figure 34).

The empiric formulas (Chapter 4.3.3.2), which were used to estimate volumes of historic events (< 70 yrs), often show an uncertainty range from 10 to 40%, depending on the made assumptions on former channel slope and the used mobility coefficient k_b. In contrast to the above mentioned fan geometry idealisation, this method has successfully been applied in recent research (Scheidl and Rickenmann, 2010, Schraml *et al.*, 2013).

The combined analyses of high-resolution data sets, derived from TLS measurement, and medium-resolution data sets, derived from ALS surveys, to detect recent events (< 10 yrs), show uncertainty values from 15 to 25%. Depending on the used approach regarding error treatment (Bremer and Sass, 2012, Wheaton *et al.*, 2010b), the uncertainty values are slightly lower or higher in this thesis (Figure 66). The largest proportion of these uncertainty volumes can be traced back to the lower resolution of the airborne laser scan data, especially in vegetated areas with large tree crowns, resulting in larger interpolated areas in the DEM.

Using a conservative error estimation, the TLS-TLS and UAV-UAV-based change detections reveal typically error ranges from 10 to 15%. These errors result from the roughness of the river bed, co-registration errors and errors inherent to the (always) slightly imprecise photogrammetric back-calculation of distortion parameters of the camera lens.

In summary, estimations of complete debris-flow fans will be still challenging in future, as reliable DEMs shortly after deglaciation are rare. Measurements are difficult to carry out and provide just a rough idea of the fan geometry and development. Recent events are often measured with newer and more sophisticated methods. Hence, the uncertainty concerning volumetric computations of eroded and deposited sediment volumes of single events typically decreases, but substantially depends on the applied error propagation and treatment (Bremer and Sass, 2012, Wheaton *et al.*, 2010b).

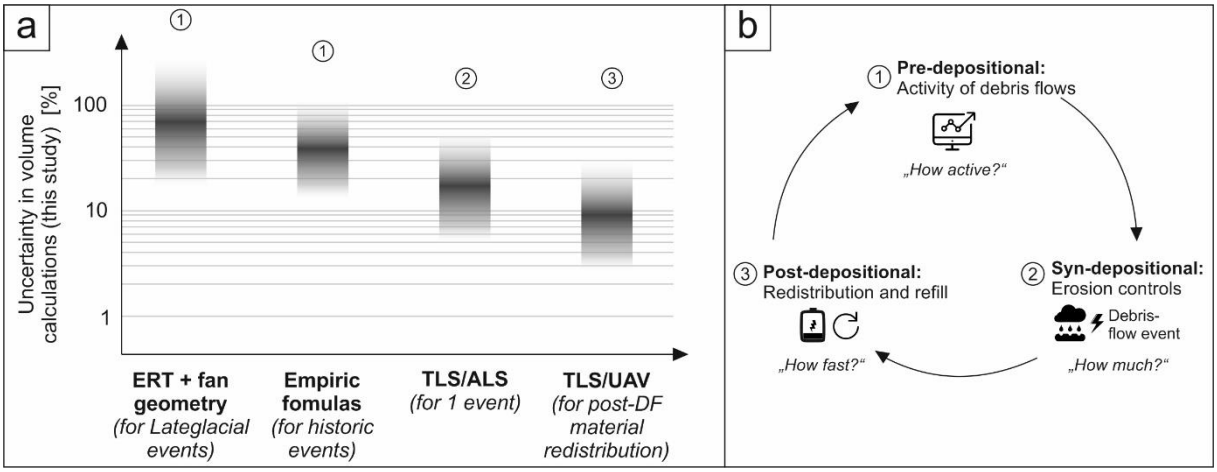

Figure 66: a) Used methods in this thesis and their uncertainties in regard to volume calculations. Encircled numbers refer to the objective shown in b. b) The three objectives and their relations covered in this thesis.

7.8 Synthesis

Why does this thesis contribute to a more reliable and transparent assessment of debris-flow related hazards in alpine regions?

(i) Imagine the following – realistic – scenario:

A debris flow occurs in an inhabited area and damages economic goods. Consequently, the residents of the affected area demand countermeasures and higher security standards to improve their personal safety (often expensive countermeasures are demanded, which would have met the requirements of this specific event or which would protect the residents from all potentially occurring events).

As debris flows do usually not occur quiet often in the same area in a short period of time (there are exceptions), the debris-flow activity and the resulting magnitudes of both historic and future events can be hardly estimated. Thus, the dimensioning of countermeasures seems sometimes to be rather guessed than based on a reproducible, scientific approach. Chapter 4 provides a methodological approach to reveal the long-term debris-flow activity in a study area to better understand the temporal and spatial variability of flow paths and debris-flow magnitudes.

In the above mentioned example, the government, who usually makes decisions, whether and which countermeasures are constructed, should take this variability into account and should communicate – in a proper way – that all-embracing safety cannot be guaranteed for all potential events as safety benefit has to be balanced with reasonable economic costs.

(ii) The debris-flow volume often considerably increases during an event due to material entrainment. The size of hazard zones and the site of potential countermeasures strongly depend on the debris-flow runout and flow height, which in turn are controlled – among other things – by the debris-flow volume. Thus, it is substantial to predict the amount of entrained material along a flow path. The results in Chapter 5 provide insights into physically-based controlling factors for these processes. The varying momentum and shear

stress of a debris flow lead to a synchronised varying material erosion and, thus, should be considered in future simulation software to better predict debris-flow endangered areas.

(iii) Debris-flow activity and volume (see (i) and (ii)) both depend on the sediment supply. After a debris-flow event, the system recharges with sediments originating from nearby slopes or material from the above lying catchment. Controlling factors on these recharge rates are still poorly understood. The results presented in Chapter 6 decipher the temporal, spatial and seasonal sediment redistribution and dynamic in the studied area. Based on these findings, an assessment of the net material recharge rate is possible, which is available for debris-flow transport and, thus, influences the potential debris-flow magnitude and runout.

In each of the presented Chapters 4 to 6, the main findings of each objective have been discussed. The results provide answers or methodological approaches to the introductory asked questions on *how active* debris flows are in an area, *how much* material is entrained and transported and *how fast* a channel gets refilled with material. Each of this topics has its own story, benefit and value in its individual research field. However, when we zoom out a little bit, the broader picture and the relationships in-between the individual studies can be seen more clearly (Figure 67). When we investigate a debris-flow channel or fan for the first time, we do usually not have a clear idea of the debris-flow activity of this individual study site (besides obviously visible indications). The presented approaches in Chapter 4 give a straight-forward guidance to analyse the activity over a larger period of time (Figure 67 → ① pre-depositional). Each occurring debris flow in that area entrains material from the channel bed and thus grows (often considerably) in magnitude. The methodology presented in Chapter 5 provides a strategy to reveal meaningful controlling factors for this erosion processes (Figure 67 → ② syn-depositional). After this debris-flow event, the channel refills with material at a given rate (Figure 67 → ③ post-depositional). Approaches to decipher processes, rates and controls are provided in Chapter 6. The recharge rate, again, governs how often debris flows can occur due to the amount of sediment supply (and how large they can grow in volume → ②) and thus affects debris-flow activity in a region → ①.

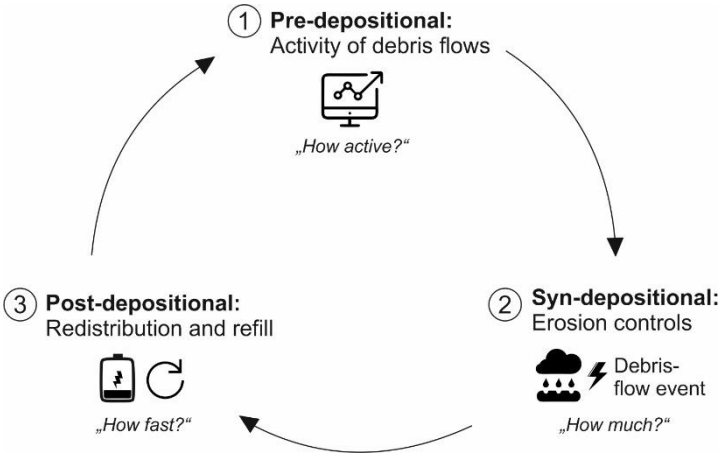

Figure 67: Figure 68: The three objectives and their relations covered in this thesis: ①: Pre-depositional – before a debris-flow event: Is an area prone to debris flows? How frequently do debris flows occur in a given area and which sediment volumes do they transport? ②: Syn-depositional – during an event: Which parameters control debris-flow erosion? ③: Post-depositional – after an event: How does a scoured channel and adjacent slopes react subsequent to a debris-flow event? How fast is a channel refilled with material?

8 Future developments and outlook

As debris-flow fans store a record of recent and past events, their history is a key requirement to analyse associated risks. In times of global climate change, the activity of debris flows affects alpine regions in different ways. Data sets to meet the challenges in these mountain regions are partly available – see Chapter 4 –, but have to be analysed by experts in detail. To draw far-reaching conclusions, concerning impacts of an enhanced rainstorm frequency on these susceptible systems, we need deeper insights in the sediment availability and productivity in alpine catchments. Therefore, evidences – as shown in Chapter 6 – should be carried out over larger areas and different lithologies. These studies might deliver substantial indications, whether potential future debris flows can transport large amount of (newly deposited or produced) sediments. Factors controlling entrainment of material on their pathways – see Chapter 5 – should be fully implemented in predictive numerical models, as they are a key requirement to design hazard zones in alpine regions.

In this thesis all new insights into debris-flow activity, debris-flow erosion and post-event sediment dynamic are based on study sites, which are limited in both areal extent and investigated time span (Figure 69). Improved or new instruments, e.g. laser scanner with a larger shot distance, less beam divergence in the atmosphere and with a faster measuring speed etc., will be able to enlarge the extents of future study areas considerably, especially in combination with an exponentially increasing computational power. Besides, better camera sensors and innovative batteries allowing for an increasing flight time and height will raise the SfM-based processing of UAV surveys to the next level.

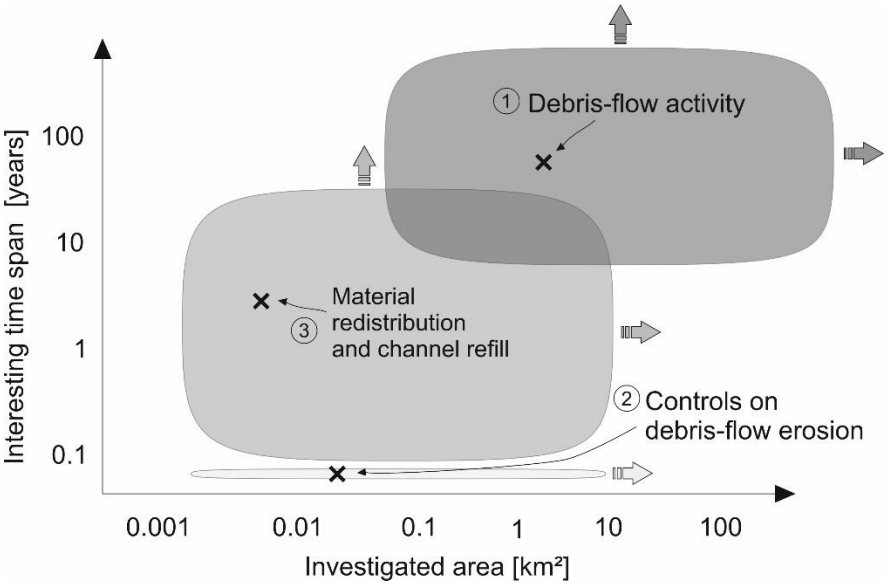

Figure 69: Objectives with typical corresponding study site extents and time spans (grey boxes). The x-symbols represent the investigated study sites and time spans in this thesis. The arrows indicate possible future extents and time spans, which can be studied with innovative approaches and new instruments.

References

ABANCO C, HURLIMANN M. 2014. Estimate of the debris-flow entrainment using field and topographical data. Natural Hazards 71: 363-383. DOI: 10.1007/s11069-013-0930-5

ABELLAN A, JABOYEDOFF M, OPPIKOFER T, VILAPLANA JM. 2009. Detection of millimetric deformation using a terrestrial laser scanner: experiment and application to a rockfall event. Natural Hazards and Earth System Sciences 9: 365-372. DOI: 10.5194/nhess-9-365-2009

ABELLAN A, VILAPLANA JM, CALVET J, GARCIA-SELLES D, ASENSIO E. 2011. Rockfall monitoring by Terrestrial Laser Scanning - case study of the basaltic rock face at Castellfollit de la Roca (Catalonia, Spain). Natural Hazards and Earth System Sciences 11: 829-841. DOI: 10.5194/nhess-11-829-2011

ALUMBAUGH DL, NEWMAN GA. 2000. Image appraisal for 2-D and 3-D electromagnetic inversion. Geophysics 65: 1455-1467. DOI: 10.1190/1.1444834

AMPFERER O. 1907. Glazialgeologische Beobachtungen in der Umgebung von Reutte. In *Verhandlungen in der K.K. Geologischen Reichsanstalt. K.K.* , Reichsanstalt KKG (ed). Geologische Reichsanstalt: Wien; 345-360.

AMPFERER O. 1924. Erläuterungen zur geologischen Spezialkarte der Republik Österreich. Blatt Lechtal. . Geologische Bundesanstalt: Wien

AMPFERER O, OHNESORG T. 1924. Erläuterungen zur geologischen Spezial-Karte der Republik Österreich. Blatt Zirl-Nassereith. Geologische Bundesanstalt: Wien

ANCEY C. 2007. Plasticity and geophysical flows: A review. Journal of Non-Newtonian Fluid Mechanics 142: 4-35. DOI: 10.1016/j.jnnfm.2006.05.005

ANGULO-MARTINEZ M, BEGUERIA S, NAVAS A, MACHIN J. 2012. Splash erosion under natural rainfall on three soil types in NE Spain. Geomorphology 175: 38-44. DOI: 10.1016/j.geomorph.2012.06.016

AUßERFERNER BOTE. 1929. Murgang am Plansee. In *Außerferner Bote*: Reutte; 3.

BADOUX A, TUROWSKI JM, MAO L, MATHYS N, RICKENMANN D. 2012. Rainfall intensity-duration thresholds for bedload transport initiation in small Alpine watersheds. Natural Hazards and Earth System Sciences 12: 3091-3108. DOI: 10.5194/nhess-12-3091-2012

BAEWERT H, MORCHE D. 2014. Coarse sediment dynamics in a proglacial fluvial system (Fagge River, Tyrol). Geomorphology 218: 88-97. DOI: 10.1016/j.geomorph.2013.10.021

BAGNOLD RA. 1954. Experiments on a gravity free dispersion of large solid spheres in a Newtonian fluid under shear. Proc. R. Sot. London 225: 49-63

BALLANTYNE CK. 2002. A general model of paraglacial landscape response. Holocene 12: 371-376. DOI: 10.1191/0959683602hl553fa

BALLIO F, BRAMBILLA D, GIORGETTI E, LONGONI L, PAPINI M, RADICE A. 2010. Evaluation of sediment yield from valley slopes: a case study. In *Montoring, Simulation, Prevention and Remediation of Dense Debris Flows Iii*, DeWrachien D, Brebbia CA (eds). Wit Press: Southampton; 149-160.

BANGEN S, HENSLEIGH J, MCHUGH P, WHEATON J. 2016. Error modeling of DEMs from topographic surveys of rivers using fuzzy inference systems. Water Resources Research 52: 1176-1193. DOI: 10.1002/2015wr018299

BARSKI M, MIESZKOWSKI R. 2014. Upper Jurassic large-scale debris flow deposits in interbiohermal basins of the sponge megafacies in Poland - new insights. Neues Jahrbuch Fur Geologie Und Palaontologie-Abhandlungen 272: 47-59. DOI: 10.1127/0077-7749/2014/0396

BARTELT P, BIELER C, BÜHLER Y, CHRISTEN M, DEUBELBEISS Y, GRAF C, MCARDELL BW, SALZ M, SCHNEIDER M. 2017. User Manual v1.7.0 Debris Flow. ETH Swiss Federal Institute of Technology Zurich: Zurich; 116.

BARTELT P, SALM B, GRUBER U. 1999. Calculating dense-snow avalanche runout using a Voellmy-fluid model with active/passive longitudinal straining. Journal of Glaciology 45: 242-254. DOI: 10.3189/s002214300000174x

BAUM R, GODT J. 2010. Early warning of rainfall-induced shallow landslides and debris flows in the USA. Landslides 7: 259-272. DOI: 10.1007/s10346-009-0177-0

BAVARIAN ENVIRONMENT AGENCY. 2015. Geologisch-wildbachkundliche Stellungnahme zum Roßbichelbach bei Oberstdorf. Bavarian Environment Agency: Augsburg; 1-14.

BAVARIAN SURVEYING AND MAPPING AUTHORITY. 2007. Airborne laser scan (04/19/2007 - 06/19/2007).

BAYERISCHES GEOLOGISCHES LANDESAMT. 1996. Erläuterungen zur geologischen Karte von Bayern 1:500000. Bayerisches Geologisches Landesamt: München

BEGUERIA S, VAN ASCH TWJ, MALET JP, GROENDAHL S. 2009. A GIS-based numerical model for simulating the kinematics of mud and debris flows over complex terrain. Natural Hazards and Earth System Sciences 9: 1897-1909

BENISTON M, DOUGLAS GF. 1996. Impacts of climate change on mountain regions. In *Climate Change 1995. Impacts, Adaptations and Mitigation of Climate Change: Scientific-Technical Analysis*, Watson RT, Zinyowera MC, Moss RH, Dokken DJ (eds). Cambridge Univ. Press: Cambridge; 191–213.

BENISTON M, STOFFEL M, HILL M. 2011. Impacts of climatic change on water and natural hazards in the Alps: can current water governance cope with future challenges? Examples from the European "ACQWA" project. . Environ. Sci. Policy 14: 734–743. DOI: doi:10.1016/j.envsci.2010.12.009

BERGER C, MCARDELL BW, SCHLUNEGGER F. 2011a. Direct measurement of channel erosion by debris flows, Illgraben, Switzerland. Journal of Geophysical Research-Earth Surface 116: 18. DOI: 10.1029/2010jf001722

BERGER C, MCARDELL BW, SCHLUNEGGER F. 2011b. Sediment transfer patterns at the Illgraben catchment, Switzerland: Implications for the time scales of debris flow activities. Geomorphology 125: 421-432. DOI: 10.1016/j.geomorph.2010.10.019

BERTI M, GENEVOIS R, LAHUSEN R, SIMONI A, TECCA PR. 2000. Debris flow monitoring in the acquabona watershed on the Dolomites (Italian alps). Physics and Chemistry of the Earth, Part B: Hydrology, Oceans and Atmosphere 25: 707-715. DOI: 10.1016/s1464-1909(00)00090-3

BERTI M, SIMONI A. 2005. Experimental evidences and numerical modelling of debris flow initiated by channel runoff. Landslides 2: 171-182. DOI: 10.1007/s10346-005-0062-4

BERTOLDI G, D'AGOSTINO V, MCARDELL BW. 2012. An integrated method for debris flow hazard mapping using 2D runout models. In *Internationales Symposion Interpraevent 2012*, Interpraevent IF (ed). Internat. Research Society Interpraevent: Grenoble; 435-446.

BERTOLO P, WIECZOREK GF. 2005. Calibration of numerical models for small debris flows in Yosemite Valley, California, USA. Natural Hazards and Earth System Sciences 5: 993-1001. DOI: 10.5194/nhess-5-993-2005

BESL PJ, MCKAY ND. 1992. A method for registration of 3-D-shapes. Ieee Transactions on Pattern Analysis and Machine Intelligence 14: 239-256. DOI: 10.1109/34.121791

BEZAK N, GRIGILLO D, URBANCIC T, MIKOS M, PETROVIC D, RUSJAN S. 2017. Geomorphic response detection and quantification in a steep forested torrent. Geomorphology 291: 33-44. DOI: 10.1016/j.geomorph.2016.06.034

BIANCO G, BROCHOT S, LAIGLE D, RUBERTO G. 2001. Mise en commun des méthods et des connaissances sur les processus des laves torrentielles pour la protection des zones habitées. In *Connexion des réseaux de données et mise en commun des connaissances et des expériences pour la gestion des risques d'inondations en région alpine: projet Interreg II France Italie.* , Zanolini F, Alzate L, Turroni E (eds). Parn: Grenoble; 133-172.

BIMBÖSE M, NICOLAY A, BRYK A, SCHMIDT K-H, MORCHE D. 2011. Investigations on intra- and interannual coarse sediment dynamics in a high-mountain river. Zeitschrift für Geomorphologie 55: 67-80. DOI: 10.1127/0372-8854/2011/0055S2-0000

BINGHAM EC, GREEN H. 1919. Paint, a plastic material and not a viscous liquid; the measurement of its mobility and yield value. Proc. Am. Sot. Test. Mater. 19: 640-664

BLASONE G, CAVALLI M, CAZORZI F. 2015. Debris-Flow Monitoring and Geomorphic Change Detection Combining Laser Scanning and Fast Photogrammetric Surveys in the Moscardo Catchment (Eastern Italian Alps). 51-54. DOI: 10.1007/978-3-319-09054-2_10

BLASONE G, CAVALLI M, MARCHI L, CAZORZI F. 2014. Monitoring sediment source areas in a debris-flow catchment using terrestrial laser scanning. Catena 123: 23-36. DOI: 10.1016/j.catena.2014.07.001

BMLFUW. 2011. Hydrographisches Jahrbuch von Österreich 2011. Bundesministerium für Land- und Forstwirtschaft: Wien

BOHM R, AUER I, BRUNETTI M, MAUGERI M, NANNI T, SCHONER W. 2001. Regional temperature variability in the European Alps: 1760-1998 from homogenized instrumental time series. International Journal of Climatology 21: 1779-1801. DOI: 10.1002/joc.689

BOLLSCHWEILER M, STOFFEL M. 2010a. Changes and trends in debris-flow frequency since AD 1850: Results from the Swiss Alps. The Holocene 20: 907-916. DOI: 10.1177/0959683610365942

BOLLSCHWEILER M, STOFFEL M. 2010b. Tree rings and debris flows: Recent developments, future directions. Progress in Physical Geography 34: 625-645. DOI: 10.1177/0309133310370283

BOLLSCHWEILER M, STOFFEL M, EHMISCH M, MONBARON M. 2007. Reconstructing spatio-temporal patterns of debris-flow activity using dendrogeomorphological methods. Geomorphology 87: 337-351. DOI: 10.1016/j.geomorph.2006.10.002

BONIELLO MA, CALLIGARIS C, LAPASIN R, ZINI L. 2010. Rheological investigation and simulation of a debris-flow event in the Fella watershed. Natural Hazards and Earth System Science 10: 989-997. DOI: 10.5194/nhess-10-989-2010

BOSSI G, CAVALLI M, CREMA S, FRIGERIO S, LUNA BQ, MANTOVANI M, MARCATO G, SCHENATO L, PASUTO A. 2015. Multi-temporal LiDAR-DTMs as a tool for modelling a complex landslide: a case study in the Rotolon catchment (eastern Italian Alps). Natural Hazards and Earth System Sciences 15: 715-722. DOI: 10.5194/nhess-15-715-2015

BOUMA AH. 1962. Sedimentology of some Flysch deposits; a graphic approach to facies interpretation. Elsevier Amsterdam

BOVIS MJ, JAKOB M. 1999. The role of debris supply conditions in predicting debris flow activity. Earth Surface Processes and Landforms 24: 1039-1054. DOI: 10.1002/(sici)1096-9837(199910)24:11<1039::aid-esp29>3.0.co;2-u

BRASINGTON J, LANGHAM J, RUMSBY B. 2003. Methodological sensitivity of morphometric estimates of coarse fluvial sediment transport. Geomorphology 53: 299-316. DOI: 10.1016/s0169-555x902)00320-3

BRASINGTON J, RUMSBY BT, MCVEY RA. 2000. Monitoring and modelling morphological change in a braided gravel-bed river using high resolution GPS-based survey. Earth Surface Processes and Landforms 25: 973-990. DOI: 10.1002/1096-9837(200008)25:9<973::aid-esp111>3.3.co;2-p

BRASINGTON J, VERICAT D, RYCHKOV I. 2012. Modeling river bed morphology, roughness, and surface sedimentology using high resolution terrestrial laser scanning. Water Resources Research 48. DOI: 10.1029/2012wr012223

BRAYSHAW D, HASSAN MA. 2009. Debris flow initiation and sediment recharge in gullies. Geomorphology 109: 122-131. DOI: 10.1016/j.geomorph.2009.02.021

BREIEN H, DE BLASIO FV, ELVERHOI A, HOEG K. 2008. Erosion and morphology of a debris flow caused by a glacial lake outburst flood, Western Norway. Landslides 5: 271-280. DOI: 10.1007/s10346-008-0118-3

BREMER M, SASS O. 2012. Combining airborne and terrestrial laser scanning for quantifying erosion and deposition by a debris flow event. Geomorphology 138: 49-60. DOI: 10.1016/j.geomorph.2011.08.024

BRUNSDEN D, PRIOR DB. 1984. Slope instability. John Wiley & Sons: New York

BÜHLER Y, GRAF C. 2013. Sediment transfer mapping in a high-alpine catchment using airborne LiDAR. In *Mattertal - ein Tal in Bewegung. Publikation zur Jahrestagung der Schweizerischen Geomorphologischen Gesellschaft 29. Juni - 1. Juli 2011, St. Niklaus*, Graf C (ed). Eidg. Forschungsanstalt WSL: Birmensdorf; 113-124.

CAINE N. 1980. The rainfall intensity-duration control of shallow landslides and debris-flows. Geogr. Ann. A62: 23–27. DOI: doi:10.2307/520449

CANNON SH, DEGRAFF J. 2009. The Increasing Wildfire and Post-Fire Debris-Flow Threat in Western USA, and Implications for Consequences of Climate Change. Springer-Verlag Berlin: Berlin

CANNON SH, GARTNER JE, WILSON RC, BOWERS JC, LABER JL. 2008. Storm rainfall conditions for floods and debris flows from recently burned areas in southwestern Colorado and southern California. Geomorphology 96: 250-269. DOI: 10.1016/j.geomorph.2007.03.019

CARRIVICK JL, GEILHAUSEN M, WARBURTON J, DICKSON NE, CARVER SJ, EVANS AJ, BROWN LE. 2013. Contemporary geomorphological activity throughout the proglacial area of an alpine catchment. Geomorphology 188: 83-95. DOI: 10.1016/j.geomorph.2012.03.029

CAVALLI M, GOLDIN B, COMITI F, BRARDINONI F, MARCHI L. 2017. Assessment of erosion and deposition in steep mountain basins by differencing sequential digital terrain models. Geomorphology 291: 4-16. DOI: 10.1016/j.geomorph.2016.04.009

CAVALLI M, MARCHI L. 2008. Characterisation of the surface morphology of an alpine alluvial fan using airborne LiDAR. Nat. Hazards Earth Syst. Sci. 8: 323-333. DOI: 10.5194/nhess-8-323-2008

CERLING TE, WEBB RH, POREDA RJ, RIGBY AD, MELIS TS. 1999. Cosmogenic ages and frequency of late Holocene debris flows from Prospect Canyon, Grand Canyon, USA. Geomorphology 27: 93-111. DOI: 10.1016/s0169-555x(98)00092-0

CHANDLER J. 1999. Effective application of automated digital photogrammetry for geomorphological research. Earth Surface Processes and Landforms 24: 51-63. DOI: 10.1002/(sici)1096-9837(199901)24:1<51::aid-esp948>3.0.co;2-h

CHEN HX, ZHANG LM. 2015. EDDA 1.0: integrated simulation of debris flow erosion, deposition and property changes. Geoscientific Model Development 8: 829-844. DOI: 10.5194/gmd-8-829-2015

CHIGIRA M, DUAN FJ, YAGI H, FURUYA T. 2004. Using an airborne laser scanner for the identification of shallow landslides and susceptibility assessment in an area of ignimbrite overlain by permeable pyroclastics. Landslides 1: 203-209. DOI: 10.1007/s10346-004-0029-x

CHRISTEN M, KOWALSKI J, BARTELT P. 2010. RAMMS: Numerical simulation of dense snow avalanches in three-dimensional terrain. Cold Regions Science and Technology 63: 1-14. DOI: 10.1016/j.coldregions.2010.04.005

CHRISTEN M, KOWALSKI J, BARTELT P. 2011. Erratum to "RAMMS: Numerical simulation of dense snow avalanches in three-dimensional terrain" [Cold Regions Science and Technology, Volume 63/1–2 (2010) pp. 1–14]. Cold Regions Science and Technology 65: 273. DOI: 10.1016/j.coldregions.2010.09.006

CLAGUE JJ, FRIELE PA, HUTCHINSON I. 2003. Chronology and hazards of large debris flows in the Cheekye River Basin, British Columbia, Canada. Environmental & Engineering Geoscience 9: 99-115. DOI: 10.2113/9.2.99

COE JA, KINNER DA, GODT JW. 2008. Initiation conditions for debris flows generated by runoff at Chalk Cliffs, central Colorado. Geomorphology 96: 270-297. DOI: 10.1016/j.geomorph.2007.03.017

COLOMINA I, MOLINA P. 2014. Unmanned aerial systems for photogrammetry and remote sensing: A review. ISPRS Journal of Photogrammetry and Remote Sensing 92: 79-97. DOI: 10.1016/j.isprsjprs.2014.02.013

COOK KL. 2017. An evaluation of the effectiveness of low-cost UAVs and structure from motion for geomorphic change detection. Geomorphology 278: 195-208. DOI: 10.1016/j.geomorph.2016.11.009

CORSINI A, CASTAGNETTI C, BERTACCHINI E, RIVOLA R, RONCHETTI F, CAPRA A. 2013. Integrating airborne and multi-temporal long-range terrestrial laser scanning with total station measurements for mapping and monitoring a compound slow moving rock slide. Earth Surface Processes and Landforms 38: 1330-1338. DOI: 10.1002/esp.3445

COSTA JE. 1984. Physical geomorphology of debris flows. In *Developments and Applications of Geomorphology*, Costa JE, Fleisher PJ (eds). Springer: Berlin; 288-317.

COSTA JE, WIECZOREK GF. 1987. Debris Flows/Avalanches: Process, Recognition, and Mitigation. Geological Society of America: Boulder

COUSSOT P, MEUNIER M. 1996. Recognition, classification and mechanical description of debris flows. Earth-Science Reviews 40: 209-227. DOI: 10.1016/0012-8252(95)00065-8

CROSTA GB, CUCCHIARO S, FRATTINI P. 2003. Validation of semi-empirical relationships for the definition of debris-flow behavior in granular materials. Millpress Science Publishers: Rotterdam

CROZIER MJ. 1986. Landslides: Causes, consequences and environment. Croom Helm: London

CRUDEN DM, VARNES DJ. 1996. Landslide Types and Processes. In *Landslides: Investigation and Mitigation, Transportation Research Board, Special Report No. 247*, Turner AK, Shuster RL (eds); 36-75.

CUBASCH U, WASZKEWITZ J, HEGERL G, PERLWITZ J. 1995. Regional climate changes as simulated in time-slice experiments. Climatic Change 31: 273-304. DOI: 10.1007/bf01095150

CUCCHIARO S, CAVALLI M, VERICAT D, CREMA S, LLENA M, BEINAT A, MARCHI L, CAZORZI F. 2018. Monitoring topographic changes through 4D-structure-from-motion photogrammetry: application to a debris-flow channel. Environmental Earth Sciences 77: 21. DOI: 10.1007/s12665-018-7817-4

CURRY AM, MORRIS CJ. 2004. Lateglacial and Holocene talus slope development and rockwall retreat on Mynydd Du, UK. Geomorphology 58: 85-106. DOI: 10.1016/s0169-555x(03)00226-5

D'AGOSTINO V. 2013. Assessment of Past Torrential Events Trough Historical Sources. In *Dating Torrential Processes on Fans and Cones*, Schneuwly-Bollschweiler M, Stoffel M, Rudolf-Miklau F (eds). Springer: Berlin; 131-146.

D'AGOSTINO V, MARCHI L. 2001. Debris flow magnitude in the Eastern Italian Alps: Data collection and analysis. Physics and Chemistry of the Earth Part C-Solar-Terrestial and Planetary Science 26: 657-663. DOI: 10.1016/s1464-1917(01)00064-2

D'AGOSTINO V, CERATO M, COALI R. 1996. Il trasporto solido di eventi estremi nei torrenti del trentino orientale. In *Proceedings Int. Symposium Interpraevent*. Internationale Forschungsgesellschaft Interpraevent: Garmisch-Partenkirchen; 377-386.

DEEMS JS, PAINTER TH, FINNEGAN DC. 2013. Lidar measurement of snow depth: a review. Journal of Glaciology 59: 467-479. DOI: 10.3189/2013JoG12J154

DIETRICH A. 2014. Vergleich von potentiell mobilisierbaren Murvolumina mit rezenten Ereignissen und holozänen Murkegeln am Plansee (Tirol, Österreich) In *Ingenieurfakultät Bau Geo Umwelt*. Technische Universität München; 177.

DIETRICH A, KRAUTBLATTER M. 2017. Evidence for enhanced debris-flow activity in the Northern Calcareous Alps since the 1980s (Plansee, Austria). Geomorphology 287: 144-158. DOI: 10.1016/j.geomorph.2016.01.013

DIETRICH A, KRAUTBLATTER M. 2019. Deciphering controls for debris-flow erosion derived from a LiDAR-recorded extreme event and a calibrated numerical model (Roßbichelbach, Germany). Earth Surface Processes and Landforms 44: 1346-1361. DOI: 10.1002/esp.4578

DONG J-J, LEE C-T, TUNG Y-H, LIU C-N, LIN K-P, LEE J-F. 2009. The role of the sediment budget in understanding debris flow susceptibility. Earth Surface Processes and Landforms 34: 1612-1624. DOI: 10.1002/esp.1850

DOWLING CA, SANTI PM. 2014. Debris flows and their toll on human life: a global analysis of debris-flow fatalities from 1950 to 2011. Natural Hazards 71: 203-227. DOI: 10.1007/s11069-013-0907-4

DWD CLIMATE DATA CENTER. 2015. Niederschlag: vieljährige Mittelwerte 1981 - 2010. Deutscher Wetterdienst.

DWD CLIMATE DATA CENTER. 2016. Historical 10-minute station observations of precipitation for Germany. Service GsNM (ed): Offenbach.

EASTERLING DR. 2000. Climate Extremes: Observations, Modeling, and Impacts. Science 289: 2068-2074. DOI: 10.1126/science.289.5487.2068

EVANS SG, CLAGUE JJ. 1994. Recent climatic change and catastrophic geomorphic processes in mountain environments. Geomorphology 10: 107-128. DOI: 10.1016/0169-555x(94)90011-6

FEUERWEHR BREITENWANG. 2010. Murenabgang L255 Planseelandesstraße. http://www.feuerwehr-breitenwang.at/MURENABGANG_L255_PLANSEELANDESSTRASSE.

FEUERWEHR BREITENWANG. 2012. Murenabgang Plansee 04.08.2012.

FONSTAD MA, DIETRICH JT, COURVILLE BC, JENSEN JL, CARBONNEAU PE. 2013. Topographic structure from motion: a new development in photogrammetric measurement. Earth Surface Processes and Landforms 38: 421-430. DOI: 10.1002/esp.3366

FORMAYER HK-K, HELGA. 2009. Hochwasser und Klimawandel.

FÖRSTNER W. 1986. A Feature Based Correspondence Algorithm for Image Matching. Int. Arch. of Photogrammetry and Remote Sensing 26: 150-166

FRANK F, HUGGEL C, MCARDELL BW, VIELI A. 2019. Landslides and increased debris-flow activity: A systematic comparison of six catchments in Switzerland. Earth Surface Processes and Landforms 44: 699-712. DOI: 10.1002/esp.4524

FRANK F, MCARDELL BW, HUGGEL C, VIELI A. 2015. The importance of entrainment and bulking on debris flow runout modeling: examples from the Swiss Alps. Natural Hazards and Earth System Sciences 15: 2569-2583. DOI: 10.5194/nhess-15-2569-2015

FRANK F, MCARDELL BW, OGGIER N, BAER P, CHRISTEN M, VIELI A. 2017. Debris-flow modeling at Meretschibach and Bondasca catchments, Switzerland: sensitivity testing of field-data-based entrainment model. Natural Hazards and Earth System Sciences 17: 801-815. DOI: 10.5194/nhess-17-801-2017

FRANZI L, BIANCO G. 2001. A statistical method to predict debris flow deposited volumes on a debris fan. Physics and Chemistry of the Earth Part C-Solar-Terrestial and Planetary Science 26: 683-688. DOI: 10.1016/s1464-1917(01)00067-8

FREI C, SCHAR C. 1998. A precipitation climatology of the Alps from high-resolution rain-gauge observations. International Journal of Climatology 18: 873-900. DOI: Doi 10.1002/(Sici)1097-0088(19980630)18:8<873::Aid-Joc255>3.0.Co;2-9

FRICKE W. 2002. Hängen vermehrte Starkniederschläge am Hohenpeißenberg mit veränderten Wetterlagen zusammen? :

FRIEDEL H. 1935. Beobachtungen an den Schutthalden der Karawanken. Carinthia II 125: 21–33

FRIEDMAN GM, SANDERS JE, KOPASKA-MERKEL DC. 1992. Principles of sedimentary deposits. Stratigraphy and sedimentology. Macmillan: New York

FU BH, SHI PL, WANG P, LI Q, KONG P, ZHENG GD. 2009. Geometry and kinematics of the 2008 Wenchuan earthquake surface ruptures around the Qushan Town of Beichuan County, Sichuan: Implications for mitigation of seismic and geologic disasters. Chinese Journal of Geophysics-Chinese Edition 52: 485-495

FUCHS S, HEISS K, HÜBL J. 2007. Towards an empirical vulnerability function for use in debris flow risk assessment. Natural Hazards and Earth System Science 7: 495-506. DOI: 10.5194/nhess-7-495-2007

FUHRER J, BENISTON M, FISCHLIN A, FREI C, GOYETTE S, JASPER K, PFISTER C. 2006. Climate risks and their impact on agriculture and forests in Switzerland. Climatic Change 79: 79-102. DOI: 10.1007/s10584-006-9106-6

FULLER IC, LARGE ARG, CHARLTON ME, HERITAGE GL, MILAN DJ. 2003. Reach-scale sediment transfers: An evaluation of two morphological budgeting approaches. Earth Surface Processes and Landforms 28: 889-903. DOI: 10.1002/esp.1011

FULLER IC, MARDEN M. 2010. Rapid channel response to variability in sediment supply: Cutting and filling of the Tarndale Fan, Waipaoa catchment, New Zealand. Marine Geology 270: 45-54. DOI: 10.1016/j.margeo.2009.10.004

FULLER IC, MARDEN M. 2011. Slope–channel coupling in steepland terrain: A field-based conceptual model from the Tarndale gully and fan, Waipaoa catchment, New Zealand. Geomorphology 128: 105-115. DOI: 10.1016/j.geomorph.2010.12.018

GABET EJ, MUDD SM. 2006. The mobilization of debris flows from shallow landslides. Geomorphology 74: 207-218. DOI: 10.1016/j.geomorph.2005.08.013

GATTER R, CAVALLI M, CREMA S, BOSSI G. 2018. Modelling the dynamics of a large rock landslide in the Dolomites (eastern Italian Alps) using multi-temporal DEMs. Peerj 6: 28. DOI: 10.7717/peerj.5903

GERTSCH E. 2009. Geschiebelieferung alpiner Wildbachsysteme bei Grossereignissen - Ereignisanalysen und Entwicklung eines Abschätzverfahrens In *Geographisches Institut der Universität Bern* Universität Bern Bern; 349.

GHUFFAR S, SZEKELY B, RONCAT A, PFEIFER N. 2013. Landslide Displacement Monitoring Using 3D Range Flow on Airborne and Terrestrial LiDAR Data. Remote Sensing 5: 2720-2745. DOI: 10.3390/rs5062720

GIRARDEAU-MONTAUT D, ROUX M, MARC R, THIBAULT G. 2005. Change detection on points cloud data acquired with a ground laser scanner. International Archives of Photogrammetry, Remote Sensing and Spatial Information Sciences 36: W19

GLADE T. 2005. Linking debris-flow hazard assessments with geomorphology. Geomorphology 66: 189-213. DOI: 10.1016/j.geomorph.2004.09.023

GOODWIN NR, ARMSTON J, STILLER I, MUIR J. 2016. Assessing the repeatability of terrestrial laser scanning for monitoring gully topography: A case study from Aratula, Queensland, Australia. Geomorphology 262: 24-36. DOI: 10.1016/j.geomorph.2016.03.007

GOODWIN NR, ARMSTON JD, MUIR J, STILLER I. 2017. Monitoring gully change: A comparison of airborne and terrestrial laser scanning using a case study from Aratula, Queensland. Geomorphology 282: 195-208. DOI: 10.1016/j.geomorph.2017.01.001

GOTTWALD S, BANDEMER H. 1995. Fuzzy Sets, Fuzzy Logic, Fuzzy Methods with Applications

GREGORETTI C, DALLA FONTANA G. 2007. Rainfall threshold for the initiation of debris flows by channel-bed failure in the Dolomites. Millpress Science Publishers: Rotterdam

GREGORETTI C, STANCANELLI LM, BERNARD M, BOREGGIO M, DEGETTO M, LANZONI S. 2019. Relevance of erosion processes when modelling in-channel gravel debris flows for efficient hazard assessment. Journal of Hydrology 568: 575-591. DOI: 10.1016/j.jhydrol.2018.10.001

GRISWOLD JP. 2004. Mobility Statistics and Hazard Mapping for Nonvolcanic Debris-flows and Rock Avalanches. Portland State University: Portland; 200

GUTHRIE RH, HOCKIN A, COLQUHOUN L, NAGY T, EVANS SG, AYLES C. 2010. An examination of controls on debris flow mobility: Evidence from coastal British Columbia. Geomorphology 114: 601-613. DOI: 10.1016/j.geomorph.2009.09.021

GUZZETTI F, PERUCCACCI S, ROSSI M, STARK CP. 2008. The rainfall intensity-duration control of shallow landslides and debris flows: an update. Landslides 5: 3-17. DOI: 10.1007/s10346-007-0112-1

HAEBERLI W, BENISTON M. 1998. Climate change and its impacts on glaciers and permafrost in the Alps. Ambio 27: 258-265

HAEBERLI W, GUODONG C, GORBUNOV AP, HARRIS SA. 1993. Mountain permafrost and climatic change. Permafrost and Periglacial Processes 4: 165-174. DOI: 10.1002/ppp.3430040208

HAEBERLI W, KAAB A, MUHLL DV, TEYSSEIRE P. 2001. Prevention of outburst floods from periglacial lakes at Grubengletscher, Valais, Swiss Alps. Journal of Glaciology 47: 111-122. DOI: 10.3189/172756501781832575

HARRIS C, STEPHENS M. 1988. A combined corner and edge detector. In *Proceedings of the fourth Alvey Vision Conference*; 147-151.

HEARN GJ, HART AB. 2011. Geomorphological Contributions to Landslide Risk Assessment: Theory and Practice. In *Geomorphological Mapping: Methods and Applications*. Elsevier Science Bv: Amsterdam; 107-148.

HELSEN MM, KOOP PJM, VAN STEIJN H. 2002. Magnitude-frequency relationship for debris flows on the fan of the Chalance torrent, Valgaudemar (French Alps). Earth Surface Processes and Landforms 27: 1299-1307. DOI: 10.1002/esp.412

HERSCHEL WH, BULKLEY R. 1926. Über die Viskosität und Elastizität von Solen. Am. Sot. Test. Mater. 26: 621-633

HIBLER IJ. 1921. Der Plansee und seine Umgebung. Wagner: Innsbruck

HÜBL J, STEINWENDTNER H. 2001. Two-dimensional simulation of two viscous debris flows in Austria. Physics and Chemistry of the Earth Part C-Solar-Terrestial and Planetary Science 26: 639-644. DOI: 10.1016/s1464-1917(01)00061-7

HUNG C-Y, CAPART H. 2013. Rotating laser scan method to measure the transient free-surface topography of small-scale debris flows. Experiments in Fluids 54: 1-17. DOI: 10.1007/s00348-013-1544-0

HUNGR O. 1995. A model for the runout analysis of rapid flow slides, debris flows, and avalanches. Canadian Geotechnical Journal 32: 610-623. DOI: 10.1139/t95-063

HUNGR O. 2005. Classification and terminology. In *Debris-Flow Hazards and Related Phenomena*, Jakob M, Hungr O (eds). Springer: Berlin; 9-23.

HUNGR O, LEROUEIL S, PICARELLI L. 2014. The Varnes classification of landslide types, an update. Landslides 11: 167-194. DOI: 10.1007/s10346-013-0436-y

HUNGR O, MCDOUGALL S. 2009. Two numerical models for landslide dynamic analysis. Computers & Geosciences 35: 978-992. DOI: 10.1016/j.cageo.2007.12.003

HUNGR O, MCDOUGALL S, BOVIS M. 2005. Entrainment of material by debris flows. In *Debris-Flow Hazards and Related Phenomena*, Jakob M, Hungr O (eds). Springer: Berlin; 135-158.

HUNGR O, MORGAN GC, KELLERHALS R. 1984. Quantitative analysis of debris torrent hazards for design of remedial measures. Canadian Geotechnical Journal 21: 663-677. DOI: 10.1139/t84-073

HÜRLIMANN M, RICKENMANN D, GRAF C. 2003. Field and monitoring data of debris-flow events in the Swiss Alps. Canadian Geotechnical Journal 40: 161-175. DOI: 10.1139/t02-087

HURRELL JW. 1995. Decadal trends in the north atlantic oscillation: regional temperatures and precipitation. Science 269: 676-9. DOI: 10.1126/science.269.5224.676

HUSSIN HY, QUAN LUNA B, VAN WESTEN CJ, CHRISTEN M, MALET JP, VAN ASCH TWJ. 2012. Parameterization of a numerical 2-D debris flow model with entrainment: a case study of the Faucon catchment, Southern French Alps. Natural Hazards and Earth System Science 12: 3075-3090. DOI: 10.5194/nhess-12-3075-2012

HUTCHINSON JN. 1968. Mass movements. In *Encyclopedia of Geomorphology*, Fairbridge RW (ed). (Reinhold Publishers: New York; 688-695.

HYDROGRAPHISCHER DIENST TIROL. 2014. Online and private database from the Hydrographischer Dienst Tirol.

HYYPPA J, HYYPPA H, LECKIE D, GOUGEON F, YU X, MALTAMO M. 2008. Review of methods of small-footprint airborne laser scanning for extracting forest inventory data in boreal forests. International Journal of Remote Sensing 29: 1339-1366. DOI: 10.1080/01431160701736489

INNSBRUCKER ZEITUNG. 1852. Österreich. In *Innsbrucker Zeitung*: Innsbruck; 1.

IRMLER R, DAUT G, MAUSBACHER R. 2006. A debris flow calendar derived from sediments of lake Lago di Braies (N. Italy). Geomorphology 77: 69-78. DOI: 10.1016/j.geomorph.2006.01.013

IVERSON RM. 1997. The physics of debris flows. Reviews of Geophysics 35: 245-296. DOI: 10.1029/97rg00426

IVERSON RM. 2000. Landslide triggering by rain infiltration. Water Resources Research 36: 1897-1910. DOI: 10.1029/2000wr900090

IVERSON RM. 2003. The debris-flow rheology myth. Millpress Science Publishers: Rotterdam

IVERSON RM. 2012. Elementary theory of bed-sediment entrainment by debris flows and avalanches. Journal of Geophysical Research-Earth Surface 117: 17. DOI: 10.1029/2011jf002189

IVERSON RM, OUYANG C. 2015. Entrainment of bed material by Earth-surface mass flows: Review and reformulation of depth-integrated theory. Reviews of Geophysics 53: 27-58. DOI: 10.1002/2013rg000447

IVERSON RM, REID ME, LAHUSEN RG. 1997. Debris-flow mobilization from landslides. Annual Review of Earth and Planetary Sciences 25: 85-138. DOI: 10.1146/annurev.earth.25.1.85

IVERSON RM, REID ME, LOGAN M, LAHUSEN RG, GODT JW, GRISWOLD JP. 2010. Positive feedback and momentum growth during debris-flow entrainment of wet bed sediment. Nature Geoscience 4: 116-121. DOI: 10.1038/ngeo1040

IVERSON RM, SCHILLING SP, VALLANCE JW. 1998. Objective delineation of lahar-inundation hazard zones. Geological Society of America Bulletin 110: 972-984. DOI: 10.1130/0016-7606(1998)110<0972:odolih>2.3.co;2

JABOYEDOFF M, OPPIKOFER T, ABELLAN A, DERRON MH, LOYE A, METZGER R, PEDRAZZINI A. 2012. Use of LIDAR in landslide investigations: a review. Natural Hazards 61: 5-28. DOI: 10.1007/s11069-010-9634-2

JAKOB M, BOVIS M, ODEN M. 2005. The significance of channel recharge rates for estimating debris-flow magnitude and frequency. Earth Surface Processes and Landforms 30: 755-766. DOI: 10.1002/esp.1188

JAKOB M, MCDOUGALL S, WEATHERLY H, RIPLEY N. 2012. Debris-flow simulations on Cheekye River, British Columbia. Landslides 10: 685-699. DOI: 10.1007/s10346-012-0365-1

JAMES MR, ROBSON S. 2012. Straightforward reconstruction of 3D surfaces and topography with a camera: Accuracy and geoscience application. Journal of Geophysical Research-Earth Surface 117: 17. DOI: 10.1029/2011jf002289

JAMES MR, ROBSON S. 2014. Mitigating systematic error in topographic models derived from UAV and ground-based image networks. Earth Surface Processes and Landforms 39: 1413-1420. DOI: 10.1002/esp.3609

JAMES MR, ROBSON S, SMITH MW. 2017. 3-D uncertainty-based topographic change detection with structure-from-motion photogrammetry: precision maps for ground control and directly georeferenced surveys. Earth Surface Processes and Landforms 42: 1769-1788. DOI: 10.1002/esp.4125

JAVEMICK L, BRASINGTON J, CARUSO B. 2014. Modeling the topography of shallow braided rivers using Structure-from-Motion photogrammetry. Geomorphology 213: 166-182. DOI: 10.1016/j.geomorph.2014.01.006

JEBUR MN, PRADHAN B, TEHRANY MS. 2014. Optimization of landslide conditioning factors using very high-resolution airborne laser scanning (LiDAR) data at catchment scale. Remote Sensing of Environment 152: 150-165. DOI: 10.1016/j.rse.2014.05.013

JOHNSON AM. 1970. Physical processes in geology: A method for interpretation of natural phenomena; intrusions in igneous rocks, fractures, and folds, flow of debris and ice. Freeman, Cooper: San Francisco

JOHNSON AM, RODINE JR. 1984. Debris flow. In *Slope Instability*, Brunsden D, Prior DB (eds). Wiley and Sons: London; 257–361.

JOHNSON JP, WHIPPLE KX. 2007. Feedbacks between erosion and sediment transport in experimental bedrock channels. Earth Surface Processes and Landforms 32: 1048-1062. DOI: 10.1002/esp.1471

JOMELLI V, BRUNSTEIN D, CHOCHILLON C, PECH P. 2003. Hillslope debris-flow frequency since the beginning of the 20th century in the Massif des Ecrins (French Alps). Millpress Science Publishers: Rotterdam

JOMELLI V, BRUNSTEIN D, GRANCHER D, PECH P. 2007. Is the response of hill slope debris flows to recent climate change univocal? A case study in the Massif des Ecrins (French Alps). Climatic Change 85: 119-137. DOI: 10.1007/s10584-006-9209-0

JOMELLI V, PECH VP, CHOCHILLON C, BRUNSTEIN D. 2004. Geomorphic Variations of Debris Flows and Recent Climatic Change in the French Alps. Climatic Change 64: 77-102. DOI: 10.1023/b:clim.0000024700.35154.44

JULIEN PY, LAN YQ. 1991. Rheology of hyperconcentrations. Journal of Hydraulic Engineering-Asce 117: 346-353. DOI: 10.1061/(asce)0733-9429(1991)117:3(346)

KAARTINEN H, HYYPPA J, YU XW, VASTARANTA M, HYYPPA H, KUKKO A, HOLOPAINEN M, HEIPKE C, HIRSCHMUGL M, MORSDORF F, NAESSET E, PITKANEN J, POPESCU S, SOLBERG S, WOLF BM, WU JC. 2012. An International Comparison of Individual Tree Detection and Extraction Using Airborne Laser Scanning. Remote Sensing 4: 950-974. DOI: 10.3390/rs4040950

KAITNA R, HUBER T. 2017. Debris Flow Activity in Permafrost Regions in Austria During the 20th Century. Springer International Publishing Ag: Cham

KAITNA R, RICKENMANN D, SCHATZMANN M. 2007. Experimental study on rheologic behaviour of debris flow material. Acta Geotechnica 2: 71-85. DOI: 10.1007/s11440-007-0026-z

KAITNA R, SCHNEUWLY-BOLLSCHWEILER M, SAUSGRUBER T, MOSER M, STOFFEL M, RUDOLF-MIKLAU F. 2013. Susceptibility and triggers for debris flows: Emergence, loading, release and entrainment. In *Dating Torrential Processes on Fans and Cones*, Schneuwly-Bollschweiler M, Stoffel M, Rudolf-Miklau F (eds). Springer: Berlin; 33-49.

KANG C, CHAN D. 2018. Numerical simulation of 2D granular flow entrainment using DEM. Granular Matter 20: 17. DOI: 10.1007/s10035-017-0782-x

KASPRAK A, WHEATON JM, ASHMORE PE, HENSLEIGH JW, PEIRCE S. 2015. The relationship between particle travel distance and channel morphology: Results from physical models of braided rivers. Journal of Geophysical Research-Earth Surface 120: 55-74. DOI: 10.1002/2014jf003310

KEAN JW, COE JA, COVIELLO V, SMITH JB, MCCOY SW, ARATTANO M. 2015. Estimating rates of debris flow entrainment from ground vibrations. Geophysical Research Letters 42: 6365-6372. DOI: 10.1002/2015gl064811

KEAN JW, MCCOY SW, TUCKER GE, STALEY DM, COE JA. 2013. Runoff-generated debris flows: Observations and modeling of surge initiation, magnitude, and frequency. Journal of Geophysical Research-Earth Surface 118: 2190-2207. DOI: 10.1002/jgrf.20148

KEEFER DK. 2002. Investigating landslides caused by earthquakes - A historical review. Surveys in Geophysics 23: 473-510. DOI: 10.1023/a:1021274710840

KEILER M, KNIGHT J, HARRISON S. 2010. Climate change and geomorphological hazards in the eastern European Alps. Philos Trans A Math Phys Eng Sci 368: 2461-79. DOI: 10.1098/rsta.2010.0047

KENNER R, BÜHLER Y, DELALOYE R, GINZLER C, PHILLIPS M. 2014. Monitoring of high alpine mass movements combining laser scanning with digital airborne photogrammetry. Geomorphology 206: 492-504. DOI: 10.1016/j.geomorph.2013.10.020

KLIR GJ, YUAN B. 1995. Fuzzy sets and fuzzy logic: theory and applications. Prentice-Hall, Inc.

KNIGHT J, HARRISON S. 2009. Sediments and future climate. Nature Geoscience 2: 230-230. DOI: 10.1038/ngeo491

KOTARBA A. 1997. Formation of High-Mountain Talus Slopes Related to Debris-Flow Activity in the High Tatra Mountains. Permafrost and Periglacial Processes 8: 191-204. DOI: 10.1002/(sici)1099-1530(199732)8:2<191::aid-ppp250>3.0.co;2-h

KRAUTBLATTER M, DIKAU R. 2007. Towards a uniform concept for the comparison and extrapolation of rockwall retreat and rockfall supply. Geografiska Annaler Series a-Physical Geography 89A: 21-40. DOI: 10.1111/j.1468-0459.2007.00305.x

KRAUTBLATTER M, MOSER M. 2009. A nonlinear model coupling rockfall and rainfall intensity based on a four year measurement in a high Alpine rock wall (Reintal, German Alps). Natural Hazards and Earth System Science 9: 1425-1432

KRAUTBLATTER M, MOSER M, SCHROTT L, WOLF J, MORCHE D. 2012. Significance of rockfall magnitude and carbonate dissolution for rock slope erosion and geomorphic work on Alpine limestone cliffs (Reintal, German Alps). Geomorphology 167: 21-34. DOI: 10.1016/j.geomorph.2012.04.007

KRONFELLNER-KRAUS G. 1984. Extreme Feststofffrachten und Grabenbildungen von Wildbächen. In *Internationales Symposion Interpraevent* Interpraevent IF (ed): Villach; 109-118.

LANE SN, WESTAWAY RM, HICKS DM. 2003. Estimation of erosion and deposition volumes in a large, gravel-bed, braided river using synoptic remote sensing. Earth Surface Processes and Landforms 28: 249-271. DOI: 10.1002/esp.483

LANG A, MOYA J, COROMINAS J, SCHROTT L, DIKAU R. 1999. Classic and new dating methods for assessing the temporal occurrence of mass movements. Geomorphology 30: 33-52. DOI: 10.1016/s0169-555x(99)00043-4

LE MAUFF B, JUIGNER M, BA A, ROBIN M, LAUNEAU P, FATTAL P. 2018. Coastal monitoring solutions of the geomorphological response of beach-dune systems using multi-temporal LiDAR datasets (Vendee coast, France). Geomorphology 304: 121-140. DOI: 10.1016/j.geomorph.2017.12.037

LEFSKY MA, COHEN WB, PARKER GG, HARDING DJ. 2002. Lidar remote sensing for ecosystem studies. Bioscience 52: 19-30. DOI: 10.1641/0006-3568(2002)052[0019:lrsfes]2.0.co;2

LEGG NT, MEIGS AJ, GRANT GE, KENNARD P. 2014. Debris flow initiation in proglacial gullies on Mount Rainier, Washington. Geomorphology 226: 249-260. DOI: 10.1016/j.geomorph.2014.08.003

LI J, CAO Z, HU K, PENDER G, LIU Q. 2017. A depth-averaged two-phase model for debris flows over erodible beds. Earth Surface Processes and Landforms. DOI: 10.1002/esp.4283

LOWE DG. 1999. Object recognition from local scale-invariant features. In *Proceedings of the Seventh IEEE International Conference on Computer Vision*; 1150-1157 vol.2.

LOWE DG. 2004. Distinctive Image Features from Scale-Invariant Keypoints. International Journal of Computer Vision 60: 91-110. DOI: 10.1023/B:VISI.0000029664.99615.94

LUGON R, STOFFEL M. 2010. Rock-glacier dynamics and magnitude-frequency relations of debris flows in a high-elevation watershed: Ritigraben, Swiss Alps. Global and Planetary Change 73: 202-210. DOI: 10.1016/j.gloplacha.2010.06.004

MA C, HU KH, ZOU Q, TIAN M. 2013. Characteristics of clustering debris flows in Wenchuan earthquake zone. Journal of Mountain Science 10: 953-961. DOI: 10.1007/s11629-013-2410-5

MALET JP, LAIGLE D, REMAÎTRE A, MAQUAIRE O. 2005. Triggering conditions and mobility of debris flows associated to complex earthflows. Geomorphology 66: 215-235. DOI: 10.1016/j.geomorph.2004.09.014

MANGENEY A. 2011. Landslide boost from entrainment. Nature Geoscience 4: 77-78. DOI: 10.1038/ngeo1077

MARAIO S, BRUNO PPG, PICOTTI V, MAIR V, BRARDINONI F. 2018. High-resolution seismic imaging of debris-flow fans, alluvial valley fills and hosting bedrock geometry in Vinschgau/Val Venosta, Eastern Italian Alps. Journal of Applied Geophysics 157: 61-72. DOI: 10.1016/j.jappgeo.2018.07.001

MARCHETTI DW, CERLING TE. 2005. Cosmogenic 3He exposure ages of Pleistocene debris flows and desert pavements in Capitol Reef National Park, Utah. Geomorphology 67: 423-435. DOI: 10.1016/j.geomorph.2004.11.004

MARCHI L, BRUNETTI MT, CAVALLI M, CREMA S. 2019. Debris-flow volumes in northeastern Italy: Relationship with drainage area and size probability. Earth Surface Processes and Landforms 44: 933-943. DOI: 10.1002/esp.4546

MARCHI L, CAVALLI M. 2007. Procedures for the documentation of historical debris flows: application to the Chieppena Torrent (Italian alps). Environ Manage 40: 493-503. DOI: 10.1007/s00267-006-0288-5

MARCHI L, D'AGOSTINO V. 2004. Estimation of debris-flow magnitude in the Eastern Italian Alps. Earth Surface Processes and Landforms 29: 207-220. DOI: 10.1002/esp.1027

MARCHI L, TECCA PR. 2006. Some observations on the use of data from historical documents in debris-flow studies. Natural Hazards 38: 301-320. DOI: 10.1007/s11069-005-0264-z

MARTÍNEZ-ESPEJO ZARAGOZA I, CAROTI G, PIEMONTE A, RIEDEL B, TENGEN D, NIEMEIER W. 2017. Structure from motion (SfM) processing of UAV images and combination with terrestrial laser scanning, applied for a 3D-documentation in a hazardous situation AU - Martínez-Espejo Zaragoza, Isabel. Geomatics, Natural Hazards and Risk 8: 1492-1504. DOI: 10.1080/19475705.2017.1345796

MATTHEWS JA, DAHL S-O, BERRISFORD MS, NESJE A, DRESSER PQ, DUMAYNE-PEATY L. 1997. A preliminary history of Holocene colluvial (debris-flow) activity, Leirdalen, Jotunheimen, Norway. Journal of Quaternary Science 12: 117-129. DOI: 10.1002/(sici)1099-1417(199703/04)12:2<117::aid-jqs296>3.0.co;2-1

MATTHEWS JA, DAHL SO, DRESSER PQ, BERRISFORD MS, LIE O, NESJE A, OWEN G. 2009. Radiocarbon chronology of Holocene colluvial (debris-flow) events at Sletthamn, Jotunheimen, southern Norway: a window on the changing frequency of extreme climatic events and their landscape impact. The Holocene 19: 1107-1129. DOI: 10.1177/0959683609344674

MAURITSCH HJ, SEIBERL W, ARNDT R, ROMER A, SCHNEIDERBAUER K, SENDLHOFER GP. 2000. Geophysical investigations of large landslides in the Carnic Region of southern Austria. Engineering Geology 56: 373-388. DOI: 10.1016/s0013-7952(99)00120-9

MAYER B, STOFFEL M, BOLLSCHWEILER M, HÜBL J, RUDOLF-MIKLAU F. 2010. Frequency and spread of debris floods on fans: A dendrogeomorphic case study from a dolomite catchment in the Austrian Alps. Geomorphology 118: 199-206. DOI: 10.1016/j.geomorph.2009.12.019

MAYER K. 2015. Mur- und Hochwasserereignis am Roßbichelbach und Faltenbach. Bavarian Environment Agency; 33.

MCARDELL BW. 2016. Field Measurements of Forces in Debris Flows at the Illgraben: Implications for Channel-Bed Erosion. International Journal of Erosion Control Engineering 9: 194-198

MCCOY SW, KEAN JW, COE JA, STALEY DM, WASKLEWICZ TA, TUCKER GE. 2010. Evolution of a natural debris flow: In situ measurements of flow dynamics, video imagery, and terrestrial laser scanning. Geology 38: 735-738. DOI: 10.1130/g30928.1

MCCOY SW, TUCKER GE, KEAN JW, COE JA. 2013. Field measurement of basal forces generated by erosive debris flows. Journal of Geophysical Research-Earth Surface 118: 589-602. DOI: 10.1002/jgrf.20041

MELIS TS, WEBB RH, GRIFFITHS PG, WISE TJ. 1995. Magnitude and frequency data for historic debris flows in Grand Canyon National Park and vicinity, Arizona. In *Water-Resources Investigations Report*.

MERGILI M, FISCHER JT, KRENN J, PUDASAINI SP. 2017. r.avaflow v1, an advanced open-source computational framework for the propagation and interaction of two-phase mass flows. Geoscientific Model Development 10: 17. DOI: 10.5194/gmd-10-553-2017

MONSERRAT O, CROSETTO M. 2008. Deformation measurement using terrestrial laser scanning data and least squares 3D surface matching. ISPRS Journal of Photogrammetry and Remote Sensing 63: 142-154. DOI: 10.1016/j.isprsjprs.2007.07.008

MORCHE D, SCHMIDT KH. 2012. Sediment transport in an alpine river before and after a dambreak flood event. Earth Surface Processes and Landforms 37: 347-353. DOI: 10.1002/esp.2263

MOTHES PA, HALL ML, JANDA RJ. 1998. The enormous Chillos Valley Lahar: an ash-flow-generated debris flow from Cotopaxi Volcano, Ecuador. Bulletin of Volcanology 59: 233-244. DOI: 10.1007/s004450050188

NAVAS A, ALBERTO F, MACHÍN J, GALÁN A. 1990. Design and operation of a rainfall simulator for field studies of runoff and soil erosion. Soil Technology 3: 385-397. DOI: https://doi.org/10.1016/0933-3630(90)90019-Y

NIKOLOPOULOS EI, CREMA S, MARCHI L, MARRA F, GUZZETTI F, BORGA M. 2014. Impact of uncertainty in rainfall estimation on the identification of rainfall thresholds for debris flow occurrence. Geomorphology 221: 286-297. DOI: 10.1016/j.geomorph.2014.06.015

NORMAN LM, SANKEY JB, DEAN D, CASTER J, DELONG S, DELONG W, PELLETIER JD. 2017. Quantifying geomorphic change at ephemeral stream restoration sites using a coupled-model approach. Geomorphology 283: 1-16. DOI: 10.1016/j.geomorph.2017.01.017

NOUWAKPO SK, WELTZ MA, MCGWIRE K. 2016. Assessing the performance of structure-from-motion photogrammetry and terrestrial LiDAR for reconstructing soil surface microtopography of naturally vegetated plots. Earth Surface Processes and Landforms 41: 308-322. DOI: doi:10.1002/esp.3787

NUNEZ-ANDRES MA, BUILL F, HURLIMANN M, ABANCO C. 2019. Multi-temporal analysis of morphologic changes applying geomatic techniques. 70 years of torrential activity in the Rebaixader catchment (Central pyrenees). Geomatics Natural Hazards & Risk 10: 314-335. DOI: 10.1080/19475705.2018.1523235

NYMAN P, RUTHERFURD ID, LANE PNJ, SHERIDAN GJ. 2019. Debris flows in southeast Australia linked to drought, wildfire, and the El Nino-Southern Oscillation. Geology 47: 491-494. DOI: 10.1130/g45939.1

O'BRIEN JS, JULIEN PY, FULLERTON WT. 1993. 2-Dimensional water flood and mudflow simulation. Journal of Hydraulic Engineering-Asce 119: 244-261. DOI: 10.1061/(asce)0733-9429(1993)119:2(244)

PALACIOS D, ZAMORANO JJ, PARRILLA G. 1998. Proglacial debris flows in Popocatepetl north face and their relation to 1995 eruption. Zeitschrift für Geomorphologie 42: 273-295

PARSONS AJ, STONE PM. 2006. Effects of intra-storm variations in rainfall intensity on interrill runoff and erosion. Catena 67: 68-78. DOI: 10.1016/j.catena.2006.03.002

PARSONS JD, WHIPPLE KX, SIMONI A. 2001. Experimental study of the grain-flow, fluid-mud transition in debris flows. Journal of Geology 109: 427-447. DOI: 10.1086/320798

PAVLOVA I, JOMELLI V, BRUNSTEIN D, GRANCHER D, MARTIN E, DÉQUÉ M. 2014. Debris flow activity related to recent climate conditions in the French Alps: A regional investigation. Geomorphology 219: 248-259. DOI: 10.1016/j.geomorph.2014.04.025

PELFINI M, SANTILLI M. 2008. Frequency of debris flows and their relation with precipitation: A case study in the Central Alps, Italy. Geomorphology 101: 721-730. DOI: 10.1016/j.geomorph.2008.04.002

PELPOLA CP, HICKIN EJ. 2004. Long-term bed load transport rate based on aerial-photo and ground penetrating radar surveys of fan-delta growth, Coast Mountains, British Columbia. Geomorphology 57: 169-181. DOI: 10.1016/s0169-555x(03)00101-6

PERROY RL, BOOKHAGEN B, ASNER GP, CHADWICK OA. 2010. Comparison of gully erosion estimates using airborne and ground-based LiDAR on Santa Cruz Island, California. Geomorphology 118: 288-300. DOI: 10.1016/j.geomorph.2010.01.009

PIERSON TC. 1986. Flow behavior of channelized debris flows, Mount St. Helens, Washington. In *Hillslope Processes*, Abrahams AD (ed). Allen and Unwin: Boston; 269-296.

PIRULLI M, SORBINO G. 2008. Assessing potential debris flow runout: a comparison of two simulation models. Natural Hazards and Earth System Sciences 8: 961-971

PLAFKER G, ERICKSEN GE, FERNÁNDEZ CONCHA J. 1971. Geological aspects of the May 31, 1970, Perú earthquake. Bulletin of the Seismological Society of America 61: 543-578

PRAGER C, ZANGERL C, PATZELT G, BRANDNER R. 2008. Age distribution of fossil landslides in the Tyrol (Austria) and its surrounding areas. Natural Hazards and Earth System Sciences 8: 377-407

PREKOPOVA M, JANOCKO J, BUDINSKY V, FRIEDMANNOVA M. 2017. Integration of seismic and sedimentological methods for analysis of Quaternary alluvial depositional systems. Environmental Earth Sciences 76: 14. DOI: 10.1007/s12665-016-6345-3

PROCHASKA AB, SANTI PM, HIGGINS JD, CANNON SH. 2008. A study of methods to estimate debris flow velocity. Landslides 5: 431-444. DOI: 10.1007/s10346-008-0137-0

PROCTER E, BOLLSCHWEILER M, STOFFEL M, NEUMANN M. 2011. A regional reconstruction of debris-flow activity in the Northern Calcareous Alps, Austria. Geomorphology 132: 41-50. DOI: 10.1016/j.geomorph.2011.04.035

PROCTER E, STOFFEL M, SCHNEUWLY-BOLLSCHWEILER M, NEUMANN M. 2012. Exploring debris-flow history and process dynamics using an integrative approach on a dolomitic cone in western Austria. Earth Surface Processes and Landforms 37: 913-922. DOI: 10.1002/esp.3207

PROSDOCIMI M, BURGUET M, DI PRIMA S, SOFIA G, TEROL E, COMINO JR, CERDA A, TAROLLI P. 2017. Rainfall simulation and Structure-from-Motion photogrammetry for the analysis of soil water erosion in Mediterranean vineyards. Science of the Total Environment 574: 204-215. DOI: 10.1016/j.scitotenv.2016.09.036

PUDASAINI SP. 2012. A general two-phase debris flow model. Journal of Geophysical Research-Earth Surface 117: 28. DOI: 10.1029/2011jf002186

RABATEL A, DELINE P, JAILLET S, RAVANEL L. 2008. Rock falls in high-alpine rock walls quantified by terrestrial lidar measurements: A case study in the Mont Blanc area. Geophysical Research Letters 35. DOI: 10.1029/2008gl033424

RATHBURN SL, RUBIN ZK, WOHL EE. 2013. Evaluating channel response to an extreme sedimentation event in the context of historical range of variability: Upper Colorado River, USA. Earth Surface Processes and Landforms 38: 391-406. DOI: 10.1002/esp.3329

REBETEZ M, LUGON R, BAERISWYL PA. 1997. Climatic change and debris flows in high mountain regions: The case study of the Ritigraben torrent (Swiss Alps). Climatic Change 36: 371-389. DOI: Doi 10.1023/A:1005356130392

REGION OF THE TYROL. 2006. Lascerscan data from the flight on the 21.11.2006 and 23.11.2006. AG BS (ed).

REID ME, COE JA, BRIEN DL. 2016. Forecasting inundation from debris flows that grow volumetrically during travel, with application to the Oregon Coast Range, USA. Geomorphology 273: 396-411. DOI: 10.1016/j.geomorph.2016.07.039

RICKENMANN D. 1995. Beurteilung von Murgängen. Schweiz. Ing. Archit 48: 1104-1108

RICKENMANN D, KOSCHNI A. 2010. Sediment loads due to fluvial transport and debris flows during the 2005 flood events in Switzerland. Hydrological Processes 24: 993-1007. DOI: 10.1002/hyp.7536

RICKENMANN D, LAIGLE D, MCARDELL BW, HÜBL J. 2006. Comparison of 2D debris-flow simulation models with field events. Computational Geosciences 10: 241-264. DOI: 10.1007/s10596-005-9021-3

RICKENMANN D, SCHEIDL C. 2013. Debris-Flow Runout and Deposition on the Fan. In *Dating Torrential Processes on Fans and Cones*, schneuwly-Bollschweiler M, Stoffel M, Rudolf-Miklau F (eds). Springer: Berlin; 75-93.

RIEGL LMS. 2013. RiSCAN Pro Manual. Riegl: Horn

RILEY KL, BENDICK R, HYDE KD, GABET EJ. 2013. Frequency–magnitude distribution of debris flows compiled from global data, and comparison with post-fire debris flows in the western U.S. Geomorphology 191: 118-128. DOI: 10.1016/j.geomorph.2013.03.008

ROSENZWEIG C, KAROLY D, VICARELLI M, NEOFOTIS P, WU Q, CASASSA G, MENZEL A, ROOT TL, ESTRELLA N, SEGUIN B, TRYJANOWSKI P, LIU C, RAWLINS S, IMESON A. 2008. Attributing physical and biological impacts to anthropogenic climate change. Nature 453: 353-7. DOI: 10.1038/nature06937

ROSSER NJ, PETLEY DN, LIM M, DUNNING SA, ALLISON RJ. 2005. Terrestrial laser scanning for monitoring the process of hard rock coastal cliff erosion. Quarterly Journal of Engineering Geology and Hydrogeology 38: 363-375. DOI: 10.1144/1470-9236/05-008

ROSSI G, TANTERI L, TOFANI V, VANNOCCI P, MORETTI S, CASAGLI N. 2018. Multitemporal UAV surveys for landslide mapping and characterization. Landslides 15: 1045-1052. DOI: 10.1007/s10346-018-0978-0

RUBIN Z, RATHBURN SL, WOHL E, HARRY DL. 2012. Historic range of variability in geomorphic processes as a context for restoration: Rocky Mountain National Park, Colorado, USA. Earth Surface Processes and Landforms 37: 209-222. DOI: 10.1002/esp.2249

RUSINKIEWICZ S, LEVOY M. 2001. Efficient variants of the ICP algorithm. Ieee Computer Soc: Los Alamitos

RYCHKOV I, BRASINGTON J, VERICAT D. 2012. Computational and methodological aspects of terrestrial surface analysis based on point clouds. Computers & Geosciences 42: 64-70. DOI: 10.1016/j.cageo.2012.02.011

SAEZ JL, CORONA C, STOFFEL M, GOTTELAND A, BERGER F, LIÉBAULT F. 2011. Debris-flow activity in abandoned channels of the Manival torrent reconstructed with LiDAR and tree-ring data. Natural Hazards and Earth System Science 11: 1247-1257. DOI: 10.5194/nhess-11-1247-2011

SAHA S, MOORTHI S, PAN HL, WU XR, WANG JD, NADIGA S, TRIPP P, KISTLER R, WOOLLEN J, BEHRINGER D, LIU HX, STOKES D, GRUMBINE R, GAYNO G, WANG J, HOU YT, CHUANG HY, JUANG HMH, SELA J, IREDELL M, TREADON R, KLEIST D, VAN DELST P, KEYSER D, DERBER J, EK M, MENG J, WEI HL, YANG RQ, LORD S, VAN DEN DOOL H, KUMAR A, WANG WQ, LONG C, CHELLIAH M, XUE Y, HUANG BY, SCHEMM JK, EBISUZAKI W, LIN R, XIE PP, CHEN MY,

ZHOU ST, HIGGINS W, ZOU CZ, LIU QH, CHEN Y, HAN Y, CUCURULL L, REYNOLDS RW, RUTLEDGE G, GOLDBERG M. 2010. THE NCEP CLIMATE FORECAST SYSTEM REANALYSIS. Bulletin of the American Meteorological Society 91: 1015-1057. DOI: 10.1175/2010bams3001.1

SALM B. 1966. Contribution to avalanche dynamics. In *International Symposium on Scientific Aspects of Snow and Ice Avalanches*. IAHS Publ.: Davos 199-214.

SASS O. 2005a. Spatial patterns of rockfall intensity in the northern Alps. In *Geomorphology in Environmental Application:*, Schmidt KH, Becht M, Brunotte E, Eitel B, Schrott L (eds). Gebruder Borntraeger: Stuttgart; 51-65.

SASS O. 2005b. Temporal variability of rockfall in the Bavarian Alps, Germany. Arctic Antarctic and Alpine Research 37: 564-573. DOI: 10.1657/1523-0430(2005)037[0564:tvorit]2.0.co;2

SASS O. 2006. Determination of the internal structure of alpine talus deposits using different geophysical methods (Lechtaler Alps, Austria). Geomorphology 80: 45-58. DOI: 10.1016/j.geomorph.2005.09.006

SASS O, KRAUTBLATTER M. 2007. Debris flow-dominated and rockfall-dominated talus slopes: Genetic models derived from GPR measurements. Geomorphology 86: 176-192. DOI: 10.1016/j.geomorph.2006.08.012

SASS O, KRAUTBLATTER M, MORCHE D. 2007. Rapid lake infill following major rockfall (bergsturz) events revealed by ground-penetrating radar (GPR) measurements, Reintal, German Alps. The Holocene 17: 965-976. DOI: 10.1177/0959683607082412

SASSA K, HUI WANG G, JAKOB M, HUNGR O. 2007. Mechanism of landslide-triggered debris flows: Liquefaction phenomena due to the undrained loading of torrent deposits. In *Debris-Flow Hazards and Related Phenomena*, Jakob M, Hungr O (eds). Springer: Berlin, Heidelberg; 81-104.

SCHAFFRATH KR, BELMONT P, WHEATON JM. 2015. Landscape-scale geomorphic change detection: Quantifying spatially variable uncertainty and circumventing legacy data issues. Geomorphology 250: 334-348. DOI: 10.1016/j.geomorph.2015.09.020

SCHEIDL C, RICKENMANN D. 2010. Empirical prediction of debris-flow mobility and deposition on fans. Earth Surface Processes and Landforms 35: 157-173. DOI: 10.1002/esp.1897

SCHEIDL C, RICKENMANN D, CHIARI M. 2008. The use of airborne LiDAR data for the analysis of debris flow events in Switzerland. Natural Hazards and Earth System Science 8: 1113-1127. DOI: 10.5194/nhess-8-1113-2008

SCHEUCHER W, RUDIGIER K. 2012. 23/2012 Technischer Einsatz Murenabgang Plansee.

SCHNEIDER D, BARTELT P, CAPLAN-AUERBACH J, CHRISTEN M, HUGGEL C, MCARDELL BW. 2010. Insights into rock-ice avalanche dynamics by combined analysis of seismic recordings and a numerical avalanche model. Journal of Geophysical Research-Earth Surface 115: 20. DOI: 10.1029/2010jf001734

SCHRAML K, KOGELNIG B, SCHEIDL C, STOFFEL M, KAITNA R. 2013. Estimation of debris flood magnitudes based on dendrogeomorphic data and semi-empirical relationships. Geomorphology 201: 80-85. DOI: 10.1016/j.geomorph.2013.06.009

SCHRAML K, OISMÜLLER M, STOFFEL M, HÜBL J, KAITNA R. 2015a. Debris-flow activity in five adjacent gullies in a limestone mountain range. Geochronometria 42. DOI: 10.1515/geochr-2015-0007

SCHRAML K, THOMSCHITZ B, MCARDELL BW, GRAF C, KAITNA R. 2015b. Modeling debris-flow runout patterns on two alpine fans with different dynamic simulation models. Natural Hazards and Earth System Sciences 15: 1483-1492. DOI: 10.5194/nhess-15-1483-2015

SCHROTT L, HUFSCHMIDT G, HANKAMMER M, HOFMANN T, DIKAU R. 2003. Spatial distribution of sediment storage types and quantification of valley fill deposits in an alpine basin, Reintal, Bavarian Alps, Germany. Geomorphology 55: 45-63. DOI: 10.1016/s0169-555x(03)00131-4

SCHÜRCH P, DENSMORE AL, IVY-OCHS S, ROSSER NJ, KOBER F, SCHLUNEGGER F, MCARDELL B, ALFIMOV V. 2016. Quantitative reconstruction of late Holocene surface evolution on an alpine debris-flow fan. Geomorphology 275: 46-57. DOI: 10.1016/j.geomorph.2016.09.020

SCHÜRCH P, DENSMORE AL, ROSSER NJ, LIM M, MCARDELL BW. 2011a. Detection of surface change in complex topography using terrestrial laser scanning: application to the Illgraben debris-flow channel. Earth Surface Processes and Landforms 36: 1847-1859. DOI: 10.1002/esp.2206

SCHÜRCH P, DENSMORE AL, ROSSER NJ, MCARDELL BW. 2011b. Dynamic controls on erosion and deposition on debris-flow fans. Geology 39: 827-830. DOI: 10.1130/g32103.1

SCHWAB M, RIEKE-ZAPP D, SCHNEIDER H, LINIGER M, SCHLUNEGGER F. 2008. Landsliding and sediment flux in the Central Swiss Alps: A photogrammetric study of the Schimbrig landslide, Entlebuch. Geomorphology 97: 392-406. DOI: 10.1016/j.geomorph.2007.08.019

SEKIGUCHI T, SATO HP. 2004. Mapping of micro topography using airborne laser scanning. Landslides 1: 195-202. DOI: 10.1007/s10346-004-0021-5

SENDERAK K, KONDRACKA M, GADEK B. 2017. Talus slope evolution under the influence of glaciers with the example of slopes near the Hans Glacier, SW Spitsbergen, Norway. Geomorphology 285: 225-234. DOI: 10.1016/j.geomorph.2017.02.023

SEPULVEDA SA, MOREIRAS SM, LARA M, ALFARO A. 2015. Debris flows in the Andean ranges of central Chile and Argentina triggered by 2013 summer storms: characteristics and consequences. Landslides 12: 115-133. DOI: 10.1007/s10346-014-0539-0

SEWELL RJ, PARRY S, MILLIS SW, WANG N, RIESER U, DEWITT R. 2015. Dating of debris flow fan complexes from Lantau Island, Hong Kong, China: The potential relationship between landslide activity and climate change. Geomorphology 248: 205-227. DOI: 10.1016/j.geomorph.2015.07.041

SIEWERT MB, KRAUTBLATTER M, CHRISTIANSEN HH, ECKERSTORFER M. 2012. Arctic rockwall retreat rates estimated using laboratory-calibrated ERT measurements of talus cones in Longyeardalen, Svalbard. Earth Surface Processes and Landforms 37: 1542-1555. DOI: 10.1002/esp.3297

SILHAN K, PANEK T, HRADECKY J, STOFFEL M. 2015. Tree-age control on reconstructed debris-flow frequencies: examples from a regional dendrogeomorphic reconstruction in the Crimean Mountains. Earth Surface Processes and Landforms 40: 243-251. DOI: 10.1002/esp.3623

ŠILHÁN K, TICHAVSKÝ R. 2016. Recent increase in debris flow activity in the Tatras Mountains: Results of a regional dendrogeomorphic reconstruction. Catena 143: 221-231. DOI: 10.1016/j.catena.2016.04.015

SOSIO R, CROSTA GB, FRATTINI P. 2007. Field observations, rheological testing and numerical modelling of a debris-flow event. Earth Surface Processes and Landforms 32: 290-306. DOI: 10.1002/esp.1391

SPREAFICO M, LEHMANN C, NAEF O. 1996. Empfehlungen zur Abschätzung von Feststofffrachten in Wildbächen, Teil II Fachliche Grundlagen und Fallbeispiele. Landeshydrologie und -geologie: Bern

STALEY DM, KEAN JW, CANNON SH, SCHMIDT KM, LABER JL. 2013. Objective definition of rainfall intensity-duration thresholds for the initiation of post-fire debris flows in southern California. Landslides 10: 547-562. DOI: 10.1007/s10346-012-0341-9

STALEY DM, WASKLEWICZ TA, KEAN JW. 2014. Characterizing the primary material sources and dominant erosional processes for post-fire debris-flow initiation in a headwater basin using multi-temporal terrestrial laser scanning data. Geomorphology 214: 324-338. DOI: 10.1016/j.geomorph.2014.02.015

STARHEIM CCA, GOMEZ C, HARRISON J, KAIN C, BREWER NJ, OWEN K, HADMOKO DS, PURDIE H, ZAWAR-REZA P, OWENS I, WASSMER P, LAVIGNE F. 2013. Complex internal architecture of a debris-flow deposit revealed using ground-penetrating radar, Cass, New Zealand. New Zealand Geographer 69: 26-38. DOI: 10.1111/nzg.12002

STEWART JP, HU JP, KAYEN RE, LEMBO AJ, COLLINS BD, DAVIS CA, O'ROURKE TD. 2009. Use of Airborne and Terrestrial Lidar to Detect Ground Displacement Hazards to Water Systems. Journal of Surveying Engineering-Asce 135: 113-124. DOI: 10.1061/(asce)0733-9453(2009)135:3(113)

STINY J. 1910. Die Muren. Universitäts-Verlag Wagner: Innsbruck

STOCK J, DIETRICH WE. 2003. Valley incision by debris flows: Evidence of a topographic signature. Water Resources Research 39: 25. DOI: 10.1029/2001wr001057

STOFFEL M. 2010. Magnitude–frequency relationships of debris flows — A case study based on field surveys and tree-ring records. Geomorphology 116: 67-76. DOI: 10.1016/j.geomorph.2009.10.009

STOFFEL M, BENISTON M. 2006. On the incidence of debris flows from the early Little Ice Age to a future greenhouse climate: A case study from the Swiss Alps. Geophysical Research Letters 33. DOI: 10.1029/2006gl026805

STOFFEL M, BUTLER DR, CORONA C. 2013. Mass movements and tree rings: A guide to dendrogeomorphic field sampling and dating. Geomorphology 200: 106-120. DOI: 10.1016/j.geomorph.2012.12.017

STOFFEL M, CONUS D, GRICHTING MA, LIÈVRE I, MAÎTRE G. 2008. Unraveling the patterns of late Holocene debris-flow activity on a cone in the Swiss Alps: Chronology, environment and implications for the future. Global and Planetary Change 60: 222-234. DOI: 10.1016/j.gloplacha.2007.03.001

SZELISKI R, KANG SB. 1994. Recovering 3D Shape and Motion from Image Streams Using Nonlinear Least Squares. Journal of Visual Communication and Image Representation 5: 10-28. DOI: https://doi.org/10.1006/jvci.1994.1002

TAKAHASHI T. 1981. Debris Flow. Annual Review of Fluid Mechanics 13: 57-77. DOI: 10.1146/annurev.fl.13.010181.000421

TAKAHASHI T. 2009. A Review of Japanese Debris Flow Research. International Journal of Erosion Control Engineering 2: 1-14. DOI: 10.13101/ijece.2.1

TAKAHASHI T, NAKAGAWA H, HARADA T, YAMASHIKI Y. 1992. Routing debris flows with particle segregation. Journal of Hydraulic Engineering-Asce 118: 1490-1507. DOI: 10.1061/(asce)0733-9429(1992)118:11(1490)

TAKEI A. 1984. Interdependence of Sediment Budget between Individual Torrents and River-System. In *Internationales Symposion Interpraevent* Interpraevent IF (ed): Villach; 35-48.

THELER D, REYNARD E, LAMBIEL C, BARDOU E. 2010. The contribution of geomorphological mapping to sediment transfer evaluation in small alpine catchments. Geomorphology 124: 113-123. DOI: 10.1016/j.geomorph.2010.03.006

THEULE JI, LIÉBAULT F, LAIGLE D, LOYE A, JABOYEDOFF M. 2015. Channel scour and fill by debris flows and bedload transport. Geomorphology 243: 92-105. DOI: 10.1016/j.geomorph.2015.05.003

THEULE JI, LIÉBAULT F, LOYE A, LAIGLE D, JABOYEDOFF M. 2012. Sediment budget monitoring of debris-flow and bedload transport in the Manival Torrent, SE France. Natural Hazards and Earth System Science 12: 731-749. DOI: 10.5194/nhess-12-731-2012

THOMA DP, GUPTA SC, BAUER ME, KIRCHOFF CE. 2005. Airborne laser scanning for riverbank erosion assessment. Remote Sensing of Environment 95: 493-501. DOI: 10.1016/j.rse.2005.01.012

TIRANTI D, RABUFFETTI D. 2010. Estimation of rainfall thresholds triggering shallow landslides for an operational warning system implementation. Landslides 7: 471-481. DOI: 10.1007/s10346-010-0198-8

TROPEANO D, TURCONI L. 2004. Using historical documents for landslide, debris flow and stream flood prevention. Applications in Northern Italy. Natural Hazards 31: 663-679. DOI: 10.1023/B:NHAZ.0000024897.71471.f2

TSUTSUI K, ROKUGAWA S, NAKAGAWA H, MIYAZAKI S, CHENG C-T, SHIRAISHI T, YANG S-D. 2007. Detection and Volume Estimation of Large-Scale Landslides Based on Elevation-Change Analysis Using DEMs Extracted From High-Resolution Satellite Stereo Imagery. IEEE Transactions on Geoscience and Remote Sensing 45: 1681-1696. DOI: 10.1109/tgrs.2007.895209

TUROWSKI JM, COOK KL. 2017. Field techniques for measuring bedrock erosion and denudation. Earth Surface Processes and Landforms 42: 109-127. DOI: 10.1002/esp.4007

VAN STEIJN H. 1996. Debris-flow magnitude—frequency relationships for mountainous regions of Central and Northwest Europe. Geomorphology 15: 259-273. DOI: 10.1016/0169-555x(95)00074-f

VAN WESTEN CJ, GETAHUN FL. 2003. Analyzing the evolution of the Tessina landslide using aerial photographs and digital elevation models. Geomorphology 54: 77-89. DOI: 10.1016/s0169-555x(03)00057-6

VARNES DJ. 1978. Slope Movement Types and Processes. Transportation and Road Research Board, National Academy of Science: Washington D.C.

VEYRAT-CHARVILLON S, MEMIER M. 2006. Stereophotogrammetry of archive data and topographic approaches to debris-flow torrent measurements: calculation of channel-sediment states and a partial sediment budget for Manival torrent (Isere, France). Earth Surface Processes and Landforms 31: 201-219. DOI: 10.1002/esp.1322

VILIMEK V, KLIMES J, VLCKO J, CARRENO R. 2006. Catastrophic debris flows near Machu Picchu Village (Aguas Calientes), Peru. Environmental Geology 50: 1041-1052. DOI: 10.1007/s00254-006-0276-3

VOELLMY A. 1955. Über die Zerstörungskraft von Lawinen. Schweizerische Bauzeitung 73 212-285. DOI: 10.5169/seals-61891

WANG GQ, JOYCE J, PHILLIPS D, SHRESTHA R, CARTER W. 2013. Delineating and defining the boundaries of an active landslide in the rainforest of Puerto Rico using a combination of airborne and terrestrial LIDAR data. Landslides 10: 503-513. DOI: 10.1007/s10346-013-0400-x

WARBURTON J. 1993. Energetics of Alpine proglacial geomorphic processes. Transactions of the Institute of British Geographers 18: 197-206. DOI: 10.2307/622362

WASKLEWICZ TA, HATTANJI T. 2009. High-Resolution Analysis of Debris Flow–Induced Channel Changes in a Headwater Stream, Ashio Mountains, Japan∗. The Professional Geographer 61: 231-249. DOI: 10.1080/00330120902743225

WEICHERT RB, BEZZOLA GR, MINOR HE. 2009. Bed erosion in steep open channels. Journal of Hydraulic Research 47: 360-371. DOI: 10.3826/jhr.2009.3128

WESTOBY MJ, BRASINGTON J, GLASSER NF, HAMBREY MJ, REYNOLDS JM. 2012. 'Structure-from-Motion' photogrammetry: A low-cost, effective tool for geoscience applications. Geomorphology 179: 300-314. DOI: 10.1016/j.geomorph.2012.08.021

WHEATON JM. 2008. Uncertainty in morphological sediment budgeting of rivers. University of Southampton: Southampton; 412.

WHEATON JM, BRASINGTON J, DARBY SE, MERZ J, PASTERNACK GB, SEAR D, VERICAT D. 2010a. Linking Geomorphic Changes to Salmonid Habitat at a Scale Relevant to Fish. River Research and Applications 26: 469-486. DOI: 10.1002/rra.1305

WHEATON JM, BRASINGTON J, DARBY SE, SEAR DA. 2010b. Accounting for uncertainty in DEMs from repeat topographic surveys: improved sediment budgets. Earth Surface Processes and Landforms 35: 136-156. DOI: 10.1002/esp.1886

WHIPPLE KX, TUCKER GE. 1999. Dynamics of the stream-power river incision model: Implications for height limits of mountain ranges, landscape response timescales, and research needs. Journal of Geophysical Research-Solid Earth 104: 17661-17674. DOI: 10.1029/1999jb900120

WHITE JC, WULDER MA, VASTARANTA M, COOPS NC, PITT D, WOODS M. 2013. The Utility of Image-Based Point Clouds for Forest Inventory: A Comparison with Airborne Laser Scanning. Forests 4: 518-536. DOI: 10.3390/f4030518

WIECZOREK GF, GLADE T. 2005. Climatic factors influencing occurrence of debris flows. In *Debris-Flow Hazards and Related Phenomena*, Jakob M, Hungr O (eds). Springer: Berlin, Heidelberg; 325-362.

WIGGINS M, SCOTT T, MASSELINK G, RUSSELL P, MCCARROLL RJ. 2019. Coastal embayment rotation: Response to extreme events and climate control, using full embayment surveys. Geomorphology 327: 385-403. DOI: 10.1016/j.geomorph.2018.11.014

WILLIAMS JG, ROSSER NJ, HARDY RJ, BRAIN MJ, AFANA AA. 2018. Optimising 4-D surface change detection: an approach for capturing rockfall magnitude–frequency. Earth Surface Dynamics 6: 101-119. DOI: 10.5194/esurf-6-101-2018

WILLIAMS RD. 2012. DEMs of difference. In *Geomorphological Techniques (Online Edition)*, Clarke LE (ed). British Society for Geomorphology 1-17.

WINCHESTER V, HARRISON S. 1994. A development of the lichenometric method applied to the dating of glacially influenced debris flows in southern chile. Earth Surface Processes and Landforms 19: 137-151. DOI: 10.1002/esp.3290190205

WINKLER G, WAGNER T, PAURITSCH M, BIRK S, KELLERER-PIRKLBAUER A, BENISCHKE R, LEIS A, MORAWETZ R, SCHREILECHNER MG, HERGARTEN S. 2016. Identification and assessment of groundwater flow and storage components of the relict Schoneben Rock Glacier, Niedere Tauern Range, Eastern Alps (Austria). Hydrogeology Journal 24: 937-953. DOI: 10.1007/s10040-015-1348-9

WOOLARD JW, COLBY JD. 2002. Spatial characterization, resolution, and volumetric change of coastal dunes using airborne LIDAR: Cape Hatteras, North Carolina. Geomorphology 48: 269-287. DOI: 10.1016/s0169-555x(02)00185-x

YAGER EM, KIRCHNER JW, DIETRICH WE. 2007. Calculating bed load transport in steep boulder bed channels. Water Resources Research 43: n/a-n/a. DOI: 10.1029/2006wr005432

YAN WY, SHAKER A, EL-ASHMAWY N. 2015. Urban land cover classification using airborne LiDAR data: A review. Remote Sensing of Environment 158: 295-310. DOI: 10.1016/j.rse.2014.11.001

YANG R, HE Z, QIU G, JIN Z, SUN D, JIN X. 2014. A Late Triassic gravity flow depositional system in the southern Ordos Basin. 41: 724-733. DOI: 10.1016/s1876-3804(14)60086-0

YIN YP, WANG FW, SUN P. 2009. Landslide hazards triggered by the 2008 Wenchuan earthquake, Sichuan, China. Landslides 6: 139-152. DOI: 10.1007/s10346-009-0148-5

YOUNG AP, OLSEN MJ, DRISCOLL N, FLICK RE, GUTIERREZ R, GUZA RT, JOHNSTONE E, KUESTER F. 2010. Comparison of Airborne and Terrestrial Lidar Estimates of Seacliff Erosion in Southern California. Photogrammetric Engineering and Remote Sensing 76: 421-427

ZACHER W. 1985. Geologische Karte von Bayern 1:100 000, Blatt 670 Oberstdorf. Bayerisches Geologisches Landesamt: München.

ZARUBA Q, MENCL V. 1982. Landslides and their control. Elsevier: Amsterdam

ZELLER J. 1985. Feststoffmessung in kleinen Gebirgseinzugsgebieten. Wasser, Energie, Luft 77: 246-251

ZHANG S, ZHANG LM. 2017. Impact of the 2008 Wenchuan earthquake in China on subsequent long-term debris flow activities in the epicentral area. Geomorphology 276: 86-103. DOI: 10.1016/j.geomorph.2016.10.009

ZIMMERMANN M, MANI P, GAMMA P. 1997. Murganggefahr und Klimaänderung – ein GIS-basierter Ansatz. Vdf Hochschulverlag: Zürich

Appendix A

Final published journal article:

Dietrich A, Krautblatter M. 2017. Evidence for enhanced debris-flow activity in the Northern Calcareous Alps since the 1980s (Plansee, Austria). Geomorphology 287: 144-158.

DOI: http://dx.doi.org/10.1016/j.geomorph.2016.01.013

Appendix B

Final published journal article:

Dietrich A, Krautblatter M. 2019. Deciphering controls for debris-flow erosion derived from a LiDAR-recorded extreme event and a calibrated numerical model (Roßbichelbach, Germany).

Earth Surface Processes and Landforms 44: 1346-1361.

DOI: https://doi.org/10.1002/esp.4578